

**WestminsterResearch**

<http://www.westminster.ac.uk/research/westminsterresearch>

**Biosynthesis of Polyhydroxyalkanoates and their medical applications.**

**Lydia Francis**

School of Life Sciences

This is an electronic version of a PhD thesis awarded by the University of Westminster. © The Author, 2011.

This is an exact reproduction of the paper copy held by the University of Westminster library.

---

The WestminsterResearch online digital archive at the University of Westminster aims to make the research output of the University available to a wider audience. Copyright and Moral Rights remain with the authors and/or copyright owners.

Users are permitted to download and/or print one copy for non-commercial private study or research. Further distribution and any use of material from within this archive for profit-making enterprises or for commercial gain is strictly forbidden.

---

Whilst further distribution of specific materials from within this archive is forbidden, you may freely distribute the URL of WestminsterResearch: (<http://westminsterresearch.wmin.ac.uk/>).

In case of abuse or copyright appearing without permission e-mail [repository@westminster.ac.uk](mailto:repository@westminster.ac.uk)

Biosynthesis of Polyhydroxyalkanoates  
and their medical applications

LYDIA FRANCIS

A thesis submitted to the University of Westminster in  
candidature for the award of the degree of Doctor of  
Philosophy

University of Westminster

2011

## **AUTHOR'S DECLARATION**

I declare that the present work was carried out in accordance with the Guidelines and Regulations of the University of Westminster.

This thesis is entirely my own work and that where any material could be construed as the work of others, it is fully cited and referenced, and/or with appropriate acknowledgement given.

**Signed Lydia Francis**

**Date: 26<sup>th</sup> May 2011**

# **Abstract**

Biomaterials have gained significant importance in the field of tissue engineering. For example, these biomaterials have been considered for the reconstruction of tissues for structural applications where the tissue morphology is of paramount importance such as bone, cartilage, blood vessels and skin etc. (Ameer *et al.*, 2002). Often these biomaterials are used for tissue regeneration when the surrounding defective tissue exhibits the inherent potential for tissue regeneration. However, in situations where the tissue lacks this ability of regeneration, relevant cells as well as growth factors have been used to accelerate tissue regeneration. In addition, these biomaterials have also been combined with drugs and used as drug delivery systems, thereby reducing the microbial infections while maximising tissue regeneration (Gomes *et al.*, 2004).

There are several factors that make polyhydroxyalkanoates (PHAs) excellent materials for use in TE, however, when used as scaffolds in bone TE, PHAs fail to actively bind to the living tissue by means of a biologically active apatite layer or meet the mechanical demands in load-bearing applications. Therefore, these polymers are combined with inorganic bioactive materials, such as bioactive glass, to increase their applicability in bone TE. Also, there is a growing need to apply these scaffolds for applications such as drug delivery.

For the first part of this study, a solid-in-oil-water (s/o/w) technique was used in an attempt to produce tailored poly(3-hydroxybutyrate) P(3HB) microspheres. The effects of different parameters used for microsphere production on the microsphere size, porosity, and drug distribution were investigated. The P(3HB) microspheres were encapsulated with the drugs such as gentamicin and tetracycline and their *in vitro* release kinetics studied.

A multifunctional P(3HB)/45S5Bioglass<sup>®</sup> composite system for bone tissue engineering was also developed which could exhibit topographical features to increase cell attachment and can also act as a carrier for controlled drug delivery *via* the immobilization of P(3HB) microspheres on the scaffold surfaces. Thus a microsphere

coating was created on the 45S5Bioglass<sup>®</sup> scaffolds resulting in a composite scaffold with increased compressive strength, surface nanotopography and bioactivity as compared to the original 45S5Bioglass<sup>®</sup> scaffold. The multifunctional scaffold was also successfully used as a drug delivery vehicle. Hence, this multifunctional scaffold can be used to deliver drugs, proteins or growth factors to treat bone related diseases. This is the first time such a multifunctional scaffold has been developed. P(3HB) were also used to prepare composite films with a combination of nanoscale bioactive glass (n-BG) for wound healing applications. The various analyses done showed that the addition of n-BG particles had increased the surface roughness of the films and improved the surface wettability. Surface mediated reactions such as clot formation was also found to decrease linearly with the increase in the amount of n-BG particles.

The microspheres were encapsulated with three model proteins BSA, Lucentis<sup>®</sup> and RNase A to understand the effect of morphology, drug distribution on the *in vitro* release profiles. The microspheres produced were of an average size of 2 $\mu$ m. P(3HB) microspheres investigated for use as drug delivery vehicles in the intraocular environment exhibited a gradual release of BSA over a period of time and the encapsulation process did not lead to any degradation of BSA. The % cumulative release of Lucentis<sup>®</sup> from both PBS and contact lens solution was for an extended period of 75 days. The microencapsulation process also did not lead to any degradation of Lucentis<sup>®</sup>. Finally the effects of solvent treatment encountered by the model protein Ribonuclease A (RNase A) during microencapsulation in P(3HB) microspheres were investigated. From the results, structural integrity of RNase A was maintained. A gradual decrease in the enzyme activity of RNase A was observed over a period of time.

# **Acknowledgements**

I would like to sincerely thank my supervisor Dr. Ipsita Roy for her patience and her expert advice, which was an invaluable contribution towards my research. I would also like to thank Prof. Tajalli Keshavarz for his belief in me and his words of encouragement throughout my stay in the University of Westminster.

I also thank Prof Aldo. R. Boccaccini for providing his support and guidance with my experimental work. Dr. Nicola Mordan, Dr. George Gergiou and Dr. Graham Palmer for their assistance with various techniques. Thanks to the University of Westminster and the Cavendish Scholarship committee for providing me this opportunity.

I am indebted to my many colleagues, technical staff and friends from the University of Westminster and 'Boots the Chemist' for their encouragement. I would like to particularly thank Ms. Diahann McEwan for her constant support and motivation.

I would like to wholeheartedly thank my parents, for their incomparable efforts in helping me finish my PhD. My heartfelt gratitude to my dear friend Faisal, my brother Gerard, sister Virginia for their unending encouragement, generosity and motivation that inspired me to give my best. Without their unconditional love, support and sacrifice, completion of this research would have been impossible.

**List of contents****List of abbreviations****List of Figures****List of Tables**

	<b>CHAPTER 1</b>	1
<b>1.1</b>	<b>Biodegradable polymers used for biomedical applications</b>	2
<b>1.1.0</b>	Synthetic polymers	2
<b>1.1.1</b>	Natural polymers	2
<b>1.1.2</b>	Polyhydroxyalkanoates	3
1.1.2.1	<u>Types of PHAs</u>	4
1.1.2.1.1	<i>Scl-PHAs</i>	4
1.1.2.1.2	<i>Mcl-PHAs</i>	5
1.1.2.2	Microorganisms involved in the production of Polyhydroxyalkanoates (PHAs) and their copolymers	5
1.1.2.2.1	<i>Scl-PHA production</i>	6
1.1.2.2.2	<i>Mcl-PHA production</i>	8
1.1.2.2.3	<i>Scl-Mcl PHA production</i>	9
1.1.2.3	Properties of Scl-PHAs	9
1.1.2.3.1	<i>Poly (3-hydroxybutyrate) P(3HB)</i>	9
1.1.2.3.2	<i>Poly(3-hydroxybutyrate-co-3-hydroxyvalerate; P(3HB-co-3HV)</i>	10
1.1.2.3.3	<i>Poly-4-hydroxybutyrate (P(4HB))</i>	11
1.1.2.3.4	<i>Poly(3-hydroxybutyrate-co-Poly-4-hydroxybutyrate) P(3HB-co-4HB)</i>	12
1.1.2.4	Properties of Mcl-PHA and Scl-Mcl PHAs	13
1.1.2.4.1	<i>P(3HO)</i>	13
1.1.2.4.2	<i>P(3HB-co-3HHx)</i>	14
<b>1.2</b>	<b>Bioactive ceramics</b>	15
<u>1.2.1</u>	<u>45S5Bioglass®</u>	15
<u>1.2.2</u>	<u>Hydroxyapatite (HA)</u>	16

---

<b>1.3</b>	<b>Composite materials</b>	16
<u>1.3.1</u>	<u>P(3HB)/bioactive ceramics composites</u>	17
<u>1.3.2</u>	<u>P(3HB-co-3HV)/bioactive ceramics composites</u>	18
<u>1.3.3</u>	<u>P(3HB-co-3HHx)/bioactive ceramics composites</u>	18
<b>1.4</b>	<b>Biomedical Applications of PHAs, inorganic bioactive materials and composite bioactive materials</b>	19
<u>1.4.1</u>	<u>Drug delivery applications of biodegradable polymers, inorganic bioactive materials and composite bioactive materials</u>	19
<u>1.4.2</u>	<u>Types of drug delivery structures</u>	19
<u>1.4.3</u>	<u>Mechanisms of action for controlled release</u>	20
1.4.3.1	Diffusion release mechanism	20
1.4.3.2	Osmotic Release	21
1.4.3.3	Degradation Release/Polymer erosion	21
<u>1.4.4</u>	<u>PHAs used for drug delivery</u>	22
1.4.4.1	Physical and mechanical properties of PHAs affecting the drug release rate	22
<i>1.4.4.1.1</i>	<i>Crystallinity</i>	22
<i>1.4.4.1.2</i>	<i>Thermal Properties</i>	23
<i>1.4.4.1.3</i>	<i>Molecular weight</i>	23
<i>1.4.4.1.4</i>	<i>Processing conditions that affect the drug release rate</i>	24
<u>1.4.5</u>	<u>Inorganic scaffolds used as drug carriers</u>	26
1.4.5.1	Factors affecting the drug release rate from inorganic scaffolds	27
<i>1.4.5.1.1</i>	<i>Processing conditions</i>	27
<u>1.4.6</u>	<u>Composites used for drug delivery</u>	28
1.4.6.1	Polyhydroxyalkanoates and bioactive ceramics in drug delivery	28
1.4.6.2	Factors affecting the drug release rate from composite scaffolds	29
<i>1.4.6.2.1</i>	<i>Processing conditions</i>	29
<u>1.4.7</u>	<u>Application routes of controlled release systems</u>	30
1.4.7.1	Oral drug delivery	30
1.4.7.2	Subcutaneous Implants	31
1.4.7.3	Intravenous administration	31

---

<b>1.5</b>	<b>Biomedical applications of PHAs</b>	32
<u>1.5.1</u>	<u>PHAs used for wound healing applications</u>	33
<u>1.5.2</u>	<u>PHAs used for Hard tissue engineering applications</u>	33
<u>1.5.3</u>	<u>PHAs used for other biomedical applications</u>	34
<b>1.6</b>	<b>Biomedical applications of Bioceramics</b>	37
<u>1.6.1</u>	<u>Bioceramics used for other hard tissue engineering applications</u>	38
<u>1.6.2</u>	<u>Bioceramics used for Bone tissue engineering</u>	38
<b>1.7</b>	<b>Biomedical applications of composite scaffolds</b>	39
<u>1.7.1</u>	<u>Composite scaffolds used for hard tissue engineering applications</u>	40
<u>1.7.2</u>	<u>Composite scaffolds used for Bone tissue engineering</u>	40
<b>1.8</b>	<b>Factors affecting material performance</b>	41
<u>1.8.1</u>	<u><i>In vitro</i> degradation</u>	41
<u>1.8.2</u>	<u><i>In vivo</i> degradation</u>	44
<u>1.8.3</u>	<u>Biocompatibility</u>	46
1.8.3.1	Biocompatibility of PHAs	46
1.8.3.2	Biocompatibility of Composite scaffolds	51
<b>1.9</b>	<b>Aims and Objectives of the present project</b>	53
	<b>CHAPTER 2</b>	56
<b>2.1</b>	<b>Materials</b>	57
<u>2.1.1</u>	<u>Water</u>	57
<u>2.1.2</u>	<u>Chemicals</u>	57
<u>2.1.3</u>	<u>Proteins</u>	57
<u>2.1.4</u>	<u>Plasmid</u>	57
<u>2.1.5</u>	<u>45S5Bioglass<sup>®</sup> and Nanobioglass (n-BG) particles</u>	57
<u>2.1.6</u>	<u>Buffers and Reagents</u>	58
2.1.6.1	Buffers for SDS-PAGE	58
2.1.6.1.1	<i>2X sample buffer for sodium dodecyl sulphate-Polyacrylamide gel electrophoresis (SDS-PAGE)</i>	58
2.1.6.1.2	<i>Resolving gel buffer</i>	58

---

2.1.6.1.3	<i>Stacking gel buffer</i>	59
2.1.6.1.4	<i>5X Reservoir Buffer</i>	58
2.1.6.1.5	<i>Protein fixing solution (for fixing proteins following SDS-PAGE)</i>	58
2.1.6.1.6	<i>Coomassie brilliant blue stain (for staining SDS-PAGE gels)</i>	58
2.1.6.1.7	<i>Destaining solution (for destaining SDS-PAGE)</i>	58
2.1.6.1.8	<i>5X TBE, pH 8.0, (g/L)</i>	58
2.1.6.2	Reagents used for preparation of simulated body fluid (SBF)	59
2.1.6.3	Reagents used for the <i>in vitro</i> drug release and <i>in vitro</i> degradation studies	59
2.1.6.3.1	<i>Contact lens solution</i>	59
2.1.6.3.2	<i>Phosphate buffered saline solution (PBS)</i>	59
<u>2.1.7</u>	<u>Cell line and cell culture materials</u>	59
<u>2.1.8</u>	<u>Bacterial cultures</u>	60
2.1.8.1	Bacterial strains and its maintenance	60
2.1.8.2	Growth media	60
<b>2.2</b>	<b>Experimental Methods</b>	61
<u>2.2.1</u>	<u>Production of P(3HB)</u>	61
2.2.1.2	Optical Density (OD)	61
2.2.1.3	Temperature, pH and dissolved oxygen tension (DOT)	61
2.2.1.4	Dry cell weight (dcw) analysis	62
2.2.1.5	Polymer extraction techniques	62
2.2.1.5.1	<i>The extraction of P(3HB) using chloroform-hypochlorite dispersion method</i>	62
<u>2.2.2</u>	<u>P(3HB) microsphere production</u>	62
2.2.2.1	Production of P(3HB) microspheres including nanobioglass (n/BG) particles	64
<u>2.2.3</u>	<u>P(3HB) microsphere film preparation</u>	64
<u>2.2.4</u>	<u>45S5Bioglass<sup>®</sup> scaffold production and coating with P(3HB) microspheres</u>	64
2.2.4.1	Agitation	65
2.2.4.2	Sonication	65

---

2.2.4.3	Immersion of the scaffold in the aqueous PVA solution	65
<u>2.2.5</u>	<u>Coating of 45S5Bioglass<sup>®</sup> scaffolds with gentamicin-loaded P(3HB) microspheres</u>	66
<u>2.2.6</u>	<u>Gentamicin loading in the 45S5Bioglass<sup>®</sup> scaffold</u>	66
<b>2.3</b>	<b>Drug/Protein quantification methods</b>	66
<u>2.3.1</u>	<u>Determination of the drugs (gentamicin and tetracycline) and proteins (BSA and RNase A) encapsulation efficiency</u>	66
<u>2.3.2</u>	<u>Liquid Chromatography Mass Spectrometry (LC-MS)</u>	67
2.3.2.1	Mobile phase used for gentamicin quantification	67
2.3.2.2	Mobile phase used for tetracycline quantification	67
<u>2.3.3</u>	<u>Bicinchoninic acid assay (BCA)</u>	67
<u>2.4</u>	<u><i>In vitro</i> drug release studies</u>	68
<b>2.5</b>	<b><i>In vitro</i> degradation and bioactivity studies</b>	69
<u>2.5.1</u>	<u>Water uptake measurement</u>	69
2.5.1.1	<i>In vitro</i> degradation studies carried out in simulated body fluid (SBF)	70
2.5.1.2	<i>In vitro</i> degradation studies carried out in 0.1M phosphate buffer saline solution (PBS) and contact lens solution	70
<u>2.5.2</u>	<u><i>In vitro</i> bioactivity tests</u>	71
2.5.2.1	Sample preparation of the (P(3HB) and P(3HB)/n-BG composite microsphere films)	71
2.5.2.2	Sample preparation of the (45S5Bioglass <sup>®</sup> and microsphere coated composite scaffolds	71
<b>2.6</b>	<b>Protein studies</b>	72
<u>2.6.1</u>	<u>Bovine Serum Albumin (BSA) adsorption test</u>	72
<u>2.6.2</u>	<u>Protein adsorption study of (P(3HB)/n-BG composite microsphere films, 45S5Bioglass<sup>®</sup> scaffolds (before and after coating with P(3HB) microspheres) and 45S5Bioglass<sup>®</sup> composite scaffolds covered with HA</u>	72
<u>2.6.3</u>	<u>Protein profile of the adsorbed proteins observed using SDS-PAGE</u>	73
<u>2.6.4</u>	<u>RNase A stability evaluation</u>	73

---

2.6.4.1	Methylene Blue activity test	73
<b>2.7</b>	<b>Biocompatibility tests</b>	74
<u>2.7.1</u>	<u>Cell culture studies on P(3HB) microsphere films (with and without drugs) and P(3HB)/n-BG composite microsphere films</u>	74
2.7.1.1	Sample preparation	75
2.7.1.1.2	<i>Sterilization of samples</i>	75
2.7.1.1.2	<i>Cell seeding on substrates</i>	75
2.7.1.2	Analysis of HaCaT cell culture studies	75
2.7.1.2.1	<i>Neutral Red assay</i>	75
<u>2.7.2</u>	<u>Cell culture studies on 45S5Bioglass<sup>®</sup> composite scaffolds</u>	77
2.7.2.1	Culturing and cyro-preservation of MG-63 cells	77
<b>2.8</b>	<b>P(3HB) microsphere, 45S5Bioglass<sup>®</sup> and P(3HB)/45S5Bioglass<sup>®</sup> composite scaffold physical characterization techniques</b>	78
<u>2.8.1</u>	<u>P(3HB) microsphere characterization techniques</u>	78
2.8.1.1	Particle size analysis	78
2.8.1.2	Surface morphology and microstructure characterization using TEM	78
2.8.1.3	Porosity	79
2.8.1.4	Density of microsphere powder	79
2.8.1.5	Determination of Residual PVA content	80
2.8.1.6	Determination of surface hydrophobicity	80
2.8.1.7	Specific surface area measurement	80
2.8.1.8	Zeta-potential analysis	81
2.8.1.9	X-Ray photoelectron spectroscopy (XPS)	81
2.8.2.0	Fourier Transform Infrared Spectroscopy (FTIR)	81
2.8.2.1	Differential Scanning Calorimetry (DSC)	82
2.8.2.2	Water contact angle study	82
2.8.2.3	White light interferometry	83
<u>2.8.3</u>	<u>45S5Bioglass<sup>®</sup> and P(3HB)/45S5Bioglass<sup>®</sup> composite scaffold physical characterization techniques</u>	83

---

2.8.3.1	Porosity measurements	83
2.8.3.2	Mechanical properties	84
2.8.3.3	X-ray diffraction analysis (XRD)	84
2.8.3.4	Scanning electron microscopy/Energy Dispersive X-Ray analysis (SEM/EDX)	84
2.8.3.5	Thromboelastograph (TEG) studies	85
2.8.3.6	Scanning Electron Microscopy (SEM) to observe cell attachment	85
2.9	Statistical analyses	85
	<b>CHAPTER 3</b>	87
<b>3.1</b>	<b>Introduction</b>	88
<u>3.1.1</u>	<u>Polyhydroxyalkanoates and their applications in drug delivery</u>	88
<b>3.2</b>	<b>Results</b>	92
<u>3.2.1</u>	<u>P(3HB) microsphere preparation</u>	92
<u>3.2.2</u>	<u>P(3HB) microsphere characterization</u>	92
3.2.2.1	Particle size	92
3.2.2.1.1	<i>The effect of polymer concentration on the particle size</i>	93
3.2.2.1.2	<i>The effect of the surfactant concentration on the microsphere size</i>	94
3.2.2.1.3	<i>The effect of stirring on the microsphere size</i>	95
3.2.2.1.4	<i>The effect of stirring on the microsphere surface area</i>	96
3.2.2.2	Surface morphology	97
3.2.2.3	Surface hydrophobicity	98
3.2.2.4	Zeta-potential analysis	99
3.2.2.4.1	<i>pH/Zeta-potential</i>	100
3.2.2.4.2	<i>Effect of zeta-potential on protein adsorption</i>	101
3.2.2.5	Internal microstructure of the microspheres	102
3.2.2.5.1	<i>Porosity</i>	102
<u>3.2.3</u>	<u>Determination of the encapsulation efficiency of P(3HB) microspheres</u>	103
<u>3.2.4</u>	<u>Determination of drug-polymer interaction</u>	104

---

3.2.4.1	Elemental composition of the surface of the microspheres	104
3.2.4.2	Fourier Transform Infrared studies (FTIR)	105
3.2.4.3	Thermal analysis of the microspheres	106
<u>3.2.5</u>	<u>In vitro degradation of the P(3HB) microspheres</u>	108
3.2.5.1	Effect of water adsorption on the thermal properties of the gentamicin loaded and unloaded P(3HB) microspheres as a function of time	109
<u>3.2.6</u>	<u>In vitro release studies</u>	112
<b>3.3</b>	<b>Discussions</b>	113
<u>3.3.1</u>	<u>The effect of polymer concentration on the microsphere size</u>	113
<u>3.3.2</u>	<u>The effect of the surfactant concentration on the microsphere size</u>	114
<u>3.3.3</u>	<u>The effect of stirring rate on the microsphere size</u>	115
<b>3.4</b>	<b>Microsphere characteristics</b>	116
<u>3.4.1</u>	<u>Surface morphology</u>	119
<u>3.4.2</u>	<u>Surface Hydrophobicity</u>	117
<u>3.4.3</u>	<u>Zeta-potential analysis</u>	118
3.4.3.1	Effect of zeta-potential on protein adsorption	118
<u>3.4.4</u>	<u>Porosity</u>	119
<u>3.4.5</u>	<u>Determination of the encapsulation efficiency of P(3HB) microspheres</u>	120
<u>3.4.6</u>	<u>Determination of drug-polymer interaction</u>	121
3.4.6.1	Elemental composition of the surface of the microspheres	121
3.4.6.2	Fourier Transform Infrared studies (FTIR)	121
3.4.6.3	Thermal analysis of the microspheres (DSC)	122
<u>3.4.7</u>	<u>In vitro degradation studies</u>	123
3.4.7.1	Effect of water adsorption on the thermal properties of the gentamicin loaded and unloaded P(3HB) microspheres as a function of time	124
<u>3.4.8</u>	<u>In vitro release studies</u>	126
<b>3.5</b>	<b>Conclusions</b>	128

---

<b>CHAPTER 4</b>	129
<b>4.1 Introduction</b>	130
<b>4.2 Results</b>	132
<u>4.2.1 P(3HB) microsphere-coated 45S5Bioglass<sup>®</sup> composite scaffolds</u>	132
<u>4.2.2 Mechanical properties</u>	136
4.2.2.1 Porosity	137
<u>4.2.3 <i>In vitro</i> bioactivity study of P(3HB) microsphere-coated 45S5Bioglass<sup>®</sup> scaffolds</u>	138
<u>4.2.4 X-Ray diffraction (XRD) analysis of the P(3HB) microsphere-coated 45S5Bioglass<sup>®</sup> scaffolds after immersion in SBF</u>	140
<u>4.2.5 Surface topography studies</u>	142
<u>4.2.6 <i>In vitro</i> drug release from P(3HB) microsphere-coated 45S5Bioglass<sup>®</sup> composite scaffolds and uncoated 45S5Bioglass<sup>®</sup> scaffolds</u>	144
<u>4.2.7 <i>In vitro</i> degradation studies</u>	146
<u>4.2.8 Protein adsorption test</u>	148
4.2.8.1 Protein profile of the adsorbed proteins observed using SDS-PAGE	149
<b>4.3 Discussions</b>	151
<u>4.3.1 45S5Bioglass<sup>®</sup> Scaffold development</u>	152
<u>4.3.2 Scaffold characterization and mechanical properties</u>	153
<u>4.3.3 <i>In vitro</i> bioactivity study of P(3HB) microsphere-coated 45S5Bioglass<sup>®</sup> scaffolds</u>	153
<u>4.3.4 Surface topography studies</u>	154
<u>4.3.5 <i>In vitro</i> drug release from P(3HB) microsphere-coated 45S5Bioglass<sup>®</sup> composite scaffolds and uncoated 45S5Bioglass<sup>®</sup> scaffolds</u>	155
<u>4.3.6 Protein adsorption test</u>	156
<u>4.3.7 <i>In vitro</i> degradation studies</u>	159
<b>4.0 Conclusions</b>	160

---

<b>CHAPTER 5</b>	161
<b>5.1 Introduction</b>	162
<b>5.2 Results</b>	166
<u>5.2.1 Nanoscale bioactive glass and P(3HB)/nBG composite microsphere characterization</u>	166
5.2.1.1 Fourier Transform Infrared studies (FTIR)	169
5.2.1.2 Scanning Electron Micrographs/Energy Dispersive X-Ray (SEM/EDX) of microsphere films	169
5.2.1.3 Thermal properties	171
5.2.1.4 Surface roughness (White light interferometry)	172
5.2.1.5 Surface wettability	173
5.2.1.6 Protein adsorption test	174
5.2.1.7 Cell attachment tests	175
5.2.1.8 Haemostatic activity of n-BG	177
<u>5.2.2 P(3HB)/n-BG composite microsphere films immersed in SBF</u>	178
5.2.2.1 Surface morphology	178
5.2.2.2 Fourier Transform Infrared studies (FTIR)	179
5.2.2.3 Scanning Electron Micrographs/Energy Dispersive X-Ray (SEM/EDX) and X-Ray diffraction (XRD) analysis of P(3HB)/nBG composite microsphere films	180
5.2.2.4 Thermal properties of P(3HB)/nBG composite microsphere films	183
5.2.2.5 Surface roughness (White light interferometry)	185
5.2.2.6 Surface wettability	187
5.2.2.7 Protein adsorption test	188
5.2.2.8 Cell attachment tests	189
<b>5.3 Discussions</b>	191
<u>5.3.1 Nanoscale bioactive glass and P(3HB)/nBG composite microsphere characterization</u>	191
5.3.1.1 <u>Surface morphology of the n-BG particles and the P(3HB)/n-BG composite microspheres</u>	191
5.3.1.2 FTIR analysis	192

---

5.3.1.3	Scanning electron microscopy /Energy dispersive X-Ray (SEM/EDX)	193
5.3.1.4	Effect of n-BG particles on the thermal properties of the P(3HB) microsphere films	193
5.3.1.5	Surface morphology and roughness of the P(3HB) and P(3HB)/n-BG composite microsphere films	194
5.3.1.6	Factors affecting the biocompatibility of the microsphere films	195
5.3.1.7	Haemostatic activity	196
<u>5.3.2</u>	<u>P(3HB)/n-BG composite microsphere films immersed in SBF</u>	197
5.3.2.1	Surface morphology of the P(3HB)/n-BG composite microsphere films	198
5.3.2.2	FTIR analysis	198
5.3.2.3	SEM/EDX and XRD analysis	199
5.3.2.4	Thermal properties	200
5.3.2.5	Surface roughness	201
5.3.2.6	Surface wettability	201
5.3.2.7	Protein adsorption	202
5.3.2.8	Cell adhesion	203
<b>5.4</b>	<b>Conclusions</b>	206
	<b>CHAPTER 6</b>	208
<b>6.1</b>	<b>Introduction</b>	209
<b>6.2</b>	<b>Results</b>	212
<u>6.2.1</u>	<u>Tetracycline loaded P(3HB) microsphere films characterizations</u>	212
6.2.1.1	Surface morphology of the P(3HB) microsphere films	212
6.2.1.2	XPS evaluation	215
6.2.1.3	Surface topography studies	217
6.2.1.4	Fourier Transform Infrared studies (FTIR)	219
6.2.1.5	X-Ray diffraction analysis (XRD)	221
6.2.1.6	Thermal analysis	223
<u>6.2.2</u>	<u>In vitro degradation studies of the tetracycline loaded P(3HB) microsphere films</u>	224

---

6.2.2.1	Thermal analysis after <i>in vitro</i> degradation studies of the P(3HB) microsphere films (with and without the drug)	228
<u>6.2.3</u>	<u><i>In vitro</i> drug release studies</u>	232
<u>6.2.4</u>	<u>Factors affecting the biocompatibility of the biodegradable polymers used as scaffolds</u>	234
6.2.4.1	Surface wettability (before protein adsorption)	234
6.2.4.2	Protein adsorption study in DMEM media	235
6.2.4.3	Surface wettability tests (after protein adsorption)	236
6.2.4.4	Cell adhesion tests	237
<b>6.3</b>	<b>Discussions</b>	240
<u>6.3.1</u>	<u>Tetracycline loaded P(3HB) microsphere films characterizations</u>	240
6.3.1.1	Surface morphology	241
6.3.1.2	X-Ray photoelectron spectroscopy (XPS)	241
6.3.1.3	Thermal analysis of the P(3HB) microspheres (with and without the drug)	242
<u>6.3.2</u>	<u><i>In vitro</i> degradation studies of the P(3HB) microsphere films (with and without the drug) in PBS</u>	243
<u>6.3.3</u>	<u>Differential Scanning Calorimetry (DSC) and X-Ray Diffraction (XRD) analysis</u>	244
<u>6.3.4</u>	<u>Factors affecting the <i>in vitro</i> drug release</u>	246
<u>6.3.5</u>	<u>Factors affecting the biocompatibility of the tetracycline loaded microsphere films</u>	248
<b>6.4</b>	<b>Conclusions</b>	251
	<b>CHAPTER 7</b>	252
<b>7.1</b>	<b>Introduction</b>	253
<b>7.2</b>	<b>Results</b>	257
<u>7.2.1</u>	<u>Characterization of Bovine serum album (BSA) encapsulated P(3HB) microspheres</u>	257
7.2.1.1	Production of BSA encapsulated P(3HB) microspheres	257

---

7.2.1.2	Bulk shape and structure of the BSA loaded P(3HB) microspheres	258
7.2.1.3	Microsphere size and its distribution	259
7.2.1.4	Encapsulation efficiency	260
7.2.1.5	<i>In vitro</i> release kinetics of BSA	261
7.2.1.6	<i>In vitro</i> degradation studies	263
7.2.1.6.1	<i>Changes in pH</i>	264
7.2.1.6.2	<i>Examination of surface morphology after in vitro degradation</i>	265
7.2.1.7	Protein profile of the BSA entrapped in the microspheres and released into PBS and contact lens solution observed using SDS-PAGE	266
<u>7.2.2</u>	<u>Lucentis<sup>®</sup> encapsulation studies</u>	267
7.2.2.1	Characterization of P(3HB) microspheres entrapped with Lucentis <sup>®</sup>	267
7.2.2.2	Encapsulation efficiency	268
7.2.2.3	<i>In vitro</i> release kinetics of Lucentis <sup>®</sup>	269
7.2.2.4	Protein profile of Lucentis <sup>®</sup> entrapped in the P(3HB) microspheres and released into PBS and contact lens solution observed using SDS-PAGE	270
<u>7.2.3</u>	<u>RNase A encapsulation studies</u>	271
7.2.3.1	Characterization of P(3HB) microspheres entrapped with RNase A	271
7.2.3.2	Microsphere size and size distribution	271
7.2.3.3	Encapsulation efficiency	272
7.2.3.4	<i>In vitro</i> release kinetics of RNase A	274
7.2.3.5	Stability of RNase A entrapped in the microspheres	274
7.2.3.5.1	<i>Fluorescence studies</i>	278
7.2.3.5.2	Protein profile of the RNase A entrapped microspheres observed using SDS-PAGE	275
7.2.3.6	Enzyme activity of RNase A using methylene blue assay	276
<b>7.3</b>	<b>Discussions</b>	278
<u>7.3.1</u>	<u>Protein loaded P(3HB) microsphere characterizations</u>	278
7.3.1.1	Bulk shape and structure of the protein loaded microspheres	278
7.3.1.2	Particle size analysis	279

---

7.3.1.3	Surface morphology	280
7.3.1.4	Porosity	280
7.3.1.5	Protein encapsulation efficiency	281
<u>7.3.2</u>	<u><i>In vitro</i> release studies</u>	283
7.3.2.1	BSA <i>in vitro</i> release studies	284
7.3.2.2	Lucentis <sup>®</sup> <i>in vitro</i> release studies	284
7.3.2.3	RNase A <i>in vitro</i> release studies	285
<u>7.3.3</u>	<u><i>In vitro</i> microsphere degradation study of P(3HB) microspheres</u>	285
<u>7.3.4</u>	<u>Protein stability tests</u>	286
7.3.4.1	Protein profile of the BSA entrapped in the microspheres and released in to PBS and contact lens solution	287
7.3.4.2	Protein profile of the Lucentis <sup>®</sup> entrapped in the microspheres and released into PBS and contact lens solution	287
7.3.4.3	RNase A stability evaluation	287
7.3.4.3.1	<i>Fluorescence tests</i>	287
7.3.4.3.2	Protein profile of the RNase A entrapped in the microspheres and released into PBS solution	288
7.3.4.3.3	<i>Methylene Blue RNase Enzyme Assay</i>	288
<b>7.4</b>	<b>Conclusions</b>	290
	<b>CHAPTER 8</b>	293
<b>8.1</b>	<b>Conclusions</b>	294
	<b>CHAPTER 9</b>	298
<b>9.1</b>	<b>Future work</b>	299
	<b>REFERENCES</b>	302
	<b>LIST OF PUBLICATIONS</b>	336

# List of Abbreviations

## PHAs

scl-PHA	Polyhydroxyalkanoates
mcl-PHA	Short chain length polyhydroxyalkanoates
lcl-PHA	Medium chain length polyhydroxyalkanoate
P(3HB)	Long chain length polyhydroxyalkanoate
P(3HB-co-3HV)	Poly(3-hydroxybutyrate)
P(4HB)	Poly(3-hydroxybutyrate-co-3-hydroxyvalerate)
P(3HB-co-4HB)	Poly(4-hydroxybutyrate)
P(3HB-co-3HHx)	Poly(3-hydroxybutyrate-co-4-hydroxybutyrate)
P(3HO-co-3HHx)	Poly(3-hydroxybutyrate-co-3-hydroxyhexanoate)
P(3HB-co-3HV-co-3HHx)	Poly(3-hydroxyoctanoate-co-3-hydroxyhexanoate)
P(3HB-co-3HV-co-4HB)	poly(3-hydroxybutyrate-co-3-hydroxyvalerate-co- 3-hydroxyhexanoate)
P(3HB-co-3HO)	Poly(3-hydroxybutyrate-co-3-hydroxyvalerate-co- 4-hydroxybutyrate)
3HB	Poly (3-hydroxybutyrate-co-3-hydroxyoctanoate)
3HV	3-hydroxybutyrate
scl-mcl-PHA	3-hydroxyvalerate
	Short chain length-medium chain length polyhydroxyalkanoate
PEG	Polyethylene glycol
BIP	Bioactive inorganic phase
Vit. E	Vitamin E
m-BG	microscale-Bioglass <sup>®</sup>
n-BG	nanoscale-Bioglass <sup>®</sup>
BG	Bioglass <sup>®</sup>
SBF	Simulated body fluid
SEM	Scanning electron microscope
TEM	Transmission electron microscope
EDX	Energy dispersive X-ray
XRD	X-ray diffraction
DSC	Differential scanning calorimetry
DMA	Dynamic mechanical analysis
LPS	lipopolysacchrides
PBS	phosphate buffer saline
NR assay	Neutral Red Asssay
DMEM	Dulbecco's modified Eagle's medium
FBS	foetal bovine serum
ALP	Alkaline phosphatase
SD	standard deviation
Pa	Pascal
$\mu$	10 <sup>6</sup> (micro)
g	grams

cm	centimetre
mm	millimetre
L	liter
wt%	mol%
$M_w$	vol%
mL	mililiter
ppm	parts per million
rpm	revolutions per minute
mM	milimolar
h	hours
min	minutes
$T_g$	glass transition temperature
$T_m$	melting temperature
$T_c$	crystallization temperature
$T_d$	degradation temperature
TS	tensile strength
E	Young's modulus
%WA	water uptake/water absorption
$\Delta H_f$	heat of fusion
$X_c$	degree of crystallinity
dcw	dry cell weight
RMS	root mean square

# **List of Figures**

## **CHAPTER 1**

- Figure 1 Figure 1: The general structure of polyhydroxyalkanoates  
Figure 2 Schematic representation of the research strategy used for this project.

## **CHAPTER 3**

- Figure 1 Schematic representation of the factors influencing the P(3HB) microsphere characteristics.
- Figure 2 Size distribution analysis of P(3HB) microspheres.
- Figure 3 The % residual PVA content of the P(3HB) microspheres.
- Figure 4 The specific surface area of the P(3HB) microspheres prepared using different conditions.
- Figure 5 Scanning electron micrographs (SEM) of the P(3HB) microspheres.
- Figure 6 Amount of Rose Bengal Dye bound onto the surface of the P(3HB) microspheres.
- Figure 7 The zeta-potential values of the P(3HB) microspheres fabricated using different conditions.
- Figure 8 pH/Zeta potential analysis of P(3HB) microspheres.
- Figure 9 Effect of zeta-potential analysis on protein adsorption.
- Figure 10 Internal microstructure of the microspheres.
- Figure 11 The percentage encapsulation efficiency, percentage of surface associated gentamicin and percentage of gentamicin present in the PVA solution of the gentamicin loaded microspheres.
- Figure 12 XPS spectra of gentamicin loaded P(3HB) microspheres.
- Figure 13 FTIR spectrum of (A) P(3HB) microspheres (B) Gentamicin loaded P(3HB) microspheres. C) The structure of gentamicin.

- Figure 14 The DSC thermograms of the A) crude P(3HB), B) unloaded P(3HB) microspheres and C) gentamicin loaded microspheres.
- Figure 15 *In vitro* degradation study of A) unloaded P(3HB) microspheres and B) the gentamicin loaded P(3HB) microspheres.
- Figure 16 pH changes observed in the SBF solution containing A) P(3HB) microspheres and B) Gentamicin loaded P(3HB) microspheres on day 1, day 15 and day 30.
- Figure 17 A comparison of the thermal properties of the unloaded P(3HB) and gentamicin loaded microspheres measured using DSC at day 1, days 15 and day 30.
- Figure 18 *In vitro* gentamicin release profile from P(3HB) microspheres.

## CHAPTER 4

- Figure 1 Diagrammatic representation of the research methodologies used in this study.
- Figure 2 SEM images of the scaffolds immersed for (A) 2 mins, (B) 5 mins, (C) 10 mins in the sonicated microsphere slurry.
- Figure 3 SEM images of 45S5Bioglass<sup>®</sup> scaffolds coated with gentamicin-loaded microspheres on the surface of the scaffold.
- Figure 4 SEM images of P(3HB) microsphere-coated 45S5Bioglass<sup>®</sup> tablets (A) before and (B) after washing with water (C) SEM image of a microsphere-coated scaffold after being in water for 28 days.
- Figure 5 Stress-strain curves of the 45S5Bioglass<sup>®</sup> porous scaffolds (A) with and (B) without the P(3HB) microsphere coatings.
- Figure 6 The compressive strength values of the uncoated and coated 45S5Bioglass<sup>®</sup> scaffold against the varying % porosity values.
- Figure 7 SEM images of P(3HB) microsphere-coated 45S5Bioglass<sup>®</sup> based glass-ceramic scaffolds immersed in SBF.
- Figure 8 XRD patterns of P(3HB) microspheres only, non-coated 45S5Bioglass<sup>®</sup> scaffold and P(3HB) microsphere-coated 45S5Bioglass<sup>®</sup> composite

scaffolds.

- Figure 9 A comparison of the average surface roughness values RMS values.
- Figure 10 Surface topography studies.
- Figure 11 *In vitro* release studies of gentamicin.
- Figure 12 *In vitro* degradation studies .
- Figure 13 Protein adsorption test.
- Figure 14 Protein profile of the adsorbed proteins observed using SDS-PAGE

## CHAPTER 5

- Figure 1 (A) SEM images of m-BG particles (B) SEM image of n-BG particles, (C) P(3HB)/n-BG composite microspheres.
- Figure 2 An elemental X-Ray mapping of the cross section of the P(3HB)/n-BG composite microspheres.
- Figure 3 FTIR spectra of the microsphere films.
- Figure 4 SEM/EDX micrographs of the microsphere films.
- Figure 5 SEM/EDX micrographs of the P(3HB)/n-BG composite microsphere films.
- Figure 6 DSC thermograms of P(3HB) microsphere films.
- Figure 7 Surface roughness studies of P(3HB) microsphere film surfaces and P(3HB)/n-BG composite microsphere films.
- Figure 8 Surface wettabilities of the P(3HB) microsphere films and P(3HB)/n-BG composite films.
- Figure 9 Total protein adsorption test carried out on the surface of P(3HB) microsphere films and P(3HB)/n-BG composites microsphere films.
- Figure 10 Cell attachment studies performed on microsphere films.
- Figure 11 SEM images of HaCaT cell attachment seen on the surface of microsphere films.

- Figure 12 Thromboelastograph plot depicting the haemostatic activity of n-BG particles.
- Figure 13 SEM images of the P(3HB)/n-BG composite microsphere films before and after immersion in SBF.
- Figure 14 FTIR spectra of the P(3HB)/n-BG composite microsphere films before and after immersion in SBF.
- Figure 15 SEM/EDX micrographs of the P(3HB)/n-BG composite microsphere films after immersion in SBF.
- Figure 16 X-Ray diffractograms of the P(3HB)/n-BG composite microsphere films after immersion in SBF.
- Figure 17 DSC thermograms of the P(3HB)/nBG composite films (before and after immersion in SBF).
- Figure 18 Surface roughness of the P(3HB)/n-BG composite microsphere films after immersion in SBF measured using white light interferometry.
- Figure 19 Surface topography of the P(3HB)/n-BG composite microsphere films after immersion in SBF.
- Figure 20 A comparison of the surface wettabilites of the P(3HB)/n-BG composite films before and after immersion in SBF.
- Figure 21 Total protein adsorption test carried out on the surface of P(3HB)/n-BG composite microsphere films (before and after immersion in SBF).
- Figure 22 Cell viability studies performed on day 3, using Neutral Red assay, on P(3HB)/n-BG composite films.
- Figure 23 SEM images of HaCaT cell attachment seen on the surface of P(3HB)/n-BG composite microsphere films before immersion in SBF and after immersion in SBF.

## **CHAPTER 6**

- Figure 1 Scanning electron micrographs of the surface of the P(3HB) microsphere films and P(3HB) microsphere films loaded with 0.5 wt% of tetracycline.
- Figure 2 Scanning electron micrographs of the surface of the P(3HB) microsphere films with tetracycline loadings of 2 wt% and 4 wt%.

- Figure 3 XPS spectra of P(3HB) microsphere film and tetracycline loaded P(3HB) microsphere films.
- Figure 4 Surface roughness quantified as root mean square of roughness (rms), for the unloaded and loaded microsphere films.
- Figure 5 Surface topography of the P(3HB) microsphere film surfaces (with and without the drug) as determined by white light interferometry.
- Figure 6 FTIR spectrum of the P(3HB) microsphere films (with and without tetracycline).
- Figure 7 X-Ray diffractograms of the P(3HB) microsphere films (with and without the drug).
- Figure 8 A comparison of the %  $X_c$  and  $T_m$  of the crude polymer and the P(3HB) microspheres (with and without the drug).
- Figure 9 A comparison of the  $T_g$  values of the crude polymer and the P(3HB) microspheres (with and without the drug).
- Figure 10 *In vitro* degradation study of the P(3HB) microsphere films (with and without tetracycline) in phosphate buffered saline solution (PBS).
- Figure 11 Changes in the pH of the 0.1 M PBS solution over a period of 30 days in the presence of the tetracycline loaded P(3HB) microsphere films is represented.
- Figure 12 A comparison of the thermal properties of the P(3HB) microsphere films (with and without the drug) measured on day 1, day 15 and day 30 using DSC.
- Figure 13 A comparison of the glass transition properties ( $T_g$ ) of the P(3HB) microsphere films (with and without the drug) measured on day 1, day 15 and day 30.
- Figure 14 A comparison of the DSC thermograms of the P(3HB) microsphere films (with and without the drug) measured at day 1, day 15 and day 30 to identify the possible drug-polymer interaction.
- Figure 15 *In vitro* kinetic profiles of tetracycline release from P(3HB) microsphere films.
- Figure 16 Surface wettabilities of the P(3HB) microsphere films (with and without the drug).

- Figure 17 Total protein adsorption carried out on the surface of the P(3HB) microsphere films (with and without the drug).
- Figure 18 Surface wettabilities of the P(3HB) microsphere films (with and without the drug) after protein adsorption.
- Figure 19 Cell attachment study performed on day 3, using Neutral Red assay, on P(3HB) microsphere films (with and without the drug).
- Figure 20 Scanning electron micrographs (SEM) of HaCaT cell attachment on day 1 and day 3 on the surface of the control (tissue culture plastic) and unloaded P(3HB) microsphere films respectively.
- Figure 21 The HaCaT cell attachment seen on day 1 and day 3 on the P(3HB) microsphere films loaded with 0.5 wt% tetracycline, 2 wt% tetracycline and 4 wt% tetracycline.

## CHAPTER 7

- Figure 1 The optical micrographs of the P(3HB) microsphere formation loaded with 0.75 wt%, 1.5 wt% and 5 wt% of BSA.
- Figure 2 SEM image of BSA loaded P(3HB) microspheres.
- Figure 3 Size distribution analysis of BSA loaded P(3HB) microspheres.
- Figure 4 Encapsulation efficiency, % of surface associated BSA and % of BSA present in the PVA solution for different BSA loadings.
- Figure 5 The 24h burst release of BSA in PBS and contact lens solution.
- Figure 6 *In vitro* cumulative release profiles of BSA loaded P(3HB) microspheres in PBS and B) contact lens solution.
- Figure 7 *In vitro* degradation studies in A) PBS and B) contact lens solution.
- Figure 8 Changes in the pH of A) PBS and B) Contact lens solution containing P(3HB) microspheres .
- Figure 9 Scanning electron micrographs of BSA-loaded PHA microspheres during *in vitro* degradation in PBS and (B) in contact lens solution.
- Figure 10 SDS-PAGE results of BSA samples taken after different time points.

- Figure 11 SEM images of Lucentis<sup>®</sup> loaded P(3HB) microspheres and Particle size distribution analysis of P(3HB) microspheres loaded with Lucentis<sup>®</sup>.
- Figure 12 The percentage encapsulation efficiency, percentage of surface associated protein and percentage of Lucentis<sup>®</sup> present in the PVA solution of the Lucentis<sup>®</sup> loaded microspheres.
- Figure 13 *In vitro* release profile of Lucentis<sup>®</sup> from P(3HB) microspheres.
- Figure 14 SDS-PAGE results of Lucentis<sup>®</sup> samples released from P(3HB) microspheres after different time points.
- Figure 15 SEM images of the of RNase A loaded P(3HB) microspheres at high magnification and Particle size distribution analysis of P(3HB) microspheres.
- Figure 16 The percentage encapsulation efficiency, percentage of surface associated protein and percentage of protein present in the PVA solution of the RNase A loaded microspheres.
- Figure 17 *In vitro* release profile of RNase A from P(3HB) microspheres.
- Figure 18 Fluorescence spectra of chloroform-treated RNase A as compared to the untreated RNase A.
- Figure 19 SDS-PAGE results of RNase A samples.
- Figure 20 A decline in the intercalation of methylene blue by RNase A was observed over a period of 30 days.
- Figure 21 % enzyme activity of the control and release samples expressed over a period of 30 days, ( $n=3$ ; error= $\pm$ s.d).

## List of Tables

### CHAPTER 1

<u>Table 1</u>	The thermal properties of the copolymer P(3HB-co-3HV) with varying 3HB and 3HV contents.
<u>Table 2</u>	Mechanical properties of P(4HB) films with varying porosity processed using different conditions (melt-processing/salt leaching conditions).
<u>Table 3</u>	The thermal properties of P(3HB-co-4HB) with varying 3HB and 4HB compositions.
<u>Table 4</u>	Anti-cancer drugs encapsulated in P(3HB) microspheres using the solvent evaporation technique. *CCNU is 1-(2 chloroethyl)-3-cyclohexylnitrosourea.
<u>Table 5</u>	Summary of common PHAs used for various biomedical applications
<u>Table 6</u>	The advantages and disadvantages of bioceramics highlighted for various applications in tissue engineering.
<u>Table 7</u>	Summary of the factors influencing <i>in vitro</i> degradation of PHAs
<u>Table 8</u>	Summary of the <i>in vivo</i> degradation characteristics of PHAs
<u>Table 9</u>	<i>In vitro</i> cell culture studies carried out on some PHAs using various cell lines.
<u>Table 10</u>	<i>In vivo</i> cell culture studies carried out using different structures of P(3HB) at various sites of implantation.

### CHAPTER 2

<u>Table 1</u>	pH of the reagents used for the <i>in vitro</i> drug release and <i>in vitro</i> degradation studies.
<u>Table 2</u>	The varying processing conditions (amount of surfactant, polymer concentration and stirring rate) used for the synthesis of P(3HB) microspheres.
<u>Table 3</u>	Drugs/Proteins loaded during P(3HB) microsphere production.
<u>Table 4</u>	Summary of the <i>in vitro</i> release studies of the different proteins and drugs.
<u>Table 5</u>	Materials investigated for the biocompatibility studies using the HaCaT keratinocyte cell line.

### CHAPTER 3

<u>Table 1</u>	The thermal properties of the crude polymer, P(3HB) microspheres and gentamicin loaded microspheres measured using DSC.
----------------	---

## **CHAPTER 4**

<u>Table 1</u>	Drug loading in uncoated 45S5Bioglass <sup>®</sup> scaffolds and P(3HB) microsphere coated 45S5Bioglass <sup>®</sup> scaffolds.
----------------	---

## **CHAPTER 5**

<u>Table 1</u>	A comparison of the thermal properties of the P(3HB) microsphere films and P(3HB)/n-BG composite microsphere films.
----------------	---

<u>Table 2</u>	Thermal properties of the P(3HB)/n-BG composite microsphere films before and after immersion in SBF.
----------------	--

## **CHAPTER 6**

<u>Table 1</u>	XPS data for the P(3HB) microspheres loaded with different amounts of tetracycline 0.5 wt%, 2wt% and 4wt%. The relative mass percentages of each compound are presented.
----------------	--

<u>Table 2</u>	The encapsulation efficiency of the P(3HB) microspheres loaded with different drug loadings.
----------------	--

## **CHAPTER 7**

<u>Table 1</u>	The different BSA loadings entrapped within P(3HB) microspheres
----------------	---

# Chapter 1

## Biosynthesis of Polyhydroxyalkanoates and their medical applications

## 1.1 Biodegradable polymers used for biomedical applications

### 1.1.0 Synthetic polymers

Synthetic polymers represent the largest group of biodegradable polymers, which have been used for a number of biomedical applications (Langer *et al.*, 2004). These synthetic polymers are known to exhibit certain positive features such as tailorable degradation rate, which make them suitable for biomedical applications. For example poly(lactic acid) PLA, a linear aliphatic polyester is produced from renewable resources such as corn starch or sugar cane and has attracted a lot of attention for biomedical applications due to its mechanical, thermal and biodegradable properties. PLA exists in two stereoisomeric forms *i.e* D-PLA and L-PLA as well as the racemic polymer, Poly(D,L-Lactic acid) PDLLA. PDLLA, a well known high molecular amorphous polymer, known for its biocompatibility, biodegradability and flexibility, has been considered suitable for various biomedical applications such as orthopaedic applications, stents, staples and sutures. These biodegradable polymers however have a risk of toxicity and immunogenicity due to their acidic by-products. Other properties such as high price lack of tailorability, presence of chemical catalysts and fast degradation rate has challenged their commercialization (Bhatia *et al.*, 2007). Nevertheless researchers like Sodian *et al.*, and Kose *et al.*, have utilised these polymers for tissue engineering applications for nerve, skin, vascular and bone tissue engineering. They have also been used as stents, staples and sutures (Sodian *et al.*, 2000, Kose *et al.*, 2003).

### 1.1.1 Natural polymers

Natural polymers such as polysaccharides and proteins have also been considered for various biomedical applications due to their lack of toxicity and inflammatory reactions when compared to the synthetic polymers. Cells adhered onto natural polymers are known to interact with the surrounding environment *via* integrins and focal adhesion proteins thereby regulating the development of various tissues. Recently collagen was used as an implant in bovine discs (Chan *et al.*, 2008). From the *ex-vivo* studies it was observed that although the disc height was restored due to the collagen implant, however after a few mechanical loadings an extrusion of the implant was observed. Thus collagen

did not possess the intrinsic mechanical properties that were required for implant in bovine discs (Chan *et al.*, 2008). Alginate, a polysaccharide derived from brown seaweed, has been used for applications such as wound healing and drug delivery due to its ability to mould into any desirable shape. Injectable alginate gel can be moulded into any shape by controlling the speed of gelation. However, the applications of these alginate gels are limited only for soft tissue engineering applications as they do not possess the mechanical strength or the osteoconductivity required for bone tissue engineering applications (Sotome *et al.*, 2004). Although these polymers have still been used for a number of biomedical applications such as cardiovascular applications, peripheral nerve regeneration and drug delivery systems, the need for polyhydroxyalkanoates has risen due to their varied mechanical properties, biocompatibility and biodegradability (Dang *et al.*, 2006).

### 1.1.2 Polyhydroxyalkanoates

Polyhydroxyalkanoates (PHAs) are water insoluble biodegradable, biocompatible polyesters that are accumulated in a large number of Gram-positive and Gram-negative bacteria. PHAs are usually produced during the stationary phase of growth under nutrient limiting conditions such as excess carbon and limited nutrients such as oxygen, nitrogen, sulphur, magnesium and phosphorous (Anderson *et al.*, 1990). PHAs accumulate as cytoplasmic inclusions in different species and these vary in the number per cell and their size (Anderson *et al.*, 1990). Polyhydroxyalkanoates (PHAs) represent a complex class of bacterial polyesters consisting of 3-, 4-, 5- and 6-hydroxyalkanoic acids, as represented in Figure 1.

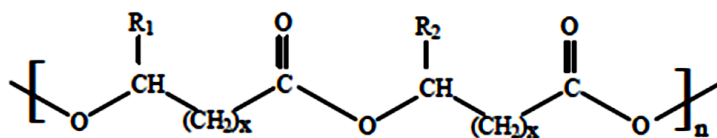


**Figure 1: The general structure of polyhydroxyalkanoates (R1/R2 = H, alkyl groups C<sub>1</sub>-C<sub>13</sub>, x = 1-4 and n = 100-30000).**

Polyhydroxyalkanoates are linear polyesters of 3-,4-,5-,6-hydroxyalkanoic acids. The hydroxyl group of each monomer is bonded to the carboxyl group of another monomer using an ester linkage. Often the variations in the length of the pendant groups extending from the polymer backbones or the distance between the ester linkages in the polymer backbones are known to cause the changes in the chemical structure of the PHAs. Due to the variations in the chemical structure, the physical properties (such as mechanical and thermal) of the polymers are affected (Valappil *et al.*, 2007).

#### 1.1.2.1 Types of PHAs

PHAs are classified as short-chain length (scl) and medium chain length (mcl) PHAs depending on the number of carbon atoms in the monomeric unit. They are also classified as homopolymers and heteropolymers depending on whether one or more than one type of hydroxyalkanoate is found as the monomer unit.

##### 1.1.2.1.1 Scl-PHAs

Scl-PHAs such as poly(3-hydroxybutyrate); P(3HB), poly(4-hydroxybutyrate); P(4HB) and P(3HB-co-3HV) have 3-5 carbon atoms in the monomer units. The types of PHAs synthesised are dependent on the microbes and the carbon source used. These carbon sources are classified into structurally related carbon sources, which give rise to monomers structurally similar the carbon source and structurally unrelated carbon source, which are known to generate monomers completely different to the carbon source used (Pouton *et al.*, 1996). Glucose has been found to be the most efficient substrate for the production of the homopolymer P(3HB) using *Alcaligenes eutrophus*, however other substrates such as sucrose, methanol and acetic acid have also been used to produce this homopolymer using the same organism. *Comamonas acidovorans* is also known to accumulate PHAs such as P(4HB) efficiently when fed with related carbon sources such as 1,4-butanediol and  $\gamma$ -butyrolactone (Pouton *et al.*, 1996). When the substrate (carbon source) is changed, organisms such as *Alcaligenes eutrophus* are capable of producing other PHAs. For example when a combination of glucose and propionate are used as carbon sources, poly(3-hydroxybutyrate-co-3-hydroxyvalerate), P(3HB-co-3HV), with varying mol% HV content could be produced. The HV content can be varied depending

on the concentration of propionate. Similarly the mol% of 4HB units in P(3HB-co-4HB) can be varied depending on the concentration of the 4-hydroxybutyric acid added in the growth medium (Saito *et al.*, 1996). PHAs have also been produced using *Bacillus cereus* SPV. *Bacillus cereus* SPV has been known to utilise a wide range of carbon sources including glucose, fructose, sucrose, various fatty acids and gluconate for the production of PHAs. This particular strain of *Bacillus* spp. was also able to synthesize various PHAs with 3-hydroxybutyrate (3HB), 3-hydroxyvalerate (3HV) and 4-hydroxybutyrate (4HB)-like monomer units from structurally unrelated carbon sources such as fructose, sucrose and gluconate (Valappil *et al.*, 2007).

#### 1.1.2.1.2 Mcl-PHAs

Mcl-PHAs such as poly(3-hydroxyhexanoate); P(3HHx) and poly(3-hydroxyoctanoate); P(3HO) have 6-14 carbon atom containing monomer units. *Pseudomonas* sp, can be grown on structurally related carbon sources such as alkenes, alkanes and aldehydes which act as precursor substrates that exhibit structures related to the constituents of the mcl-PHAs. For example, *Pseudomonas oleovorans* when grown in hexane produced a copolymer containing 83 mol% of 3(HHx), 12 mol% of P(3HO) and 4.9 mol% of poly(3-hydroxydecanoate) P(3HD). However, when grown in heptane the same organism was able to produce 97.5 mol% of 3-hydroxyheptanoate, P(3HHp), 2.5 mol% of poly(3-hydroxyvalerate), P(3HV) (Preusting *et al.*, 1990). Structurally unrelated carbon sources such as glucose and gluconate have also been used for the production of mcl-PHAs. For example, *Pseudomonas putida* KT2442 when grown in the presence of glucose, 3-hydroxydecanoate, 3HD was produced predominantly as the major constituent and other minor constituents such as 3HHx, 3HO and 3-hydroxydodecanoate, 3HDD were also incorporated into the polymer (Kim *et al.*, 2007).

#### 1.1.2.2 Microorganisms involved in the production of Polyhydroxyalkanoates (PHAs) and their copolymers

PHA producing bacteria accumulate PHA when their cell growth is inhibited by the limitation of essential nutrients such as nitrogen, carbon, phosphorous, magnesium,

potassium and oxygen and have excess carbon. Therefore, several fermentation strategies have been designed to enhance the production of PHAs based on this knowledge.

#### 1.1.2.2.1 *Scl*-PHA production

Poly(3-hydroxybutyrate) P(3HB), is the most common and simplest member of the group of PHAs, which has been extensively characterised. A number of Gram-positive, Gram-negative, photosynthetic species, lithotrophs and organotrophs have been used for the production of P(3HB). *Bacillus cereus* SPV have been known to accumulate a variety of different PHAs using different carbon sources. For example when grown in Kannan and Rehacek medium containing a structurally unrelated carbon source such as gluconate (20% w/v), a tercopolymer containing 3HB, 3HV and 4HB-like monomer was produced. The dry cell weight (dcw) was 1.943 g/L and a PHA concentration of 0.814 g/L. Similarly when grown in Kannan and Rehacek medium containing fructose or sucrose (20% w/v) as the sole carbon source, a copolymer similar to P(3HB-co-4HB) was produced. The dcw was 1.6 g/L and PHA concentration of 0.640 g/L was produced when sucrose was used as the sole carbon source; a dcw of 1.2 g/L and a PHA concentration of 0.5g/L was produced when fructose was used as a sole carbon source. *Bacillus cereus* SPV have also been grown in a medium containing different n-alkanoates (30mM final concentration) for the introduction of a different monomer. In this study, as expected the even-chain fatty acids such as acetate, hexanoate, decanoate and dodecanoate produced P(3HB). A maximum dcw 0.59g/L and a PHA concentration of 0.44g/L were produced when decanoate was used as the carbon source. However in the presence of odd chain fatty acids such as propionate, heptanoate and nonanoate, P(3HB-co-3HV) was produced. The highest dcw of 0.496 g/L and PHA concentration of 0.234g/L was observed in the presence of nonanoate (Valappil *et al.*, 2006). An increase in the carbon to nitrogen ratio in the growth medium has been found to increase the PHA accumulation in the cells (Wilkinson *et al.*, 1958). Suzuki *et al.*, determined that only a minimum concentration of nitrogen source was required for the production of P(3HB) (Suzuki *et al.*, 1988). For example, Zinn *et al.*, carried out an efficient production of P(3HB) in a two-step fed batch process using *Alcaligenes latus*, a Gram-negative bacteria. In this study the cells were grown to a desired concentration and then transferred in a nutrient-limiting medium

in the second phase. The cell growth and PHA accumulation were dependent on the ratio of the concentration of the carbon source to the limiting nutrient concentration and the dilution rate. In this study a cell concentration of  $111.7 \text{ g/L}^{-1}$  and a P(3HB) productivity of  $4.94 \text{ g/L}^{-1}$  was successfully achieved (Zinn *et al.*, 2005). Although, P(3HB) production has been successfully carried out from Gram-negative bacteria, the presence of lipopolysaccharides (LPS), known to act as endotoxins, that co-purify with the P(3HB) are known to induce a strong immunogenic reaction, thus proving to be a disadvantage. Therefore, efforts are now focussed on the production of P(3HB) from Gram-positive bacteria, which can be used for biomedical applications. P(3HB) was first isolated from the Gram positive genus *Bacillus* by Lemoigne in 1923. Since then several strains of *Bacillus* have been used to produce a range of different PHAs (Valappil *et al.*, 2007). For example, *Bacillus cereus* INT005 has been found to produce P(3HB), P(3HB-co-3HV), poly(3-hydroxybutyrate-co-3-hydroxyhexanoate) P(3HB-co-3HHx) and poly(3-hydroxybutyrate-co-6-hydroxyhexanoate-3-hydroxyhexanoate).P(3HB-co-6HHx-co-3HHx) when grown in a medium containing different carbon sources (Tajima *et al.*, 2003). Similarly, when fed with  $\epsilon$ -caprolactone as the main carbon source *Bacillus cereus* UW85 produced a tercopolymer containing 3-hydroxybutyrate (3HB), 3-hydroxyvalerate (3HV) and 3-hydroxyhexanoate (3HHx) (Labuzek *et al.*, 2001).

Poly(3-hydroxybutyrate-co-4-hydroxybutyrate), P(3HB-co-4HB), copolymer has been produced using a number of different Gram-negative and Gram positive organisms such as *Bacillus cereus* SPV, *Alcaligenes latus*, *Comamonas acidovorans*, and *Cupriavidus* sp. Several carbon sources such as 4-hydroxybutyric acid,  $\gamma$ -butyrolactone, 1,4-butanediol, 1,6-hexanediol and 4-chlorobutyric acids have been used for the production of this copolymer (Caballero *et al.*, 2005). Copolyesters of 3-hydroxybutyrate and 4-hydroxybutyrate, P(3HB-co-4HB) have been synthesised by *Ralstonia metallidurans* in a two step fermentation. When grown under aerobic conditions at  $30^\circ\text{C}$  in a medium containing butyric acid as the sole carbon source and additives such as ammonium sulphate and potassium dihydrogen citrate, for 120 hours, was observed to synthesise copolymers with a wide range of compositions (70 to 100 mol% 4HB) (Doi *et al.*, 1995). Biosynthesis of P(3HB-co-4HB) was also carried out using a *Cupriavidus* sp

(USMAA24), isolated from a soil sample. In this study, a two-step cultivation process was employed which was similar to methods described by other researchers (Sudesh *et al.*, 2000). *Cupriavidus* sp (USMAA24) was initially grown in a nutrient broth medium for 24h and then transferred to a mineral medium containing different concentrations of 1,4-butanediol and  $\gamma$ -butyrolactone. A linear increase in the 4HB composition was observed when the concentration of  $\gamma$ -butyrolactone in the medium was increased. Similarly, with an increase in 1, 4-butanediol concentration in the medium, the 3HB content was found to increase (Chee *et al.*, 2008). Gram-positive strains such as *Bacillus cereus* SPV were also observed to produce P(3HB-co-4HB) when grown in a media containing either glucose or fructose as the sole carbon source. The polymer yield in this study was observed to be 40.3% dry cell weight with a 75 mol% of 3HB and 25 mol% of 4HB when fructose was used as a sole carbon source. Similarly the polymer yield was observed to be 38.4% dry cell weight with a 90 mol% 3HB and 10 mol% 4HB when sucrose was used a sole carbon source (Valappil *et al.*, 2006).

#### 1.1.2.2.2 Mcl-PHA production

Mcl-PHAs synthesised by *Pseudomonas* sp are almost always a copolymer, where 3-hydroxyoctanoate is produced as the main monomer when grown in a medium containing even number of carbon atoms and 3-hydroxynonanoate is produced when grown in a medium containing odd number of carbon atoms (Kim *et al.*, 2007). To date more than 150 units of mcl-PHA monomers have been produced by culturing various *Pseudomonas* sps on different carbon sources. Some microorganisms such as *Pseudomonas putida*, *Pseudomonas oleovorans* and *Pseudomonas fluorescens* have been known to accumulate both aromatic and aliphatic mcl-PHAs from aromatic hydrocarbons. *Pseudomonas putida* CA-3 is known to accumulate a copolymer of mcl-PHAs containing 3-hydroxyhexanoic acid, 3-hydroxyoctanoic acid and 3-hydroxydecanoic acid monomers when grown in a medium containing styrene and phenyl acetic acid (Ward *et al.*, 2005).

### 1.2.2.2.3 Scl-Mcl PHA production

*Pseudomonas* spp can be grown on both structurally related and unrelated carbon sources to produce PHAs. The low substrate specificity of the mcl-PHA synthase, the key enzyme involved in the polymerization of the medium chain length hydroxyl CoA into mcl-PHA is mainly responsible for the diversity of the mcl-PHA monomers (Kim *et al.*, 2007). Scl-Mcl PHAs such as Poly(3-hydroxybutyrate-co-3-hydroxyhexanoate), P(3HB-co-3HHx), have been produced using a two-stage batch fermentation at 30°C. Amongst the range of alkanolic acids used; the highest production of P(3HB-co-3HHx) (33 wt%) was seen in a medium containing lauric acid. The 3-hydroxyhexanoate fraction of the copolymer was increased from 11-20 mol% when the concentration of lauric acid was increased from 5-30 g/L (Doi *et al.*, 1995).

### 1.1.2.3 Properties of Scl-PHAs

Scl-PHAs such as P(3HB), P(3HB-co-3HV) and P(4HB) have been fully characterised for various biomedical applications (Williams *et al.*, 1999; Misra *et al.*, 2006, Chen *et al.*, 2005). The physical and mechanical properties of the polymers described below highlight the importance of these properties for use in biomedical applications.

#### 1.1.2.3.1 Poly (3-hydroxybutyrate) P(3HB)

P(3HB) is a stereo-regular, isotactic polyester which has been extracted from bacteria with a high degree of purity. In addition to its biocompatible and biodegradable properties, P(3HB) is also known to exhibit piezoelectric properties which can stimulate bone growth and healing (Misra *et al.*, 2006, Knowles *et al.*, 1991). The relatively high crystallinity and rigidity of P(3HB) is due to its short methyl side chain. P(3HB) is a semi-crystalline thermoplastic with a degree of crystallinity ranging from 60-80 %. It has a regular structure due to its biological origin. It also has an ortho-rhombic structure with a right-handed helix, a fibre repeat of 5.95 Å and two parallel chain molecules that pass through the sub-cell. The crystallization of the polymer occurs as soon it is extracted from the cells using non-polar solvents therefore it is amorphous in nature in its native state. Depending on the crystallization rate and the molecular weight of P(3HB), the polymer chains form 'spherulites' when crystallised from the melt (Kumagai *et al.*,

1992a). P(3HB) also undergoes crystallization upon storage at room temperature (Kumagai *et al.*, 1992a). P(3HB) is known to exhibit a melting temperature ( $T_m$ ) of 160 to 177°C and a glass transition temperature ( $T_g$ ) of -4 to 15°C. However, the thermal properties of P(3HB) is known to vary from each sample largely due to the extraction techniques used and the variations in the molecular weight and polydispersity index of the extracted polymers (Misra *et al.*, 2006). P(3HB) has mechanical properties which are comparable to those of degradable polyesters such as polylactides. The Young's modulus exhibited by P(3HB) is 400 MPa and compressive elastic modulus of 317 MPa (Misra *et al.*, 2006). Although P(3HB) has a relatively high brittleness, the mechanical properties can be improved by blending with other degradable polymers or inorganic materials. For example P(3HB)/10 vol% hydroxyapatite exhibited a higher tensile Young's modulus of 500 MPa and compressive elastic modulus of 419 MPa when compared to P(3HB) alone (Wang *et al.*, 2005a).

#### 1.1.2.3.2 Poly(3-hydroxybutyrate-co-3-hydroxyvalerate); P(3HB-co-3HV)

P(3HB-co-3HV) is a copolymer of P(3HB) with a possible variability in the mol% of 3-hydroxyvalerate (3HV) units. Copolymers such as P(3HB-co-3HV) have been found to be less crystalline than P(3HB). The degree of crystallinity can be controlled by increasing/decreasing the HV content. Often, the previous thermal history of the polymer and the conditions used to fabricate the polymer affect the crystallinity. When higher than 40 mol% of 3HV is used, the 3HB units are known to crystallise within the P(3HV) lattice. This ability of 3HB and 3HV units to co-crystallize has been termed as 'isodimorphism' (Bluhm *et al.*, 1986; Scandola *et al.*, 1992, Pouton *et al.*, 1996). The increasing HV content is also known to effect thermal properties of P(3HB-co-3HV). The melting points of the copolymers vary depending on the HV and HB content as shown in Table 1. Similarly, the addition of HV increases the flexibility and reduces the mechanical strength of the polymer. This makes the polymer more processable than P(3HB) (Galego *et al.*, 2000). The increase in the 3HV content is also known to reduce the water contact angle of the P(3HB-co-3HV) films, thereby increasing the hydrophilicity of the films (Misra *et al.*, 2006).

**Table 1:- The thermal properties of the copolymer P(3HB-co-3HV) with varying 3HB and 3HV contents (Scandola *et al.*, 1992).**

<b>3HB mol%</b>	<b>3HV mol%</b>	<b>T<sub>m</sub> °C</b>	<b>ΔH<sub>f</sub> J/g</b>
100	0	176	95
92	8	170	70
81	19	117	62
66	34	96	48
59	41	83	48
45	55	83	57
29	71	86	71
18	82	104	83
5	95	106	87

#### 1.1.2.3.3 Poly-4-hydroxybutyrate (P(4HB))

A single P(4HB) crystal has an orthorhombic structure and is semi-crystalline in nature. Each of these crystals has stacks of lamellae that are both transparent and opaque in nature. The P(4HB) molecular chains have been folded within the lamella in a highly folded and twisted condition (Martin *et al.*, 2003). The thermal properties of P(4HB) are characterised as T<sub>g</sub> of -50°C, the crystallization temperature (T<sub>c</sub>) of 15 °C, T<sub>m</sub> of 54 °C and the enthalpy of fusion ΔH<sub>f</sub> as 11.0 cal/g. An increase in the ΔH<sub>f</sub> value indicates the higher crystallinity of a polymer. Due to its high melt viscosity, 4HB remains fairly stable at temperatures of 200°C and there is an insignificant reduction in the molecular weight (Martin *et al.*, 2003). The mechanical properties of P(4HB) films with varying porosity processed using different conditions (melt-processing/salt leaching conditions) is represented in Table 2 (Martin *et al.*, 2003). A decrease in the elastic modulus and increase in the tensile strength and elongation at break were observed at lower porosity when compared to the films with higher porosity. It is a strong thermoplastic pliable polymer with mechanical properties comparable to other high molecular weight polymers such as polyethylene. It is incredibly flexible with an elongation to break at around 1000% (Doi *et al.*, 1990; Martin *et al.*, 2003).

**Table 2: - Mechanical properties of P(4HB) films with varying porosity processed using different conditions (melt-processing/salt leaching conditions) (Martin *et al.*, 2003).**

PHA	Elastic modulus (MPa)	Tensile strength (MPa)	Elongation at Break (%)
4HB crude polymer	230	36	1140
Dense film	64.8	51.7	1000
4HB (50%) porous	14.9	6.2	164
4HB (80%) porous	1.8	1.2	100

#### 1.1.2.3.4 Poly(3-hydroxybutyrate-co-Poly-4-hydroxybutyrate) P(3HB-co-4HB)

The crystallinity of the copolymer P(3HB-co-4HB) is known to decrease with the increase in the amount of 4HB units in the copolymer. During the synthesis of the copolymer P(3HB-co-4HB), the bulky 4HB units do not get incorporated into the 3HB crystal lattice. Therefore, the copolymer with 0-29 mol% 4HB fraction exhibits only one 3HB crystal lattice indicating that the 4HB content does not get incorporated into the crystal lattice (Saito *et al.*, 1996; Chee *et al.*, 2008). However, with the increase in the 4HB fraction from 85-100 mol%, 4HB units get incorporated within the P(3HB) crystal lattice. Thus with the increase the 4HB fraction a decrease in the  $T_m$  of the copolymer was observed which indicated a reduction in the crystallinity. With the increase in the 4HB content (0-100 mol%) of the copolymer, P(3HB-co-4HB), synthesised from *A. eutrophus*, the  $T_g$  of the copolymer showed a significant reduction from 4 to  $-50^\circ\text{C}$  as shown in Table 3 (Nakamura *et al.*, 1992). The tensile strength of the copolymer also decreased from 43MPa to 26MPa in the presence of 16 mol% 4HB content (Martin *et al.*, 2003).

**Table 3: - The thermal properties of P(3HB-co-4HB) with varying 3HB and 4HB compositions (Nakamura *et al.*, 1992).**

3HB mol%	4HB mol%	T <sub>m</sub> °C	ΔH <sub>f</sub> J/g	T <sub>g</sub> °C
100	0	177	20.8	4
94	6	162	13.5	-1
90	10	159	13.0	-3
72	28	-	-	-15
15	85	48	8.6	-41
10	90	50	10.2	-44
6	94	51	11.0	-46
0	100	54	11.0	-50

#### 1.1.2.4 Properties of Mcl-PHA and Scl-Mcl PHAs

Mcl-PHAs such as P(3HO) and Scl-Mcl PHAs such as P(3HB-co-3HHx) have been used for various biomedical applications (Sanchez *et al.*, 2003). The physical and mechanical properties of the polymers described below highlight the importance of these properties for use in biomedical applications.

##### 1.1.2.4.1 P(3HO)

P(3HO) is less crystalline than the scl polymers and this difference is due to the presence of irregular pendant side chain group/alkyl groups which is responsible for the formation of a crystalline array as opposed to the formation of a closely packed 3-dimensional structure. The isotactic and syndiotactic structure sequences/configuration of these polymers are the determining factors in the formation of a crystallite. Gagnon *et al.*, observed a 30% crystallinity in P(3HO) from <sup>13</sup>C NMR results. For this study, the authors' proposed that the lower crystallinity was due to a two phase morphology of P(3HO) such as the amorphous and crystalline phase (Gagnon *et al.*, 1992). Mcl-PHAs are highly elastomeric in nature due to their low T<sub>m</sub> (42 to 61 °C) and low glass transition temperature (with a range between -25 to 62 °C) (Steinbuechel *et al.*, 2003). At temperatures higher than its T<sub>m</sub>, the polymer appears sticky and amorphous. P(3HO) is known to exhibit a T<sub>g</sub> of -35 °C which is associated to the glass-rubber transition and a T<sub>m</sub> of 60 °C. A low T<sub>g</sub> and T<sub>m</sub> value for P(3HO) was observed due its lower crystallinity of the polymer when compared to the crystallinity of P(3HB) (Dufresne *et al.*, 2000).

The crystalline parts of the mcl-PHAs are known to act as physical crosslinks due to which their mechanical properties are very different from those of scl-PHAs and its copolymers. In a study conducted by Marchessault *et al.*, the stress-strain curve for P(3HO) exhibited no yield stress which was typical to that observed for elastomers. Similarly a Young's modulus of 17MPa and an elongation to break of 250-350% was observed (Marchessault *et al.*,1990).

#### 1.1.2.4.2 P(3HB-co-3HHx)

In the case of the mcl copolymers there is no crystallinity seen due to the presence of functional groups, which prevent the regular arrangement of the polymer chain. Some mcl copolymers do not crystallise at all due to which no  $T_m$  value is observed. For example P(3HB-co-3HHx) is semi-crystalline in nature with crystallinity similar to that of P(3HB). However, the crystallinity is contributed by the 3HB units and not by 3HHx (Van der Walle *et al.*, 2001). An increase in the average length of the pendant group in the polymer has a significant effect on the thermal properties of the polymer, such as a decrease in the  $T_g$  when the mobility of the polymer chains is increased and the degree of crystallinity is reduced (Van der Walle *et al.*, 2001). For example, when *Pseudomonas oleovorans* was grown in a medium containing hexanoate, the  $T_g$  of the P(3HB-co-3HHx) was  $-25^\circ\text{C}$  when compared to the  $T_g$  of the polymer grown in decanoate which was  $-40^\circ\text{C}$  (Gross *et al.*,1989). The introduction of a comonomer into the P(3HB-co-3HHx) backbone is also known to increase the flexibility (elongation to break) and toughness of the polymer thereby decreasing the Young's modulus. For example, P(3HB-co-3HHx) containing 2.5 mol% of 3HHx exhibited a tensile strength of 27.5MPa when compared to 8.8MPa exhibited by P(3HB-co-3HHx) when the 3HHx content was increased to 9.5 mol% (Asrar *et al.*, 2002).

## 1.2 Bioactive ceramics

Ceramics have been classified as either bioinert or bioactive depending on the type of interaction with the host tissues (Marti *et al.*, 2000). Bioactive glass ceramics or silicates/phosphate glasses have been widely used in medicine and dentistry (Misra *et al.*, 2006). Bioactive glass is also known for its excellent properties such as high osteoconductivity (Chen *et al.*, 2006). When immersed in simulated body fluid (SBF) they form a microcrystalline hydroxyapatite (HA). Dissolution of the Bioactive glass products is also known to initiate angiogenesis (Chen *et al.*, 2006).

### 1.2.1 45S5Bioglass<sup>®</sup>

This is one of the well studied bioceramic in the field of hard tissue engineering. A high degree of bioactivity is the most significant property of 45S5Bioglass<sup>®</sup> which facilitates the attachment of living bone tissue, leading to successful applications *in vivo* (Hench *et al.*, 1998a). Researchers like Hench *et al.*, have reported that upon immersion of 45S5Bioglass<sup>®</sup> in body fluids the dissolution of 45S5Bioglass<sup>®</sup> takes place forming a crystalline silica-hydrated gel layer ( $\text{Na}_2\text{Ca}_2\text{Si}_3\text{O}_9$ ). Following this, an amorphous calcium phosphate layer from the hydrated silica gel layer is formed. The formation of a highly crystalline  $\text{Na}_2\text{Ca}_2\text{Si}_3\text{O}_9$  layer is often dependent on the sintering conditions of the 45S5Bioglass<sup>®</sup> which controls the crystallinity of the  $\text{Na}_2\text{Ca}_2\text{Si}_3\text{O}_9$  layer (Chen *et al.*, 2006). Finally, on prolonged immersion of the 45S5Bioglass<sup>®</sup> scaffold in a simulated body fluid (SBF), the transformation from a crystalline silica-gel layer ( $\text{Na}_2\text{Ca}_2\text{Si}_3\text{O}_9$ ) to an amorphous Ca-P layer takes place. Due to this transformation, the degradability of the 45S5Bioglass<sup>®</sup> scaffold occurs at a much faster rate when compared to tricalcium phosphate or wollastonite (Chen *et al.*, 2006). Moreover, studies have shown that upon dissolution of 45S5Bioglass<sup>®</sup> the released ions can activate the complex gene transduction pathways in cells, thereby enhancing cell differentiation and osteogenesis (Xynos *et al.*, 2001). Microarray analysis of osteoblast gene expression has shown that genes with known roles in processes relevant to osteoblast metabolism and bone homeostasis can be induced by the ionic products of bioactive glass dissolution treatment and integrin, which promotes cell-cell and cell-matrix attachment (Xynos *et al.*, 2001).

### 1.2.2 Hydroxyapatite (HA)

Hydroxyapatite is a principal constituent of bone. Hydroxyapatite is considered as a suitable bioactive ceramic due to its thermodynamic stability and its ability to form strong chemical bonds with the surrounding bone. HA are known to show good bioactive properties, however the resorbability of HA is reduced in comparison to tricalcium phosphate. For example, HA is known to remain integrated into the regenerated bone tissue even after implantation whereas tricalcium phosphate is completely resorbed after regeneration of the new bone tissue (Navarro *et al.*, 2008). Apart from its ability to support bone in growth and osteointegration, hydroxyapatite has also been used for dental and maxillofacial applications (Misra *et al.*, 2006). Although hydroxyapatite does not have the mechanical strength for long term load bearing applications, it has led to an increase in the elastic modulus of composites with PHAs. Hydroxyapatite has also been used as coatings on metallic implants (Misra *et al.*, 2006).

### **1.3 Composite materials**

Bioactive ceramics are known to have poor mechanical properties and non-uniform pore size distributions due to which they pose a problem for applications in hard tissue engineering. Similarly polymers are also known to lack the mechanical strength needed for hard tissue engineering as they are too flexible and weak (Misra *et al.*, 2006, Bonfield *et al.*, 1981). Thus composites made using a combination of biodegradable polymers and bioactive ceramics can provide the inherent strength necessary for the inorganic part of the bone. In the presence of the bioactive ceramic, a tenacious bond with the surrounding tissue *via* the hydroxyapatite (HA) formation can be achieved. Also, the biocompatibility of the scaffolds can also be enhanced due to the changes in the surface characteristics in the presence of the ceramic, which will be favourable for protein adhesion as well as cell attachment (Misra *et al.*, 2006). A combination of P(3HB), P(3HB-co-3HV) and P(3HB-co-3HHx) and ceramics used as fillers and coatings have been extensively studied. The different composite systems developed over the recent years are described below.

### 1.3.1 P(3HB)/bioactive ceramics composites

Hydroxyapatite (HA) is the most extensively used bioactive ceramic that is used in combination with polymers to form composites. Apart from imparting a positive effect on the mechanical properties of the composite systems, HA is also known to induce a high rate of bioactivity *i.e.* the formation of additional hydroxyapatite when immersed in physiological fluids. Bone apposition was reported to occur within one month of implantation in an *in vivo* study at the P(3HB)/hydroxyapatite interface, this was followed by the formation of bone after 6 months (Lunkinska *et al.*, 1997). Therefore, these studies proved that the addition of HA had a positive effect on the composite systems.

Highly porous 45S5Bioglass<sup>®</sup> scaffolds were coated with a biodegradable polymer, P(3HB) and the *in vitro* bioactivity test was evaluated by soaking in a simulated body fluid (SBF). Compression strength tests were performed before and after immersion in SBF exhibited higher values than that of the uncoated samples. An increase in the compression strength was observed due to the polymer coating which filled the microcracks and struts thus having an effect on the mechanical properties of the scaffold. The scaffolds coated with the polymer also proved to be highly bioactive, as after a few days of immersion in SBF a hydroxyapatite-like layer was formed on the scaffold's surface (Bretcanu *et al.*, 2007). P(3HB)/45S5Bioglass<sup>®</sup> composite films were also fabricated in the form of solvent cast films to study the effect of 45S5Bioglass<sup>®</sup> addition on the mechanical properties of the P(3HB)/45S5Bioglass<sup>®</sup> composite films. The presence of 45S5Bioglass<sup>®</sup> led to a reduction in the crystallinity of the polymer along with increasing the hardness of the P(3HB)/45S5Bioglass<sup>®</sup> composite films. However a decrease in the Young's modulus of the P(3HB)/45S5Bioglass<sup>®</sup> composite films from 1.1 GPa to 0.84 GPa were observed with the increase in the 45S5Bioglass<sup>®</sup> addition. For example, at 20 wt% 45S5Bioglass<sup>®</sup> concentration the interfacial strength between the polymer and the 45S5Bioglass<sup>®</sup> particles reduced due to which the Young's modulus was reduced (Misra *et al.*, 2007).

### 1.3.2 P(3HB-co-3HV)/bioactive ceramics composites

P(3HB-co-3HV) has been widely used in combination with ceramics such as HA, tricalcium phosphate (TCP) and wollastonite (Chen *et al.*, 2002). The addition of HA to P(3HB-co-3HV) has been known to have an influence on the mechanical properties of the composites when compared to ceramics such as TCP. In the presence of HA, the micro-hardness, Young's modulus and the dynamic modulus of the composite systems increased (Li *et al.*, 2004). Researchers like Galego *et al.*, observed that at 40wt% of HA, a sharp decline in the elastic modulus was observed. At a higher concentration of HA, the interfacial strength between the HA particles and the polymer was found to decrease due to this the propagation of cracks can occur under mechanical stress (Boeree *et al.*, 1993).

### 1.3.3 P(3HB-co-3HHx)/bioactive ceramics composites

Scl-Mcl PHAs are known for their high flexibility and low stiffness therefore they are more suitable for soft tissue regeneration applications such as heart valves, nerves and skin. However they lack the mechanical strength needed for hard tissue engineering and their inability to form a strong interfacial bonding with the surrounding bone tissue by means of a biologically active layer on the implant surface. Due to these limitations research is now carried out using a combination of bioactive and biodegradable composite materials. For example in a study conducted by Xi *et al.*, composite of P(3HB-co-3HHx) and hydroxyapatite (HA) were fabricated using a phase separation and subsequent sublimation technique. The composite scaffolds obtained by this technique had a porosity of more than 88% and the compressive modulus and the compressive stress were significantly increased. A good adhesion between the P(3HB-co-3HHx) matrix and HA was observed, where most of the HA were attached onto the surfaces of the solid walls of the pores of the matrix (Xi *et al.*, 2008). However different techniques used to fabricate P(3HB-co-3HHx)/bioactive ceramics have been observed to have an influence on the mechanical properties of the composite systems. For example in a study conducted by Wang *et al.*, a decrease in the compressive elastic modulus from 1.73 GPa to 0.068 GPa was observed when hydroxyapatite particles (HA) were blended into the P(3HB-co-3HHx) scaffolds using a salt leaching technique (Wang *et al.*, 2005).

## **1.4 Biomedical Applications of PHAs, inorganic bioactive materials and composite bioactive materials**

### 1.4.1 Drug delivery applications of biodegradable polymers, inorganic bioactive materials and composite bioactive materials

Drug delivery systems used for controlled drug delivery is gradually replacing the conventional methods of drug administration. The common problems encountered while administering conventional dosage forms is the inability to deliver the drug at a concentration that can trigger a pharmacological response (Pouton *et al.*, 1996). Therefore, the dosage frequency has to be increased thereby increasing the risks of side-effects. In a controlled release study, the slow drug release rate reduces the fluctuations seen in the plasma drug levels, therefore a lower incidence of toxicity is observed. The understanding of both the physical and biocompatible properties of the polymer and the drug is paramount for the success of drug delivery (Pouton *et al.*, 1996). Furthermore, the biodegradable polymer properties and structure can be designed according to the environment of the release. Composites of biodegradable polymers and ceramics such as Bioactive glass and hydroxyapatite have also been used for drug delivery for treating bone diseases such as osteomyelitis while acting as a scaffold for hard tissue engineering.

### 1.4.2 Types of drug delivery structures

The type of drug delivery structure and its influence on the drug release is an important aspect for therapeutic applications. For example the mechanism and extent of degradation, drug distribution or entrapment of drugs, the mechanism of drug release and its kinetics can be influenced by the type of drug delivery structures. For example in a study conducted by Korsatko *et al.*, the *in vitro* and *in vivo* release of the drug 7-hydroxytheophylline (HET) compressed in P(3HB) tablets implanted subcutaneously into the neck folds of female mice was investigated. From the results the authors' observed a difference in the *in vitro* release which was dependent on the drug loading. A higher drug release was observed within a period of 24 hours with an increased drug loading of 60-80%. The compaction pressures used to make the tablets did not influence the HET release (Korsatko *et al.*, 1984). However, in another study conducted by Gould

*et al.*, a much slower release of the drug was observed when P(3HB-co-3HV) compressed tablets were used when compared to the P(3HB) compressed tablets. The differences in the drug release between the two polymers were largely attributed to the matrix porosity, structure and the copolymer composition (Gould *et al.*, 1987). P(3HB) microspheres have been used to study the release of several anti-cancer drugs (Juni *et al.*, 1987). The authors' observed that the release of these anti-cancer drugs occurred in a slow and sustained manner. For example 13% of the drug aclarubicin hydrochloride released only 10% of the drug after a period of 5 days. Increased release rates of the drug sulphamethizole was observed when irregularly shaped P(3HB) microspheres were used (Juni *et al.*, 1987). *In vitro* release of the crude extract mitragynine from P(3HB-co-4HB) solvent cast films were investigated by Chee *et al.*, 2008. From the results the authors' observed a constant release rate which was attributed to the polymer degradation rate. The polymer degradation rate was in turn dependent on the molecular weight, crystallinity, thermal properties and water permeability of the solvent cast films (Chee *et al.*, 2008).

### 1.4.3 Mechanisms of action for controlled release

In order to achieve a desired drug release rate, three common mechanisms of action, diffusion, osmosis and degradation are considered.

#### 1.4.3.1 Diffusion release mechanism

In this type of mechanism there are two main types of devices used.

- a) Monolithic device
- b) Reservoir device

In the monolithic device, the active pharmaceutical ingredient (API) is mixed with the polymeric solution or dispersed uniformly within the polymer. Here, the API is slowly released into the physiological fluid by dissolution followed by diffusion. Although, a complete zero-order release may not be achieved it is considered as the simplest method of delivery. In the reservoir device, the API is placed in the core of the polymer film. The dissolution of the drug from the core of the film is dependent on the thickness of the film

and the porosity of the film (Paul *et al.*, 1976). However, if the drug has low aqueous solubility then the drug diffusion could be stopped. Similarly, a highly soluble drug can cause a burst release increasing the drug concentration in the surrounding area (Dash *et al.*, 1992).

#### 1.4.3.2 Osmotic Release

Osmotic systems for controlled drug delivery employ osmotic pressure gradient as the driving force for drug delivery. In this type of delivery, the API is present in the core of the tablet, which is then coated by a semi-permeable material. This type of drug delivery system is mostly suitable for oral administration where a compressed tablet is coated with a semi-permeable membrane. For example cellulose acetate has been used as a cellulosic membrane. The permeability of this membrane is largely dependent on the degree of acetylation where an increase in the permeability is observed when the acetyl content is increased. Upon immersion in an aqueous media, the hydrostatic pressure within compressed tablets is known to increase due to the increased diffusion of water through the semi-permeable membrane. The thickness of this material which is around 200-300 $\mu\text{m}$  is able to resist the hydrostatic pressure when the water penetrates the material. However, once the internal osmotic pressure is raised sufficiently, the drug solution is expelled through the membrane. Initially 60-80% of the drug is released at a zero-order rate, which is then followed by a slower release rate where the residual dissolved drug is released (Park *et al.*, 1994).

#### 1.4.3.3 Degradation Release/Polymer erosion

One of the key properties of biodegradable polymers used in drug delivery is their biodegradability. This property is advantageous when compared to the surgical intervention required to remove the non-degradable matrix (Hasirci *et al.*, 2000). Degradation occurs *via* two main mechanisms such as surface or bulk erosion. Surface erosion is known to occur when the rate of erosion exceeds the rate of water penetration into the bulk of the polymer. Bulk erosion is known to occur when the water molecules penetrate within the polymer matrix at a rate faster than erosion. Drug release from biodegradable polymers occurs in three main mechanisms. In the first mechanism the

drug is covalently attached to the polymer backbone and is concomitantly released when the polymer backbone is hydrolytically cleaved. In the second mechanism, the drug is embedded within the core of the biodegradable polymer and is released when the polymer eventually undergoes degradation. In this mechanism the rate of drug release is dependent on the rate of polymer degradation. In the third mechanism, the drug release is dependent on rate of diffusion from the polymeric device and a combination diffusion and erosion of the polymer (Dash *et al.*, 1992).

#### 1.4.4 PHAs used for drug delivery

The properties of PHAs such as biocompatibility, biodegradability and the ability to control the drug release kinetics by suitably engineering the chemical composition of the PHA matrix, have made PHAs an excellent matrix material for controlled drug delivery. Both scl and mcl-PHAs have been used for drug delivery. Since scl-PHAs are degraded by surface erosion, scl-PHAs are considered ideal for drug delivery. However the rate of drug release from some of these matrices can be quicker, as the number of pores on the surface is increased due to polymer crystallinity and hydrophobicity (Pouton *et al.*, 1996). Mcl-PHAs on the other hand can be used to provide a more controlled drug delivery, due to their lower melting point and crystallinity. However the inability to produce mcl-PHAs in large quantities has limited research on mcl-PHAs.

##### 1.4.4.1 Physical and mechanical properties of PHAs affecting the drug release rate

###### *1.4.4.1.1 Crystallinity*

The degree of crystallinity of a polymer is an important parameter that affects drug release kinetics. Crystalline regions of a polymer are considered to be tougher mechanically than their amorphous counterparts. In this region the intermolecular interactions of the polymer are increased, thus a more compact structure is formed. The compact structure of the polymer becomes impermeable to the diffusing molecules, thus affecting the permeability. Therefore, the reduced permeability affects the drug dissolution and the hydrolysis of the crystalline region of the polymer, finally affecting the drug release kinetics. The drug release rate from P(3HB-co-3HV) is comparatively faster than the homopolymer P(3HB). Researchers like Bissery *et al.*, have used

homopolymers like P(3HB) to deliver anti-cancer drugs like Imoustine® *in vitro*. In this published study a continuous release of the drug was observed for a period of 7 days. However, the drug distribution was affected by the irregularities in the spherical nature of the microspheres due to the crystallinity of the polymer; as a result, large aggregates of the microspheres were formed (Bissery *et al.*, 1985). However, in order to alter the crystalline properties of the polymer and the drug release rates, some researchers have blended P(3HB) with additives such as ethyl and butyl esters of fatty acids into the microspheres. The authors' noticed that although the crystalline properties of the polymer could not be altered, the drug release rates were enhanced due to the release of the additives, which facilitated the diffusion of the drugs from within the microspheres (Kubota *et al.*, 1988; Kawaguchi *et al.*, 1992).

#### 1.4.4.1.2 Thermal Properties

The presence of drugs within the polymer can act as an impurity thereby affecting the thermal properties of the drug. Potent contraceptive drugs such as levo-norgestrol (LNG) have been encapsulated in P(3HB) microspheres to be used as a long acting delivery system. DSC reports showed no characteristic peak such as  $T_m$  for LNG in the thermograms of LNG encapsulated P(3HB) microspheres, thus indicating that the drug was present in such low concentrations relative to the polymer that the drug  $T_m$  was unobservable. (Lu *et al.*, 2001). Copolymers like P(3HB-co-3HV) have  $T_g$  values ranging from -5 to 20 °C, the varying mol% of 3HV in the polymer chain has an impact on the crystallinity and the thermal properties of the polymer. Akthar and Pouton conducted experiments to identify the interactions of the P(3HB-co-3HV) with methyl red used as a model drug and its influence on the  $T_g$  values. X-ray diffraction studies of the methyl red loaded copolymer showed no difference in the rate of crystallization. However, the shape and the breadth of the melt endotherm broadened suggesting that the drug had the effect of an impurity (Akthar *et al.*, 1991).

#### 1.4.4.1.3 Molecular weight

The molecular weight of the polymer is an important factor as it affects the drug release kinetics (Pouton *et al.*, 1996). The molecular weight of a polymer extracted is affected by a number of factors such as the fermentation conditions used, the type of

microorganism, concentration of the carbon and the pH of the media. In addition to these factors, conditions like the solvents used to extract the polymer and the subsequent steps for the purification of the polymer can also affect the molecular weight of the polymer (Pouton *et al.*, 1996). The varying chain lengths of the polymer affect the hydrophobicity of the polymer, thus affecting the drug release kinetics both *in vivo* and *in vitro*. Microspheres prepared using higher molecular weight polymers have been observed to be irregularly shaped and coalesced together, due to which the surface area of the drug-loaded particles is reduced affecting the drug release rate (Pouton *et al.*, 1996). In a study conducted by Khang *et al.*, the *in vitro* release of the anti-cancer drug 5-fluoro-2'-deoxyuridine from P(3HB) microspheres with different molecular weights (65000, 135000 and 450000Da) were studied. The authors' observed that the drug release rate from the P(3HB) microspheres with the lowest molecular weight of 65000Da was higher when compared to the P(3HB) microspheres with a higher molecular weight of 135000 and 450000Da (Khang *et al.*, 1992). Higher molecular weight polymers are compact in nature and sometimes these molecular weight chains can get entangled which can prevent the surrounding media from entering into the polymeric vehicle, thereby preventing the drug release, resulting in a slower drug release (Pouton *et al.*, 1996).

#### 1.4.4.1.4 Processing conditions that affect the drug release rate

The processing conditions used to fabricate the biodegradable polymers as drug delivery vehicles also affect the drug release rate. For example factors such as porosity, particle size, viscosity and drug distribution vary under the different processing conditions (Berkland *et al.*, 2003). Microsphere preparation using the emulsion technique is the most common method used to encapsulate the drugs. Microsphere preparation using the solvent evaporation method to encapsulate the drug is affected by the types of solvents used, surfactants used and the viscosity of the emulsion phase due to the polymer and surfactant concentration.

The types of solvents used for microsphere preparation are known to affect the surface morphology of the microspheres. For example progesterone encapsulation in P(3HB) and P(3HB-co-3HV) microspheres were significantly affected by the solvents used for the solvent evaporation technique. When chloroform was used, a very porous and irregular

surface was formed but when the solvent was replaced with methylene chloride, a smooth surface with high encapsulation efficiency of 80% was observed. The *in vitro* release of progesterone was the slowest using the P(3HB-co-3HV) microspheres as it was less porous when compared to the P(3HB) microspheres (Nobes *et al.*, 1998).

The surfactants used in the solvent evaporation technique during microsphere preparation are known to affect the encapsulation efficiency of the drugs. For example polyvinyl alcohol (PVA), an emulsifier used in the emulsion phase during microsphere preparation, is known to influence the drug distribution within the microspheres, thereby having an influence on the *in vitro* drug release profile. Yang *et al.*, observed the uniform drug distribution and slower BSA release from PCL (polycaprolactone) and PLGA (poly DL-lactic-co-glycolic acid) 65:35 microspheres when PVA was used as an emulsifier (Yang *et al.*, 2001). Similarly in another study conducted by Bouissou *et al.*, the encapsulation efficiencies of fibronectin FIII9V-10 in PLGA microspheres using different surfactants such as PVA, Tween 20 and Tween 80 were compared. In this study a higher encapsulation efficiency of 25% was observed when PVA was used as a surfactant when compared to 15% and 11% encapsulation efficiency when Tween 20 and Tween 80 were used respectively. The microspheres fabricated using Tween 20 and Tween 80 exhibited surface minor ridges with hollow structures which contributed to the lower encapsulation efficiency. However the microspheres fabricated using PVA retained the FIII9V-10 thus exhibiting higher encapsulation efficiency (Bouissou *et al.*, 2004).

Other factors such as viscosity of the emulsion phase used for fabricating the microspheres have an effect on the microsphere size. For example the increase in the polymer concentration leads to an increase in the viscosity of the solution due to which the smaller microspheres are not broken down. In a study conducted by Bonarstev *et al.*, it was observed that the P(3HB) microspheres fabricated by the oil-emulsion technique encapsulating the antibiotic dipyridamole (DPD) produced microspheres which were larger in size. The largest microparticle sizes were 92 $\mu\text{m}$  (Bonarstev *et al.*, 2007). The *in vitro* release profiles of the drugs also vary considerably due to the variations in the microsphere sizes (Nobes *et al.*, 1998). The *in vitro* release rate of various drugs from microspheres with various sizes is listed in Table 4.

**Table 4:- Anti-drugs encapsulated in P(3HB) microspheres using the solvent evaporation technique.**

\*CCNU is 1-(2 chloroethyl)-3-cyclohexylnitrosourea.

Drugs	Type of PHA	Particle size ( $\mu\text{m}$ )	Release rate	References
*CCNU	P(3HB)	1-15	90% in 10h	Bissery <i>et al.</i> , 1985
Alcarubicin	P(3HB)	158-214	10% in 120h	Juni <i>et al.</i> , 1986
Tetracaine	P(3HB)	20-40	50% in 2h	Akthar <i>et al.</i> , 1989
Rifampicin	P(3HB)	120-200	40% in 24h	Kassab <i>et al.</i> , 1997

#### 1.4.5 Inorganic scaffolds used as drug carriers

Bioactive ceramic scaffolds such as bioactive glass ceramics or silicates/phosphates, hydroxyapatite and calcium phosphates have been used for hard tissue engineering. However, in addition to being used to provide structural integrity required for hard tissue engineering they can also serve as a drug delivery vehicle by controlling the kinetics of the therapeutic drug without the requirement of an additional drug carrier. These bioactive glasses have the advantage of being easily shaped into different forms such as pellets, films and powders, therefore these scaffolds when used as implants have also been considered for drug delivery applications. For example, in order to diminish the infections associated with the scaffold, researchers like Domingues *et al.*, have incorporated antibiotics such as tetracycline within the bioactive glass scaffold as a carrier for the drug. In this study the authors' observed that the tetracycline release from the bioactive glass lasted for a period of 80 days. Although a burst release of 12% was observed in the first 8h, a cumulative release of 22% at the end of the study was observed. From this study it was concluded that the bioactive glasses could be used as an efficient system for slow release of the drug (Domingues *et al.*, 2004). Hydroxyapatite (HA) is another inorganic material, which is a major component of the bone. Porous HA has largely been used as a filling material for bone defects and augmentation (Wang *et al.*, 2007). This porous morphology of HA has been used a fundamental feature while using HA as a potential drug release agent. For example in a study conducted by Palazzo *et al.*, ibuprofen-lysine and hydrocortisone sodium-succinate from two cylindrical hydroxyapatitic grafts with the same porosity were used as drug delivery matrices. The authors had observed that the drug hydrocortisone sodium-succinate was released at

much slower rate when compared to ibuprofen-lysine during the first 40 minutes (Palazzo *et al.*, 2005).

#### 1.4.5.1 Factors affecting the drug release rate from inorganic scaffolds

##### 1.4.5.1.1 Processing conditions

Several techniques have already been developed to fabricate these scaffolds with added advantage of a drug delivery capability. However the methods that were employed to fabricate these scaffolds have a considerable effect on the drug release rate. In the template technique, the scaffolds are prepared by dissolving the polyurethane sponge in ceramic particles where the surplus slurry is then removed and sintered at a high temperature to obtain a porous three-dimensional scaffold (Chen *et al.*, 2006). In order to impregnate the drugs within the scaffolds, they are further immersed in drug containing phosphate-buffered saline solution (PBS). In a study conducted by Zhu *et al.*, the *in vitro* release study of gentamicin from both mesoporous bioactive glass (MBG) and the bioactive glass (BG) ceramics fabricated using the polyurethane sponge technique were compared. The authors' observed that in the MBG scaffold the drug uptake capacity was two-fold higher than that of the BG scaffold due to its increased surface area and pore volume. Although BG and MBG scaffolds exhibited an initial burst release followed by a relatively slower release, the *in vitro* release of gentamicin from the MBG scaffolds was much slower when compared to the drug release from the BG scaffolds. For the MBG scaffolds an initial burst release of 52% was observed in the first 12h followed by a sustained release of 66% of the initial drug loaded for a period of 7 days. While for the BG scaffolds a higher initial burst release of 73% was observed in the first 12h, followed by 96% cumulative release of gentamicin after 7 days. It was observed that the gentamicin molecules were hosted deep inside the mesoporous channels in the MBG scaffolds which contributed towards its slower release. The BG scaffolds on the other hand were dense with the presence of some disordered pores on the surface. A higher percentage of the gentamicin molecules were located on the surface of the BG scaffolds, which had explained the faster release of gentamicin. Thus from this study it was concluded that MBG scaffolds were a better system for local drug delivery (Zhu *et al.*, 2009).

#### 1.4.6 Composites used for drug delivery

Although numerous techniques have been developed to fabricate inorganic scaffolds incorporating the drug there are some disadvantages that render them unsuitable for drug delivery. For example the drug release rate in the template technique cannot be controlled as the ceramic scaffolds are loaded with the drug by simply immersing in the drug containing solution (Habraken *et al.*, 2007). In the thermal technique which involves the sintering of the scaffold at temperatures around  $>800^{\circ}\text{C}$ , the drugs incorporated within these scaffolds are often degraded at high temperatures (Vallet-Regi *et al.*, 2008). Scaffolds with high porosity and large interconnectivity do not have the capacity to retain the drug at the required site for a longer period of time (Murino *et al.*, 2009). Thus several studies are now focused on the combination of biodegradable polymers and bioactive ceramics such as fibres or particles as composite scaffolds for drug delivery studies. Composite scaffolds offer a convenient alternative as they combine the advantages of both the biodegradable polymers and bioactive ceramics. For example biodegradable polymers can be used to control the drug release rate due to their degradation rate (Hutmacher 2000). On the other hand the presence of the bioactive ceramics in the composites can improve the mechanical strength and the structural integrity of the composite scaffolds.

##### 1.4.6.1 Polyhydroxyalkanoates and bioactive ceramics in drug delivery

Although synthetic biodegradable polymers and bioactive ceramic scaffolds have been used as drug delivery vehicles, some synthetic polymers such as poly(methyl methacrylate) and poly(propylene glycol-fumarate) could not be used *in vivo* as they provoked an adverse tissue response due to their acidic degradation products (Murino *et al.*, 2009). Therefore, the need to fabricate biocompatible composite scaffolds has been in demand (Murino *et al.*, 2009). Polyhydroxyalkanoates (PHAs) exhibit biocompatible properties as well as support cell growth. They can be easily fabricated into any complex shape and structure. PHAs have been combined with bioactive ceramics, thus in addition to improving the mechanical properties of the composite scaffolds, this combination of polymers and ceramics also lead to formation of multi-functional scaffolds with a drug delivery capability (Misra *et al.*, 2008). For example, Wang *et al.*, fabricated P(3HB-co-

3HV) and HA nanoparticles encapsulating gentamicin for a controlled release study. Although, an initial burst release of gentamicin from these composite nanoparticles was observed, the total drug release period lasted for 10 weeks. With an equal weight ratio of HA and P(3HB-co-3HV) (1:1), a higher encapsulation efficiency compared to HA alone was observed due to the formation of a strong bond between the drug and HA. Thus, this composite system proved to be promising for a long-term release system (Wang *et al.*, 2007). Other drugs such as alendronate (AL) used to prevent osteoporosis have been incorporated into HA and P(3HB-co-3HV) microspheres (Huang *et al.*, 2009). Composites of Wollstanite and P(3HB-co-3HV) microspheres encapsulating the drug gentamicin have been used in a powder form as bone fillings and as an effective bioactive drug delivery system. The drug was incorporated into the composites by a solid-in-oil-in-water technique. These microspheres were later lyophilized and stored under vacuum. By this method a high encapsulation efficiency of 65.2% was observed for the composite scaffolds when compared to the P(3HB-co-3HV) microspheres, which was 51.8% (Li *et al.*, 2005).

#### 1.4.6.2 Factors affecting the drug release rate from composite scaffolds

##### 1.4.6.2.1 Processing conditions

One of the simplest approaches of incorporating a drug in the composite scaffolds is by coating the drug containing polymer solution onto the three-dimensional structure of the bioceramic scaffolds. This is achieved by immersing the scaffold in the drug containing solution. In this method the sustained release of the drug is dependent on the thickness of the polymer coating, initial drug loading and the percentage of porosity. For example in a study conducted by Kim *et al.*, tetracycline hydrochloride was incorporated within porous HA scaffolds by dip coating the scaffolds in poly( $\epsilon$ -caprolactone) solution. The drug release from the composite scaffolds increased sharply when compared to the HA scaffolds alone during the first 2h, after which a sustained release of the drug was observed. In this study the initial burst release was attributed to the unbound drug particles present on the surface of the scaffolds. However, with the increase in the immersion time, the drug release was largely dependent on the hydrolytic degradation of the PCL layer as well as release of those drugs embedded within the porous matrix of the

scaffolds. Therefore, it was observed that the drug release in this system was largely dependent on the thickness of the polymeric coating and internal porosity (Kim *et al.*, 2004).

#### 1.4.7 Application routes of controlled release systems

Several types of controlled release systems carrying drugs or other bioactive agents have been formulated with the aim of a desired controlled release at the site of action. Targeted drug delivery reduces the amount of dosage thus reducing the toxic side effects on healthy cells.

##### 1.4.7.1 Oral drug delivery

Delivery of larger macromolecules orally has always been a challenge. Some larger protein and peptide based drugs have stringent demand on the way they are delivered in the body (Yang *et al.*, 2001). It is important for these molecules to retain their structure until they reach the delivery site. However, the enzyme activity in the stomach significantly affects the bioactivity, stability, pharmacodynamics and the pharmacokinetics of these molecules. In addition, the mucosal lining of the stomach prevents the successful penetration of the drugs, thus proving to be an obstacle (Elridge *et al.*, 1990). P(3HB) compressed tablets containing anti-hypersensitive drugs were used for slow drug delivery. The slow and sustained releases of drugs from these tablets were dependant on the molecular weight of the polymer. The drug release rate increased when molecular weight was increased from 3000kDa to 6000kDa (Korsatko *et al.*, 1984). P(3HB) compression moulded compact discs were used to deliver tetracycline for the treatment of periodontal disease. In the presence of the tablets a significant improvement in the reduction of the gingival infection was seen over a period of 10 days. Adequate therapeutic levels of tetracycline were also maintained in the saliva (Collins *et al.*, 1989; Deasy *et al.*, 1989). P(3HB) microspheres encapsulating 50% sulphamethizole was orally administered in greyhound dogs. A good correlation in the *in vitro* release profile and *in vivo* absorption was observed (Pouton *et al.*, 1991). Diltrazem, a vasodilator was compressed in P(3HB) tablets and the construct was used to study the *in vitro* release rate (Kharenko *et al.*, 1999). In this study, a higher/faster release rate was

seen with higher drug loadings. At 45% drug loading a complete release of the drug was seen (Kharenko *et al.*, 1999).

#### 1.4.7.2 Subcutaneous Implants

Transdermal delivery provides the opportunity to deliver small lipophilic drugs, which are usually destroyed by the liver when taken orally. The skin however is an impenetrable barrier consisting of corneocytes and a hydrophobic lipid layer which provides a highly tortuous pathway for the diffusion of most drugs, therefore many novel approaches have been applied to achieve a practical transdermal delivery (Metcalf *et al.*, 2006). Due to the skin's innate impermeability both passive and active methods have been employed. In the passive method, a range of formulations are applied to enhance drug delivery without applying any physical force whereas in the active method physical forces such as heat, electrical current, laser light or ultrasound is employed to deliver the drug (Merino *et al.*, 1997). Mcleod *et al.*, in 1988 compressed gonadotropin releasing hormone (GnRH) in P(3HB) tablets and placed subcutaneously in sheep. This hormone is used to stimulate the luteinizing hormone (LH), which is used to promote the preovulatory follicle growth and induce ovulation in sheep. P(3HB) containing this hormone was able to release about 40-50 pg of GnRH consistently for a period of 2-4h, thereby maintaining a constant elevated plasma level of LH. This study proved to be successful and a high incidence of ovulation was seen when two implants per animal was used (Mcleod *et al.*, 1988). Mcl-PHA with a polyamidoamine dendrimer was considered for transdermal drug delivery (Wang *et al.*, 2003). In this study the model drug Tamsulosin was efficiently delivered by permeating through a snake skin model. The clinically required amount of drug was delivered due to the presence of the dendrimer (Wang *et al.*, 2003).

#### 1.4.7.3 Intravenous administration

P(3HB) microspheres (1-12  $\mu\text{m}$  in size) encapsulating the anti-cancer drug 'Imoustine' was intravenously injected into Lewis lung carcinoma mice (Bissery *et al.*, 1985). The drug release from the P(3HB) microspheres lasted for a period of 24h when compared to the release rate from poly(lactic acid) (PLA) which lasted only for a period of 90 hours (Bissery *et al.*, 1985). Saito *et al.*, intravenously injected  $^{14}\text{C}$  labelled P(3HB)

microspheres in both mice and rat. The microspheres of an average size of 1-12 $\mu\text{m}$  when administered in mice were found to be 47% in the lungs, 14% in the liver and 2.1% in the spleen. However, when microspheres of 0.3-0.5  $\mu\text{m}$  were injected in the tail vein of rats, 86% of the radioactivity from the microspheres was found in the liver, 2.5% in the spleen and 2.4% in the lungs. Here, the difference in the radioactive distribution was due to the variation or irregularity in the particle size (Saito *et al.*, 1991).

## **1.5 Biomedical applications of PHAs**

### 1.5.1 PHAs used for wound healing applications

Skin comprises a major part of the body, any damage due to injury, burns and disease can have a major physiological or functional consequence. Therefore, several tissue engineered skin substitutes are being designed to treat acute and chronic skin wounds (Metcalf *et al.*, 2007; Macneil *et al.*, 2008). In tissue engineering, a biomaterial is designed that can be used to replace the damaged organ or tissue. However for skin tissue regeneration or wound healing, the biomaterial should possess the strength to promote the growth of skin cells such as keratinocytes, melanocytes and fibroblasts. They should be non-toxic, non-antigenic and facilitate angiogenesis while being incorporated with minimal scarring and pain. In addition to this, biomaterials are also required to act as an artificial extracellular matrix (ECM) for the cells to attach. Therefore, natural polymers such as polypeptides, hyaluronan, glycosaminoglycans and synthetic materials such as polylactide (PLA), polylactide-co-glycolide (PLGA) were used as skin substitutes. Although these materials have been successfully used as skin substitutes, some disadvantages that prohibited their use were their inability to support appropriate cellular activity such as the molecular signalling cascades which prevented the clinicians from manipulating it in a surgical setting. Therefore other replacements such as biodegradable polyhydroxyalkanoates are being considered for skin tissue engineering/regeneration (Metcalf *et al.*, 2006). Techniques such as electrospinning and three-dimensional printing are being considered to provide an accurate pore size and porosity so that the internal architecture of the scaffold can support cell attachment (Metcalf *et al.*, 2006). Biocompatibility of the scaffolds is one of the pre-requisites for skin replacement. For *in vitro* studies, keratinocytes are used. These cells are known to have the same behaviour

both *in vitro* and *in vivo*. The disaggregated autologous keratinocytes when added on a scaffold are known to create a stratified epithelial layer. When large numbers of keratinocytes are grown over a period of two to three weeks, they organise themselves within the substitute and recreate the anatomical composition of a skin (Metcalf *et al.*, 2006). Copolymers of poly(3-hydroxybutyrate-co-5mol%-hydroxyhexanoate), poly(3HB-co-5mol%-3HHx) and poly(3-hydroxybutyrate-co-7mol%-4-hydroxybutyrate), poly(3HB-co-7mol%-4HB) and poly(3HB-co-97mol%-4HB) were electrospun into scaffolds and then subcutaneously implanted in rats to study their bioabsorption behaviour and tissue response. The scaffolds were observed to be well tolerated with minimal inflammatory response as seen from the histological evaluations (Ying *et al.*, 2008). P(3HB) and P(3HB-co-3HV) sutures have also been used for healing myofascial wounds (Valappil *et al.*, 2006). These sutures did not cause any necrosis, inflammation or carcinogenesis when implanted *in vivo* in female wistar rats for a period of 1 year. No adverse reactions were seen in comparison to the controls and the reactions exhibited were characteristic of the wound process and of a reaction to a foreign body invasion. The presence of the HV content in the copolymer films also did not induce any changes in the intensity or duration of the inflammatory reactions or fibrous capsule formation around the sutures (Valappil *et al.*, 2006). P(3HB) fibres used as wound dressings were pre-treated with a strong acid or base to improve the surface properties for cell attachment. Human epithelial cells when added on the pre-treated fibres appeared well spread with good adhesion (Valappil *et al.*, 2006).

### 1.5.2 PHAs used for Hard tissue engineering applications

Natural and synthetic polymers for example collagen, poly(ethyleneglycol), polyhydroxyalkanoates and poly(lactide-co-glycolide) have been considered for bone tissue engineering applications due to their favourable properties such as biocompatibility (cell attachment and differentiation) and tailorable mechanical and degradable properties (Yang *et al.*, 2001). Although the above mentioned polymers have been used for load bearing applications such as fracture fixation devices, one of the main disadvantages that limit their applicability in hard tissue engineering is their fast degradability. Due to this, polyhydroxyalkanoates such as poly(3-hydroxybutyrate) P(3HB) and poly(3-

hydroxybutyrate-co-3-hydroxyvalerate) P(3HB-co-3HV) with long term degradation profiles have been considered. P(3HB) also has the capacity to induce osteogenesis and healing due to its piezoelectric properties. Therefore P(3HB) has the ability to strengthen and repair bone which is an added feature comparable to that of natural bone (Ferrier *et al.*, 2002). P(3HB) implants when used *in vivo* for connecting osteotomies whereby a bone is cut to shorten, in the tibia of rats, completely resorbed after 24 weeks. Similarly, when used as osteosynthetic patches anchored with two P(3HB) bolts to repair the zygomatic arches of rabbits, they were able to successfully cover the defects of osseous skull and the fracture of the visceral cranium (Misra *et al.*, 2006). Other polyhydroxyalkanoates such as poly(3-hydroxybutyrate-co-3-hydroxyhexanoate) P(3HB-3HHx) have also been used as a scaffold material in bone tissue engineering. *In vitro* cell attachment studies using osteoblast cells have shown high alkaline phosphatase (ALP) activity, strong calcium deposition and fibrillar collagen synthesis when compared to films of P(3HB) and PLA (Wang *et al.*, 2005). The alkaline phosphatase activity of the cells grown on P(3HB-co-3HHx) scaffolds was up to about 65 U/g scaffolds, 50% higher than that of P(3HB) and PLA, respectively (Wang *et al.*, 2005). In another study conducted by Deng *et al.*, chondrocytes isolated from rabbit articular cartilage were seeded onto P(3HB-co-3HHx), P(3HB) and the blend of P(3HB-co-3HHx)/P(3HB) scaffolds for a period of 28 days. From the results it was observed that a higher chondrocyte proliferation was observed on the P(3HB-HHx)/P(3HB) scaffolds rather than the P(3HB) scaffolds alone. Thus from this study it was proven that P(3HB-co-3HHx) films exhibited higher affinity for chondrocyte attachment, proliferation and differentiation when compared to the other films (Deng *et al.*, 2002).

### 1.5.3 PHAs used for other biomedical applications

P(3HB) has also been used as pericardial patches, anastomoses tubes, separating films, repair of peripheral nerves and as a substitute for covering damaged tissue of gastrointestinal tract (Ljungberg *et al.*, 1999; Novikov *et al.*, 2002; Freier *et al.*, 2002). Mcl-PHAs on the other hand are more applicable for soft tissue engineering such as heart valve tissue engineering and skin tissue engineering due to their soft and elastomeric properties. Mcl-PHAs such as P(3HO-co-3HHx) have been used in soft tissue

engineering as substitutes to repair heart valves, blood vessels and vascular grafts (Sodian *et al.*, 2000a; Stock *et al.*, 2000). Whereas P(3HB-co-3HHx) has been used in hard tissue engineering for the repair of cartilage and bone (Deng *et al.*, 2002; Wang *et al.*, 2004). Although, mcl-PHAs exhibit a higher structural diversity when compared to the scl-PHAs, their main limitation lies in the inability to produce these polymers in large quantities. A detailed summary of the use of PHAs in tissue regeneration is shown in Table 5.

Table 5:- Summary of common PHAs used for various biomedical applications

Applications of PHAs	Types of PHAs used	Site of implantation	Remarks	References
Nerve regeneration	P(3HB)	P(3HB) conduits to bridge the gap in the rat sciatic nerve	Successful migration of Schwann cells and axonal regeneration was identified	Mosahebi <i>et al.</i> , 2002
		P(3HB) nerve conduits to support rabbit common nerve injury	P(3HB) conduits take a long time to undergo degradation therefore they provide the mechanical support required during regeneration. Lesser risk of accumulating large amount of acidic degradation products	Wu <i>et al.</i> , 2009
	P(4HB)	Tubular constructs of P(4HB) was seeded with ovine vascular smooth muscle cells	Provided mechanical support. The constructs supported cell adhesion	Martin <i>et al.</i> , 2003
Cardiovascular Patches/Heart valves	P(3HB)	Non-woven patches used as pericardial substitutions, enlargement of pulmonary artery and the repair of arterial septal defects	In the presence of the pericardial patches, the coronary artery was well preserved even after 30 days of implantation. The mechanical strength was retained. The constructs supported cell adhesion and prevented the dilation of the regenerating tissue.	Freier <i>et al.</i> , 2002
Skin regeneration	Terpolyesters of 3-hydroxybutyrate 3HB, 4-hydroxybutyrate (4HB) and 3-hydroxy-hexanoate (3HHx); P(3HB-co-4HB-co-3HHx),	Films used as skin implants were seeded with L929 mouse fibroblasts, human keratinocyte (HaCaT) cells	The cell morphology and viability analyzed using SEM and methylthiazol tetrazolium (MTT) assay proved that all the three cell types exhibited higher cellular activity on the P(3HB-co-4HB-co-3HHx) films. SEM images revealed well spread cell shape with large number of pseudopods indicating strong cell-to-cell and cell to material interactions	Liu <i>et al.</i> , 2008
	P(3HB-co-3HV-co-3HHx), novel terpolyesters of poly(3-hydroxybutyrate-co-3-hydroxyvalerate-co-3-hydroxyhexanoate),	human keratinocyte (HaCaT) cells	Films made of P(3HB-co-3HV-co-3HHx), were soft and exhibited the flexibility that was required for skin tissue engineering, P(3HB-co-3HV-co-3HHx), films seeded with HaCaT exhibited the highest cell density and viability	Ji <i>et al.</i> , 2008

## 1.6 Biomedical applications of Bioceramics

### 1.6.1 Bioceramics used for other hard tissue engineering applications

Alumina, a bioinert ceramic has a higher Young's modulus of 380GPa and lower wear rates therefore it is used for dental implants. HA has been used as dental implants and coatings for chemical bonding. 45S5Bioglass<sup>®</sup> has also been used as dental implants, coatings for chemical bonding and as maxillofacial reconstruction devices. Phosphate glasses have been used as vertebral prosthesis and orthopaedic fixation devices (Hench *et al.*, 2004 and Huang *et al.*, 2008). The advantages, disadvantages of bioceramics highlighted for various applications in tissue engineering have been listed in Table 6.

**Table 6:- The advantages and disadvantages of bioceramics highlighted for various applications in tissue engineering (Misra *et al.*, 2006; Chen *et al.*, 2006).**

Types of Material	Shape of materials	Advantages	Disadvantages
Inorganic calcium phosphates example HA, $\beta$ -tricalcium phosphate, $\alpha$ - tricalcium phosphate	Films 3D scaffolds	Biocompatibility, and osteoconductivity	Slow degradation rate and brittle
Bioactive glasses and glass ceramics	Films 3D scaffolds Foams	Biocompatibility, osteoconductivity angiogenic and tailorable resorption	Inflammatory response  lack of compression strength and poor stiffness

### 1.6.2 Bioceramics used for Bone tissue engineering

Bone tissue regeneration or repair has been the most common yet complicated problem in the field orthopaedic surgery. Often the main problems associated with treating bone defects were biocompatibility and its immunological response (Goldberg *et al.*, 1987). In addition, the size of the bone defects caused due to trauma or disease pose considerable difficulty as they cannot be repaired by the natural growth of the host tissue.

There is the need to fill these defects with a porous material, usually known as a scaffold, which in addition to bridging the gap, can also promote the regeneration of a new bone tissue (Hench *et al.*, 1998). Those biomaterials which exhibit bioactive properties *i.e.*, the ability to form a biologically active hydroxyapatite layer when immersed in physiological fluids is used for bone tissue engineering applications. The bioactive property of these biomaterials, allow the formation of tenacious bonds to bone or osseointegration thereby transferring the load to and from the living bone (Chen *et al.*, 2006). In addition, other properties such as porosity and mechanical strength are also required for bone tissue engineering applications. For example the average porosity required for bone tissue engineering is 90% with a pore size of  $>100 \mu\text{m}$ . This high porosity is known to facilitate the proliferation of cells for new tissue regeneration while also enabling the mass transport of oxygen and nutrition (Rezwan *et al.*, 2006). These biomaterials are classified as either conductive *i.e.* the ability to provide physical support to facilitate tissue regeneration or inductive *i.e.* the ability to induce specific biological responses (Rezwan *et al.*, 2006). The most commonly used biomaterials are bioceramics such as silicate glasses, glass-ceramics, and hydroxyapatites as well amorphous or crystalline calcium phosphates (Rezwan *et al.*, 2006). For example alumina bioinert ceramics have lower wear rates and higher Young's modulus, therefore can be used for load bearing orthopaedic applications. Bioactive glasses such as 45S5 Bioglass<sup>®</sup> have exhibited higher bioactivity through the formation of a biologically active hydroxycarbonate apatite layer. It has been used as orthopaedic fixation devices. Calcium phosphates such as tricalcium phosphates have been used as temporary bone space fillers due to their higher dissolution rate, as a result they are replaced by bone during implantation. Glass ceramics such as phosphate glasses and wollastonite have also been extensively used as bone substitutes and vertebral prosthesis (Hench *et al.*, 2004; Huang *et al.*, 2008; Rezwan *et al.*, 2006).

## **1.7 Biomedical applications of composite scaffolds**

### 1.7.1 Composite scaffolds used for hard tissue engineering applications

Composite films of P(3HB-co-3HV)/TCP and P(3HB-co-3HV)/HA manufactured using the compression moulding technique have been used for maxillofacial reconstruction. The addition of TCP enhanced the mechanical properties of the films, while the presence of HA increased the storage modulus and bioactivity of the composite films (Misra *et al.*, 2006; Chen *et al.*, 2006).

### 1.7.2 Composite scaffolds used for Bone tissue engineering

Bioactive ceramics are often known to lack the mechanical properties (fracture toughness) needed for bone tissue engineering due to their relatively high stiffness. In contrast, lack of mechanical strength is the disadvantage of using polyhydroxyalkanoates for load bearing applications. In addition, although some polymers have been moulded into complex shapes and structures, they generally lack the bioactive function which is imperative for bone tissue engineering applications. Due to their inability to form a strong bond to the natural bone they become too weak to meet the physical demands in surgery (Bonfield *et al.*, 1981). Therefore, in order to achieve the optimal mechanical and biological property, both degradable polymers and inorganic bioactive particles have been combined to form composite materials (Misra *et al.*, 2006). These composite materials are known to possess several advantages such as improved mechanical properties including higher stiffness, tailorable degradation behaviour and increased bioactivity due to the formation of a tenacious bond with bone. Finally, the surface characteristics of the composite materials such as surface roughness and wettability were observed to be improved due to the presence of the bioactive inorganic phases in the composite materials leading to better adsorption of proteins and cell growth (Li *et al.*, 2005; Wei *et al.*, 2004). The bioactive inorganic ceramics as well as polyhydroxyalkanoates are often incorporated in the form of fibres. Mechanical and bioactive properties of the composite materials are often affected by the size and distribution of the particles within the composite materials. For example the higher specific surface area of the nanoparticles are known to contribute towards an increased

bioactivity when compared to the microparticles (Li *et al.*, 2005; Wei *et al.*, 2004). The host tissue response to nanostructure surfaces is also different when compared to the other surfaces. Some examples of the common composites used in bone tissue engineering are discussed below.

Polyhydroxyalkanoates such as P(3HB-co-3HV) have been used in combination with HA and TCP in the form of films. The presence of HA in the composite films increased the storage modulus and bioactivity of the films (Ni *et al.*, 2002). P(3HB) composite films incorporating 45S5Bioglass<sup>®</sup> particles in different concentrations such as 5 and 20wt% were fabricated by Misra *et al.*, to study the effects of 45S5Bioglass<sup>®</sup> particles on the thermal and mechanical properties of the composite films. The authors observed that with the increase in the 45S5Bioglass<sup>®</sup> concentrations, the crystallinity of the polymer matrix was reduced and an increase in the glass transition temperature was observed. The storage modulus of the composite films had increased to  $2.4 \times 10^9$  Pa in the presence of 20wt% of the 45S5Bioglass<sup>®</sup> particles as compared to  $1.8 \times 10^9$  Pa in the case of P(3HB) (Misra *et al.*, 2007). P(3HB)/bioactive glass composite films with three different concentrations of m-BG and n-BG (10, 20 and 30 wt%, respectively) prepared by a solvent casting technique were examined for changes in the mechanical and structural properties. From the results it was observed that the addition of n-BG particles had a significant stiffening effect on the composites, modulus when compared with m-BG. The nanometric size of the n-BG particles contributed to a 50% increase in the stiffness of the composites (up to a 50% increase). Similarly an increase in the Young's modulus in the PHA/n-BG composites was also observed which related to the higher interfacial surface area was provided by the nanoparticles, which enhanced the load transfer between the matrix and the stiff inclusions when compared to the m-BG particles. Thus the results from this confirmed that the addition of nanosized bioactive glass particles had a more significant effect on the mechanical and structural properties of a composite system in comparison with microparticles (Misra *et al.*, 2008).

## 1.8 Factors affecting material performance

### 1.8.1 *In vitro* degradation

*In vitro* degradation studies are performed in simple aqueous solutions so it would be possible to predict the *in vivo* degradation behaviour of an implant. It is normally carried out in phosphate buffered saline (PBS) solution, cell growth media such as Dulbecco's Modified Eagle Medium (DMEM) or in human serum containing inflammatory cells at 37 °C, under static or dynamic condition. After the incubation period, the samples were analysed for changes in mechanical properties, molecular mass and surface morphology (Freier *et al.*, 2002a). PHAs have also been known to undergo both *in vitro* as well as *in vivo* degradation, in the context of biocompatibility, as discussed below (Freier *et al.*, 2002a, Jendrossek *et al.*, 2002). A summary of some of the important results obtained from *in vitro* degradation of PHAs is given in Table 7. *In vitro* degradation of P(3HB) in buffer solutions resulted in a decrease in the molecular weight after 80 days of incubation (Doi *et al.*, 1989). The degradation of P(3HB) is observed to take place through random scission in both the amorphous and crystalline regions of the polymer matrix (Freier *et al.*, 2002). This study concludes that P(3HB) undergoes slow *in vitro* degradation where the mass loss half life in the buffer solution occurs in the range of 56 to 152 weeks (Freier *et al.*, 2002). The *in vitro* degradation rate of P(3HB-co-3HV) is dependent on the varying HV content which has a significant effect on the molecular weight, crystallinity and porosity of the P(3HB-co-3HV) polymers. In order to accelerate the rate of degradation, P(3HB-co-3HV) films have been blended with alginate, dextrin, amylose and talcum powder (Table 7) (Yasin *et al.*, 1989). The highly crystalline regions of the polymer P(3HO-co-3HHx) films are responsible for the slow degradation process when immersed in the buffer solution (pH 7.4 and 37°C). In order to accelerate the degradation, the P(3HO-co-3HHx) films have been blended with gelatin (Wang *et al.*, 2005). The rate of degradation of the films had increased because the crystallinity of the blended films had reduced due to the blending of gelatin. Furthermore, the blending of gelatin had also created a porous surface in the films, which had increased the surface area of the films for hydrolytic attack (Wang *et al.*, 2005). Hydrophilic polymers such as poly(lactic acid) PLA and poly-ethylene glycol (PEG) have also been grafted onto the reactive backbone

of polymers such as poly(3-hydroxyoctanoate-co-3-hydroxyundecenoate) P(3HO-co-3HU), to increase the hydrophilicity of the polymers by incorporating hydrophilic molecules in the polymer chains. Such surface modifications improved the water uptake and swelling of the polymer matrix, leading to an improved hydrolysis or degradation of the polymer (Renard *et al.*, 2003).

Wollastonite has been used as a filler in P(3HB-co-3HV) film as an aid in the degradation of the composites. In a study conducted by Li *et al.*, the *in vitro* degradation of three-dimensional composite scaffolds made of P(3HB-co-3HV) and wollastonite were investigated for a period of 15 weeks in PBS. The results of this study revealed that with the addition of wollastonite in the composite films, an increase in the water absorption capacity and weight loss of the films were observed. The addition of wollastonite in the range of 0-40 wt% had decreased the water contact angle from 66° to 16°. The weight loss of the composite scaffolds with 10 wt% and 20 wt% wollastonite had increased from 27% to 35% during the first 3 weeks of incubation when compared to P(3HB-co-3HV) scaffolds where a weight loss of only 12% was observed at the end of 15 weeks. Thus from these results it was observed that the degradation rate of the composite films could be adjusted with the addition of wollastonite (Li *et al.*, 2005). The addition of 45S5Bioglass<sup>®</sup> glass is also known to improve the water uptake of the P(3HB) composite films when compared to the P(3HB) films alone (Misra *et al.*, 2008). In a study conducted by Misra *et al.*, an increase in the water uptake of P(3HB)/45S5Bioglass<sup>®</sup> films was observed when the concentration of the 45S5Bioglass<sup>®</sup> was increased from 10 wt% to 30 wt%. For example, at end of the one month period, an increase in the water uptake capacity to 25% was observed when 30 wt% of 45S5Bioglass<sup>®</sup> particles were incorporated whereas 10wt % of 45S5Bioglass<sup>®</sup> exhibited only 10% of water uptake capacity (Misra *et al.*, 2008).

Table 7: Summary of the factors influencing *in vitro* degradation of PHAs

Types of PHAs	Influences on the rate of degradation	Remarks	References
P(3HB)	Glycerin was incorporated into the films	The porous surface created by glycerine increased the surface area of the polymer matrix exposing it to degradation after the glycerine was leached out from the film	Abe <i>et al.</i> , 1994, Kurcok <i>et al.</i> , 1995
	lipase, amylase, trypsin and protease	The degradation rate of P(3HB) increased three-fold in comparison to the films that were subject to simple hydrolysis	Freier <i>et al.</i> , 2002
P(HB-co-HV)	Gama-irradiation and steam sterilization	A significant loss in the molecular weight and mechanical properties were observed when the films were exposed to different sterilization methods	Shishatskaya <i>et al.</i> , 2004
	alginate, dextrin, amylose and talcum powder	The rate of degradation of the films were accelerated after leaching of the additives out from the films	Yasin <i>et al.</i> , 1999
	PLA, PEG	A change in the rate of weight loss of the films was observed after rapid dissolution of PEG and hydrolysis of PLA	Renard <i>et al.</i> , 2003
P(3HO)	Monoacrylate–poly(ethylene glycol)-grafted poly(3-hydroxyoctonate) (PEGMA-g-PHO)	The hydrolytic degradation of the blends was dependent on the number of PEGMA groups on the P(3HO) chain, with an increase in the concentration of the PEGMA group, the degradation rate increased	Kim <i>et al.</i> , 2005

### 1.8.2 *In vivo* degradation

The host reaction to an implant/biomaterial is often dependent on the degradation products released by the biomaterial. Several biologically active species such as enzymes and lipids are known to influence the degradation kinetics of the biomaterial after implantation. The physicochemical characteristics of the biomaterial may also trigger the inflammatory system thus creating an aggressive environment for the biomaterial. Often, the *in vivo* degradation of an implant is governed by the enzymatic action of the phagocytic cells (Ali *et al.*, 1994). In response to the degradation products the host body releases either pro- or anti-inflammatory mediators, which can cause initial acute inflammation, which is followed by a chronic inflammation and possible ultimate rejection of the biomaterial. *In vivo* degradation rates of various PHAs and the animal models used are summarised in Table 8. Malm *et al.*, have shown that P(3HB) degrades at a much slower rate *in vivo* when compared to other polylactides such as poly(D,L lactic acid) PDLLA and poly(L-lactic acid) PLLA. It was also observed that these films were completely absorbed *in vivo* in 24 to 30 months, where a reduction in the crystallinity was observed at 4 weeks with a steady reduction in the Young's modulus and microhardness (Malm *et al.*, 1992). Similarly Williams *et al.*, observed that mcl-PHAs such as poly(3-hydroxyoctanoate-co-3-hydroxyhexanoate) P(3HO-co-3HHx), when implanted subcutaneously as films in mice, led to a reduction in the molecular weight from 137,000Da to 65,000Da over a period of 40 weeks (Williams *et al.*, 1999).

Table 8: - Summary of the *in vivo* degradation characteristics of PHAs

Types of PHA	site of implantation for the study of <i>in vivo</i> degradation	Degradation results	References
P(3HB)	Tibial osteotomies of rabbits	Complete degradation after 6 months of implantation	Vainionpää <i>et al.</i> , 1986
	Intermedullary region of sheep	Slight reduction in the hardness after 24 months of implantation	Herold <i>et al.</i> , 2002
	Mandibular region of rats	Complete degradation after 6 months	Kostopoulous <i>et al.</i> , 1994
	Condyles of rabbits	Degradation until 6 months of implantation	Luklinska <i>et al.</i> , 1997
P(3HB-co-HV)	Subfascial region of sheep	Complete resorption after 3 months	Sadowski <i>et al.</i> , 1998
	Rabbits (subcutaneous)	4 mol% reduction- 5 months	Jones <i>et al.</i> , 2000
P(3HB-co-10% 4HB)	Rats (Intraperitoneal)	80 mol% reduction-4 months	Sudesh <i>et al.</i> , 2000
	Rats (subcutaneous)	55 mol% reduction-1 year	Ishikawa <i>et al.</i> , 1996
P(3H0-co-3HHx)	Mice (subcutaneous)	30 mol% reduction -6 months	Marois <i>et al.</i> , 1999

### 1.8.3 Biocompatibility

#### 1.8.3.1 Biocompatibility of PHAs

Biocompatibility of an implant or biomaterial is an important factor in tissue engineering. The purity of the biomaterial, the shape, size of the implant and the chemical nature can affect the biocompatibility. Biocompatibilities of PHAs are also affected by factors like the porosity, surface hydrophilicity and the surface energy of the material (Zhao *et al.*, 2003). The natural occurrence of the PHA degradation products in the human body is the primary reason for the lack of toxicity (Williams *et al.*, 1999). 3-hydroxybutyric acid is a natural/common metabolite that is found in all higher living beings at concentrations of 3-10 mg per 100 mL (Hocking *et al.*, 2004). It has also been used as an irrigation solution after an ocular surgery. Several toxicity tests done on P(3HB) have revealed that it can be safely administered subcutaneously, intravenously and intraperitoneally. Histocompatibility tests and *in vivo* studies have revealed minimal inflammatory reactions. The degradation product of P(4HB), 4-hydroxybutyric acid, is a natural constituent found in human brain, lung, liver, kidney and muscle. After a series of cytotoxicity, sensitization, intracutaneous activity and haemocompatibility tests, the FDA proved that P(4HB) is non toxic and biocompatible (Nelson *et al.*, 1981). Owing to this, PHAs have been used for a number of biomedical applications such as wound management, orthopaedics, drug delivery and vascular system applications (Williams *et al.*, 1999; Chen *et al.*, 2005; Pouton *et al.*, 1996 and Sodian *et al.*, 2000b).

Several cell lines such as osteoblasts, fibroblasts and chondrocytes have been used to study the biocompatibility of P(3HB). These studies have proven excellent biocompatibility and lack of toxicity of P(3HB) towards these cell lines (Kose *et al.*, 2003). For example Shishatskaya *et al.*, studied the effect of P(3HB) microspheres on the cell morphology and viability of mouse fibroblast cells. From this study it was concluded that the cell proliferation rate, cell viability and the morphological changes remained unaffected, thus proving that the microspheres were highly biocompatible (Shishatskaya *et al.*, 2004). Similarly, the *in vitro* biocompatibility of P(3HB-co-3HV) has also been tested using several cell lines. For example the effect on the growth of fibroblasts and its cytotoxicity was studied by Chaput *et al.*, It was

observed that with the increase in the HV content a slight cytotoxic effect was recorded. Other researchers like Rivard *et al.*, observed no characteristic change in the morphology or cell proliferation of cell lines like osteoblasts and fibroblasts when grown on P(3HB-HV) films (Rivard *et al.*, 1995).

Several attempts have also been made to improve the biocompatibility of the PHA implants. Kai *et al.*, showed that the introduction of P(3HHx) in the P(3HB-co-3HHx) blend had improved the biocompatibility of the blend. Due to the low degree of crystallization of the blend, less stress due to the molecular chain arrangement was produced. Thus a fairly regular and smooth surface with small pores was formed for the blend. This surface morphology had provided a regular surface for the cells to attach and grow (Kai *et al.*, 2002). The P(3HB) films however were more irregular and had a lesser surface area for the cells to attach (Kai *et al.*, 2002). Researchers like Wei *et al.*, have synthesised novel polyesters such as P(3HB-4HB-3HHx) from *Aeromonas hydrophila*. These authors observed that this novel polyester had exhibited a high biocompatibility when compared to poly(L-lactic acid) (PLLA) or P(3HB-co-3HHx) films. The 3HHx content in the films had remarkably reduced the crystallinity of the film. This change in the crystallinity of the films had affected the surface physicochemical properties of the film. Similarly, the increase of 4HB content also contributed to the surface roughness and hydrophilicity of the film. Therefore, the increased hydrophilicity, reduced crystallinity and increased surface roughness had contributed to the better attachment of the human mesenchymal cell (MSC) and increased the proliferation rate when compared to the tissue culture plate (TCP) (Wei *et al.*, 2008). A sample of the different *in vitro* cell culture studies carried out using a number of cell lines have been listed in Table 9.

Table 9: - *In vitro* cell culture studies carried out on some PHAs using various cell lines.

Type of application	Cell lines used for <i>in vitro</i> studies	Observations	References
P(3HB) microspheres	Mouse fibroblast cells (L929)	Cell proliferation rate, cell viability and the morphological changes remained unaffected therefore proving that the microspheres were highly biocompatible	Shishatskaya <i>et al.</i> , 2007
P(3HB) films (treated with lipase)	Mouse fibroblast cells (L929)	Better adherence when compared to untreated films	Wang <i>et al.</i> , 2005
P(3HB) films (treated with ammonia and fibronectin coating)		Due to an appropriate balance maintained between the hydrophobic and hydrophilic surface properties, an increasing protein adsorption and cell adhesion was observed	Wang <i>et al.</i> , 2003
Blends of P(3HB-co-4HB)/P(3HB-co-3HHx) as films	Rabbit chondrocytes	The blend showed a fairly rough surface (average roughness 0.8 $\mu\text{m}$ ). Other factors that contributed to the cell attachment was the surface charge, where the higher concentration of the polar component had increased the fibronectin adsorption	Luo <i>et al.</i> , 2009
Films of P(3HB-co-3HV)	Human retinal pigment epithelial cells	Cell proliferation and good cell spreading observed.	Tezcaner <i>et al.</i> , 2003
P(3HO)Films	Chinese hamster ovary cells (CHO)	Plasma treatment was carried out to surface modify the P(3HO) films. The surface modified P(3HO) films exhibited increased hydrophilicity and an improved cell attachment	Kim <i>et al.</i> , 2002
Films of (P(3HB-co-3HV-co-4HB)	Mesenchymal stem cells (MSC)	Higher surface roughness, hydrophobicity had rendered it suitable for cell differentiation and cell proliferation into osteoblasts	Wei <i>et al.</i> , 2008
Films of P(3HB-co-3HHx)	Human Bone marrow	Exhibited good biocompatibility and cells differentiated into osteoblasts	Yang <i>et al.</i> , 2004

Unverdorben *et al.*, observed mild inflammatory reactions when P(3HB) stents were implanted *in vivo*. P(3HB-co-3HV) films have been surface functionalised to promote biocompatibility by inducing cell adhesion and proliferation. Several methods such as grafting polymethacrylic acid (PMMA) or  $\gamma$  radiation on P(3HB-co-3HV) films have been attempted to improve cell adhesion on the films (Tesema *et al.*, 2004). *In vivo* biocompatibility of mcl-PHAs such as P(3HO-co-3HHx) in the form of tubes, microspheres and pellets have been studied by Williams *et al.*, 2005. These implants like the scl-PHAs also showed mild inflammatory response with the formation of a fibrous capsule around the samples. The samples showed no evidence of macrophages and the tissue response continued to be mild even after 40 weeks of implantation. Histological analysis revealed a thin layer of fibroblasts surrounded by collagen on the polymer samples (Williams *et al.*, 2005). Blends of P(3HB-co-3HHx) and polyethylene glycol (PEG) with different weight ratios such as 1:1 and 1:5 have been implanted subcutaneously in rabbits. Although, this polymer appeared to be non cytotoxic, the degradation product of the polymer accelerated due to the presence of PEG which induced a strong tissue response involving the presence of lymphocytes, eosinophils and vascularisation (Qua *et al.*, 2006). In contrast, P(3HB-co-HHx) shows good biocompatibility, with a gradual degradation rate of only 10% weight loss after six months of implantation. There were no neutrophils observed in the fibrous capsule surrounding the polymer sample thus indicating that the tested materials were non-cytotoxic (Qua *et al.*, 2006). A summary of some of the *in vivo* cell culture studies carried out on some PHAs using various cell lines are represented in Table 10.

**Table10: - *In vivo* cell culture studies carried out using different structures of P(3HB) at various sites of implantation.**

Type of application	Site of implantation	Observations	References
P(3HB) microspheres	Intramuscular injection in Wistar rats	An inflammatory response was observed during the first 24 hours of injection. A thin fibrous capsule formation at the interface of the microspheres and the tissue is formed- after 2 weeks of implantation,	Shishatskaya <i>et al.</i> , 2007
P(3HB) compressed tablets	Subcutaneous implantation in rat neck folds	Neutrophil granulocytes changed to lymphocytes after implantation, without any formation of a necrotic tissue after 20 weeks of implantation	Korsatko <i>et al.</i> , 1987
P(3HB) microspheres encapsulating anti-tumor drug rubomycin	Injected in mice with ascetic Ehrlich carcinoma	Drug released at a controlled rate had significantly inhibited the proliferative activity of cancer cells and improved the cell survival of mice	Shishatskaya <i>et al.</i> , 2007
P(3HB) microspheres encapsulating the drug 2', 3'-diacyl-5-fluoro-2'-deoxyuridine	intraperitoneal injection in mice with P388 leukemia	Higher antitumor effects were observed for a period of 5 consecutive days. The polymer microspheres also showed low toxicity and good biocompatibility	Kawaguchi <i>et al.</i> , 1992
P(3HB) patches	Pericardial patches in sheep	Minimal inflammatory response where only a small number of lymphocytes were produced. A dense collagen layer was seen on the patch, which was comparable to that of the native pericardium	Malm <i>et al.</i> , 1992a
P(3HB) films	Subcutaneously implanted in mice for a period of 12 weeks	During 4-6 weeks of implantation the thickness of the fibrous capsule was reduced from 200 $\mu\text{m}$ to 60 $\mu\text{m}$ . At 48 weeks, the capsule formation around the implant was minimal with no mono and polynuclear macrophages seen	Volova <i>et al.</i> , 2003
P(3HB-co-3HV) rods incorporated with drugs such as Sublactam and Cefoperazone	Implanted in rat tibia	A limited necrotic area was observed around the implant at 15 days of incubation. Disappearance of initial inflammatory reaction around the implant was observed after 30 days.	Yagmurlu <i>et al.</i> , 1999

### 1.8.3.2 Biocompatibility of Composite scaffolds

*In vitro* biocompatibility tests of inorganic/organic composite scaffolds such as glass-ceramics and biodegradable polymers have also been carried out. In a study conducted by Bretcanu *et al.*, the *in vitro* biocompatibility of 45S5Bioglass<sup>®</sup> scaffolds coated with a P(3HB) were tested using a human osteosarcoma cell line (HOS-TE85). The biocompatibility tests done revealed that the HOS cells are seen to adhere and spread on the polymer coated scaffolds. A higher number of cells were also observed on the polymer coated scaffolds when compared to the uncoated scaffolds after a period of 7 days in the cell culture media. This study further confirmed that 45S5Bioglass<sup>®</sup>/P(3HB) scaffolds have potential as osteoconductive tissue engineering substrates (Bretcanu *et al.*, 2009). *In vivo* studies using cylindrical specimens of P(3HB-co-3HV)/HA composites were carried out in rabbit tibias. After one month of implantation a well developed lamellar bone structure around the implant surface was observed. In this study it was observed that HA not only had the ability to bond with the surrounding tissue but it also provided the adequate support for cell growth and was tolerant towards the new tissue formation (Luklinska *et al.*, 2003). The *in vivo* biocompatibility and anti-microbial activity of bioactive glasses (BG) with a composition of  $(\text{SiO}_2)_{0.80} (\text{P}_2\text{O}_5)_{0.04} (\text{CaO})_{0.16}$  loaded with tetracycline was investigated. The histological analysis of the samples after implantation for the first 6h did not reveal any reaction. After 24h polymorphonuclear cells were observed around the bioactive glasses with a composition of  $(\text{SiO}_2)_{0.80} (\text{P}_2\text{O}_5)_{0.04} (\text{CaO})_{0.16}$  scaffolds loaded with tetracycline. However, after 72h, an acute inflammatory reaction was observed which was characterized as moderate in intensity (Domingues *et al.*, 2004). In another study, porous P(3HB-co-3HV) and calcium phosphate-loaded collagen (CaP-Gelfix) foams were tested for their *in vivo* bone formation capacity and their suitability for use in bone tissue engineering. The composite scaffolds were seeded with rat bone marrow stromal cells and implanted into defects created in rat femurs. Although some initial inflammation was observed in the CaP-Gelfix group, minimal inflammation was observed at all stages. Histological examination revealed higher fibrous connective tissue formation and in the CaP-Gelfix group when compared with the P(3HB-co-3HV) samples (Kose *et al.*, 2004). In a study conducted by Misra *et al.*, porous P(3HB) foams impregnated with 10 wt% of 45S5Bioglass<sup>®</sup> particles

were fabricated and tested for their *in vitro* and *in vivo* bioactivity. The P(3HB)/BG foams exhibited a high level of total protein adsorption which was a 1000 $\mu$ g when compared to 800 $\mu$ g of P(3HB) scaffolds on their own. The porous microstructure of the composite foams was also found to be suitable for MG-63 cell attachment and proliferation. The composite foams when implanted subcutaneously in rats did not exhibit any foreign body reaction after one week of implantation, thereby proving to be non-toxic as well as biocompatible (Misra *et al.*, 2010). In another study conducted by Misra *et al.*, the effects of introducing micro (m-BG) and nanoscale (n-BG) bioactive glass particles on the biocompatibility of P(3HB)/bioactive glass composite systems were investigated. In this study the presence of n-BG particles improved the surface nanotopography which had considerably improved the total protein adsorption on the n-BG composites compared to the unfilled polymer and the m-BG composites. A cell proliferation study using MG-63 cells demonstrated the good biocompatibility of both types of P(3HB)/45S5Bioglass<sup>®</sup> glass composite where an increase in cell proliferation during the 7 day period, in tandem with the trend for the tissue culture plastic used as a control was observed (Misra *et al.*, 2008).

## 1.9 Aims and Objectives of the present project

The aim of this research project was to use lipopolysacchride (LPS) free P(3HB) isolated from Gram-positive bacteria, *Bacillus cereus* SPV, in combination with the bioactive ceramic 45S5Bioglass<sup>®</sup> for various biomedical applications including drug delivery, bone TE and wound healing. A schematic representation of the research strategy used for this project is represented in Figure 2

The specific objectives to fulfil the above aims include

**1.9.1 Large scale production of LPS-free P(3HB)** - Production of LPS-free P(3HB) using *acillus cereus* SPV, in a 20L scale fermentation. LPS present on the outer layer or membrane of Gram-negative bacteria act as endotoxins thereby inducing a severe immunogenic reaction when in contact with blood. These endotoxins are known to contaminate the PHA during the recovery/extraction of PHAs.

**1.9.2 Production of P(3HB) microspheres** - A solid-in-oil-water (s/o/w) technique will be used in an attempt to produce tailored poly(3-hydroxybutyrate) P(3HB) microspheres. The effects of different parameters used for microsphere production on the microsphere size, porosity and drug distribution will be investigated. Following optimization, the microspheres will be characterised using Scanning Electron Microscopy; SEM, thermal properties using Differential Scanning Calorimetry; DSC, particle size distribution using particle size analyser.

**1.9.3 Application of the P(3HB) microspheres in drug delivery** -The P(3HB) microspheres will also be encapsulated with drugs gentamicin and tetracycline to be used for potential drug delivery purposes. The microspheres will also be used to produce structures with various morphologies such as microsphere films and their *in vitro* drug release rate monitored.

**1.9.4 Use of polymer as drug delivery agents in polymer/composite scaffolds** -3D composite scaffolds will be made using P(3HB) and 45S5Bioglass<sup>®</sup> to form scaffolds for combined application in hard tissue regeneration and drug delivery. P(3HB)/45S5Bioglass<sup>®</sup> composite microsphere films will also be prepared with nanoscale bioactive glass particles (n-BG) for potential wound healing applications. The effect of the n-BG particles on the thermal and biocompatible properties of the composite

microsphere films will be investigated. In addition, the effect of the n-BG particles on the bioactivity as well as its haemostatic efficacy for applications in wound healing will be examined. The polymer/composite scaffolds will be analysed for their microstructural properties using Scanning Electron Microscopy, SEM, thermal properties using Differential Scanning Calorimetry; DSC, mechanical properties using Compressive strength Analysis, and X-Ray Diffraction; XRD.

#### **1.9.5 Determination of the *in vitro* biocompatibility and bioactivity of the drug**

**delivery constructs and scaffolds** -Biocompatibility of the drug delivery constructs will be carried out using HaCaT and MG-63 cell lines and the bioactivity of the 3D scaffolds will be measured *in vitro* using SBF.s

**1.9.6 Application of the P(3HB) microspheres in protein delivery** - P(3HB) microspheres for protein delivery will be investigated. In this study three different proteins, bovine serum albumin (BSA), Lucentis<sup>®</sup> and ribonucleic acid (RNase A) will be encapsulated within P(3HB) microspheres and their *in vitro* drug release rate monitored. P(3HB) microspheres encapsulated with BSA and Lucentis<sup>®</sup> will be used as drug delivery vehicles for the intraocular environment. RNase A has the same molecular weight as the functional agents such as bone morphogenic proteins (BMP-2) which is useful for inducing the formation of bone and cartilage. Thus the results obtained from the RNase A study can later be extrapolated to BMP-2. RNaseA activity and structural integrity of all the proteins during the encapsulation process will be investigated.

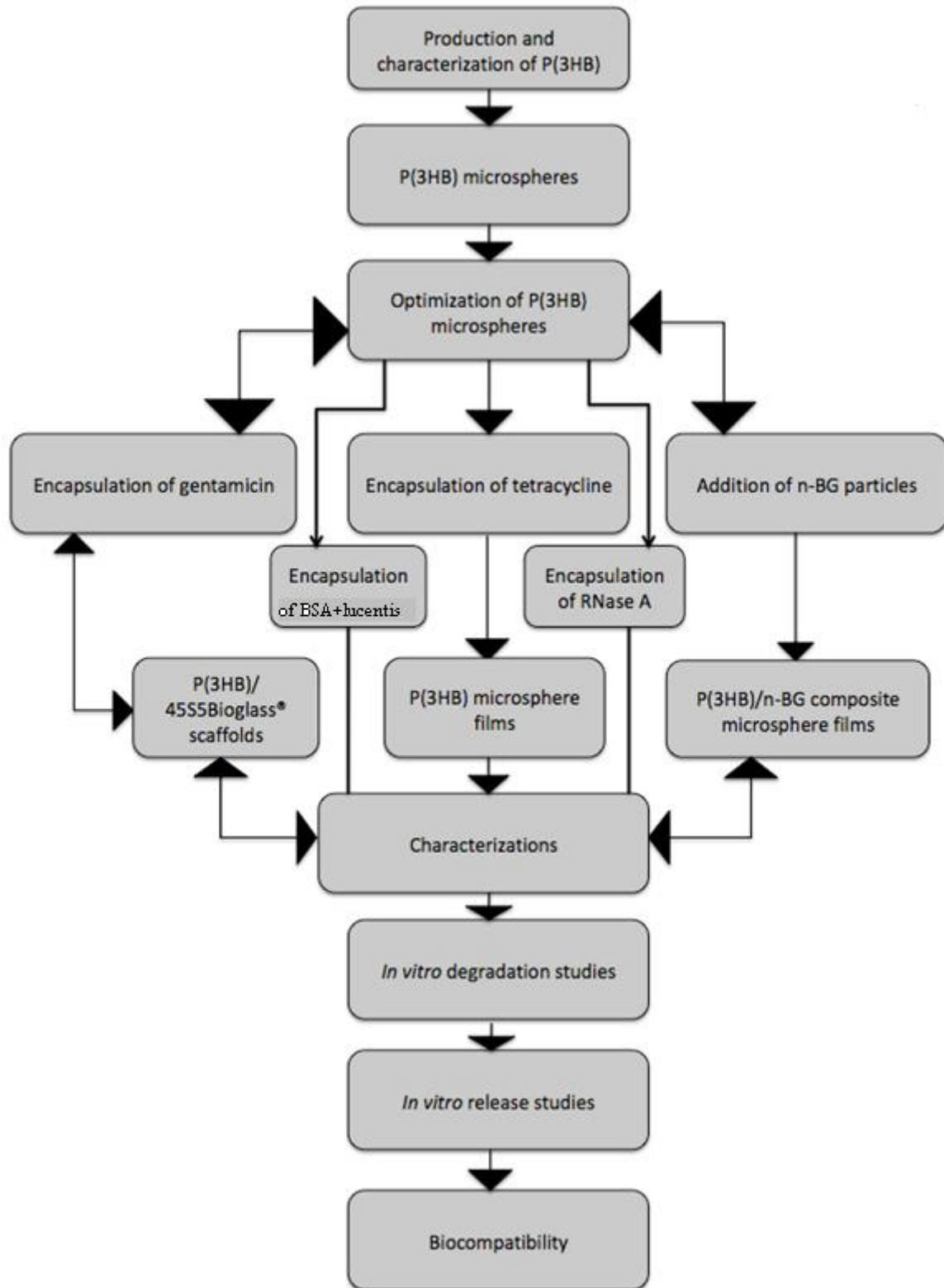


Figure 2:- Schematic representation of the research strategy used for this project.

# Chapter 2

## Materials and Methods

## 2.1 Materials

### 2.1.1 Water

Distilled and (high performance liquid chromatography) HPLC grade water were used where appropriate. The two types of water used for P(3HB) microsphere production and drug quantification were obtained from Elga Pure Lab Options distillation units.

### 2.1.2 Chemicals

All the chemicals, buffers and drugs used were purchased from Sigma-Aldrich, (Dorset UK). Care was taken to make sure that the chemicals used were of the best grade available (analytical or HPLC where appropriate) for the experiment.

### 2.1.3 Proteins

The broad range protein molecular weight marker and ribonuclease A (pancreatic RNase A) was purchased from Promega, UK. Bovine serum albumin fraction V (BSA) used in the bicinchoninic acid (BCA) assay was purchased from Sigma-Aldrich, (Dorset UK). Lucentis<sup>®</sup> (Ranibizumab 10mg/mL) was purchased from Novartis Europharm Ltd, U.K.

### 2.1.4 Plasmid

The green fluorescent protein (GFP) containing plasmid (pTP6) used to transfect the MG63 osteoblast cells were obtained from Dr. Mark Clements, University of Westminster, London.

### 2.1.5 45S5Bioglass<sup>®</sup> and Nanobioglass (n-BG) particles

The melt-derived 45S5Bioglass<sup>®</sup> powder (particle size ~10–20  $\mu\text{m}$ ) purchased from NovaMin Technology Inc. (Florida, USA) was obtained from Professor Boccaccini, Department of Materials Science, Erlangen, Germany. The composition of 45S5Bioglass<sup>®</sup> is 45 wt.%  $\text{SiO}_2$ , 24.5 wt.%  $\text{Na}_2\text{O}$ , 24.5 wt.%  $\text{CaO}$  and 6 wt.%  $\text{P}_2\text{O}_5$  (Hench *et al.*, 1998a). Flame spray synthesis used to prepare nanobioglass particles (n-BG) and this was also obtained from Prof Boccaccini, Department of Materials Science, Erlangen, Germany. The composition of n-BG particles is 46.08 wt%  $\text{SiO}_2$ , 22.96 wt%  $\text{Na}_2\text{O}$ , 27.18 wt %  $\text{CaO}$  and 3.77 wt%  $\text{P}_2\text{O}_5$ .

## 2.1.6 Buffers and Reagents

### 2.1.6.1 Buffers for SDS-PAGE

#### *2.1.6.1.1 2X sample buffer for sodium dodecyl sulphate-Polyacrylamide gel electrophoresis (SDS-PAGE)*

The components are 0.125 M Tris-HCl, pH 6.8, 15% glycerol (v/v), 6% SDS, and 0.005% bromophenol blue. 50  $\mu$ L of  $\beta$ -mercaptoethanol was added to 1 mL of sample loading buffer.

#### *2.1.6.1.2 Resolving gel buffer*

The components are 1.5 M Tris-HCl, 0.4% SDS, (No pH adjustment was required).

#### *2.1.6.1.3 Stacking gel buffer*

The components are 0.5 M Tris-HCl, 0.4% SDS

#### *2.1.6.1.4 5X Reservoir Buffer*

The components are Tris Base 15g, 72g glycine, 5g SDS (g/L)

#### *2.1.6.1.5 Protein fixing solution (for fixing proteins following SDS-PAGE)*

Methanol (HPLC grade), acetic acid (100%) and water mixed in the ratio 5:1:4 respectively.

#### *2.1.6.1.6 Coomassie brilliant blue stain (for staining SDS-PAGE gels)*

0.025% Brilliant Blue R stain dissolved in 10 mL acetic acid (100%) and 90 mL water.

#### *2.1.6.1.7 Destaining solution (for destaining SDS-PAGE)*

10% acetic acid (100%) in water.

#### *2.1.6.1.8 5X TBE, pH 8.0, (g/L)*

The components are Tris Base 54, Boric acid 27.5, EDTA 4.5

### 2.1.6.2 Reagents used for preparation of simulated body fluid (SBF)

The components are ultra pure water 1500 mL, sodium chloride 15.92g, sodium bicarbonate, 0.72g; potassium chloride, 0.44g; potassium phosphate dibasic trihydrate 0.45g; magnesium chloride hexahydrate, 0.61g; calcium chloride, 0.55g; sodium sulphate, 0.142g; TRIZMA<sup>®</sup> base, 12.11g; hydrochloric acid-appropriate amount to adjust the pH to 7.25.

### 2.1.6.3 Reagents used for the *in vitro* drug release and *in vitro* degradation studies

#### 2.1.6.3.1 Contact lens solution

Bausch and Lomb, Multi-purpose contact lens solution, Kingston upon-Thames UK was used for the *in vitro* drug release studies.

#### 2.1.6.3.2 Phosphate buffered saline solution (PBS)

Phosphate buffered saline solution (PBS) purchased from Sigma-Aldrich, (Dorset UK) was used for the *in vitro* drug release studies. The pH of the reagents used for the *in vitro* drug release and *in vitro* degradation studies is shown in Table 1.

**Table 1:- pH of the reagents used for the *in vitro* drug release and *in vitro* degradation studies.**

Reagents	pH
Contact Lens solution	7.17
Phosphate buffered saline solution (PBS)	7.4

### 2.1.7 Cell line and cell culture materials

The human keratinocyte cell line (HaCaT) was obtained from Dr. I. C. Locke, University of Westminster London, UK. MG63 human osteosarcoma cell line for *in vitro* cell culture studies on 45S5Bioglass<sup>®</sup> samples were obtained from Dr. Mark Clements, University of Westminster London, UK. All chemicals, reagents, buffers and dyes for cell culture were purchased from Sigma-Aldrich (Poole, U.K) and VWR International (Poole, U.K) unless otherwise specified. Cell culture media components were purchased from Invitrogen LTD

(Paisley, U.K) and foetal calf serum (FCS) was purchased from Biosera LTD (Ringmer, U.K). Cell culture flasks were purchased from BD Biosciences (Oxford, UK) and penicillin and streptomycin was purchased from Invitrogen (Paisley, UK).

#### 2.1.8 Bacterial cultures

P(3HB) was isolated from the Gram-positive bacteria *Bacillus cereus* SPV which was obtained from the culture collection of University of Westminster, London, U.K. All chemicals required for the growth of *Bacillus cereus* SPV and extraction of polymer from the bacterial cells were obtained from Sigma-Aldrich Company Ltd. and VWR Chemicals (England) except for nutrient broth and yeast extract, which was obtained from DIFCO (BD UK Ltd., Oxford, UK). Antifoam (FG-10) was purchased from Dow corning (Edison, NJ, USA) for fermentation study.

##### 2.1.8.1 Bacterial strains and its maintenance

The *Bacillus cereus* SPV cells obtained from the culture collection (-80 °C) were grown in an incubator (New Brunswick Scientific C25KC incubator shaker, USA) at 30°C for 24h in 30 mL of sterile nutrient broth. This 24h grown culture was then streaked on sterile nutrient agar plates (30 mL of sterile nutrient agar solution on petri-plates) in order to obtain single bacterial colonies. The plates were incubated for 48h at 30°C and then stored at 4°C. Glycerol (acting as a cyro-preservant) deeps of the culture were also prepared for long-term storage by adding 500µL of the 24h grown culture and 500µL of sterile 40% glycerol. The mixture was vortexed and stored in 1.5 mL eppendorfs at -20°C for further use (Valappil *et al.*, 2007).

##### 2.1.8.2 Growth media

The components of the nutrient broth are 1.0 g/L; yeast extract, 2.0 g/L; peptone, 5.0 g/L; sodium chloride, 5.0 g/L and maintained at 4 °C after growth on nutrient agar: yeast extract, 2.0 g/L; peptone, 5.0 g/L sodium chloride, 5.0 g/L; agar, 15.0 g/L. The production medium, glucose, 20 g/L; Difco yeast extract, 2.5 g/L; potassium chloride, 3 g/L; ammonium sulphate, 5.0 g/L; 100mL of defatted soyabean dialysate (prepared from 10g of defatted soyabean meal in 1000mL of distilled water for 24h at 4°C) was used.

## 2.2 Experimental Methods

### 2.2.1 Production of P(3HB)

P(3HB) production was carried out in 20 L fermentor with a 14 L working volume using *Bacillus cereus* SPV. The inoculum (1.4 L) culture was prepared using a single bacterial colony obtained from a nutrient agar plate. This was incubated at 30°C for 24h on a rotary shaker at 250 rpm. The fermentors containing only the salts of the production medium were sterilized separately without the addition of glucose and soyabean dialysate. Glucose and soyabean dialysate sterilized separately were added to the fermentor along with the inoculum. The pH of the medium was adjusted to 6.8 using 1N NaOH. The dissolved oxygen tension (DOT) was set to 100% air saturation at the beginning of the run. The pH, DOT, glucose concentration and optical cell density were monitored throughout the run. The impeller speed was maintained at 250 rpm (revolutions per minute), airflow rate at 1.0 vvm (volumetric air flow rate) and at a temperature of 30°C.

#### 2.2.1.2 Optical Density (OD)

OD of the culture was recorded at different time points, in order to measure the bacterial growth. OD readings were taken at 600 nm (absorbance) in a standard spectrophotometer (Novaspec II visible spectrophotometer, UK) and for all cases nutrient broth was used as blank. The optimal OD of 1.3 nm was used for inoculating in the production medium.

#### 2.2.1.3 Temperature, pH and dissolved oxygen tension (DOT)

Temperature and DOT levels were monitored online using the temperature and DOT probes (polarographic oxygen-sensing probe (Inglold, Metler-Toledo Ltd., Beaumont Leys, Leicester, UK) which were connected to the fermentor vessel. The pH of the production medium was measured offline (Jenway pH meter 3305, UK) by collecting samples from the fermentor at regular intervals.

#### 2.2.1.4 Dry cell weight (dcw) analysis

15 mL of the culture from the fermentation run were taken at different time points to measure the dry cell weight. The culture was centrifuged at 4500 rpm for 10 mins and the cells were freeze-dried before recording the cell mass.

#### 2.2.1.5 Polymer extraction techniques

The bacterial cells were harvested from the culture by centrifugation and stored at -80°C for 24h. The frozen cells were then lyophilised (Savant Modulyo D Freeze drier, Thermo electron Corp, UK) for up to 48h in a freeze drier at -47°C and at a pressure of 133 mbar. The freeze-dried cells were then weighed and designated as dry cell weight (dcw). Subsequently, the polymer was extracted from the cells by using the chloroform-hypochlorite dispersion method as mentioned below.

##### 2.2.1.5.1 *The extraction of P(3HB) using chloroform-hypochlorite dispersion method*

A dispersion solution containing 50 mL of chloroform and 50 mL of diluted (30%) sodium hypochlorite solution in water was used to extract P(3HB) from the freeze-dried cells. The freeze-dried cells (1g) were added to the dispersion solution and treated at 37°C for 1h in an orbital shaker at 100 rpm. Three different phases were obtained from the solution containing the mixture after it was centrifuged at 3680g for 10 minutes. P(3HB) present in the bottom phase of the mixture was extracted by precipitation in 10 volumes of ice-cold methanol (Vallappil *et al.*, 2007).

#### 2.2.2 P(3HB) microsphere production

A solid-in-oil-in-water emulsion technique was used for P(3HB) microspheres preparation. Quantities of 1 or 3 g of P(3HB) were dissolved in 8 mL of chloroform and agitated for 3 min (Table 2). This mixture was then transferred into the first water-in-oil emulsion (w/o) of 40 mL of 1% or 0.5% w/v aqueous polyvinyl alcohol (PVA) solution, and stirred at 1000 rpm for 3 min. This solution was then added to a second water-in-oil-in water emulsion (w/o/w) of 500 mL of 0.5% or 0.05% w/v aqueous PVA solution, forming the second-oil-in-water emulsion. This emulsion was stirred either at 300 rpm or 800 rpm for 4h to form P(3HB) microspheres. The resulting microspheres were isolated

by centrifugation at 3680 g for 5 min and then washed with distilled water three times, air dried and stored in a desiccator until further use.

**Table 2:- The varying processing conditions (amount of surfactant, polymer concentration and stirring rate) used for the synthesis of P(3HB) microspheres.**

Samples	Polymer concentration (g/L)	PVA concentration (%)	Stirring rate (rpm)
1	1	0.5	800
2	3	0.5	300
3	1	1	300
4	3	1	800

The drug/protein loaded microspheres were also prepared using the same solid-oil-in-water emulsion technique. For this the drug/proteins were added to the first water-in-oil emulsion (w/o) of 40 mL of 1% or 0.5% w/v aqueous polyvinyl alcohol (PVA) solution and then transferred to a second water-in-oil-in water emulsion (w/o/w) of 500 mL of 0.5% or 0.05% w/v aqueous PVA solution. Following centrifugation the microspheres were lyophilised and stored at 4°C for further use. The different drugs/proteins loaded during P(3HB) microsphere production is shown in Table 3.

**Table 3:- Drugs/Proteins loaded during P(3HB) microsphere production.**

Drugs/Proteins loaded during P(3HB) microsphere production	Drug/Protein Loadings (wt%)
Gentamicin	2 wt%
Tetracycline	0.5 wt%, 2 wt%, 4 wt%
Bovine Serum Albumin (BSA)	0.75 wt%, 1.5 wt% and 5 wt%
Lucentis <sup>®</sup>	5 wt%
Ribonucleic Acid A (RNase A)	50 wt%

### 2.2.2.1 Production of P(3HB) microspheres including nanobioglass (n/BG) particles

10 wt% of n-BG particles were added to the polymer solution to yield P(3HB)/n-BG composite microsphere films. This mixture was further sonicated for 1-2 min (Ultrasonic Homogenizers US200, Phillip Harris Scientific, UK) to improve the dispersion of the n-BG particles by disaggregating possible agglomerations. The P(3HB)/n-BG was then transferred into 40 mL of 1% w/v aqueous polyvinyl alcohol (PVA) solution, and stirred at 800 rpm for 3 minutes. This solution was then added to 500 mL of 0.5% w/v aqueous PVA solution, forming the second-oil-in-water emulsion. This emulsion was stirred for 4h at the same agitation speed as before to form the P(3HB) microspheres. The resulting microspheres were isolated by centrifugation at 3680 g for 5 min and then washed with distilled water three times, air dried and stored in a desiccator until further use.

### 2.2.3 P(3HB) microsphere film preparation

0.1g of the lyophilised microspheres were uniaxially compressed to form a disc using a hydraulic hand press and a force of 0.09 MPa to the films of (diameter=12.87mm and thickness=0.87mm) had a surface area of 1.13cm<sup>2</sup> (Naraharisetti *et al.*, 2005). P(3HB) microsphere (0.1g) loaded with 0.5 wt%, 2 wt% and 4 wt% of tetracycline was uniaxially compressed to form a disc. Similarly 0.1g of the lyophilised microspheres with the n-BG particles were uniaxially compressed to form a disc using the same protocol.

### 2.2.4 45S5Bioglass<sup>®</sup> scaffold production and coating with P(3HB) microspheres

45S5Bioglass<sup>®</sup>-based glass-ceramic scaffolds were produced by the foam replica technique introduced in a previous investigation (Chen *et al.*, 2006). Briefly, a PU foam cut to the desired size (the size of the foam determines the final dimensions of the scaffold)-nominally 10 x 10 x 10 mm<sup>3</sup> was immersed in a well-mixed 45S5Bioglass<sup>®</sup> slurry made by dissolving 45S5Bioglass<sup>®</sup> powder in poly (DL-lactic acid)-dimethyl carbonate solution, which consequently infiltrated the foam structure. Glass particles adhered to the surfaces of the polymer foam. The coated foam is normally squeezed vigorously after it has been taken out of the slurry to give a reasonably homogeneous coating (assessed by visual inspection). The foams were then dried under a fume hood in

air at room temperature for at least 12h. Finally the foams were sintered using an optimized heat treatment programme to eliminate the sacrificial PU template and to densify the struts. In this project, the polymer was slowly burned out at 550°C for 3h in order to minimize the damages to the glass coating. Once the polymer was removed, the glass foam was sintered at 1100 °C for 2h. This experiment was carried at Imperial College, London with the assistance of Mr. Decheng Meng.

The sintered 45S5Bioglass<sup>®</sup> scaffolds were coated with P(3HB) microspheres by dipping the scaffolds for 2, 5 or 10 min into an aqueous slurry made with P(3HB) microspheres, and different approaches were investigated to achieve a high-quality P(3HB) microsphere coating on the scaffolds, as described below.

#### 2.2.4.1 Agitation

A 1% w/v microsphere solution was prepared using ultrapure water and agitated using a mechanical stirrer for 3h; this was followed by immersing the 45S5Bioglass<sup>®</sup> scaffold in the slurry with the help of a copper wire gently entwined in the pores of the scaffold. The coated scaffolds were then removed and allowed to air dry in desiccators at room temperature.

#### 2.2.4.2 Sonication

The 1% and 3% w/v microsphere slurries in water were sonicated using a USC300D VWR ultrasonic for 2, 5 and 10 mins to improve the dispersion of the microspheres by separating possible microsphere agglomerations. This was followed by immersing the 45S5Bioglass<sup>®</sup> scaffold in the slurry with the help of a copper wire gently entwined in the pores of the scaffold. The coated scaffolds were then removed and allowed to air dry in desiccators at room temperature.

#### 2.2.4.3 Immersion of the scaffold in the aqueous PVA solution

In an alternative approach, the scaffolds were immersed in the PVA solution during microsphere preparation. It was anticipated that the microspheres, while settling down, could penetrate through the scaffold pores and crevices, thoroughly coating the scaffold.

### 2.2.5 Coating of 45S5Bioglass<sup>®</sup> scaffolds with gentamicin-loaded P(3HB) microspheres

To coat the 45S5Bioglass<sup>®</sup> scaffolds with gentamicin-loaded P(3HB) microspheres, a slurry of the drug-loaded microspheres was made using the highly non-polar solvent, hexane, because gentamicin, being hydrophilic, would diffuse into the water phase if an aqueous slurry was used. The coating was obtained by adding the microsphere slurry drops onto the scaffold using a pipette (1 mL of the suspension for every 0.05g of the scaffold).

### 2.2.6 Gentamicin loading in the 45S5Bioglass<sup>®</sup> scaffold

In an attempt to incorporate the drug directly onto the scaffold for the purpose of comparison, gentamicin solution at a concentration of 2 mg/mg was added drop wise to the 45S5Bioglass<sup>®</sup> scaffolds (5x5x10 mm<sup>3</sup>) using a pipette. The scaffolds were weighed before and after the loading process and the amount of drug loaded on the sample was estimated from the weight change. Upon addition of the solution, scaffolds were left to dry at room temperature in desiccators.

## **2.3 Drug/Protein quantification methods**

### 2.3.1 Determination of the drugs (gentamicin and tetracycline) and proteins (BSA, Lucentis<sup>®</sup> and RNase A) encapsulation efficiency

The encapsulation efficiency (EE %) of the drug/protein-loaded microsphere prepared under different conditions as mentioned in section 2.2.2. was determined using equation 1.

$$EE\% = \frac{\text{experimental drug loading}}{\text{actual drug loading}} \dots\dots\dots (1)$$

To determine the EE values, 5mg of the drug/protein loaded microspheres were dissolved in 1mL of chloroform, to which 5mL of water was added after the microspheres were well dissolved. Drugs and proteins used in this study being hydrophilic in nature, separated into the water phase on vortexing. The water phase was then analysed for the

drug content using liquid chromatography-mass spectrometry (LC-MS) and the proteins in the aqueous phase was then quantified using the bicinchoninic acid (BCA assay) after centrifugation.

### 2.3.2 Liquid Chromatography Mass Spectrometry (LC-MS)

Liquid Chromatography Mass Spectrometry (LC-MS) was used for analysing the drug content from the release buffer. 15  $\mu$ L samples collected at different time points were injected onto the HPLC column (Dionex HPLC) coupled with an atmospheric pressure (AP)-electrospray ionization (ESI) mass spectrometer (Dionex). Separation was carried out at 50°C on a reversed-phase C18 60 RP column of dimensions 250 mm x 4 mm.

#### 2.3.2.1 Mobile phase used for gentamicin quantification

The mobile phase used for gentamicin quantification was an isocratic flow of 60% pentafluoropropionic acid (20 mM in ultra-pure water from Fluka Chemicals, Buchs, Switzerland) and 40% methanol at flow rate of 0.5 mL/min. The standard curve was plotted for gentamicin concentrations ranging between 1.0 and 2000  $\mu$ g mL<sup>-1</sup>.

#### 2.3.2.2 Mobile phase used for tetracycline quantification

The mobile phase used for tetracycline quantification was an isocratic flow of a mixture of water, 5% formic acid, acetonitrile and methanol (23:40:25:12) at flow rate of 0.2 mL/min (Zhu *et al.*, 2001). The standard curve was plotted for tetracycline concentrations ranging between 1.0 and 2000  $\mu$ g/mL.

### 2.3.3 Bicinchoninic acid assay (BCA)

0.1 mL of each standard and unknown sample replicate was pipetted into labeled test tubes. To this 2.0 mL of the working reagent (50 parts of BCA Reagent A with 1 part of BCA Reagent B 50:1, Reagent A: B) was added. The tubes were covered with aluminum foil and incubated at 37°C for 30 minutes (working range = 20-2,000  $\mu$ g/mL). The tubes with the standard and samples were covered and cooled to room temperature. The total protein adsorbed was quantified using a bicinchoninic acid (BCA) reagent kit (Thermo scientific). The optical density of the samples was measured at 562nm using a standard

spectrophotometer (Novaspec II Visible spectrophotometer, UK) against a calibration curve at concentrations ranging from 1.0 and 2000 $\mu\text{g}/\text{mL}$  using bovine serum albumin (BSA), as per the manufacturer's protocol.

#### **2.4 *In vitro* drug release studies**

The *in vitro* release experiments were performed in an incubator at 37°C for different time points. Drug/protein loaded P(3HB) microspheres, microsphere-coated and 45S5Bioglass<sup>®</sup> uncoated scaffolds, were immersed in different release buffers and 1mL samples were collected at regular intervals. Each aliquot was replaced with fresh buffer and the tubes returned to the shaker. At each time point the samples were taken out in triplicates and the results averaged. The drug content was determined by injecting 15 $\mu\text{L}$  of the samples onto a high-performance liquid chromatography (HPLC) column and the gentamicin concentration quantified using the standard curve. The experiments were repeated three times. The protein concentrations in the release samples were determined by the BCA assay using the standard plot generated by the BSA standard. Thus based on the determined initial loading of the microspheres and the amount of protein detected in the release medium, the percentage of BSA release as a function of time was detected. The BCA assay does not reach a true end point as a result the colour development will continue even after cooling. Thus all tubes should be made within 10 mins, however if the rate of colour development occurs at low temperature then no error will be introduced.

A summary of the *in vitro* release studies of the different proteins and drugs are represented in the Table 4.

**Table 4:-Summary of the *in vitro* release studies of the different proteins and drugs.**

Drugs/Proteins loaded in P(3HB) microspheres, microsphere-coated and 45S5Bioglass <sup>®</sup> uncoated scaffolds	Release buffer	Time points at which samples were taken (days)
Gentamicin	SBF	1, 2, 3, 4, 7, 12, 18, 22, 26 and 30 days
Tetracycline	PBS	1, 2, 3, 4, 7, 12, 18, 22, 26 and 30 days
Bovine Serum Albumin (BSA)	PBS, Contact lens solution	1, 2, 3, 4, 7, 12, 18, 22, 26 and 30 days
Lucentis <sup>®</sup>	PBS, Contact lens solution	1, 2, 3, 4, 7, 12, 18, 22, 26 and 30, 35, 40, 45, 47, 50, 55, 57, 60, 65, 70, 75 days
Ribonucleic Acid A (RNase A)	PBS	1, 2, 3, 4, 7, 12, 18, 22, 26 and 30 days

## 2.5 *In vitro* degradation and bioactivity studies

### 2.5.1 Water uptake measurement

All the samples were weighed before immersion ( $M_{o, dry}$ ) in SBF/PBS/contact lens solution and incubated at 37°C. At specified time points such as (1, 3, 7, 14 and 30 days), the samples were collected and analysed for water uptake (%WA). For measuring the water adsorption (%WA), the immersed samples were removed, the surface gently wiped with blue roll (except for the microspheres, they were centrifuged at 3680g for 5 mins and the supernatant removed) and the weight was measured ( $M_{t, wet}$ ). Similarly the weight losses (%WL) of the samples were also calculated after drying the samples ( $M_{t, dry}$ ) at 37°C overnight in an incubator.

The water absorption and weight loss were calculated using the following equations

$$\%WA = \frac{M_{t,wet} - M_{t,dry}}{M_{t,dry}} \dots\dots\dots (2)$$

$$\%WL = \frac{(M_{0,dry} - M_{t,dry})}{M_{0,dry}} \dots\dots\dots(3)$$

( $M_{0, dry}$ ) is the weight of the samples before immersion

( $M_{t, wet}$ ) is the weight of the wet samples

( $M_{t, dry}$ ) is the weight of the samples after drying

#### 2.5.1.1 *In vitro* degradation studies carried out in simulated body fluid (SBF)

The *in vitro* degradation studies of the (P(3HB) microspheres (gentamicin loaded and unloaded), 45S5Bioglass<sup>®</sup> and P(3HB)/45S5Bioglass<sup>®</sup> composite scaffolds were carried out in simulated body fluid (SBF), which has similar ionic concentration to human blood plasma (Kokubo *et al.*, 1990; 1991). The reagents mentioned in section 2.1.6.2, were dissolved in deionised water to prepare 2L of final volume and the pH adjusted to 7.25. Freshly prepared SBF was used for all the analysis and when needed, was stored at 4°C for no more than 14 days. The samples were kept in a 37°C incubator under static conditions and at desired time points the samples were collected, gently washed with deionised water and left to dry at 37 °C in an incubator overnight for further analysis. The water uptake measurement of all the samples were carried out using the same protocol as mentioned in section 2.5.1 and the %WA and %WL of the films measured using equations 2 and 3.

#### 2.5.1.2 *In vitro* degradation studies carried out in 0.1M phosphate buffer saline solution (PBS) and contact lens solution

The *in vitro* degradation studies of the P(3HB) microsphere films (tetracycline loaded and unloaded) were performed in 0.1M PBS. Similarly the *in vitro* degradation studies of the P(3HB) microsphere loaded with BSA was carried out in 0.1M PBS as well as contact lens solution. The water uptake measurement of all the samples were carried out using the same protocol as mentioned in section 2.5.1 and the %WA and %WL of the films measured using equations 2 and 3.

### 2.5.2 In vitro bioactivity tests

*In vitro* bioactivity tests such as hydroxyapatite formation were carried out using acellular simulated body fluid (SBF) as developed by Kukubo *et al.*, 1990. The pH of SBF was adjusted to 7.25 at 37°C using HCl and it has the ionic concentrations approximately equal to those of human blood plasma (pH7.3). The reagents were dissolved in HPLC (high performance liquid chromatography) grade water. Freshly prepared SBF was used for all the analysis and when needed, was stored at 4°C for no more than 14 days. The SBF was refreshed after 48h of incubation followed by every 3 days. Hydroxyapatite is formed by the rapid exchange of Na<sup>+</sup> and ions with H<sup>+</sup> or H<sub>3</sub>O<sup>+</sup> ions from the solution. With the increase in the hydroxyl concentration formation of Si-O-Si layer occurs after the condensation and repolymerization of SiO<sub>2</sub> rich layer. Amorphous CaO and P<sub>2</sub>O<sub>5</sub> layer is formed after the adsorption of Ca<sup>2+</sup> and PO<sub>4</sub><sup>3-</sup> groups on the surface. Finally the crystallization of the CaO and P<sub>2</sub>O<sub>5</sub> layer takes place and a hydroxyapatite layer is formed.

#### 2.5.2.1 Sample preparation of the (P(3HB) and P(3HB)/n-BG composite microsphere films)

The P(3HB) and P(3HB)/n-BG composite microsphere films were collected after 1, 3 and 7 days of incubation, washed with deionised water and vacuum-dried before further examination.

#### 2.5.2.2 Sample preparation of the (45S5Bioglass<sup>®</sup> and microsphere coated composite scaffolds

The 45S5Bioglass<sup>®</sup> scaffolds of dimensions 10x10x10 mm<sup>3</sup> coated with P(3HB) microspheres and sintered 45S5Bioglass<sup>®</sup> tablets of dimensions 10 mm (diameter) x 0.2 mm (thickness) were also used as controls for the SBF study. The scaffolds were collected after 1, 3, 7, 14 and 30 days of incubation, washed with deionised water and left to dry at ambient temperature in a desiccator for further examination. These samples were then characterised using SEM and XRD to determine the formation of hydroxyapatite on their surfaces.

## 2.6 Protein studies

### 2.6.1 Bovine Serum Albumin (BSA) adsorption test

In order to determine the protein adsorption onto the surface of the microspheres 25 mg of the microspheres prepared using different conditions, as mentioned in section 2.2.2, were added to 5 mL of distilled water containing 1 mg of BSA. The microspheres were then removed by centrifugation and the concentration of BSA in the supernatant after adsorption on the surface of the microspheres was determined using UV spectroscopy (Eppendorf Biophotometer, U.K). The absorbance was measured at 280 nm wavelength. A calibration curve was prepared using known concentrations of BSA. The protein adsorbed ( $q$ ) on the surface of the microspheres was calculated using equation 4.

$$q = \frac{C_i - C_f}{m} V \dots\dots\dots(4)$$

Where  $C_i$  are the initial and  $C_f$  are the final BSA concentration and the BSA concentration in the supernatant after adsorption studies, respectively;  $V$  is the total volume of the solution (5mL); and  $m$  is the weight of the microspheres added into the solution (Patil *et al.*, 2007).

### 2.6.2 Protein adsorption study of (P(3HB)/n-BG composite microsphere films, 45S5Bioglass<sup>®</sup> scaffolds (before and after coating with P(3HB) microspheres) and 45S5Bioglass<sup>®</sup> composite scaffolds covered with HA

The protein adsorption study was carried out by placing the (P(3HB)/n-BG composite microsphere films, 45S5Bioglass<sup>®</sup> scaffolds (before and after coating with P(3HB) microspheres) and 45S5Bioglass<sup>®</sup> composite scaffolds covered with HA in 2 mL of the cell culture media (Dulbecco's Modified Eagle Medium supplemented with 10% foetal calf serum, 2mM L-glutamine, and 1% w/v penicillin and 1% w/v streptomycin solution at 37°C for 24h to determine the amount of serum protein adsorbed on the surface. The 45S5Bioglass<sup>®</sup> scaffolds (before and after coating with P(3HB) microspheres) were washed with Hank's balanced salt solution, pH 7.4 both after 1h and 24h. The samples

were then treated with 1 mL of 3% Triton X-100 (Ghannam *et al.*, 1999). The total protein adsorbed was quantified using a bicinchoninic acid (BCA) reagent kit (Thermo scientific). The optical density of the samples was measured at 562 nm using a standard spectrophotometer (Novaspec II Visible spectrophotometer, UK). The total proteins adsorbed on the surface of the samples were normalized for the surface area.

### 2.6.3 Protein profile of the adsorbed proteins observed using SDS-PAGE

The protein profile of the protein extracted from the surface of the samples (45S5 Bioglass<sup>®</sup>, 45S5Bioglass<sup>®</sup> composite scaffolds (coated with microspheres), P(3HB)/45S5Bioglass<sup>®</sup> composite scaffolds covered with hydroxyapatite (HA) and the BSA and RNase A encapsulated from P(3HB) microspheres were analysed using SDS-PAGE. The proteins of the samples were extracted and denatured with (12% SDS and 20%  $\beta$ -mercaptoethanol) and compared with protein BSA present in the serum. The size estimation was carried out using the molecular weight reference markers from Promega, UK. Protein samples of 20 $\mu$ g were diluted in reducing 2X sample buffer (Section 2.6.1.8), boiled for 5 mins and allowed to cool down to room temperature. Electrophoresis was carried out using a 12% and 15% polyacrylamide gel. The samples were run at a constant voltage of 200V in a Tris/glycine/SDS buffer using a Bio-Rad Mini-Protean II electrophoresis system. After migration, the gels were stained with Coomassie Blue in methanol-acetic acid-water (2.5:1:6.4) to reveal protein, destained and dried (Igartua *et al.*, 1998).

### 2.6.4 RNase A stability evaluation

#### 2.6.4.1 Methylene Blue activity test

RNA solution was prepared by dissolving 100 mg of RNA in 10 mL 3-(N-morpholino) propanesulfonic acid (MOPS) buffer (0.1M MOPS -HCl, pH 7.5, 2mM EDTA). Methylene blue buffer was prepared by dissolving 1 mg methylene blue in 100 mL MOPS buffer and the absorbance taken at 688 nm was adjusted to  $0.5 \pm 2\%$  using MOPS buffer. Due to the light sensitivity of the dye, the methylene blue buffer was stored in the dark. RNA solution (2.5-100 $\mu$ L) was mixed with methylene blue buffer to a final volume of 1 mL in cuvettes. The sample requires preincubation at 25°C for 10 mins in the

spectrophotometer in the dark. The RNase A release samples were analysed for specific activity and compared to the activity of free RNase A in solution (control) placed in contact with the unloaded microspheres and subjected to the same release medium and temperature. 10  $\mu$ L of the release samples as well as the control taken at different time points were added to 1 mL of the preincubated RNA solution (0.8 mg mL<sup>-1</sup>) in methylene blue buffer and the change in absorbance at 688nm (Novaspec II Visible spectrophotometer, UK) was recorded. The absorbance change was recorded immediately between 1 and 3 mins. One unit of enzyme activity (EU) was defined as the amount of RNase that leads to an absorbance change of 0.01 min<sup>-1</sup> at 25°C at a substrate concentration of 0.8 mg RNA mL<sup>-1</sup>. The enzyme activity of the native enzyme is 61 EU/mg of protein. (Stoeffele *et al.*, 1996).

RNase A is a protein whose fluorescence spectrum is mainly due to the tyrosine residues present in its structure therefore it has an emission maximum around 303nm (Nellore *et al.*, 1997). The fluorescence emission spectra were measured using a Perkin Elmer LS50 fluorescence spectrophotometer at an excitation wavelength of 268nm (Perkin Elmer Corporation, Rockville, USA).

## **2.7 Biocompatibility tests**

### 2.7.1 Cell culture studies on P(3HB) microsphere films (with and without drugs) and P(3HB/n-BG composite microsphere films

All media including buffers, trypsin and dyes were filter-sterilised prior to use and warmed to 37°C. The human keratinocyte cell line (HaCaT) was grown in Dulbecco's Modified Eagle Medium (DMEM), supplemented with 10% foetal calf serum, 2 mM L-glutamine and 1% w/v penicillin and 1% w/v streptomycin solution. The medium was changed every 2 days. The cell cultures were maintained at 37°C, 5% CO<sub>2</sub> and passaged on confluence by trypsin treatment. Following cell detachment, fresh medium was added to the cell suspension, which was then centrifuged at 500g for 10 mins. The resulting cell pellet was resuspended in fresh medium and transferred to 75 cm<sup>2</sup> tissue culture flasks as required (Prashar *et al.*, 2002).

### 2.7.1.1 Sample preparation

#### 2.7.1.1.2 Sterilization of samples

All the samples were sterilised using ultra-violet (UV) light. The samples were kept in 24-well microplates and placed under UV for 30 minutes, for each side of the sample. Shortwave 254nm UV sterilization was used in a SI-950 UV Benchtop incubator with a height of 18 inches. The samples were handled using a sterilized spatula. This form of sterilization was employed, as it has been shown to be more effective compared to washing with alcohol or autoclaving (Shishatskaya *et al.*, 2004).

#### 2.7.1.1.2 Cell seeding on substrates

The semi-confluent HaCaT cells were released from the flasks by trypsinisation and concentrated to pellet form by centrifugation (400g, 5 min). A cell seeding density of 20,000 cells/cm<sup>2</sup> was used for the films, respectively. The samples were placed in a polystyrene 24 well flat bottomed tissue culture plate with the film samples placed in the centre of the well and 2 mL of the cell suspended media was added for attachment of the keratinocytes. The plates were incubated in a humidified environment (37°C, 5% CO<sub>2</sub>) for a period of 3 days. Standard tissue culture plastic was used as the control surface. Neutral Red (NR) assay was used to check the cell viability.

### 2.7.1.2 Analysis of HaCaT cell culture studies

#### 2.7.1.2.1 Neutral Red assay

The cell attachment study was carried out using the Neutral Red (NR) assay (Prashar *et al.*, 2002). Briefly, the films were incubated with 2 mL of media containing 40 mg/mL of NR, which was filter-sterilised. The growth on the standard tissue culture plate was used as control. The 24 well plates containing the films were then further incubated for 3h at 37°C to allow for uptake of the dye by viable, uninjured cells. The NR containing medium was removed after 3h and the films gently removed and placed in another 24 well plate. The films were then quickly washed with 200 mL of fixative (1% CaCl<sub>2</sub>-0.5% formaldehyde). Next, 200mL of another solution containing 1% acetic acid and 50% ethanol solution was added to each well to extract the dye. The plates were then

allowed to stand at room temperature for 10 minutes followed by rapid agitation on a microtitre plate shaker. The absorbance of the extracted dye (100 mL) was then read at 540 nm on a Thermomax microtitre plate reader (MDS Analytical Technologies (UK) Ltd., Wokingham, UK). All experiments were performed at least three times. The total NR uptake was a measure of viability (% NR uptake is directly proportional to the number of live, uninjured cells). Control plates containing only cells and medium were run alongside every experiment (Prashar *et al.*, 2002). The percentage viability was calculated using equation 5.

$$\% \text{ Cell viability} = \frac{\text{Mean absorbances of cells on films}}{\text{Mean absorbances of cells on tissue culture plates}} \dots(5)$$

All NR assay values were expressed as a percentage of the growth relative to the tissue culture plate. The baseline of 100% viability was set as the absorbance of the test cells. Background absorbance due to non-specific reactions between the test materials and the NR dye were deducted from the exposed cell values. The difference in the surface areas of the tissue culture plastic (1.86 cm<sup>2</sup>) and the films (1.13 cm<sup>2</sup>) were considered and the correction factor was applied to determine the % cell viability on the films. The samples analysed for biocompatibility are listed in Table 5.

**Table 5:- Materials investigated for the biocompatibility studies using the HaCaT keratinocyte cell line.**

Chapters	Samples analysed	Neutral Red Assay (NR)	SEM
Chapter 5,6	P(3HB)	√	√
Chapter 6	P(3HB)/tetracycline loaded with 0.5 wt%, 2 wt% and 4 wt%	√	√
Chapter 5	P(3HB) immersed in SBF for 1, 3, 7 days	√	√
Chapter 5	P(3HB)/n-BG	√	√
Chapter 5	P(3HB)/n-BG immersed in SBF for 1, 3, 7 days	√	√

### 2.7.2 Cell culture studies on 45S5Bioglass<sup>®</sup> composite scaffolds

All media including buffers, trypsin and dyes were filter-sterilised prior to use and warmed to 37°C. The MG-63 osteoblast cells, human osteosarcoma cell line was grown in Dulbecco's Modified Eagle Medium (DMEM), supplemented with 10% foetal calf serum (FCS), 2mM L-glutamine and 1% w/v penicillin and streptomycin solution.

#### 2.7.2.1 Culturing and cyro-preservation of MG-63 cells

The osteoblast cells were resurrected from their frozen state by thawing them and transferring them quickly to centrifuge tubes containing 10 mL Low-glucose Dulbecco's Modified Eagle Medium (DMEM) (supplemented with 10% foetal calf serum, 100µg/mL penicillin and 100 µg/mL of streptomycin). The cell suspension was centrifuged at room temperature for 3 mins at 1000 rpm. The cell pellet was re-suspended using 5mL of DMEM and 2mL of the resuspended cell suspension was added to the tissue culture flasks (the flasks had gas permeable caps and a surface area of 80 cm<sup>2</sup>) followed by 8mL of fresh DMEM. The flasks were incubated in a humidified atmosphere, in 5% CO<sub>2</sub> and at 37°C. The spent medium of the flask was changed after every 2 days and the flasks were also checked for contamination using an optical microscope. Once the cells were grown to 70-90% confluency they were sub-cultured to maintain healthy growth.

For sub culturing, the spent medium was removed from the flask and washed with 5 mL of PBS followed by adding 2-3 mL (1 mL/cm<sup>2</sup>) of trypsin onto the washed cell monolayer and incubated at 37°C for 2 mins. The cells were examined under inverted phase microscope to observe the detachment of the cells and 8 mL (3-4 times the volume of trypsin) of fresh DMEM was added to the flask. The cell suspension was then centrifuged for 3 mins at 1000 rpm. The cell pellet was resuspended using 5mL of fresh DMEM. 3mL of the resuspended cell suspension was further divided into three new flasks (1 mL) and 9mL of fresh DMEM was added. The cells were then further allowed to grow until the start of new experiments. The cells were not passaged for more than 3-4 times and they were frozen in ampoules and stored in liquid nitrogen for further use. For cyro-preservation the cell lines were preserved in liquid nitrogen for long term-storage. The cells were subjected to trypsinisation and centrifugation as mentioned earlier. After

centrifugation the cell pellet was re-suspended in freezing medium (70% growth medium, 20% foetal calf serum and 10% dimethyl sulfoxide) at a concentration of  $0.5-1 \times 10^6$  cells/mL. 1 mL aliquots were further pipetted into cyro-protective vials and stored at  $-80^\circ\text{C}$  overnight. Frozen vials were then transferred to the liquid nitrogen storage vessel and preserved until further use.

## **2.8 P(3HB) microsphere, 45S5Bioglass<sup>®</sup> and P(3HB)/45S5Bioglass<sup>®</sup> composite scaffold physical characterization techniques**

### 2.8.1 P(3HB) microsphere characterization techniques

#### 2.8.1.1 Particle size analysis

Malvern Mastersizer particle size analyzer (Worcestershire, UK) was used to measure the particle size of the microspheres at Imperial College London, UK. Microspheres were dispersed well in water and following a background measurement; the suspensions were added dropwise to the analyser until the ideal concentration was reached.

#### 2.8.1.2 Surface morphology and microstructure characterization using TEM

P(3HB) microspheres were observed using a JEOL 5610LV scanning electron microscope at Imperial College London, UK by Mr. Decheng Meng. The samples were placed on 8 mm diameter aluminum stubs using a sticky tag to hold the sample. A gold sputtering device (EMITECH-K550) was used to coat the samples, operating at a pressure of  $7 \times 10^{-2}$  bar and deposition current of 20 mA for 2 mins; images were taken at various magnifications to analyze the samples. The cross-sections of single microspheres and the crystallinity of the polymer were analysed by transmission electron microscopy (TEM) using a JEOL JEM-2010 transmission electron microscope operated at 200kV. The sample for TEM was prepared using the focused ion beam method (FIB; FEI FIB200-SIMS). The microspheres were coated first with gold, then with platinum. A Ga<sup>+</sup> beam of 30 keV between 30 and 100 pA was used to cut the sample. Images were taken in secondary electron mode. Once the samples had been polished to the desired thickness, they were extracted using an *ex-situ* lift-out technique onto a 3 mm Formuar-coated copper grid for TEM analysis (Giannuzzi *et al.*, 2005).

## 2.8.1.3 Porosity

The porosity ( $\epsilon$ ) of the microspheres was measured according to equation 5, using the liquid displacement method (Chang *et al.*, 2006). Briefly, 5 mL of ethanol was used as the displacement liquid in a measuring cylinder and weighed. The P(3HB) microspheres immersed in ethanol in the cylinder was sonicated in a water bath to assist penetration of ethanol within the pores. The sample porosity was calculated using equation 6.

$$\begin{aligned}
 V_p(\text{the volume of the matrix pores}) &= (W_2 - W_3 - W_s) / \rho_e \\
 V_s(\text{the volume of the matrix polymer phase}) &= (W_1 - W_2 + W_s) / \rho_e \\
 \epsilon = V_p / (V_p + V_s) &= (W_2 - W_3 - W_s) / (W_1 - W_3) \quad \dots(6)
 \end{aligned}$$

$W_1$  is the weight of the cylinder filled with ethanol before the immersion of the microsphere sample,  $W_2$  is the weight of the cylinder, the ethanol and the sample after removing the excess ethanol above the 5 mL mark,  $W_3$  is the weight of the cylinder and ethanol after removing the microsphere sample saturated with ethanol, and  $W_s$  is the weight of the microsphere sample used in the measurement.

## 2.8.1.4 Density of microsphere powder

The density of the microsphere powder ( $\rho_{\text{msp}}$ ) was determined at Imperial College, London using a 25 mL pycnometer and applying the equation 7.

$$\rho_{\text{msp}} = \frac{(m_{p2} - m_{p1})}{(m_{p4} - m_{p1}) - (m_{p3} - m_{p2})} \rho_L \quad \dots\dots\dots (7)$$

Where  $m_{p2}$  is the mass of the microsphere sample and the measuring cylinder in grams,  $m_{p1}$  is the mass of the measuring container,  $m_{p4}$  is the mass of the specific amount of immersion liquid which was water and the measuring container,  $m_{p3}$  is the mass of the specific amount of the microsphere sample, the immersion liquid and the measuring container, and  $\rho_L$  is the density of the immersion on liquid at measuring temperature.

#### 2.8.1.5 Determination of Residual PVA content

The % residual PVA content present on the surface of the microspheres prepared using different conditions were determined by the formation of a coloured complex between two adjacent hydroxyl groups of PVA solution and an iodine molecule (Yang *et al.*, 2008). Briefly, 2 mg of the lyophilized microsphere samples prepared using the different conditions were treated with 2mL of 0.5 M sodium hydroxide (NaOH) for 15 minutes at 60°C. Each of the samples was then neutralized with 900 $\mu$ L of 1 N hydrochloric acid (HCl) and the volume was adjusted to 5mL with distilled water. To each of the samples, 3mL of 0.65 M solution of boric acid, 0.5 mL of iodine solution (I<sub>2</sub>)/Potassium iodide (KI) (0.05 M/0.15 M) and 1.5 mL of distilled water were added. Finally, the absorbance of the samples was measured at 690 nm (Novaspec II Visible spectrophotometer, UK) after 15 mins of incubation. A standard plot of PVA was also prepared under identical conditions (Sahoo *et al.*, 2002).

#### 2.8.1.6 Determination of surface hydrophobicity

1 mg microsphere samples prepared using different conditions, as mentioned in section 2.2.2, were incubated with different concentrations of Rose Bengal dye (4-20 $\mu$ g/mL) for 3h at room temperature. The samples were then centrifuged at 110000g for 30 minutes in a microcentrifuge (Sorvall legend RT, UK) to spin down the particles. The supernatant from each of the samples was analysed at 542.7nm (Novaspec II Visible spectrophotometer, UK) to determine the unbound dye. The dye solution without any microspheres were used as a control and run each time under the same condition to account for the dye bound to the centrifuge tubes (Sahoo *et al.*, 2002).

#### 2.8.1.7 Specific surface area measurement

The specific surface area (SSA) of the microspheres was measured according to Brunauer-Emmett-Teller (BET) method at Imperial College, London by Dr. Julian Jones. The physical adsorption of gas molecules on a solid surface were measured using a Micromeritics Tristar instrument after degassing for 1h at 150°C. The particle diameter ( $d_{\text{BET}}$ ) for P(3HB) was calculated for the SSA value, using equation 8.  $\rho$  = density of P(3HB) *i.e* 1.26 g/cm<sup>3</sup>, SSA= Specific surface area.

$$d_{\text{BET}} = \frac{6}{\rho \times SSA} \dots\dots\dots(8)$$

### 2.8.1.8 Zeta-potential analysis

The zeta-potential analysis of the microspheres prepared using the different conditions as mentioned in section 2.2.2 were carried out in Poland by Mr. Decheng Meng, 2g of the P(3HB) microspheres mixed with water were stirred using a magnetic stirrer for 30 minutes. Following that the microspheres were centrifuged and re-dispersed in 5mL of water and stirred once again for 30 minutes. Water and HEPES buffer was used as the dispersant for the microspheres to measure their zeta-potential. The zeta-potential analysis of the microspheres was measured using an Agilent 7020 Zeta Probe (Foster City, USA). 1N NaOH and 1N HCl solutions were added as necessary to adjust the pH (Patil *et al.*, 2007).

### 2.8.1.9 X-Ray photoelectron spectroscopy (XPS)

The surface chemistry of the tetracycline and gentamicin loaded microspheres were analysed by Dr D J Morgan, Cardiff Catalysis Institute, Cardiff. Axis Ultra DLD system (Kratos Axis Ultra., Cardiff, U.K) with the following acquisition parameters; monochromated 120 W X-ray Power (10 mA emission x 12 kV), 20 eV Pass energy, Analysis Area 700 x 300  $\mu\text{m}^2$ ) were used to analyse the samples.

### 2.8.2.0 Fourier Transform Infrared Spectroscopy (FTIR)

Chemical characterization and molecular bonding of the drug loaded and unloaded P(3HB) microspheres were carried out at University College London, Eastman Dental Institute using the FTIR system 2000, Perkin Elmer, USA spectroscopy) with the following conditions: spectral range, 400-4000  $\text{cm}^{-1}$ ; window material, CsI;16 scans; resolution 4  $\text{cm}^{-1}$ ; temperature stabilised coated FR-DTGS detector.

### 2.8.2.1 Differential Scanning Calorimetry (DSC)

The thermal properties of the samples (drug loaded and unloaded) microspheres and microsphere films taken out at different time points before and after the water uptake studies were measured at University College London, UCL using a Perkin-Elmer Pyris Diamond DSC (Perkin-Elmer Instruments, USA). The sample masses for each of the measurements were in the range of 5-7mg. The samples were encapsulated in standard aluminium pans and all tests performed under nitrogen atmosphere. The samples were heated/cooled/heated at a rate of  $20^{\circ}\text{C min}^{-1}$  between  $-50^{\circ}\text{C}$  and  $250^{\circ}\text{C}$ . All measurements were carried out in triplicates. The crystallinity percentage was determined by measuring the enthalpy of fusion from the differential scanning calorimetry curve using equation 9.

$$\% \text{Crystallinity} = \frac{\Delta H_{f(\text{sample})}}{\Delta H_{f(100\% \text{ crystallinity})}} \dots\dots\dots(9)$$

where  $\Delta H_{f(\text{sample})}$  is the enthalpy of fusion for the extracted P(3HB) sample and  $\Delta H_{f(100\% \text{ crystallinity})}$  is the enthalpy of fusion of commercial P(3HB)

### 2.8.2.2 Water contact angle study

Static water contact angle measurements of the P(3HB) microsphere films (tetracycline loaded and unloaded; P(3HB)/n-BG composite microsphere films) were carried out University College London, Eastman Dental Institute in order to evaluate the wettability of the samples. The experiment was carried out on a KSV Cam 200 optical contact angle meter (KSV Instruments Ltd., Finland). An equal volume of water ( $<12 \mu\text{L}$ ) was placed on every sample by means of a gas light micro-syringe, forming a drop. Photos (frame interval-1s, number of frames-20) were taken to record the shape of the drops. The water contact angles on the specimens were measured by analyzing the record drop images (n=3) using the Windows based KSV-Cam software. An image was recorded by the KSV-Cam software every second for 30 s in order to monitor the contact angle as a function of time. The image processing software was used to determine the contact angle

by fitting the measured drop profile with the Young-Laplace Equation.

### 2.8.2.3 White light interferometry

2D and 3D plots of the surface topography was obtained by the means of white light interferometry (ZYGO<sup>®</sup>, New View 200 OMP 0407C, UK) at Imperial College London, London with the assistance of Mr. Decheng Meng in order to evaluate the topography and the surface roughness of the samples. P(3HB) and P(3HB)/n-BG microsphere films were analyzed at 10X magnification using a 100 $\mu$ m bipolar scan. Three analyses per sample were performed to get an average rms measurement.

### 2.8.3 45S5Bioglass<sup>®</sup> and P(3HB)/45S5Bioglass<sup>®</sup> composite scaffold physical characterization techniques

The physical characterization techniques employed were chosen to highlight the fictionalization aspect provided by the addition of P(3HB) microspheres in the 45S5Bioglass<sup>®</sup> scaffolds. The different techniques carried out on the 45S5Bioglass<sup>®</sup> and composite scaffolds are mentioned below.

#### 2.8.3.1 Porosity measurements

The porosities of scaffolds before ( $P_1$ ) and after ( $P_2$ ) coating with P(3HB) microspheres were determined using the equation 10.

$$P_1 = 1 - \left( \frac{W_1}{\rho_{BG} V_1} \right) P_2 = 1 - \left[ \frac{\left( \frac{W_1}{\rho_{BG}} \right) + \left( \frac{W_2 + W_1}{\rho_{P(3HB)}} \right)}{V_2} \right] \dots \dots \dots (10)$$

Where  $W_1$  and  $W_2$  are the weights of the scaffold before and after coating, and  $V_1$  and  $V_2$  are the volumes of the scaffold before and after coating with P(3HB) microspheres, which were determined from measurements of scaffold dimensions using a digital

calliper (Mitutoyo, Germany). The theoretical densities of 45S5Bioglass<sup>®</sup> and P(3HB) are ( $\rho_{\text{BG}} = 2.70 \text{ g cm}^{-3}$ ) (Hench *et al.*, 1998) and ( $\rho_{\text{P(3HB)}} = 1.23 \text{ g cm}^{-3}$ ) (Misra *et al.*, 2006), respectively.

### 2.8.3.2 Mechanical properties

The compressive strength of 45S5Bioglass<sup>®</sup> scaffolds before and after coating with P(3HB) microspheres was measured using a Zwick/Roell Z010 universal testing machine at Imperial College London, as described by Bretcanu *et al.*, 2007. Five microsphere-coated and five 45S5Bioglass<sup>®</sup> uncoated scaffolds were carefully shaped to prismatic specimens of dimensions  $5 \times 5 \times 10 \text{ mm}^3$ . A load of 1 kN was applied onto the  $5 \times 5 \text{ mm}^2$  face until the compressive strain reached 70%. The crosshead speed was  $0.5 \text{ mm min}^{-1}$ .

### 2.8.3.3 X-ray diffraction analysis (XRD)

X-ray diffraction (XRD) analysis were performed on a Brüker D8 Advance diffractometer in flat geometry, using Ni filtered Cu K $\alpha$  radiation at Imperial College London, with the assistance of Mr. Decheng Meng. Data were collected from 10 to 100° in  $\theta$ - $\theta$  mode with a primary beam slit size of 0.6 mm. A Brüker Lynx Eye silicon strip detector was used and a size of  $0.00196671^\circ$  and a count time of 0.1s per step (Misra *et al.*, 2008).

### 2.8.3.4 Scanning electron microscopy/Energy Dispersive X-Ray analysis (SEM/EDX)

Microstructural observations of uncoated and microsphere coated 45S5Bioglass<sup>®</sup> scaffolds were performed using a JEOL 5610LV scanning electron microscope at Imperial College London, by Mr. Decheng Meng. Scanning electron microscopy (SEM) was also used to characterise the changes that occurred on the scaffold surfaces upon immersion in SBF. The increase in the amounts of phosphorus (P) and calcium (Ca) and the decrease in the amounts of sodium (Na) and silicon (Si) were detected by energy-dispersive X-ray (EDX) analysis. EDX spectra (Ka) of the composite samples were taken at different time points of immersion in SBF. These measurements were carried out at 10 kV in a field emission gun scanning electron microscope (EDX, INCA Oxford instruments).

### 2.8.3.5 Thromboelastograph (TEG) studies

The haemostatic efficacies of the n-BG particles were measured using a thromboelastograph (TEG) haemostasis analyser 5000 at St Thomas' Hospital, London U.K. In a TEG, the polyethylene cup containing blood is rotated  $\pm 5^\circ$  around a torsion wire. The time until the bimodal symmetric viscoelasticity curve's amplitude is 2 mm is referred to as R (min) and represents the initial detection of clot formation. The maximum separation of the curves is referred to as MA and represents the maximum clot strength (dyn/cm<sup>2</sup>) (Ostomel *et al* 2006). Kaolin a standardised reagent consisting of kaolin, buffered stabilizers and a blend of phospholipids was used for this study. Kaolin containing vials were warmed to room temperature initially. The vials were gently tapped and 1.0 mL of native blood was added into each vial and then gently inverted for a few times. Then 340  $\mu$ L of the citrated blood was added into TEG analyzer cups containing 20 $\mu$ L of 0.2M calcium chloride. The lever was moved to the start position and the test and sample run were carried out until the MA parameter was defined. The TEG analyzer was attached to a computer running the TEG analytical software (Haemoscope Corporation).

### 2.8.3.6 Scanning Electron Microscopy (SEM) to observe cell attachment

Samples were examined under SEM to observe the HaCaT cell attachment and spreading on the surface to the samples. Specimens from day 1 and day 3 were fixed in 3% glutaraldehyde in 0.1 M cacodylate buffer for 12h at 4°C. Subsequent dehydration using a series of graded ethyl alcohols (50%, 70%, 90% and 100%) was performed. Samples were dried by immersion in hexamethyldisilazane for 2 min and left in a fume cupboard for 2h. The dried samples were then attached to aluminium stubs, gold coated and examined under SEM (JEOL 5610LV, USA) at various magnifications.

## 2.9 Statistical analyses

All data are expressed as mean  $\pm$  standard deviation. The data were compared using Student's *t*-test and analysis of variance (ANOVA) was used to assess significant difference among selected factors. If the factor effect was significant a Bonferroni comparison Post Hoc test was done to assess for the presence of significant differences.

The differences were considered significant when  $*p < 0.05$ , very significant  $**p < 0.01$  and highly significant  $***p < 0.001$ , respectively. A  $p$ -value higher than 0.05 ( $p > 0.05$ ) was taken as indicating no significant difference. Statistical analysis was performed using Graphpad PRISM software (Graphpad Software Inc., La Jolla, USA) and PASW 18 (SPSS) software (SPSS Inc., Chicago, Illinois).

# Chapter 3

Drug delivery using Poly(3-hydroxybutyrate) microspheres

### 3.1 Introduction

#### 3.1.1 Polyhydroxyalkanoates and their applications in drug delivery

Polymeric drug delivery systems are designed to deliver drugs to the local site of action for extended periods of time, so that the therapeutic levels of the drug with short *in vivo* half-lives can be maintained (Pouton *et al.*, 1996). In addition, different forms of drug delivery devices are used to reduce the fluctuations in the plasma drug levels, so a slower drug release rate can be achieved, which can then provide an effective pharmacological response (Pouton *et al.*, 1996). Microencapsulation of a drug within a polymeric device is considered as one of the most common methods of drug delivery (Nobes *et al.*, 1996). Drug encapsulated microspheres require less frequent drug administration when compared to the conventional dosage forms. Also, the drugs that are encapsulated within the microspheres are kept separate from other microspheres; as a result multiple drug administration in a single injection can be achieved, which would have not been possible otherwise owing to drug compatibility issues (Pouton *et al.*, 1996). Apart from being orally administered, microspheres can also be administered through a number of parenteral pathways such as intraocular, intravenous, intra-arterial, intraspinal and intraosseous (Edlund *et al.*, 2002). Often the site of administration influences the performance of the drug delivery due to the difference in the local tissue environment such as pH and enzyme activity (Edlund *et al.*, 2002).

The solvent evaporation method is the most frequently used method to prepare polymeric microspheres. The characteristics of the microspheres produced are largely dependent on the type of polymer and drug used. Other processing parameters such as solvent type and concentration of the emulsifier, drug/polymer ratio and stirring rate are also known to affect the physicochemical properties of the microspheres (Bazzo *et al.*, 2008). The surface morphology and porosity of the microspheres are known to be particularly affected due to which the drug release rate from the microspheres is also affected. However the encapsulation efficiency of drugs within the microspheres is largely dependent on the type of microencapsulation procedure as well as the solubility of the drug. For example in the single emulsion method (*o/w*), a predetermined quantity of the polymer dissolved in the solvent is added to deionized water (inner aqueous phase,  $w_1$ )

containing polyvinyl alcohol PVA, which is used as a surfactant for the production of microspheres. The solvent from the microspheres are removed from the inner aqueous phase and evaporated through the emulsion-air interface. The polymer precipitation is accelerated giving rise to the final microsphere characteristic once the solvent evaporation is initiated. However the encapsulation efficiency of highly hydrophilic drugs in the o/w method is affected by the fast shrinkage of the microspheres as a result the encapsulated drug is drained out of the microspheres during the solvent removal. Therefore the o/w method is more suitable for the entrapment of less hydrophilic drugs as they will agglomerate toward the microsphere surface due to their hydrophobic nature. In the double emulsion method ( $w_1/o/w_2$ ) the initial emulsion phase ( $w_1$ ) is added to a second aqueous phase containing PVA ( $w_2$ ) where during solvent evaporation, small microdroplets formed within the microspheres coalesce forming a honeycomb structure. During solvent evaporation, the precipitating polymer wall also forms holes through which the entrapped drug is partly removed. This honeycomb structure is considered most suitable for efficient entrapment of hydrophilic drugs (Rosca *et al.*, 2004).

Double emulsion method has been used by several researchers to entrap highly hydrophilic drugs such as gentamicin within biodegradable microspheres (Yang *et al.*, 2001; 2007; Lecàroz *et al.*, 2006). Gentamicin a highly water soluble drug, is an aminoglycoside that had been used against a wide range of Gram-positive and Gram-negative bacteria. For example gentamicin has been used for the treatment of osteomyelitis, an inflammatory bone disease. Osteomyelitis is the microbial infection of the bone medullary cavity, cortex and periosteum that is known to occur during post-operative sepsis after an orthopaedic procedure. However, for the treatment of osteomyelitis, a prolonged systemic antibiotic treatment such as the use of gentamicin, either oral or parenteral, for a period of 4-6 weeks, is known to cause systemic toxicity and patient discomfort. Therefore, localised delivery at the infected site was introduced by injecting drug loaded microspheres. By this method the risk of high dose administration and possibility of building drug resistance could be avoided (Huang *et al.*, 2001). In a study conducted by Huang *et al.*, PLA microspheres containing gentamicin was used for the treatment of bone infection. PLA microspheres with an average size of  $178\mu\text{m}$  were entrapped with gentamicin sulphate for the treatment of osteomyelitis,

where 80% of gentamicin sulphate was released within 3 weeks of implantation (Sampath *et al.*, 1992).

Thus in this chapter, P(3HB) microspheres containing gentamicin for the treatment of bone infections such as osteomyelitis were developed since they do not possess the risk of toxicity and immunogenicity due to their acidic byproducts which is a disadvantage when PLA is used. The processing conditions that particularly affect the characteristics of the P(3HB) microspheres were investigated so that microspheres with a high gentamicin loading efficiency, controllable porosity and uniform drug distribution could be achieved. Firstly, the P(3HB) microsphere preparation using a double emulsion/solvent evaporation technique by varying the polymer concentration, emulsifier concentration and the stirring rate is discussed. The effects of the final characteristics of the microspheres on the properties of the microspheres such as surface hydrophilicity, zeta-potential analysis and protein adsorption were also monitored. Their surface chemistry was analysed for the presence of any surface bound drugs that may contribute to the initial burst release (Naraharisetti *et al.*, 2005). X-ray photoelectron spectroscopy was used to analyse the surface chemistry of the microspheres. Infrared spectroscopy was used to evaluate the chemical interaction of gentamicin with the P(3HB) microspheres (Stephens *et al.*, 2000). Secondly, the changes in microsphere characteristics such as surface morphology and porosity in the presence of the drug (gentamicin) and its effect on the drug release kinetics was also investigated. Also, the effect of the processing conditions and the presence of the drug on the thermal properties of P(3HB) was studied. Finally, the *in vitro* degradation behaviour of the gentamicin loaded P(3HB) microspheres as compared to unloaded P(3HB) microspheres were studied. A schematic representation of the microsphere preparation as well as the various characterization techniques used to analyse the gentamicin loaded and unloaded microspheres are shown in Figure 1.

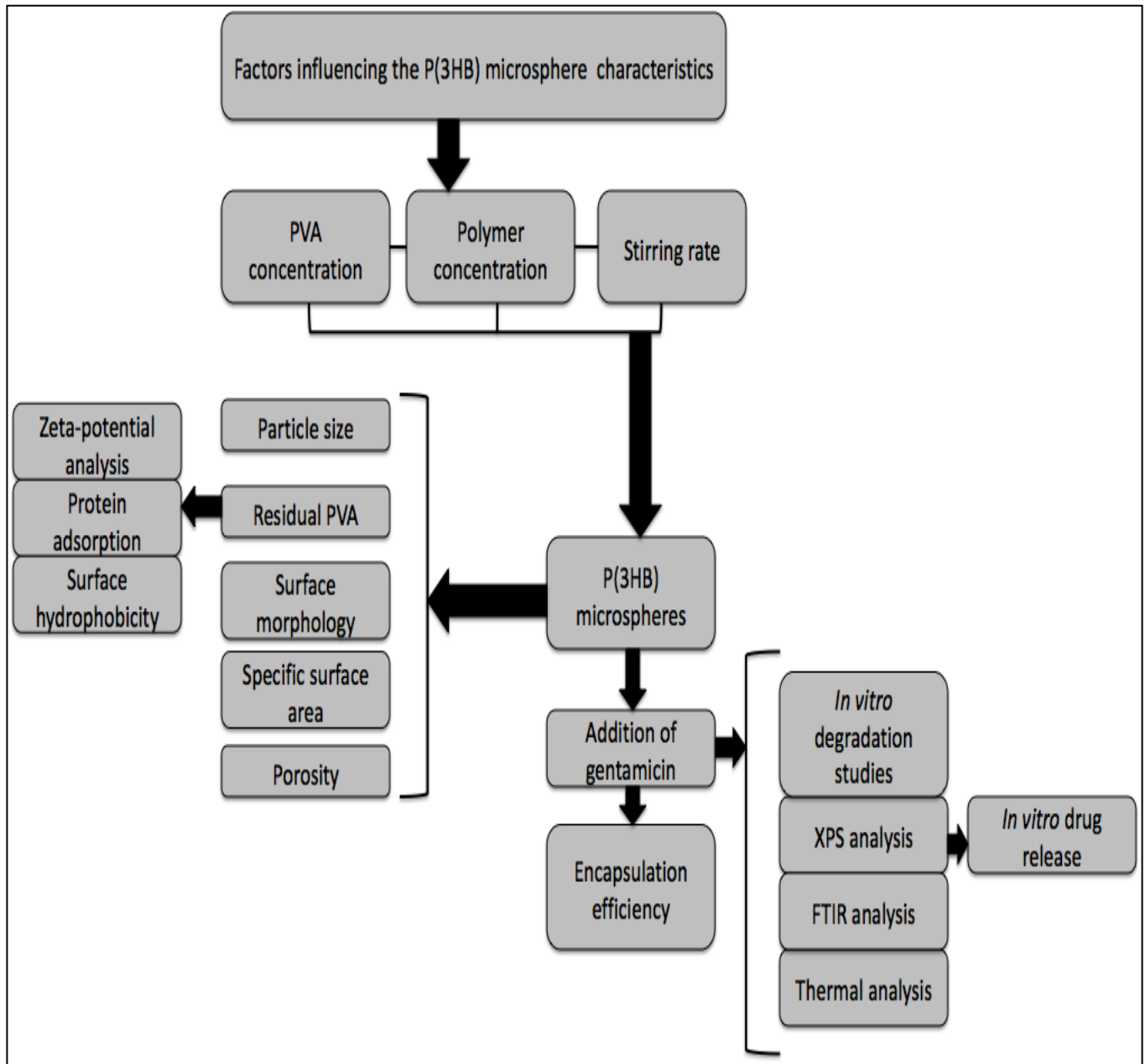


**Figure 1:- Schematic representation of the factors influencing the P(3HB) microsphere characteristics and the different characterizations described in this chapter.**

## 3.2 RESULTS

### 3.2.1 P(3HB) microsphere preparation

The P(3HB) microspheres were prepared by the solid-oil-in-water (s/o/w) technique using different conditions presented as described in Chapter 2, section 2.2.2, Table 2. In order to optimise the microspheres for maximum encapsulation efficiency the conditions for microsphere preparation including polymer concentration, the surfactant concentration and the stirring rate were varied. The conditions were decided using partial factorial analysis (Govender *et al.*, 2005). This allowed the determination of optimal processing conditions using limited experiments.

### 3.2.2 P(3HB) microsphere characterization

#### 3.2.2.1 Particle size

The particle size distribution curve of the P(3HB) microspheres prepared using different conditions shown in Chapter 2, section 2.2.2, Table 2 are represented in Figure 2 (A, B, C, D). Figure 2A shows that the size range of the measured particles were around 1-15 $\mu\text{m}$ , where 80% of the measured particles had a mean particle size ranging from 1.5 to 2.0 $\mu\text{m}$  and 90% of the microspheres had diameters below 5 $\mu\text{m}$ . Figure 2B shows that the size range of the measured particles were around 1-10 $\mu\text{m}$ , where 50% of the measured particles had a mean particle size ranging from 1.5 to 2.0 $\mu\text{m}$  and 90% of the microspheres had diameters below 5 $\mu\text{m}$ , similarly Figure 2C also showed that 50% of the measured particles had a mean particle size ranging from 1.5 to 2.0 $\mu\text{m}$  and 90% of the microspheres had diameters below 5 $\mu\text{m}$ . Figure 2D shows that the size range of the measured particles were around 1-10 $\mu\text{m}$ , where 90% of the measured particles had a mean particle size ranging from 1.5 to 2.0 $\mu\text{m}$  and 80% of the microspheres had diameters below 5 $\mu\text{m}$ .

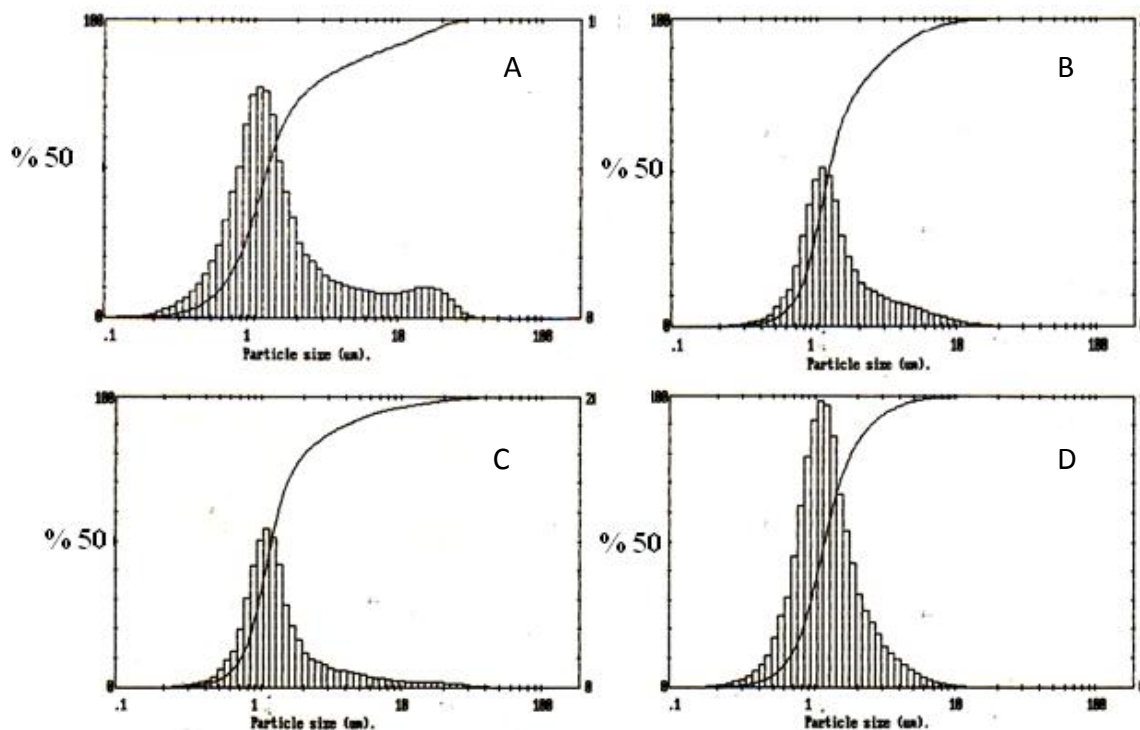


Figure 2:- Size distribution analysis of P(3HB) microspheres prepared using different conditions. A sample 1 (polymer concentration of 1g/L, PVA concentration of 0.5wt% and stirrer speed of 800 rpm), B sample 2 (polymer concentration of 3g/L, PVA concentration of 0.5wt% and stirrer speed of 300 rpm), C sample 3 (polymer concentration of 1g/L, PVA concentration of 1wt% and stirrer speed of 300 rpm), D sample 4 (polymer concentration of 3g/L, PVA concentration of 1wt% and stirrer speed of 800 rpm).

#### 3.2.2.1.1 The effect of polymer concentration on the particle size

The amount of P(3HB) used per unit volume of the solvent in this study were varied from 1g to 3g respectively. The microspheres prepared under conditions 1 (polymer concentration of 1g/L, PVA concentration of 0.5wt% and stirring rate of 800 rpm) and 2 (polymer concentration of 3g/L, PVA concentration of 0.5wt% and stirring rate of 300 rpm) (Chapter 2, section 2.2.2, Table 2) had an average size of  $2\mu\text{m}$  and  $1.7\mu\text{m}$  as shown in Figure 2A and B. These microspheres were slightly larger than  $1.58\mu\text{m}$  and  $1.54\mu\text{m}$  average microsphere size (Figure 2C and D).

### 3.2.2.1.2 The effect of the surfactant concentration on the microsphere size

Polyvinyl alcohol (PVA) concentration, which was used as a surfactant, was varied from 0.5% w/v to 1% w/v as shown in Chapter 2, section 2.2.2, Table 2. For conditions 1 (polymer concentration of 1g/L, PVA concentration of 0.5wt% and stirring rate of 800rpm) and 2 (polymer concentration of 3g/L and stirring rate of 300 rpm), a lower PVA concentration of 0.5% w/v was used and in conditions 3 (polymer concentration of 1g/L and stirring rate of 300 rpm) and 4 (polymer concentration of 3g/L and stirring rate of 800 rpm), a PVA concentration of 1% w/v was used in the emulsion phase. The mean particle size, as seen from Figure 3, increased with the decrease in the PVA concentration in the emulsion phase.

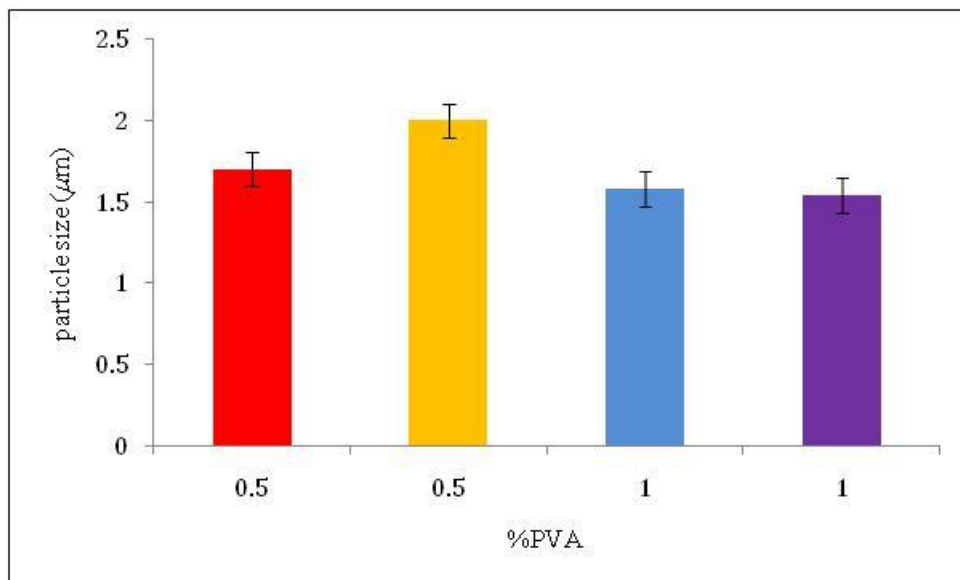


**Figure 3:** - The effect of the surfactant concentration on the P(3HB) microsphere size sample 1 (polymer concentration of 1g/L, PVA concentration of 0.5wt% and stirrer speed of 800 rpm), sample 2 (polymer concentration of 3g/L, PVA concentration of 0.5wt% and stirrer speed of 300 rpm), sample 3 (polymer concentration of 1g/L, PVA concentration of 1wt% and stirrer speed of 300 rpm), sample 4 (polymer concentration of 3g/L, PVA concentration of 1wt% and stirrer speed of 800 rpm), plotted against particle size ( $\mu\text{m}$ ).

### *3.2.2.1.3 The effect of stirring on the microsphere size*

In order to study the effect of stirring rate on the microsphere size, the stirring rate was maintained at 300 rpm and 800 rpm in the final emulsification step under varying PVA concentrations and P(3HB) concentrations, as explained in section 3.2.2.1.2. The microsphere sizes were  $2\mu\text{m}$  and  $1.54\mu\text{m}$  when prepared under conditions 1 (polymer concentration of 1g/L and PVA concentration of 0.5wt %) and 4 (polymer concentration of 3g/L and PVA concentration of 1wt %) with a stirrer speed of 800 rpm. Similarly, the microspheres prepared under condition 2 (polymer concentration of 3g/L and PVA concentration of 0.5wt%) and 3 (polymer concentration of 1g/L and PVA concentration of 1wt%) with a stirrer speed of 300 rpm exhibited an average size of  $1.7\mu\text{m}$  and  $1.58\mu\text{m}$ , respectively.

#### 3.2.2.1.4 The effect of stirring on the microsphere surface area

The specific surface area of the microspheres prepared varied depending on the different conditions used as represented in Figure 4. An increase in the specific surface area was observed when the average particle size was decreased (Figure 4). The microspheres with an average particle size of  $1.54\mu\text{m}$  and  $1.58\mu\text{m}$  in diameter (sample 3 and sample 4 Chapter 2, section 2.2.2, Table 2) exhibited a specific surface area of  $9.60\text{ m}^2/\text{g}$  and  $9.52\text{ m}^2/\text{g}$ . However, microspheres with slightly larger particle size of  $2\mu\text{m}$  and  $1.7\mu\text{m}$  in diameter (sample 2 and sample 1, Chapter 2, section 2.2.2, Table 2), exhibited a specific surface area of  $6.05\text{ m}^2/\text{g}$  and  $9.4\text{ m}^2/\text{g}$ .

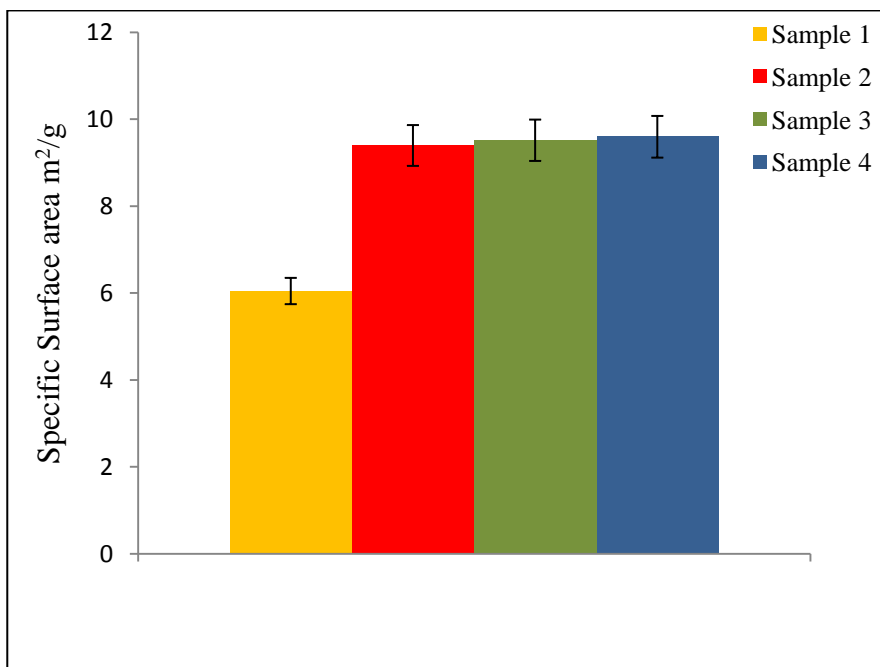


**Figure 4:** - The specific surface area of the P(3HB) microspheres prepared using different conditions.

### 3.2.2.2 Surface morphology

The surface morphology of the microspheres prepared by the solvent evaporation method using different conditions was viewed under scanning electron microscopy (SEM) (Figure 5). The microspheres prepared under the different conditions as explained in section Chapter 2, section 2.2.2, appeared spherical in shape with a smooth surface morphology.

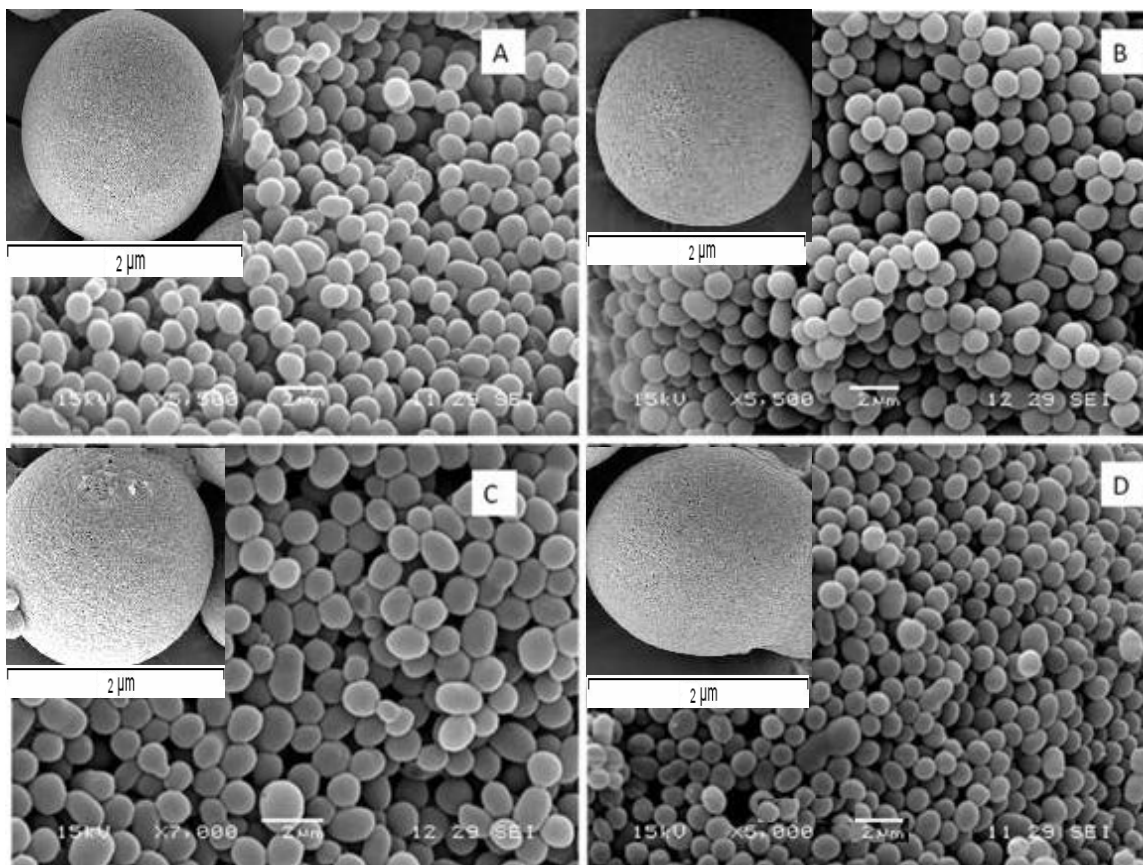


**Figure 5:-** Scanning electron micrographs (SEM) of the P(3HB) microspheres prepared under different conditions described in Table 1 sample 1 (polymer concentration of 1g/L, PVA concentration of 0.5wt% and stirrer speed of 800 rpm), sample 2 (polymer concentration of 3g/L, PVA concentration of 0.5wt% and stirrer speed of 300 rpm), sample 3 (polymer concentration of 1g/L, PVA concentration of 1wt% and stirrer speed of 300 rpm), sample 4 (polymer concentration of 3g/L, PVA concentration of 1wt% and stirrer speed of 800 rpm). Numbers in the insets indicate size at magnification x22,000.

## 3.2.2.3 Surface hydrophobicity

The surface hydrophobicity of the microspheres fabricated using higher and lower concentrations of PVA was determined by comparing the amount of Rose Bengal dye that was adsorbed per mg of the microspheres. As seen in Figure 6, the amount of Rose Bengal bound to the surface of the microspheres decreases with the increase in the PVA concentration. The microspheres fabricated under conditions 3 (polymer concentration of 1g/L, PVA concentration of 1wt% and stirrer speed of 300 rpm) and 4 (polymer concentration of 3g/L, PVA concentration of 1wt% and stirrer speed of 800 rpm) exhibited a higher % residual PVA and hence bound a lesser amount of Rose Bengal Dye when compared to the microspheres fabricated under conditions 1 (polymer concentration of 1g/L, PVA concentration of 0.5wt% and stirrer speed of 800 rpm) and 2 (polymer concentration of 3g/L, PVA concentration of 0.5wt% and stirrer speed of 300 rpm). For example, at the highest concentration of 12 mg/mL of Rose Bengal dye, the microsphere samples 3 and 4 bound 0.72 mg/mg and 0.63 mg/mg of the dye when compared to 1.03 mg/mg and 1.07 mg/mg for the microsphere samples 1 and 2.

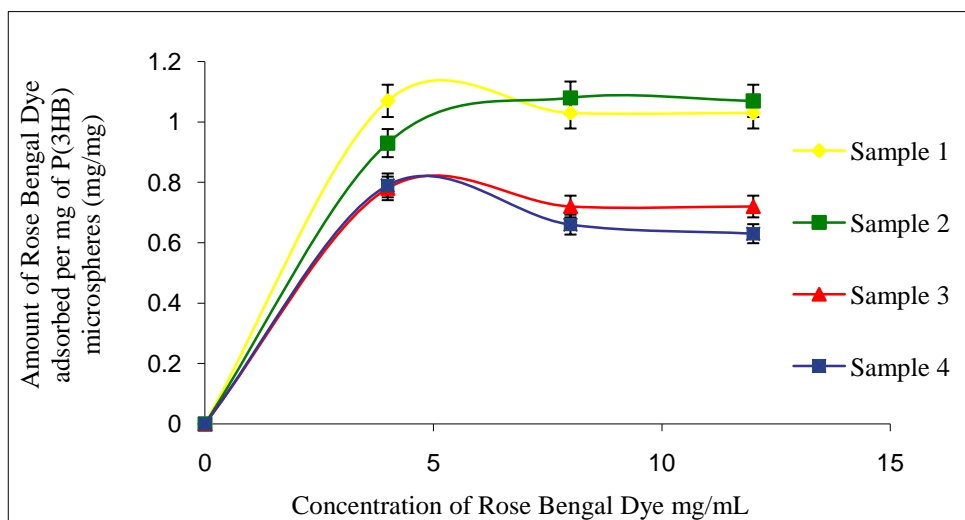


**Figure 6:- Amount of Rose Bengal Dye bound onto the surface of the P(3HB) microspheres sample 1 (polymer concentration of 1g/L, PVA concentration of 0.5wt% and stirrer speed of 800 rpm), sample 2 (polymer concentration of 3g/L, PVA concentration of 0.5wt% and stirrer speed of 300 rpm), sample 3 (polymer concentration of 1g/L, PVA concentration of 1wt% and stirrer speed of 300 rpm), sample 4 (polymer concentration of 3g/L, PVA concentration of 1wt% and stirrer speed of 800 rpm) as a function of an increase in the Rose Bengal dye concentration.**

## 3.2.2.4 Zeta-potential analysis

The microspheres prepared with a higher PVA concentration in conditions 3 (polymer concentration of 1g/L, PVA concentration of 1wt% and stirrer speed of 300 rpm) and 4 (polymer concentration of 3g/L, PVA concentration of 1wt% and stirrer speed of 800 rpm) at pH 7 exhibited a much lower zeta-potential value of -14.2 mV & -14 mV when compared to the zeta-potential values of -32.2 mV and -33.7mV of the microspheres prepared under conditions 1 (polymer concentration of 1g/L, PVA concentration of 0.5wt% and stirrer speed of 800 rpm) and 2 (polymer concentration of 3g/L, PVA concentration of 0.5wt% and stirrer speed of 300 rpm), as seen in Figure 7.

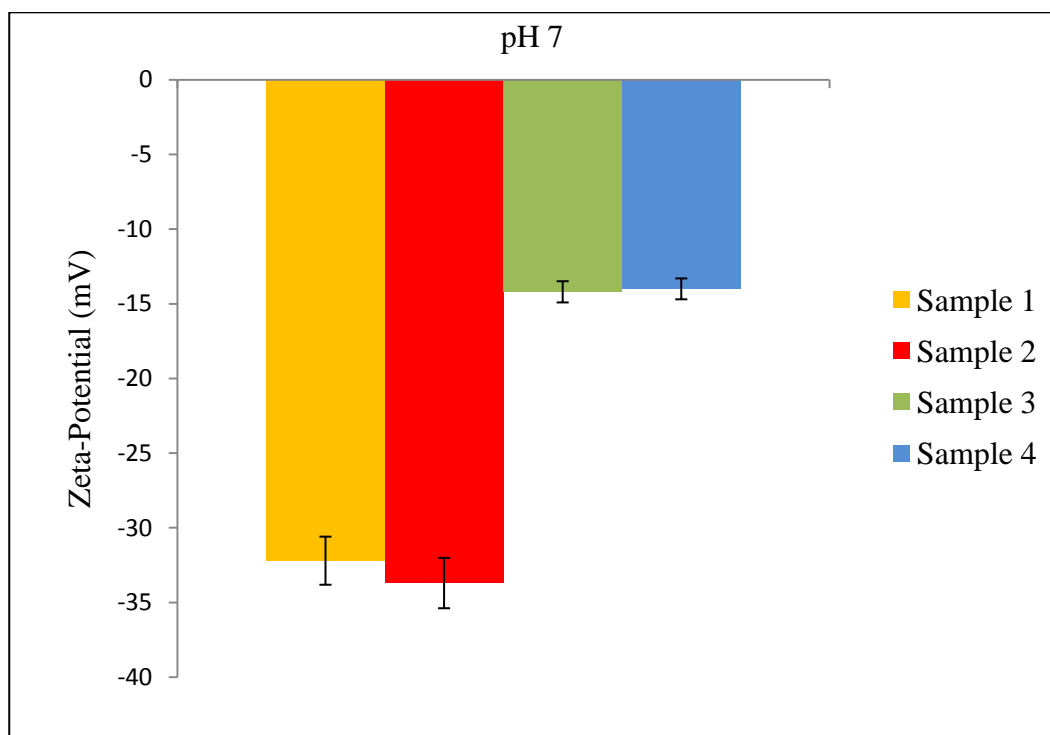


**Figure 7:- The zeta-potential values of the P(3HB) microspheres fabricated using different conditions at pH 7.**

## 3.2.2.4.1 pH/Zeta-potential

To measure the zeta-potential of the microsphere samples as a function of pH, a suspension of the microsphere samples were prepared 0.001 M HEPES buffer and the pH adjusted either with 0.1 M HCl or 0.1 M NaOH. From the zeta-potential-pH profiles it was observed that all the microspheres exhibited a negative surface charge at pH 7 as shown in Figure 7. However at a lower pH, the microspheres exhibited a positive zeta-potential value (Figure 8). The microspheres fabricated using conditions 3 (polymer concentration of 1g/L, PVA concentration of 1wt% and stirrer speed of 300 rpm) and 4 (polymer concentration of 3g/L, PVA concentration of 1wt% and stirrer speed of 800 rpm) exhibited lower positive zeta-potential charge when compared to the microspheres fabricated using conditions 1 (polymer concentration of 1g/L, PVA concentration of 0.5wt% and stirrer speed of 800 rpm) and 2 (polymer concentration of 3g/L, PVA concentration of 0.5wt% and stirrer speed of 300 rpm).

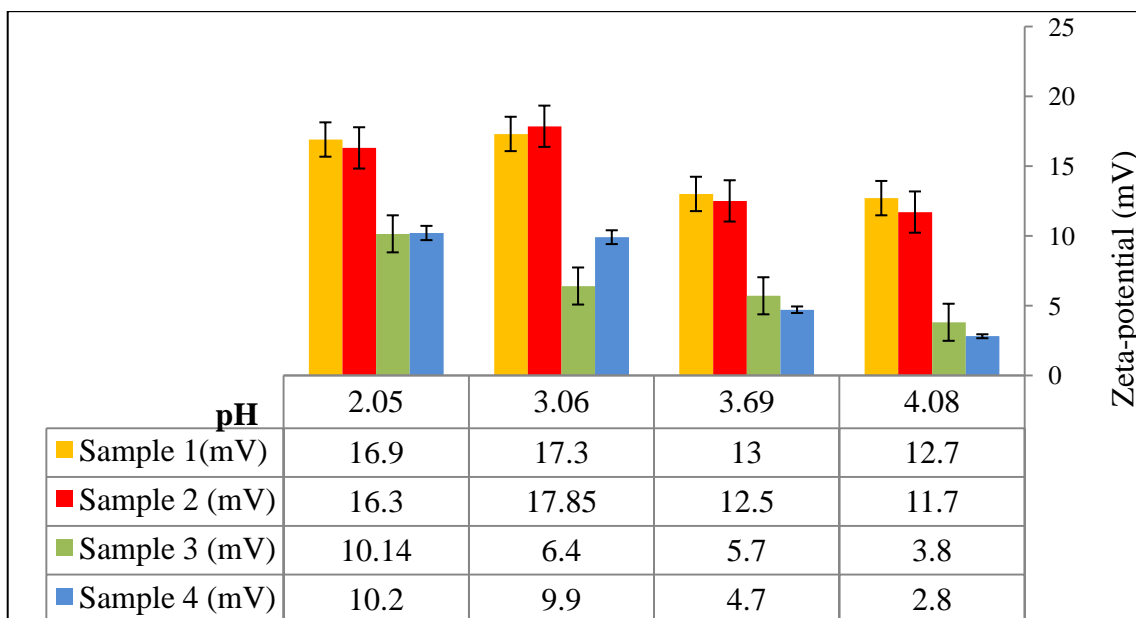


**Figure 8:- The zeta-potential values of the P(3HB) microspheres fabricated using different conditions at different pH .**

### 3.2.4.1.2 Effect of zeta-potential on protein adsorption

The comparison of protein (BSA) adsorption and zeta-potential of the microspheres fabricated under the different conditions are represented in Figure 9. From the results, the microspheres prepared under conditions 3 (polymer concentration of 1g/L, PVA concentration of 1wt% and stirrer speed of 300 rpm) and 4 (polymer concentration of 3g/L, PVA concentration of 1wt% and stirrer speed of 800 rpm) adsorbed a slightly higher amount of protein which was 327 mg/g and 324.4 mg/g when compared to 315mg/g and 240mg/g of proteins adsorbed on the microspheres prepared under conditions 1 (polymer concentration of 1g/L, PVA concentration of 0.5wt% and stirrer speed of 800 rpm) and 2 (polymer concentration of 3g/L, PVA concentration of 0.5wt% and stirrer speed of 300 rpm).

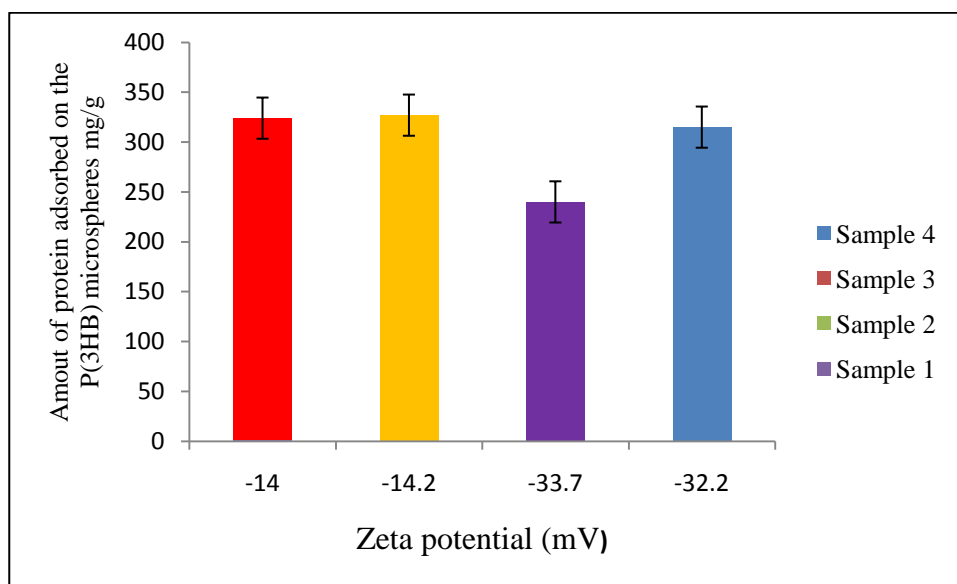


**Figure 9:-** Amount of BSA adsorbed on the surface of the P(3HB) microspheres, sample 1 (polymer concentration of 1g/L, PVA concentration of 0.5wt% and stirrer speed of 800 rpm), sample 2 (polymer concentration of 3g/L, PVA concentration of 0.5wt% and stirrer speed of 300 rpm), sample 3 (polymer concentration of 1g/L, PVA concentration of 1wt% and stirrer speed of 300 rpm), sample 4 (polymer concentration of 3g/L, PVA concentration of 1wt% and stirrer speed of 800 rpm) as a function of its zeta-potential.

### 3.2.2.5 Internal microstructure of the microspheres

The internal microstructure of the microspheres fabricated using condition 4 as seen in Table 1 was examined using TEM (Figure 10). An individual microsphere was selected and cut to the desired thickness. Figure 10A shows the cross-section of a typical microsphere inside the focused ion beam (FIB) instrument. The TEM image of the cross-section of the microsphere, Figure 10B, indicated that there were many nanosized pores inside the microsphere. The pore sizes were in the range of ~5 to ~20 nm. As seen in Figure 10C, the polymer appeared well crystallised with the crystals randomly oriented.

#### 3.2.2.5.1 Porosity

All the microspheres prepared under different conditions as shown in Table 1 exhibited internal porosity which was measured using equation 6 as described in Chapter 2, section 2.8.1.3. The average porosity of the microspheres prepared using condition 1, 2, 3 and 4 (sample 1, 2, 3 and 4, Table 1), was 50%, 53%, 54% and 55% respectively.

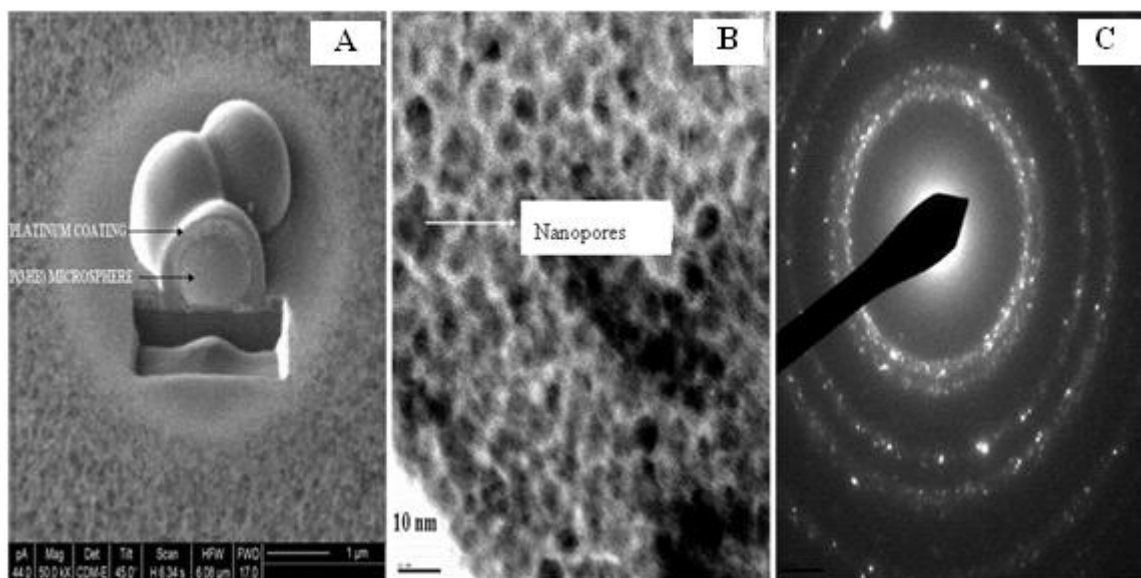


**Figure 10:-** A) Focussed Ion Beam images (FIB) showing the cross-section of a microsphere, (B) TEM image of a cross section of a microsphere, (C) Randomly oriented crystalline structure of P(3HB). Arrows indicating the presence of nanopores within the microsphere (B).

### 3.2.3 Determination of the encapsulation efficiency of P(3HB) microspheres

In order to achieve higher drug loadings, the effects of polymer concentration, PVA concentration and stirring rate on encapsulation efficiency during microsphere preparation was investigated. In this study, gentamicin, a model drug with an initial drug loading of 2 mg/g was encapsulated within the microspheres fabricated using different conditions described in Chapter 2, section 2.3.1. In this study although the initial drug loading was kept constant, the highest encapsulation efficiency (equation 1, Chapter 2, section 2.4.1) of 48%, 34% and 32% were observed in microspheres that were prepared under the conditions 4, 3 and 2 respectively, as compared to 11% for the microspheres prepared under the condition 1. The total amount of gentamicin present in the final PVA solution and the surface associated gentamicin bound to the microspheres are represented in Figure 11.

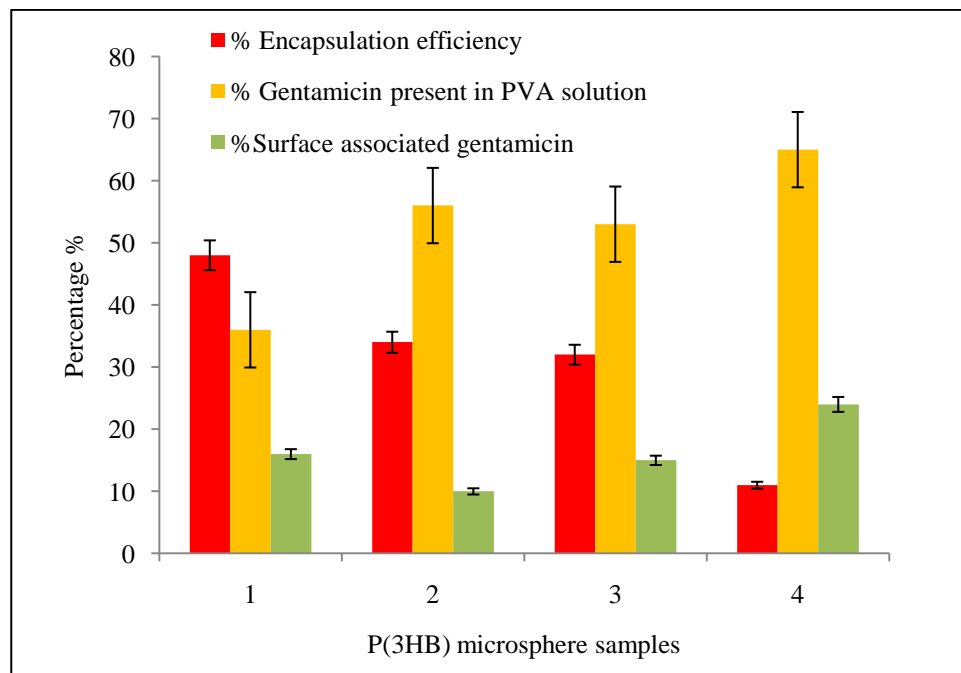


**Figure 11:-** The percentage encapsulation efficiency, percentage of surface associated gentamicin and percentage of gentamicin present in the PVA solution of the gentamicin loaded microspheres, ( $n=3$ ; error= $\pm$ s.d).

### 3.2.4 Determination of drug-polymer interaction

In order to study the effect of the drug-polymer interaction on the *in vitro* release kinetics of the drug, analysis such as XPS analysis, Fourier Transform Infrared (FTIR) and Dynamic scanning analysis were carried out.

#### 3.2.4.1 Elemental composition of the surface of the microspheres

The surface chemistry of the microspheres with the highest encapsulation efficiency of 48% was investigated using XPS analysis. As shown in Figure 12, the presence of carbon, nitrogen and oxygen content present on the surface of the gentamicin-loaded microspheres was examined using a soft X-Ray excitation. Nitrogen present in gentamicin was used to estimate the amount of drug entrapped during the microsphere fabrication procedure. The surface chemical composition of the tested sample was found to be 67.29% carbon, 31.25% oxygen and 1.05% of nitrogen. The binding energy of nitrogen N-1s is  $E_b=399.5$  eV which corresponds to the single bonded nitrogen as shown in Figure 13B. The binding energy of the nitrogen N-1s present on the gentamicin-loaded microspheres was found to be 396.13 eV, which was quite close to the value for singly bonded nitrogen.

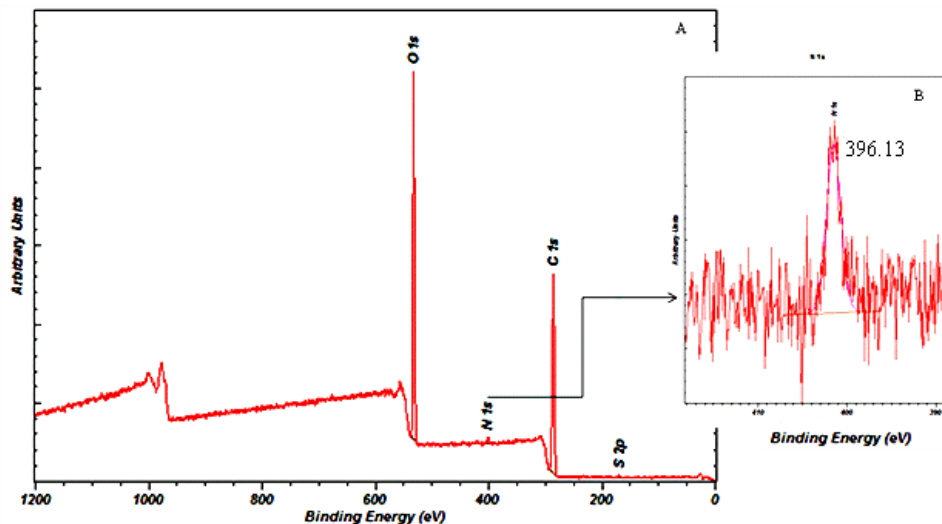


Figure 12:- A) XPS spectra of gentamicin loaded P(3HB) microspheres, B) Magnification of the nitrogen peak with a binding energy of 396.13 eV is depicted.

## 3.2.4.2 Fourier Transform Infrared studies (FTIR)

FTIR spectra of the unloaded P(3HB) microspheres and gentamicin loaded P(3HB) microspheres were carried out to identify the possible chemical drug-polymer interaction. The FTIR spectra of the unloaded P(3HB) microspheres is shown in Figure 13A, where the absorption bands at  $980\text{cm}^{-1}$ ,  $1230\text{cm}^{-1}$ ,  $1282\text{cm}^{-1}$  and  $1782\text{cm}^{-1}$  were attributed to the crystalline phase of the polymer and bands at  $1184\text{cm}^{-1}$  and  $1741\text{cm}^{-1}$  were attributed to the amorphous phase of the polymer. The stretching vibrations of the amorphous and crystalline carbonyl groups were seen at  $1741\text{cm}^{-1}$  and  $1728\text{cm}^{-1}$ . (Vallapil *et al.*, 2007; Shih *et al.*, 2006). The characteristic peaks for the gentamicin spectrum seen at wavenumbers  $1642\text{cm}^{-1}$ , attributed to the secondary amide bond was not seen in the gentamicin loaded microspheres (Figure 13B). Due to the low concentration of gentamicin in the P(3HB) microspheres, no chemical shift in the FTIR spectra of P(3HB) in the presence of gentamicin was observed, hence, no possible covalent bonding had taken place between gentamicin and P(3HB).

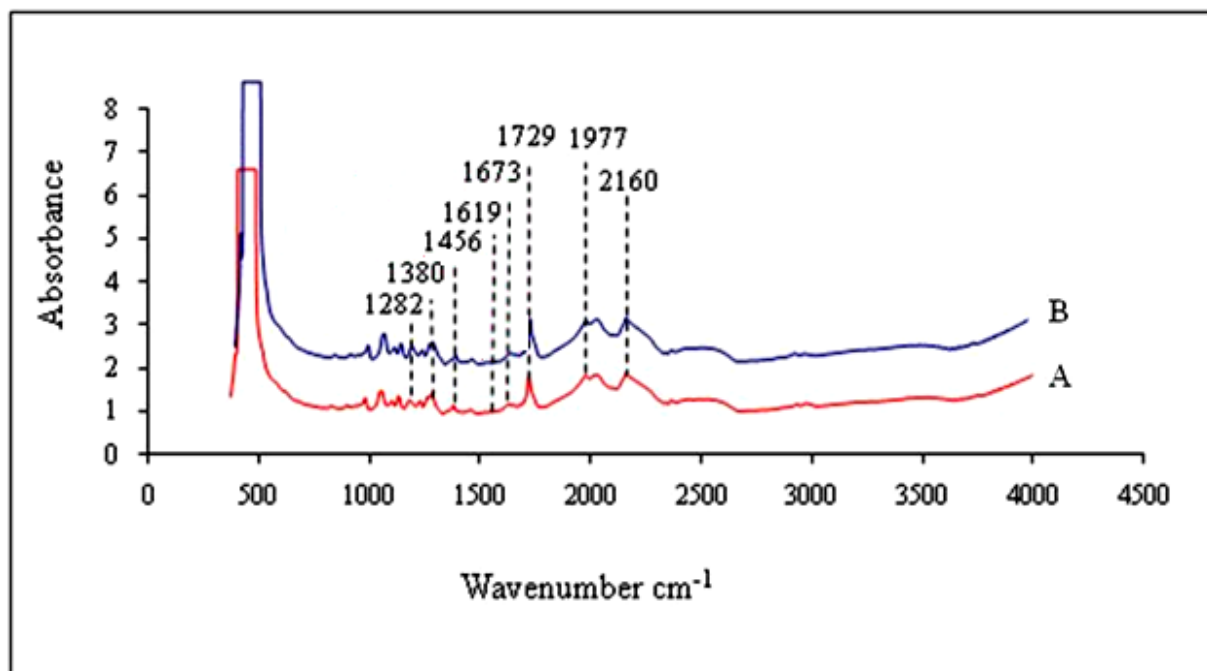


Figure 13: FTIR spectrum of (A) P(3HB) microspheres (B) Gentamicin loaded P(3HB) microspheres.

### 3.2.4.3 Thermal analysis of the microspheres

Differential Scanning Calorimetry (DSC) was used to determine the thermal properties of the gentamicin loaded and unloaded P(3HB) microspheres (Table 1). The melting temperature ( $T_m$ ) of the polymer on its own was 175.76°C, the unloaded P(3HB) microspheres were 174.72°C and the gentamicin loaded microspheres was 174.46°C. The thermograms obtained from DSC for the polymers, unloaded P(3HB) microspheres and gentamicin loaded P(3HB) microspheres, are shown in Figure 14 (A, B & C).

The crystallinity (% $X_c$ ) of the crude polymer P(3HB) microspheres and the gentamicin loaded P(3HB) microspheres were 50.44 %, 47.83 %, 44.72 % respectively as calculated using equation 9, Chapter 2, section 2.8.2.1.

The  $T_g$  of the crude polymer was around 4.35°C, which was lower than that of the P(3HB) microspheres and the gentamicin loaded P(3HB) microspheres which were 4.60°C and 4.98°C, respectively. The  $T_g$  value of the gentamicin loaded microspheres before immersion in SBF was 4.98°C which was much higher when compared to 4.60°C of the unloaded P(3HB) microspheres before immersion.

Gentamicin a complex mixture made up of three major components, gentamicin  $C_1$  with a  $T_m$  of 94-100°C, gentamicin  $C_{1a}$  and gentamicin  $C_2$  with a  $T_m$  of 107°C and 124°C did not appear as a separate peak in the DSC thermograms of the gentamicin loaded microspheres as seen in Figure 13C, when compared to the thermograms of the P(3HB) microspheres.

**Table 1:- The thermal properties of the crude polymer, P(3HB) microspheres and gentamicin loaded microspheres measured using DSC (n=3).**

Thermal Properties	$T_g$ ( $^{\circ}\text{C}$ )	%Xc	$T_m$ ( $^{\circ}\text{C}$ )
Crude Polymer	4.35	50.44	175.76
P(3HB) microspheres	4.6	47.83	174.72
Gentamicin loaded P(3HB) microspheres	4.98	44.72	174.46

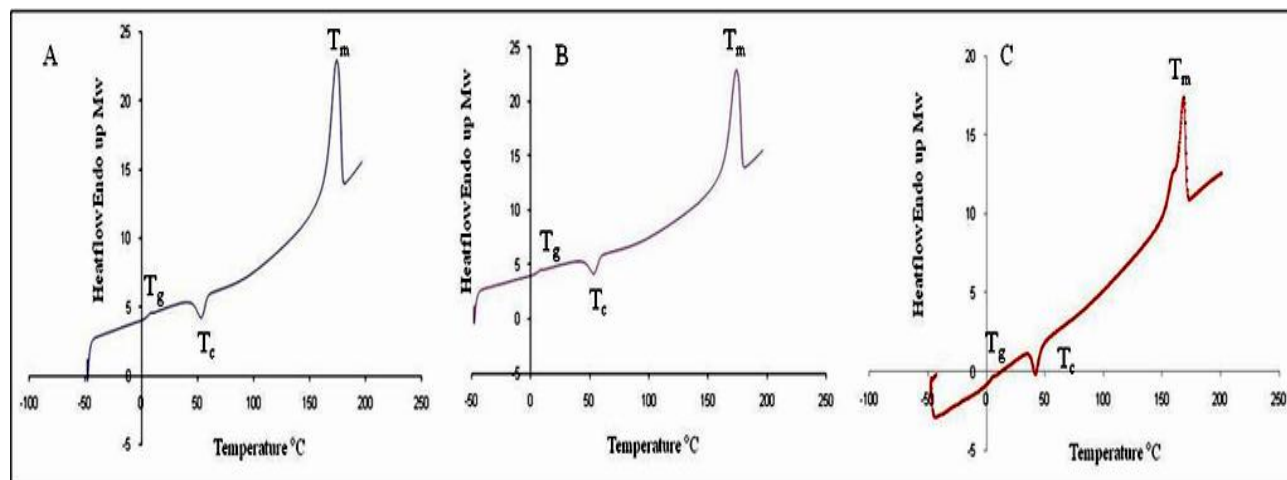


**Figure 14:- The DSC thermograms of the A) crude P(3HB), B) unloaded P(3HB) microspheres and C) gentamicin loaded microspheres (n=3).**

### 3.2.5 *In vitro* degradation of the P(3HB) microspheres

The water uptake and weight loss studies of the gentamicin loaded and unloaded P(3HB) microspheres carried out in simulated body fluid (SBF) over a period of 30 days are represented in Figure 15. The % water adsorption (% WA) for the gentamicin loaded microspheres exhibited a gradual increase from 507% to 552% over a period of 30 days when compared to the % WA of 228.11% to 584% from day 1 to day 30 of the unloaded P(3HB) microspheres (Figure 15A). Similarly, the % weight loss (% WL) of the gentamicin loaded microspheres also increased from 37% to 87% from day 1 to day 30 when compared to the %WL of 5.81% to 11.75% of the unloaded P(3HB) microspheres as seen in Figure 15B.

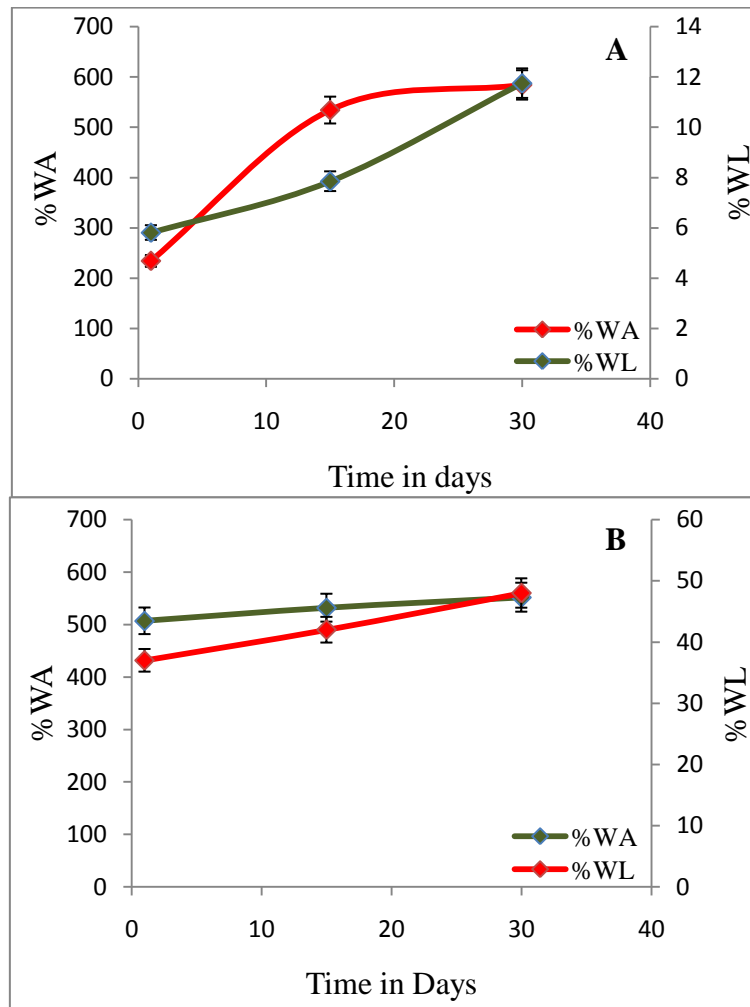


**Figure 15:- *In vitro* degradation study of A) unloaded P(3HB) microspheres and B) the gentamicin loaded P(3HB) microspheres immersed in simulated body fluid (SBF) showing (% water absorption and % weight loss) (n=3; error bars = $\pm$  SD).**

A gradual change in the pH of SBF was observed with the increase in the immersion time of the gentamicin loaded microspheres (Figure 16). The pH of SBF with the unloaded P(3HB) microspheres changed from 7.25 to 7.00 over a period of 30 days. However, the pH of SBF with the gentamicin loaded P(3HB) microspheres changed from 7.0 to 6.85 over a period of 30 days as seen in Figure 16.

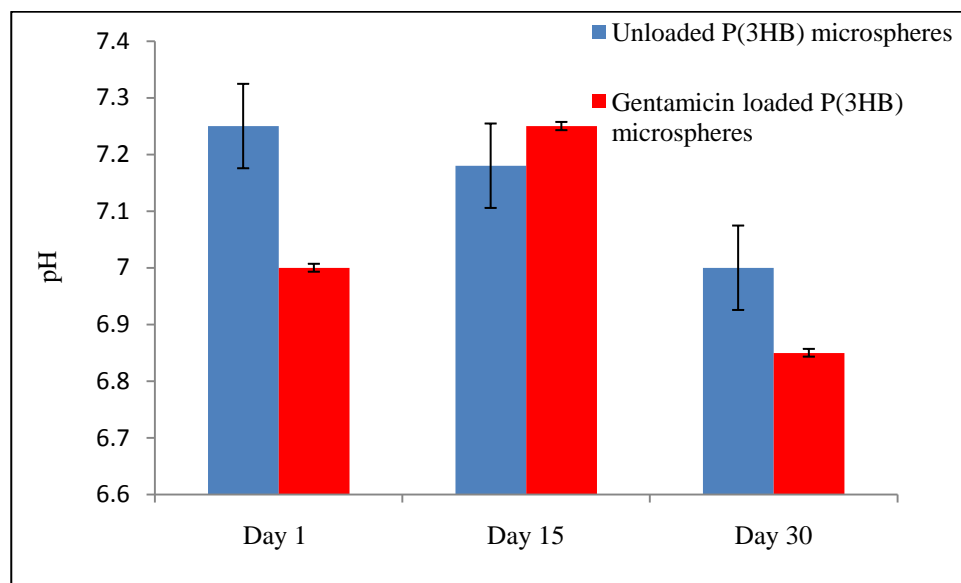


**Figure 16:- pH changes observed in the SBF solution containing unloaded P(3HB) microspheres and Gentamicin loaded P(3HB) microspheres on day 1, day 15 and day 30, (n=3; error bars = $\pm$  SD).**

### 3.2.5.1 Effect of water adsorption on the thermal properties of the gentamicin loaded and unloaded P(3HB) microspheres as a function of time

The thermal properties of the gentamicin loaded and unloaded P(3HB) microspheres after the *in vitro* degradation studies in SBF were also investigated (Figure 17). The DSC thermograms of the gentamicin loaded and unloaded P(3HB) microspheres are represented in Figure 17A, and 17B.

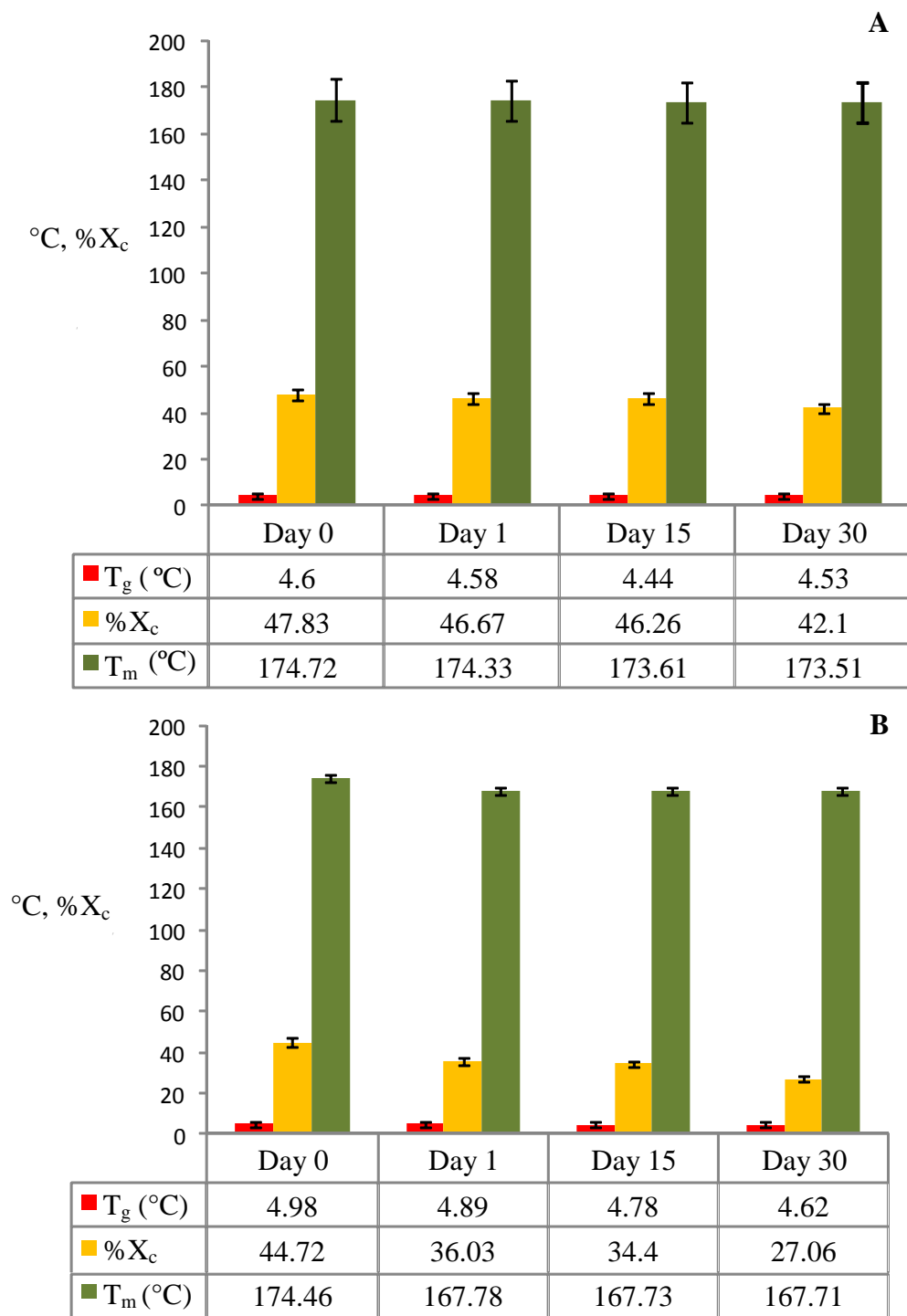


**Figure 17:- A comparison of the thermal properties of the A) unloaded P(3HB) and B) gentamicin loaded microspheres measured using DSC at day 1, days 15 and day 30 (n = 3; error bars=±SD).**

The  $T_g$  value of the unloaded P(3HB) microspheres remained almost constant after immersion in SBF, only a slight change from  $4.60^\circ\text{C}$  to  $4.53^\circ\text{C}$  was observed after immersion for over a period of 30 days. However the  $T_g$  value of the gentamicin loaded microspheres decreased from  $4.98^\circ\text{C}$  before immersion to  $4.62^\circ\text{C}$  after immersion in SBF for over a period of 30 days (Figure 16).

Changes in the other thermal properties such as the degree of crystallinity ( $\%X_c$ ) and melting temperature ( $T_m$ ) were also observed in both the unloaded and gentamicin loaded P(3HB) microspheres before and after immersion in SBF over a period of 30 days. The  $\%X_c$  of the gentamicin loaded P(3HB) microsphere before immersion was 44.72%, however after immersion in SBF for 1 day the  $\%X_c$  was reduced to 36.03%. The  $\%X_c$  of the unloaded P(3HB) microspheres before immersion was 47.83% and after immersion it reduced to 46.67%. The  $\%X_c$  of the gentamicin loaded P(3HB) microspheres on prolonged immersion in SBF for a period of 30 days was reduced from 36.03% to 34.4% and 27.06% on day 1, day 15 and day 30 respectively, when compared to the  $\%X_c$  values of the unloaded P(3HB) microspheres which was 46.67 %, 46.26 % and 42.10% on day 1, day 15 and day 30 respectively.

The  $T_m$  values of the gentamicin loaded microspheres before immersion in SBF was  $174.46^\circ\text{C}$ , which was reduced to  $167.78^\circ\text{C}$  after immersion in SBF for 1 day and continued to decrease to  $167.73^\circ\text{C}$  and  $167.71^\circ\text{C}$  over a period of 30 days. The  $T_m$  values of the unloaded P(3HB) microspheres were  $174.72^\circ\text{C}$  before immersion in SBF and reduced to  $174.33^\circ\text{C}$  after immersion in SBF for 1 day and continued to decrease to  $173.61^\circ\text{C}$  and  $173.51^\circ\text{C}$  over a period of 30 days.

### 3.2.6 *In vitro* release studies

The cumulative *in vitro* release of gentamicin from P(3HB) microspheres prepared using condition 4 (sample 4) is shown in Figure 18. In this study the release profile is seen to be biphasic, where an initial burst release was observed followed by controlled release. Gentamicin released from the microspheres in the SBF solution at 37°C of pH 7.4, was measured after periods of 1 h, 5 h, 12 h and 20 h. During the initial burst release phase (0 minutes to 1 hour) the drug released was 90.56  $\mu\text{g}/\text{mL}$ , which was 60 % of the total encapsulated drug. This phase was followed by the controlled release period which was from 5 hours to 12 hours, where small amounts of the drug *i.e* 24.56 $\mu\text{g}/\text{mL}$  to 18 $\mu\text{g}/\text{mL}$  slowly diffused from the microspheres into the release buffer. Finally, after 20 h, the cumulative drug release was 95.33%.

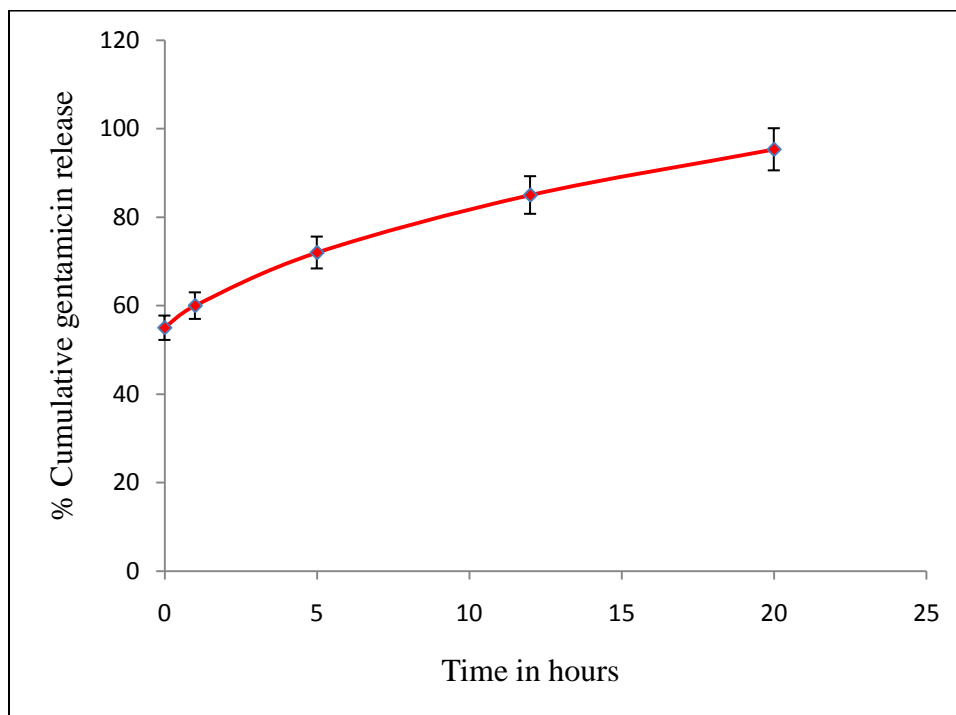


Figure 18:- *In vitro* gentamicin release profile from P(3HB) microspheres (sample 4) (n = 3; error bars= $\pm$ SD).

### 3.3 Discussions

Biodegradable polymers have been used in a number of different forms such as tablets, films and rods; however the interest in microencapsulation of the drugs within the polymeric device such as microspheres for drug delivery has accelerated. Thus, in this study a solid/oil/water emulsion (s/o/w) technique was used to fabricate the gentamicin loaded microspheres, so that a higher drug loading as well as higher encapsulation efficiency can be achieved. Three important factors such as the surfactant concentration, polymer concentration and the stirring rate were varied to study its effect on the microsphere structure.

#### 3.3.1 The effect of polymer concentration on the microsphere size

The amount of P(3HB) used per unit volume of the solvent in this study was varied from 1g to 3g respectively. Microspheres prepared under conditions 1 and 2 had an average size of  $1.7\mu\text{m}$  and  $2\mu\text{m}$ , as shown in Figure 1A and B. These microspheres were slightly larger than microspheres prepared under conditions 3 and 4 (Figure 1C and D) which were of mean size  $1.58\mu\text{m}$  and  $1.54\mu\text{m}$  respectively. The effect of varying the polymer concentration on the final microsphere structure was studied. The size of the microspheres prepared using lower concentrations of P(3HB) such as the microspheres prepared using conditions 1 were slightly smaller than the microspheres prepared using higher concentrations of P(3HB) (condition 2). It was observed that at higher concentrations of the polymer in the emulsion phase, the viscosity of the solution increases. At higher viscosities the solution is difficult to disperse due to which slightly larger microspheres are produced (Yang *et al.*, 2001). However the microspheres prepared using conditions 4 in this study with polymer concentrations of 3 g/L exhibited a smaller particle size when compared to the microspheres prepared using conditions 3. Although the increasing polymer concentration of 3 g/L in condition 4 had increased the viscosity of the emulsion phase other factors such as surfactant concentration and stirrer speed would have dominated contributing to the small size of the microspheres.

### 3.3.2 The effect of the surfactant concentration on the microsphere size

In this study PVA was used as the surfactant and the concentrations of PVA in the first emulsion phase were varied to study its effect on the microsphere particle size. The PVA concentration in the emulsion phase was varied from 0.5% w/v to 1% w/v. An increase in the PVA concentration from 0.5% w/v to 1% w/v resulted in slight differences in the sizes of microspheres such as microspheres prepared under conditions 1 and 2 had an average size of  $1.7\mu\text{m}$  and  $2\mu\text{m}$  and the microspheres prepared under conditions 3 and 4 which were of mean size  $1.58\mu\text{m}$  and  $1.54\mu\text{m}$  respectively. In addition, the microspheres had a smoother finish to the surface and were not coalesced together. An optimal viscosity of the emulsion phase is often required as this prevents the solids from precipitating out of the solution leading to the formation of smoother finished microspheres (Yang *et al.*, 2001). For e.g. in a study conducted by Yang *et al.*, it was observed that at lower PVA concentrations such as 0.025% w/v, the water droplets inside the microspheres coalesced with each other, thereby forming interconnecting water channels which increased the release rate of BSA. These water channels then increased in size eventually leading to the collapse of the microspheres (Yang *et al.*, 2001). Higher concentrations of PVA on the other hand is known to increase the viscosity of the external phase, thus making it increasingly difficult to break the emulsion droplets into smaller sizes. Hence, larger microspheres are produced. However in this study only slight differences in the microsphere sizes were observed with increasing PVA concentrations as there is a maximum PVA concentration which influences the size of the microsphere beyond which an increase in the viscosity due to the PVA concentration does not have any further influence on the size of the microspheres and the stirrer speed was found to be the dominant factor.

Once the microspheres were prepared they were washed three times with water to remove the presence of any residual PVA that was present on the surface of the microspheres. Residual PVA on the surface of the microspheres can have a significant effect on the physical properties of the microspheres such as the surface charge, surface hydrophobicity, *in vitro* drug release rate and rate of protein adsorption (Sahoo *et al.*, 2002). In this study despite the washings, residual PVA was still found associated with

the microspheres. Samples 1 and 2 (condition 1 and 2) exhibited a lower percentage of residual PVA which was 0.14% and 0.13% when compared to 0.6% and 0.54% of % residual PVA present in samples 3 and 4 (condition 3 and 4). After solvent evaporation, PVA is generally known to be bound irreversibly on the surface of the microspheres. The amount of PVA that binds to the curvature of the microspheres is again dependent on the microsphere size (Lee *et al.*, 1999). It was observed that with the decrease in the microsphere size and an increase in the PVA concentration, the PVA transfer rate from the oil/water interface onto the newly formed curved interface of the microsphere would increase (Lee *et al.*, 1999). This observation was in agreement with the results obtained in this study, where an increase in the PVA content on the surface of the microspheres was observed, when the PVA concentration in the external phase was increased. Lee *et al.*, also observed that when PVA concentrations of 0.1% w/w, 1% w/w and 10% w/w were used, the PVA content on the surface of the PLGA microspheres varied from 7.4 mg/g, 15.2 mg/g, 23.7 mg/g, thus a higher concentration of PVA was observed on the microspheres prepared using 10% w/w of PVA (Lee *et al.*, 1999).

As expected, the surface area of the microspheres increased with a decrease in the average size of the microspheres. The microspheres with a higher specific surface area also exhibited an increase in the higher % residual PVA adsorbed on the surface. Researchers like Poletto *et al.*, have also observed an increase in the specific surface area from  $33\text{m}^2/\text{g}$  to  $120\text{m}^2/\text{g}$  of the P(3HB-co-3HV) microspheres when the particle size was reduced from  $360\mu\text{m}$  to  $190\mu\text{m}$  (Poletto *et al.*, 2007).

### 3.3.3 The effect of stirring rate on the microsphere size

In order to study the effect of stirring rate on microsphere size, the stirring rate was maintained at 300 rpm and 800 rpm in the final emulsification step under varying PVA and P(3HB) concentrations. The microsphere sizes were  $1.7\mu\text{m}$  and  $1.54\mu\text{m}$  when prepared under conditions 1 and 4 (sample 1 and 4, Table 1), with a stirrer speed of 800 rpm. Similarly, the microspheres prepared under condition 2 and 3 (sample 2 and 3, Table 1), with a stirrer speed of 300 rpm exhibited an average size of  $2\mu\text{m}$  and  $1.58\mu\text{m}$  respectively. It has been previously observed that at an increased stirring rate of 800 rpm,

the microsphere size is significantly reduced (Kassab *et al.*, 1997). From the results obtained in this study, it can be concluded that the stirrer speed may have contributed to the small size of the microspheres. A highly viscous solution is difficult to disperse at a lower stirrer speed, due to which larger sized microspheres are produced. Martin *et al.*, observed the formation of larger P(3HB) microspheres of  $100\mu\text{m}$  to  $250\mu\text{m}$  when the stirrer speed was reduced to 500 rpm when compared to the smaller microspheres (5 to  $10\mu\text{m}$ ) produced when the stirrer speed was increased to 800 rpm (Martin *et al.*, 2000). Similar observations were made in this study where at a higher stirrer speed of 800 rpm smaller sized microspheres were produced when compared to those produced at 300 rpm. Thus the stirrer speeds could have provided the required energy to disperse the oil phase in water producing smaller sized microspheres. It was also observed that the average microsphere size in this study varied from only 1 to  $5\mu\text{m}$  despite the increasing viscosity of the emulsion phase in the presence of both PVA and polymer. In this study the effect of the stirrer speed had a dominant effect on the microsphere size as there is a maximum viscosity which influences the size of the microsphere beyond which an increase in the viscosity due to the PVA and polymer concentration does have any further influence on the size of the microspheres (Yang *et al.*, 2001).

### **3.4 Microsphere characteristics**

#### 3.4.1 Surface morphology

In this study, the surface morphology of the microspheres analysed using SEM revealed the presence of uniform spherical shaped microspheres, under the different preparation conditions used. The type of solvent and the volume used also influenced the surface morphology of the microspheres. In this study chloroform was chosen as the solvent as opposed to dichloromethane due to lesser miscibility of chloroform in water, which is 1 in 200 parts when compared to dichloromethane, which is 1 in 50 parts (Sahoo *et al.*, 2002). An increased amount of PVA is known to partition into the polymer phase when the organic solvent exhibits an increased miscibility in water because of higher hydrophilicity (Sahoo *et al.*, 2002). Thus in order to avoid a higher deposition of residual

PVA on the surface of the microspheres chloroform was used as the solvent. Although the presence of residual PVA was detected on the surface of the microspheres, the small amount of surface associated PVA may have not contributed to the changes in the surface morphology. The volume of chloroform used in this study however would have contributed to the production of uniform, spherical shaped microspheres. A decrease in the volume of the solvent is also known to affect the surface morphology of the microspheres thereby increasing the number of surface pores at a lower volume of the solvent. At a lower solvent volume the water droplets entrapped within the microspheres are known to evaporate leaving behind empty spaces both on the surface as well as within the microspheres thus contributing to a rough surface morphology. However in this study, since no surface associated pores were observed, the volume of the solvent may have been optimal for the production of smooth microspheres. Yang *et al.*, observed a rough surface morphology with increased surface porosity when a low volume of methylene chloride was used as the solvent for the fabrication of PCL and PLGA (65:35) microspheres (Yang *et al.*, 2001).

#### 3.4.2 Surface Hydrophobicity

Microspheres fabricated with a higher PVA (1%) concentration appeared to be more hydrophilic in nature as compared to those that were formulated with 0.5% PVA, as seen from the lesser amounts of Rose Bengal Dye bound to their surfaces. In a relevant study Sahoo *et al.*, observed a lower binding of  $0.005\mu\text{g/mL}$  of Rose Bengal dye on the surface of nanoparticles which were formulated with 5% PVA when compared to  $0.024\mu\text{g/mL}$  bound on nanoparticles formulated with a 0.5% PVA concentration. During microsphere preparation, hydrophobic ends of PVA penetrate into the organic phase and interact with P(3HB) microspheres due to which an irreversible binding of PVA occurs on the surface of microspheres when the solvent evaporates. An increased amount of PVA is known to partition into the polymer phase when the organic solvent exhibits an increased miscibility in water because of higher hydrophilicity. Since PVA is a hydrophilic polymer, therefore the higher amount of residual PVA on the surface of the microspheres would have accounted for the higher hydrophilicity (Sahoo *et al.*, 2002).

### 3.4.3 Zeta-potential analysis

The zeta-potential values reflected the change in the surface charge due to the deposition of PVA on the surface of the microspheres (Wang *et al.*, 2007). The COOH groups on the microspheres exhibited a negative charge at due to deprotonation (pH 7), however at a lower pH a charge reversal from negative to positive was observed. This phenomenon was observed for all microspheres prepared using different conditions. Similarly, decreases in positive zeta-potential values were observed when the concentration of residual PVA on the surface of microspheres was increased. Often non-ionic surfactants such as PVA are known to strongly adhere on the microsphere surface by anchoring the hydrophobic tail into the polymer only when it is hydrophobic, leaving the polar head protruded on the surface (Sahoo *et al.*, 2002). During the microsphere preparation, hydrophobic ends penetrate into the organic phase and interact with P(3HB) microspheres due to which an irreversible binding of the PVA occurs on the surface of microspheres when the solvent evaporates. Thus, when P(3HB) is fabricated into microspheres, PVA used as a surfactant coats the surface thereby shielding the surface charge of PHB. Due to this, P(3HB) processed into microspheres carries a much less negative charge at neutral pH when compared to the negative charge of the neat P(3HB) (-40 mV at neutral pH). In acidic solutions such as pH <4.0, C=O of the ester present on the surface of microspheres gets protonated. As a result, at lower pH the negative surface charge is reversed to a positive surface charge. Similar observations were also made by Lee *et al.*, [18] who showed that with an increase in PVA concentration from 0.5% to 5%, the zeta-potential values of the PLGA nanoparticles decreased from -15.4 mV to -08.0 mV at neutral pH. However in acidic solutions (pH<5.0), the zeta-potential values of microspheres with lower PVA concentration (0.5% w/v) showed a relatively high positive charge when compared to the lower surface charge of microspheres prepared with higher PVA concentration (1% w/v) (Lee *et al.*, 2002).

#### 3.4.3.1 Effect of zeta-potential on protein adsorption

The changes in the surface properties of the microspheres can have a significant impact on their use for biological applications (Patil *et al.*, 2007). Thus in this study the protein adsorption in the presence of varying surface charges were studied. In this study, a higher

amount of protein was adsorbed on microspheres with a lesser negative charge when compared to those with a higher negative charge. BSA adsorption on a surface of an adsorbent at a neutral pH occurs due to electrostatic interactions. Since BSA is negatively charged at neutral pH and the microspheres fabricated using different conditions also exhibited a negative surface charge at neutral pH, other interactive factors such as van der Waals, and steric interactions could have also contributed to the protein-adsorbent interaction (Robertson *et al.*, 1990). Similar observations were made by Patil *et al.*, where 10 mg/mg (nanoparticles) of protein adsorption on the nanoparticles with a negative charge of -17.72 mV was observed. However 67.40 mg/mg (nanoparticles) of protein adsorbed on cerium oxide nanoparticles with a zeta-potential charge of 59.32 mV. The authors' had observed an increasing protein adsorption on nanoparticles with a positive zeta-potential charge, further confirming that the electrostatic interaction was the primary reason for the protein adsorption.

#### 3.4.4 Porosity

In this study, the internal porosity within the microspheres measured using the liquid displacement technique showed no significant differences in the differently sized microspheres. During the formation of the microspheres after the solvent is removed, the water droplets within the microspheres are quickly trapped, which are later dried out leaving pores behind. The outer wall of the microspheres prevents further influx of water and the formation of large water droplets within the microspheres (Yang *et al.*, 2001). The interpenetration of the surfactant at higher concentrations within the polymer matrix prevents the coalescing of the water droplets together and formation of one hollow core within. However at lower concentrations of PVA the water droplets are known to coalesce with each other forming interconnecting water channels eventually forming much non-uniform bigger pores. Yang *et al.*, also observed the formation of much bigger pores when low PVA concentrations of 0.025% w/v was used. However, in the presence of 0.5% w/v of PVA the water droplets were stabilised preventing them from coalescing thus leading to uniform internal porosity. Thus in this study, the rapid solidification of the microspheres as well the PVA concentration from 0.5% w/v and 1% w/v was optimal and contributed to an even pore distribution throughout the polymer matrix.

#### 3.4.5 Determination of the encapsulation efficiency of P(3HB) microspheres

In another part of this study, the microspheres prepared under the different conditions were loaded with the drug gentamicin during microsphere formation to study the efficacy of these microspheres as drug delivery vehicles. Thus in order to achieve higher encapsulation efficiencies various factors such as drug/polymer ratio, type of solvent, and PVA concentrations on the encapsulation efficiencies were studied. In this study the drug concentration was kept constant at 2 mg/g (during microsphere preparation, Chapter 2 section 5.3.1) and the polymer and PVA concentration varied. The microspheres prepared under condition 4, exhibited the highest encapsulation efficiency of 48% when compared to the microspheres produced using other conditions. In this study, the faster rate of solvent removal in the microspheres with a smaller size led to the rapid entrapment of the drug. Sendil *et al.*, also observed an increase in the encapsulation efficiency with a decrease in microsphere size. P(3HB-co-3HV) microspheres with average size of 399 $\mu\text{m}$  in diameter exhibited lower encapsulation efficiency of 20.2% when compared to 30.1% encapsulation efficiency exhibited by the smaller microspheres (340 $\mu\text{m}$ ) (Sendil *et al.*, 1999).

Microspheres fabricated with higher concentrations of PVA are known to yield stable emulsions which prevent the transfer of the encapsulated drugs into the surroundings; as a result the drug is more evenly distributed within the interior of the microspheres (Yang *et al.*, 2001). This could also explain the higher encapsulation efficiency of gentamicin in the P(3HB) microspheres fabricated with a higher PVA concentration used in this study when compared to the lower encapsulation of 11% observed within the P(3HB) microspheres fabricated with a lower PVA concentration.

Variations in the polymer/drug ratio influence the encapsulation efficiency (Wang *et al.*, 2007). In the presence of high concentrations of the polymer and fixed drug concentrations, higher concentrations of the drug are encapsulated within the microspheres thus exhibiting higher encapsulation efficiency (Wang *et al.*, 2007). This could be another reason why higher encapsulation efficiency was observed in sample 4 where an increased polymer content of 3g was used when compared to the microspheres

fabricated with a lower polymer content of 1g. In this study, the highest encapsulation efficiency of 48% was observed in microspheres that were prepared under condition 4 (sample 4), were chosen for the *in vitro* drug release studies.

#### 3.4.6 Determination of drug-polymer interaction

Other analyses such as XPS, FTIR and thermal analysis were also carried out on these particular microspheres to study the changes in the physicochemical properties of the polymer in the presence of the drug.

##### 3.4.6.1 Elemental composition of the surface of the microspheres

The assessment of the gentamicin adsorption on the microsphere surface prepared under condition 4 (sample 4, Table1) was done on the basis of nitrogen content present on the samples since the nitrogen species is unique to the drug and is absent in the P(3HB) microspheres. From the XPS data a significant increase in the nitrogen content on the surface of the gentamicin loaded samples was observed when compared to the unloaded P(3HB) microspheres, where, as expected, only carbon and oxygen were seen. This result therefore indicated that apart from being encapsulated, some amount of gentamicin was bound onto the microsphere surface. Similar results were also observed by Naraharisetti *et al.*. They also observed the presence of surface bound drugs (gentamicin) on the microspheres made using poly-L-lactide (PLLA) and copolymers of DL-lactic-co-glycolic acid (PLGA) (Naraharisetti *et al.*, 2005). The microspheres with the highest encapsulation efficiency of 64.5% and largest particle size of 308 $\mu$ m in diameter exhibited the highest % of nitrogen on the surface, which was 2.01%. This indicated that gentamicin, in addition to being encapsulated within the microspheres, it was also found on the surface (Naraharisetti *et al.*, 2005).

##### 3.4.6.2 Fourier Transform Infrared studies (FTIR)

The drug and polymer interaction can play a very important role in the drug release characteristics. This chemical interaction between the drug/polymer is known to affect the *in vitro* release profile (Stephens *et al.*, 2000). In this study Fourier Transform Infrared spectroscopy (FTIR) was used to analyse the possible interaction between the

drug gentamicin and P(3HB). From the FTIR results the characteristic bands of gentamicin at  $1642\text{cm}^{-1}$  attributed to the secondary amide structure was not detected in the microsphere samples loaded with the gentamicin. The concentration of the drug present within the microspheres could have been too low to detect any interaction with the polymer using a not so sensitive technique such as FTIR. Some researchers such as Stephens *et al.*, have used other techniques such as NMR and mass spectroscopic analysis to study the effect of the drug on the drug release rate. From the results the authors' observed that the drug release was retarded due to the amide formation between gentamicin sulphate and the polyanhydride matrix (Stephens *et al.*, 2000). Although FTIR analysis revealed no possible bond formation in this study, more sensitive techniques such as NMR and mass spectroscopic analysis should be employed in the future.

#### 3.4.6.3 Thermal analysis of the microspheres (DSC)

Differential Scanning Calorimetry is also another method of detecting the existence of a possible interaction between the drug and the polymer. In this study the thermal behaviour of the crude polymer, unloaded P(3HB) microspheres and the gentamicin loaded microspheres were compared to study the effect of the processing conditions and drug loading on the thermal properties of the polymer. From the thermograms of the crude polymer and the unloaded microspheres obtained from DSC, it was noticed that the glass transition temperature ( $T_g$ ) of the unloaded polymer had increased from  $4.35^\circ\text{C}$  to  $4.6^\circ\text{C}$ . This indicated that the processing conditions of the polymer had increased the crystallinity of the polymer (Martin *et al.*, 2000). Also, an increase in the  $T_g$  value ( $4.98^\circ\text{C}$ ) of the gentamicin loaded microspheres were also observed when compared to the unloaded P(3HB) microspheres. This difference in the  $T_g$  values between the gentamicin loaded and unloaded P(3HB) microspheres indicated that with an increase in the concentration of the emulsion in the presence of the drug, the mobility of the polymer chains is reducing the  $T_g$  value of the polymer (Chang *et al.*, 2006). The  $T_m$  of the gentamicin loaded microspheres of  $174.46^\circ\text{C}$  was also lower than that of the unloaded P(3HB) microspheres, indicating that the crystalline properties of the gentamicin loaded P(3HB) microspheres decreased in the presence of the drug, probably due to the

incorporation of the drug within the crystalline structure of the polymer hence disrupting the crystal structure. However, from the DSC thermograms of the gentamicin loaded P(3HB) microspheres in this study, the thermal properties of only the polymer dominated the thermogram and no thermal properties of the drug itself could be observed. The drug ratio of drug/polymer was too low to be detected as a result the thermal properties of the drug itself could not be detected. Researchers like Bidone *et al.*, have also observed a decrease of 10°C in the  $T_m$  of ibuprofen loaded P(3HB) microspheres when compared to the unloaded P(3HB) microspheres. It was found that ibuprofen had coexisted as both a crystalline and molecular dispersion within the P(3HB) matrix thereby affecting the crystalline properties of the polymer in the microspheres. The thermal properties of ibuprofen were observed in the DSC thermograms due to the crystalline properties of the drug within the P(3HB) microspheres (Bidone *et al.*, 2009).

In this work the crystalline properties of the polymer were also altered after the solvent evaporation procedure as well as in the presence of the drugs. Shih *et al.* also conducted a study where P(3HB) and chitosan microspheres were synthesised using a single and double emulsion method and analysed by X-ray diffraction and FTIR techniques to identify the interaction of PVA used as a surfactant in the emulsion phase. From the results a minor phase indicative of PVA was observed in the XRD and FTIR data. This result indicated that the solvent evaporation techniques had an influence on the physical properties of the polymer (Shih *et al.*, 2007). Thus for this study the presence of PVA used for the fabrication of the microspheres would have acted as an impurity thus influencing the crystalline properties of the P(3HB).

#### 3.4.7 In vitro degradation studies

In this study the water uptake and weight loss studies of the unloaded P(3HB) microspheres and the gentamicin loaded microspheres were carried out for a period of 30 days to investigate the influence of the drug on the degradation properties of the microspheres. The gentamicin loaded microspheres exhibited a higher weight loss when compared to the unloaded P(3HB) microspheres. Similarly the water absorption by the gentamicin loaded microspheres also gradually increased exhibiting a simultaneous increase in the weight loss over a period of 30 days. For the gentamicin loaded P(3HB)

microspheres, the presence of the hydrophilic drug as well the % residual PVA on the surface of the microspheres would have also contributed to the increased water uptake when compared to the unloaded P(3HB) microspheres with just a coating of PVA. The water adsorption in the gentamicin loaded microsphere also increased due to the higher solubility or hydrophilicity of the drug (Frank *et al.*, 2004). In this study, the rapid dissolution of the drug may have created additional pores leading to the increased water uptake and subsequent weight loss of the gentamicin loaded microspheres due to hydrolysis when compared to the unloaded P(3HB) microspheres. Bazzo *et al.*, observed the rapid ingress of water within the P(3HB) microspheres due to the desorption of the drug crystals (Piroxicam) on the surface of the microspheres, this further led to the increased water uptake within the pores (sizes between 40 to 100Å) created due to the drug solubilisation in the dissolution medium (Bazzo *et al.*, 2008). However the water adsorption in the unloaded microspheres in this study was relatively low when compared to the gentamicin loaded P(3HB) microspheres with no appreciable water uptake due to a physical properties of the polymer such as high crystallinity.

#### 3.4.7.1 Effect of water adsorption on the thermal properties of the gentamicin loaded and unloaded P(3HB) microspheres as a function of time

In this study the thermal properties of the gentamicin loaded and unloaded P(3HB) microspheres were compared after the immersion studies in SBF, in order to investigate the effect of water adsorption and simultaneous degradation on the thermal properties as a function of time. The results from this study showed that no significant changes occurred in the  $T_g$  values of both the unloaded and gentamicin loaded P(3HB) microspheres after immersion in SBF on day 1 when compared to the microspheres before immersion. The high crystallinity of the polymer may have contributed to the insignificant changes in the  $T_g$  values on day 1 of both the gentamicin loaded and unloaded P(3HB) microspheres (Frank *et al.*, 2004). However, with the increase in the immersion time (from day 1 to day 15), the gentamicin loaded microspheres as well as the unloaded microspheres exhibited a reduction in the  $T_g$  value, which also coincided with the increased water uptake of the microspheres. A similar trend in the reduction of the  $T_g$  values of both the gentamicin loaded and unloaded P(3HB) microspheres were observed until day 30 with the highest

reduction in the  $T_g$  values observed for the 30 days immersion sample. This decrease in the  $T_g$  value occurred alongside an increase in the water uptake of the microspheres. Hence, the polymer chains must become more mobile due to the presence of water (Siepmann *et al.*, 2001). Therefore, with the increase in the water uptake into the polymeric matrix, the  $T_g$  is reduced, causing the polymer chains to be more mobile (Siepmann *et al.*, 2001). Frank *et al.*, made a similar observation when the  $T_g$  values of the lidosalt-loaded poly(lactide-co-glycolide) (PLGA) microspheres started to decrease after about 14 days of immersion in the buffer. During the initial lag phase the  $T_g$  value was 39°C after which the  $T_g$  value reached about 33°C after 30 days. A linear decrease in the  $T_g$  values along with the molecular weight was also observed (Frank *et al.*, 2004).

The degree of crystallinity ( $\%X_c$ ) and  $T_m$  values for the gentamicin loaded P(3HB) microspheres also exhibited a significant reduction ( $n=3, ***p<0.001$ ) from day 1 to day 30 when compared to the unloaded P(3HB) microspheres over a period of 30 days. This change in the  $\%X_c$  and  $T_m$  values of the gentamicin loaded microspheres was possibly due to the initial degradation that takes place in the amorphous region, followed by the degradation caused due to the chain scission in the crystalline domains, thus decreasing the overall crystallinity of the polymeric matrix.

### 3.4.8 *In vitro* release studies

The *in vitro* drug release rate is largely dependent on the size of the microspheres (Edlund *et al.*, 2002). Larger microspheres (100-300 $\mu\text{m}$ ) tend to release the drug slowly and for a much longer time when compared to the smaller microspheres (Berkland *et al.*, 2002). This slow release is due to the reduced drug diffusion path within microspheres and the decreased specific surface area of larger microspheres when compared to smaller microspheres. Thus in this study, drug release within a period of 24h was observed which can probably be attributed to the small size (1.54 $\mu\text{m}$  in diameter) of the microspheres.

The *in vitro* drug release is also dependent on the drug distribution within the microspheres. The high initial burst release is often attributed to the presence of surface associated drugs (Kassab *et al.*, 1997). In this study gentamicin, in addition to being encapsulated within the microspheres, was also adsorbed on the surface of the microspheres, as confirmed by the XPS analysis. As a result, an initial burst release of 60% of the total encapsulated drug was recorded in this study. After an initial burst release, a slow and controlled release of the drug was observed.

Often factors such as the type of encapsulated drug and polymer determine the rate of slow and sustained release (Poletto *et al.*, 2007). In this study, a sustained release phase from 5 hours to 12 hours was observed where small amounts of the drug, slowly diffused from the microspheres into the release buffer. The length of the sustained release phase of polymeric matrices is largely dependent on the type of polymer used (Naraharisetti *et al.*, 2005). Polymers are known to undergo degradation either by surface erosion or bulk degradation or a combination of both. With the increase in the penetration of water molecules into the polymeric matrix, homogenous surface erosion starts to occur which is followed by bulk degradation.

In this study, the total cumulative release of 95.33% was found to occur within a period of 20 hours, therefore drug release by either surface erosion or degradation was not considered due to the slow degradable nature of the polymer. The drug release in the final stage occurred most likely through the water channels that were created by the diffused drugs. Further in this study, it was observed that in the presence of the hydrophilic drug

and PVA, the water uptake rate of the polymer was accelerated, thereby having a significant impact on drug release.

### 3.5 Conclusions

In this study, a solid-in-oil-water (s/o/w) technique was used in an attempt to produce tailored poly(3-hydroxybutyrate) P(3HB) microspheres. The effects of several parameters such as polymer precipitation, surfactant concentration and stirring rate were considered. The average size of the microspheres varied from  $2\mu\text{m}$  to  $1.54\mu\text{m}$  with specific surface areas from  $9.60\text{ m}^2/\text{g}$  to  $6.05\text{ m}^2/\text{g}$ . The microspheres produced using low stirring rates of 300 rpm produced slightly larger microspheres when compared to the smaller microspheres produced when the stirring rate was increased to 800 rpm. The solvent (chloroform) removal from the emulsion after microsphere fabrication did not produce any change in the surface morphology of the microspheres when observed under SEM. The presence of PVA used as a surfactant and the polymer concentration influenced the drug distribution within the microspheres. The presence of PVA in the internal water phase enhanced the stabilization of the inner water droplets and the surface associated PVA prevented the microspheres from coalescing. The presence of residual PVA on the surface of the microspheres affected factors such as zeta-potential, surface hydrophobicity, protein adsorption and the encapsulation efficiency of the microspheres.

The surface and internal morphology, drug distribution and release kinetics of the microspheres exhibiting the highest encapsulation efficiency (48%), were investigated. The DSC analysis showed that the microsphere preparation process had influenced the thermal behaviour of the microspheres. The glass transition temperature  $T_g$ , of the microspheres had increased and the  $T_g$  and  $\%X_c$  decreased in the presence of the drug (gentamicin). The hydrophilic nature of the drug also had an influence on the polymeric degradation as well as the drug release behaviour. The *in vitro* release of gentamicin was biphasic where an initial burst release was observed followed by a diffusion mediated sustained release.

The knowledge gained in this work about the different factors influencing the drug release will have important implications for the controlled delivery of potent drugs in various therapeutic applications.

# Chapter 4

Multi-functional P(3HB)  
microsphere/45S5Bioglass<sup>®</sup>-based  
composite scaffolds for bone tissue  
engineering

#### 4.1 Introduction

There are several factors that make polyhydroxyalkanoates (PHAs) excellent candidate materials for use in TE and other biomedical applications, such as biocompatibility, ability to support cell growth, cell adhesion and biodegradability (Chen *et al.*, 2005; Zhao *et al.*, 2003). However, when used as scaffolds in bone TE, PHAs fail to actively bind to the living tissue by means of a biologically active apatite layer or meet the mechanical demands in load-bearing applications. Therefore, these polymers are combined with inorganic bioactive materials, such as bioactive glass or hydroxyapatite (HA), to increase their applicability in bone TE (Misra *et al.*, 2006). The addition of bioceramics have also been observed to alter the degradation rate of the polymer composite by having an effect on certain parameters such as water absorption, weight loss and pH (Misra *et al.*, 2010). The addition of bioactive ceramics in the composite polymeric system is also known to affect the biocompatibility of the composite systems due to the changes incorporated in the surface roughness, surface wettability and protein adsorption rate (Chen *et al.*, 2006; Rainer *et al.*, 2008). There is a growing need to make multifunctional scaffolds to include applications such as drug delivery. One of the major problems or complications associated with the use of implants or scaffolds for bone treatment is the occurrence of infections. Often, microorganisms adhere to the biomaterials used, forming a biofilm on the surface, which is a major contributor to the pathogenesis of implant-associated infections. These biofilms often exhibit a high antibiotic resistance. Osteomyelitis is one such bone infection, which is hard to treat (Korsatko *et al.*, 1984). The main causative agent for osteomyelitis is *Staphylococcus aureus*, *Streptococcus* and *Haemophilus influenzae*. To counteract bone infection following implantation, gentamicin is often used, an aminoglycoside antibiotic with a broad spectrum of activity against both Gram-positive and Gram-negative bacteria (Brin *et al.*, 2008; Solberg *et al.*, 1999). Thus the need for functionalizing polymer/composite scaffolds with improved surface topography for cell attachment as well as a substrate for delivering drug is growing.

In the present chapter, a series of experiments is designed to develop a multifunctional P(3HB)/Bioglass<sup>®</sup> composite system with extra functionalities for tissue engineering

applications. The major tasks carried out are schematically represented in Figure 1. In this strategy, the drug is encapsulated in the polymer phase, which uniformly coats the 3-D bioactive glass or ceramic scaffold. The goal is to deliver the drug at a controlled rate, while the rigid inorganic scaffold maintains the structural integrity of the construct. In the present investigation, novel scaffolds based on bioactive glass (45S5 Bioglass<sup>®</sup>) foams combined with P(3HB) microspheres as drug carriers have been developed for bone tissue engineering. The reason for using gentamicin, as the drug for this study was its broad spectrum of activity against both Gram-positive and Gram-negative bacteria.

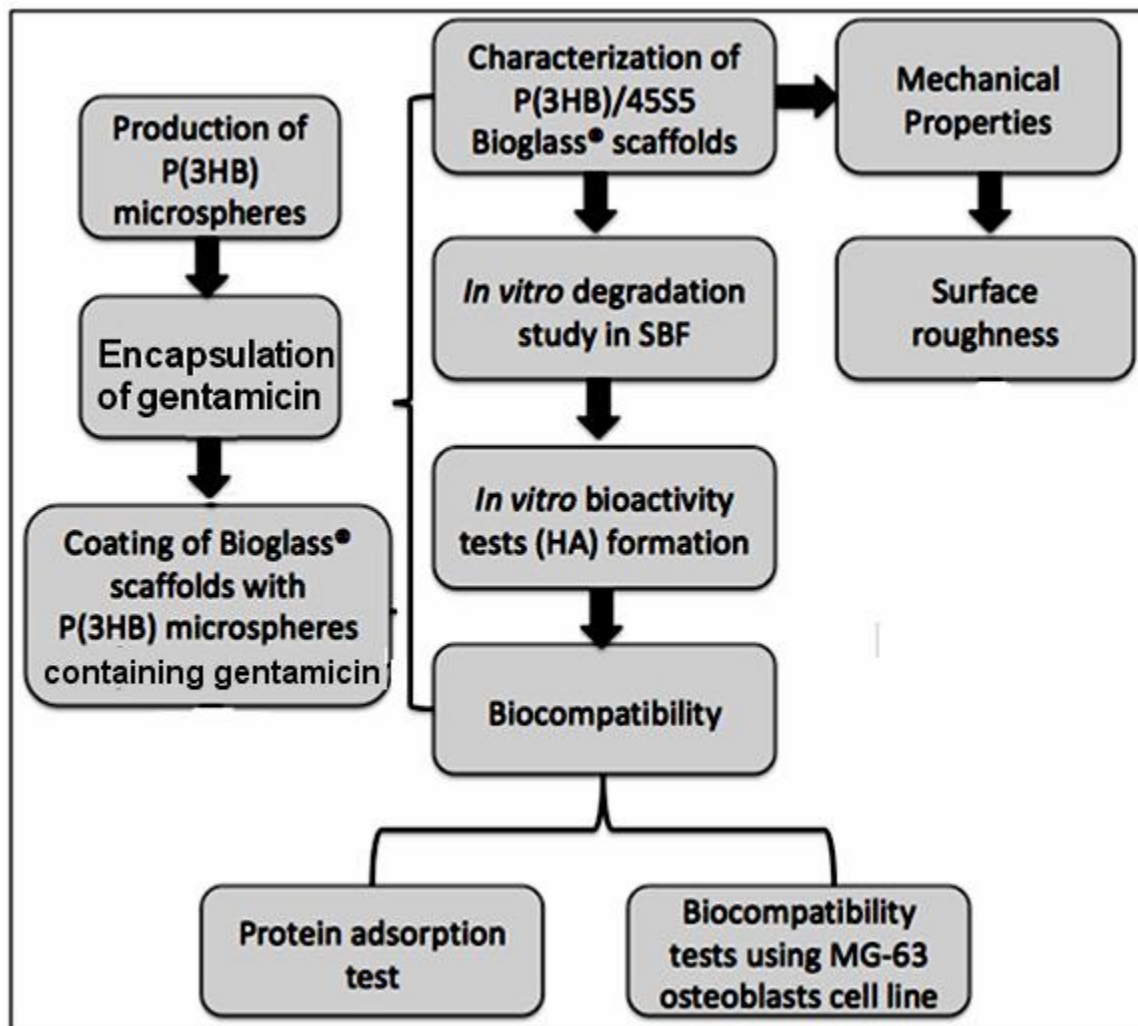
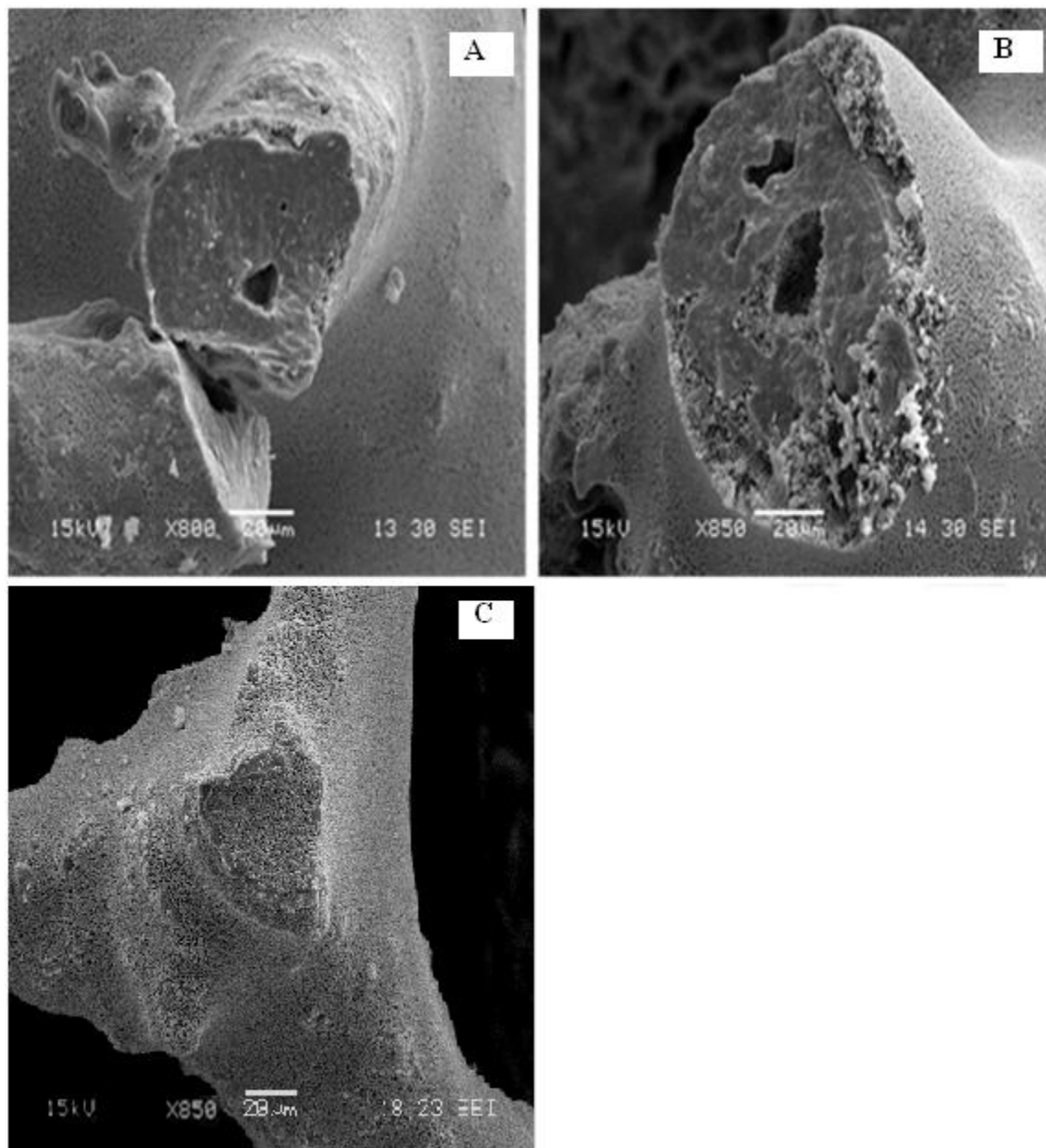


Figure 1: - Diagrammatic representation of the research methodologies used in this study.

## 4.2 Results

### 4.2.1 P(3HB) microsphere-coated 45S5Bioglass<sup>®</sup> composite scaffolds

The first goal in the task of fabricating the microsphere-coating on the scaffold was to achieve a homogenous and structurally robust coating throughout the three-dimensional (3-D) structure of the scaffold. Therefore, methods such as agitation and sonication, described in Chapter 2 section 2.2.4.1 and 2.2.4.2 were used to coat 45S5Bioglass<sup>®</sup> scaffolds with P(3HB) microspheres. Besides using the slurry-dipping technique to coat the scaffold, the scaffolds were also immersed in the final PVA emulsion during microsphere production, as described in Chapter 2 section 2.2.4.3, and it was expected that the scaffolds would be well coated with the microspheres after the evaporation of the emulsion. In both the agitation and sonication methods similar results in terms of homogeneity of the coating were achieved, indicating that both techniques are in principle suitable for coating 3-D porous scaffold with P(3HB) microspheres. When the scaffolds were left in the final PVA emulsion, it was found that not only a non-homogenous coating was observed, but also etching of the 45S5Bioglass<sup>®</sup> surface had been initiated. The sonication technique, in which the scaffold was immersed in the microsphere slurry after sonication for different time periods, scaffolds were seen to acquire a microsphere coating both on the surface and within the crevices and scaffold pores, as seen in Figure 2. Therefore, after detailed investigation, the optimum condition chosen for coating was sonication of 1 wt% of aqueous microsphere suspension for 5 mins followed by dip coating the scaffold for 5 minutes.



**Figure 2:- SEM images of the 45S5Bioglass<sup>®</sup> scaffolds immersed for (A) 2 mins, (B) 5 mins, (C) 10 mins in the sonicated microsphere slurry. Uniform coatings of microspheres on the surface of the scaffold are seen in images (A) 800x, (B) 850x C) 1500x.**

The gentamicin-loaded microspheres were seen to attach both onto the 4S5Bioglass<sup>®</sup> scaffolds surface and within the crevices forming a fairly homogenous coating, as revealed by the SEM micrographs shown in Figure 3. The thickness of the coating varied from being a single-microsphere layer, and therefore 2 $\mu$ m thick, to a multi-microsphere layer with a thickness of ~5–6  $\mu$ m.

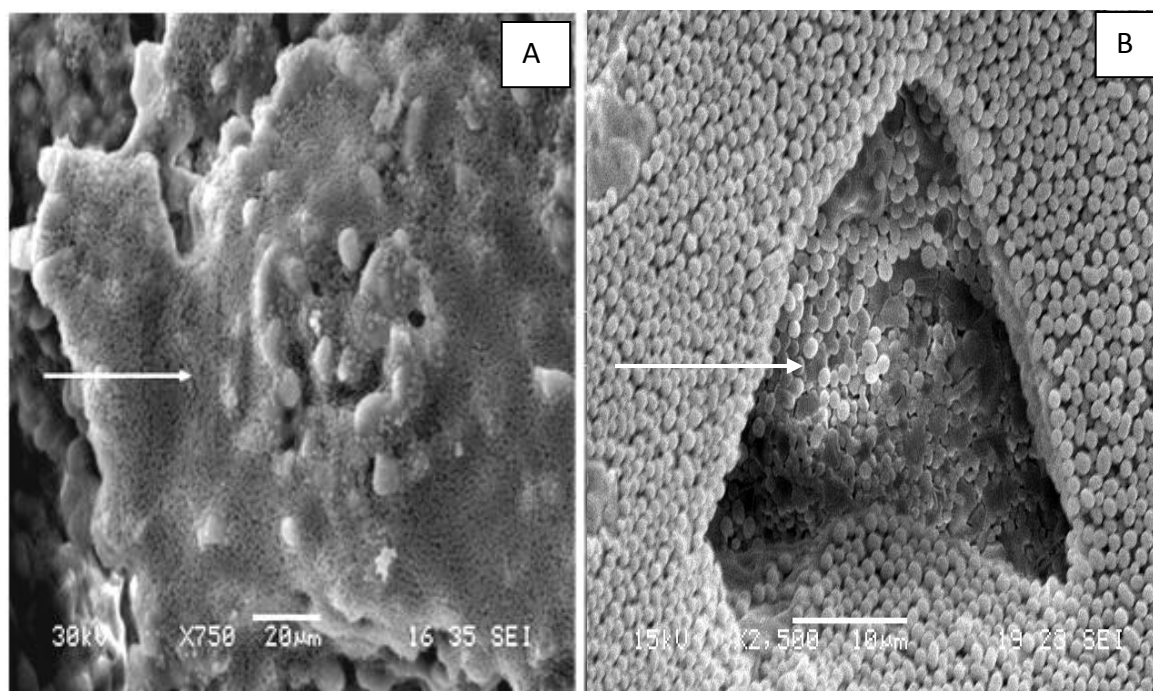


**Figure 3:- SEM images of 4S5Bioglass<sup>®</sup> scaffolds coated with gentamicin-loaded microspheres on the surface of the scaffold as seen in image A) 750 x and within the crevices of the scaffold B) 2500x. Arrows indicate a uniform coating of microspheres both on the surface and within the scaffolds.**

In order to determine the adhesion of the microspheres coating to the glass-ceramic surface, a 4S5Bioglass<sup>®</sup>-derived glass-ceramic tablet was fabricated (applying the same heat-treatment condition used to fabricate the scaffolds) and coated with microspheres (using the same coating condition as for the scaffolds). The coated tablet was dried overnight at room temperature. It was then gently washed with 30 mL of distilled water using a pipette. The weight of the tablet was recorded before and after washing. From the

SEM images of tablet surfaces, Figure 4A and 4B, no difference in the P(3HB) microsphere-coated 45S5Bioglass<sup>®</sup> tablets (A) before and (B) after washing with water were observed. SEM image of a P(3HB) microsphere-coated 45S5Bioglass<sup>®</sup> composite scaffold after being in water for 28 days, Figure 4C also showed the high level of adhesion of the microspheres to the glass-ceramic surface.

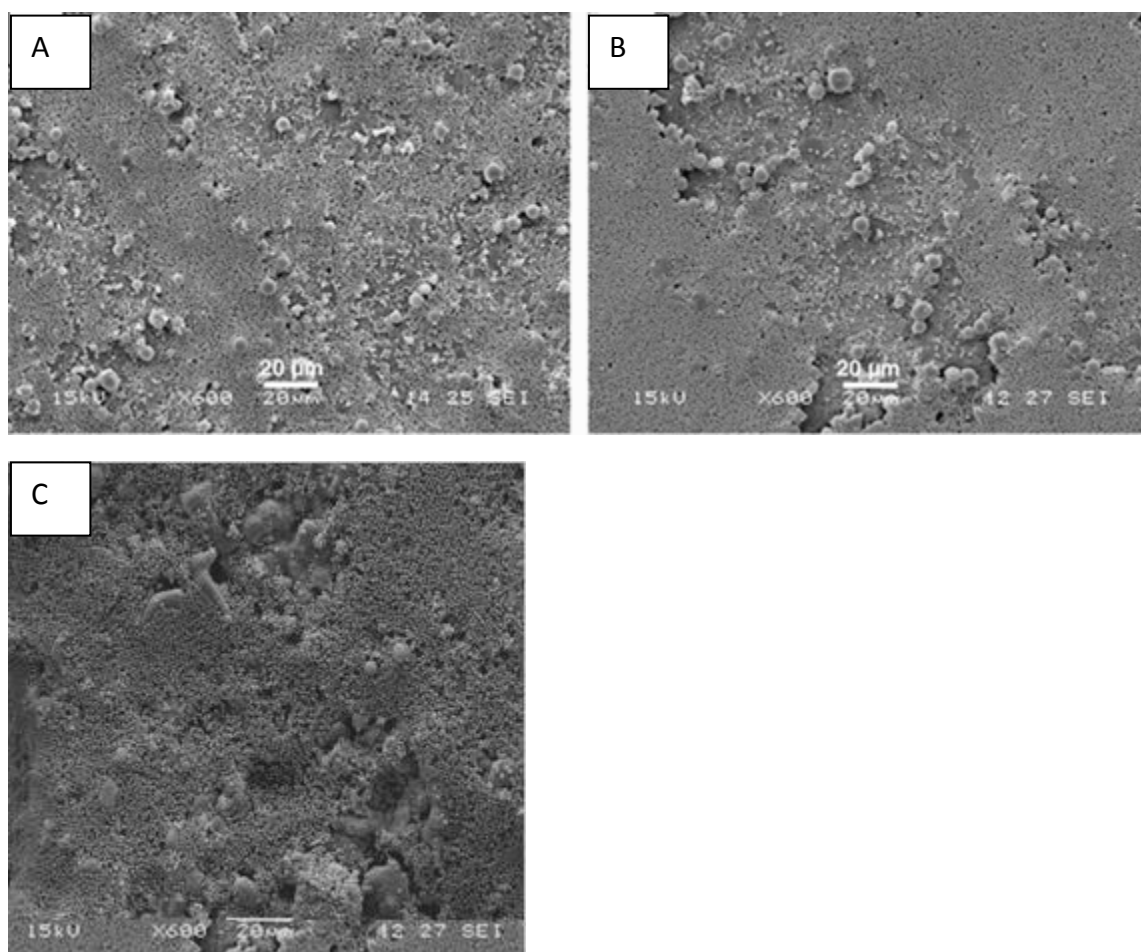


**Figure 4:- SEM images of P(3HB) microsphere-coated 45S5Bioglass<sup>®</sup> tablets (A) before and (B) after washing with water (C) SEM image of a microsphere-coated scaffold after being in water for 28 days showing the high level of adhesion of the microspheres to the glass-ceramic surface.**

#### 4.2.2 Mechanical properties

The mechanical properties of scaffolds coated and uncoated with microspheres were investigated by the compressive strength test. Typical stress *vs* strain plots of both samples are shown in Figure 5. The mean compressive strength of microsphere-coated scaffolds was determined to be 0.27MPa, which is double the value obtained for uncoated samples. The work of fracture is related to the total area under the stress *vs* strain curves. The larger the area, the higher is the fracture toughness of the material. The area under the stress *vs* strain curve of the microsphere-coated scaffold sample was calculated to be 4.83 mm<sup>2</sup> (using Origin™ programme), and that of the uncoated scaffold, was 1.92 mm<sup>2</sup>. Hence the work of fracture of the microsphere-coated scaffolds was much higher than that of the uncoated scaffolds.

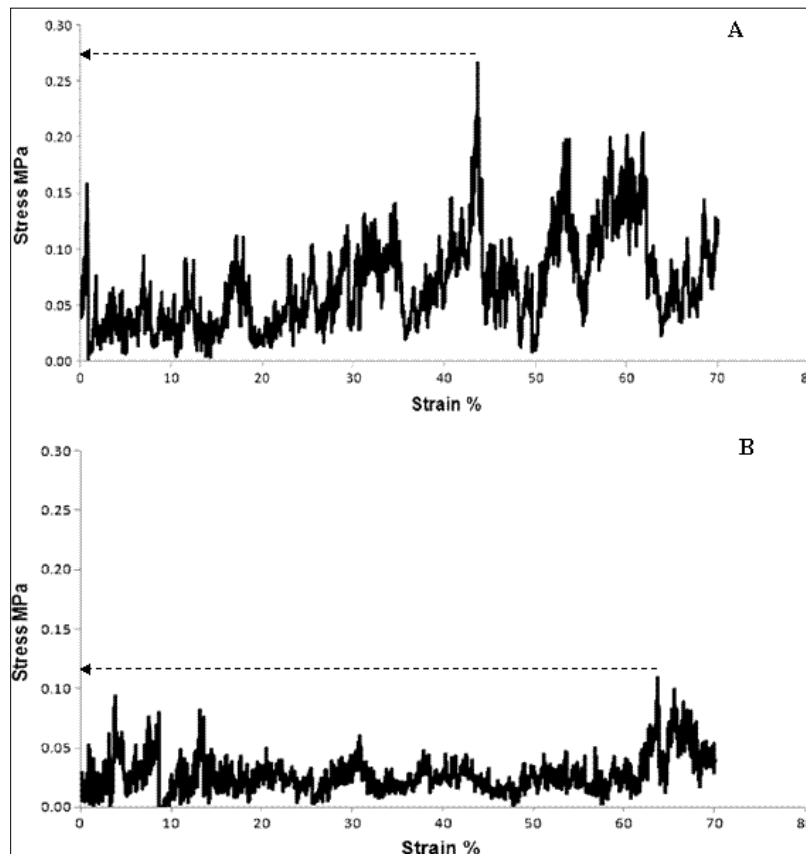
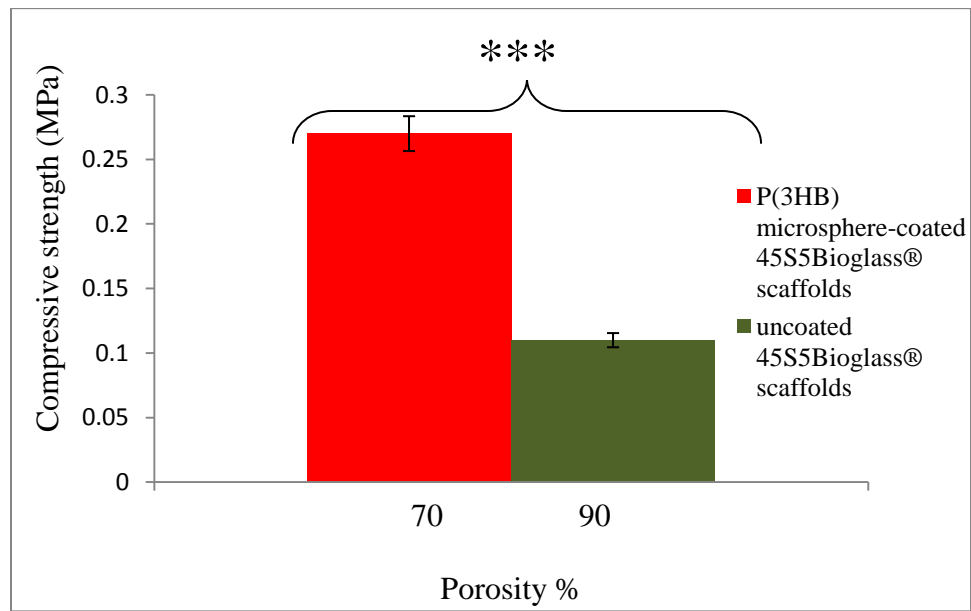


Figure 5:- Stress-strain curves of the 45S5Bioglass<sup>®</sup> porous scaffolds (A) with and (B) without the P(3HB) microsphere coatings, (n = 3; error bars=±SD).

## 4.2.2.1 Porosity

The porosity of the P(3HB) microsphere-coated 45S5Bioglass<sup>®</sup> scaffolds was calculated using equation 6, Chapter 2, section 2.8.3.1. After coating, the porosity reduced from the original ~90% to ~70%, as a result of which the compressive strength of the coated samples increased significantly as shown in Figure 6. Thus the P(3HB) microsphere coating decreased the overall porosity of the scaffolds somewhat and therefore the scaffold strength was predicted to increase.



**Figure 6:-** The compressive strength values of the uncoated and coated 45S5Bioglass<sup>®</sup> scaffold against the varying % porosity values is represented. The data (n = 3; error bars= $\pm$ SD) were compared using ANOVA and the differences were considered significant at (F(1,4)=34.691),\*\*\* $p$ <0.0001.

#### 4.2.3 *In vitro* bioactivity study of P(3HB) microsphere-coated 45S5Bioglass<sup>®</sup> scaffolds

As is common practice in the field of biomaterials (Hench *et al* 1998; Tanahashi *et al* 1994), the bioactivity of the present P(3HB) microsphere-coated 45S5Bioglass<sup>®</sup> scaffolds was assessed by measuring HA formation on the scaffolds' surface upon their immersion in SBF. It is therefore important to identify whether or not the P(3HB) microsphere-coating would affect the formation of HA on the scaffolds upon immersion in SBF. SEM was used to detect the presence of these HA crystals on the scaffold surfaces. The results of the SEM investigation carried out on scaffolds after immersion in SBF are presented in Figure 7. Figure 7A shows no formation of HA on a scaffold immersed for 24h in SBF. However, HA was seen to form by day 3, when a needle-like crystalline structure appeared on the surface of the scaffold, as illustrated in Figure 7B and C. By day 7, as seen in Figure 7D, the surface of the scaffold was almost fully covered by HA crystals (indicated by the arrow in the image). From the images in Figure 7F1, it can be clearly seen that HA crystals have grown around the microspheres, the HA crystalline structures are indicated using arrows in these images. This observation provides good evidence to conclude that most of the microspheres were eventually embedded underneath a thick HA layer. This fact was established by the image in Figure 7D1.

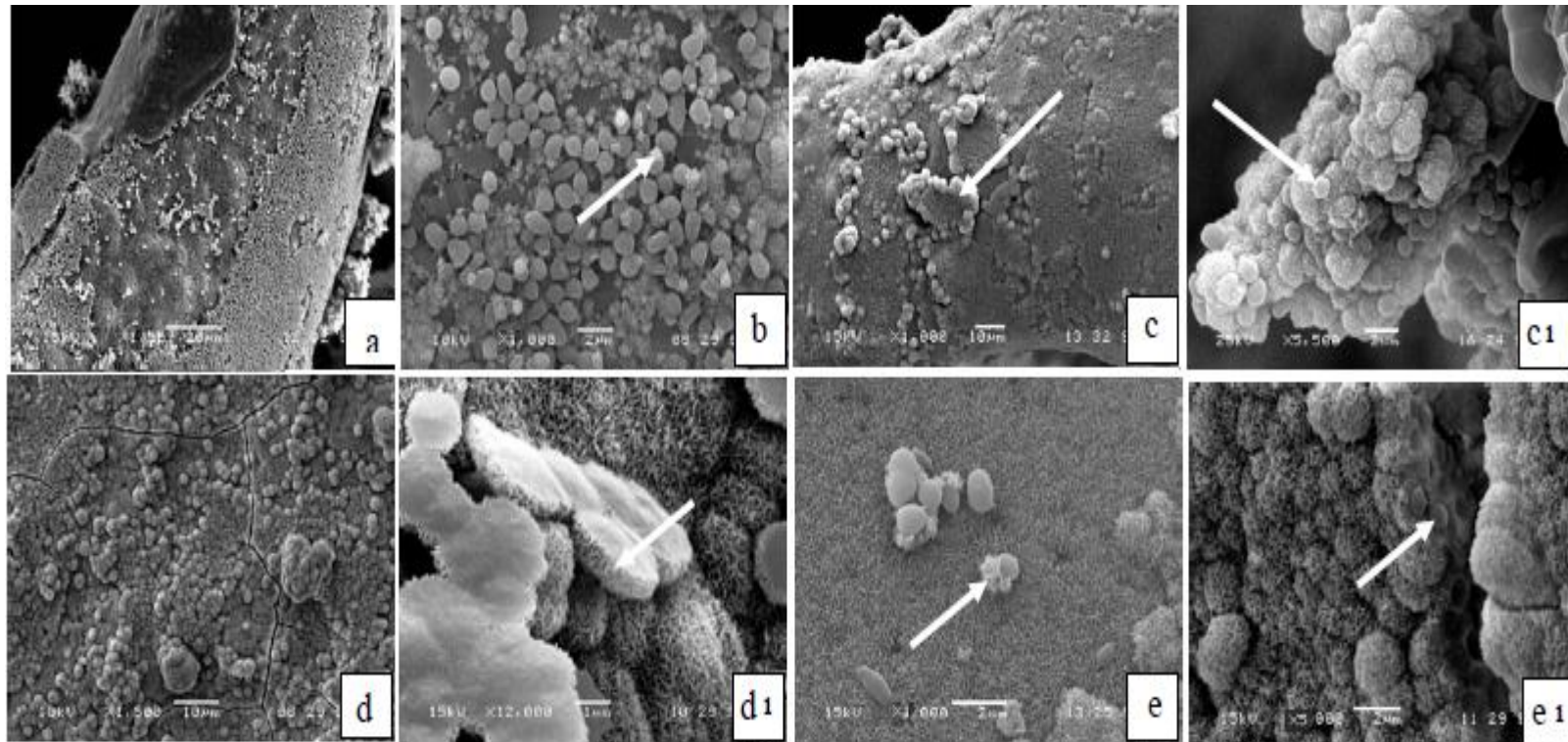


**Figure 7:- SEM images of P(3HB) microsphere-coated 45S5Bioglass<sup>®</sup> based glass-ceramic scaffolds immersed in SBF after (A) 24 h, 1,000 x, (B) 3 days, 1000 x, (C) 7 days, 1000 x; (C1) 7 days 5,500 x (high magnification); (d) 14 days, 1000 x; (d1) 14 days 12,000 x (high magnification) and (e) 30 days, 1000 x; (F1) 30 days, 5000 x. Arrows indicate the presence of hydroxyapatite (b, c, c1, d1) and arrows in figure e and e1 indicates the growth of hydroxyapatite on the surface of the microspheres.**

#### 4.2.4 X-Ray diffraction (XRD) analysis of the P(3HB) microsphere-coated 45S5Bioglass<sup>®</sup> scaffolds after immersion in SBF

To further investigate HA formation on the material's surface after immersion in SBF, XRD analysis was conducted on P(3HB) microsphere-coated 45S5Bioglass<sup>®</sup> composite scaffolds after immersion in SBF for 1 day, 3 days, 7 days, 2 weeks, 3 weeks and 4 weeks. P(3HB) microspheres on their own and uncoated 45S5Bioglass<sup>®</sup> scaffolds were also characterized by XRD to determine their crystalline phases, as shown in Figure 8. All scaffolds exhibit XRD patterns characteristic of a glass-ceramic structure, which has been discussed in detail elsewhere (Chen *et al.*, 2006). Although a characteristic diffraction pattern was obtained on the P(3HB) microspheres (Figure 8), due to the relatively small quantity of the microspheres present on the coated scaffolds as compared to the amount of 45S5Bioglass<sup>®</sup>, the intensity of their diffraction pattern was too low and the pattern could not be distinguished from the spectrum of the sintered 45S5Bioglass<sup>®</sup> scaffold, which is dominated by the sodium calcium silicate phase,  $\text{Na}_2\text{Ca}_2\text{Si}_3\text{O}_9$  (Chen *et al.*, 2006).

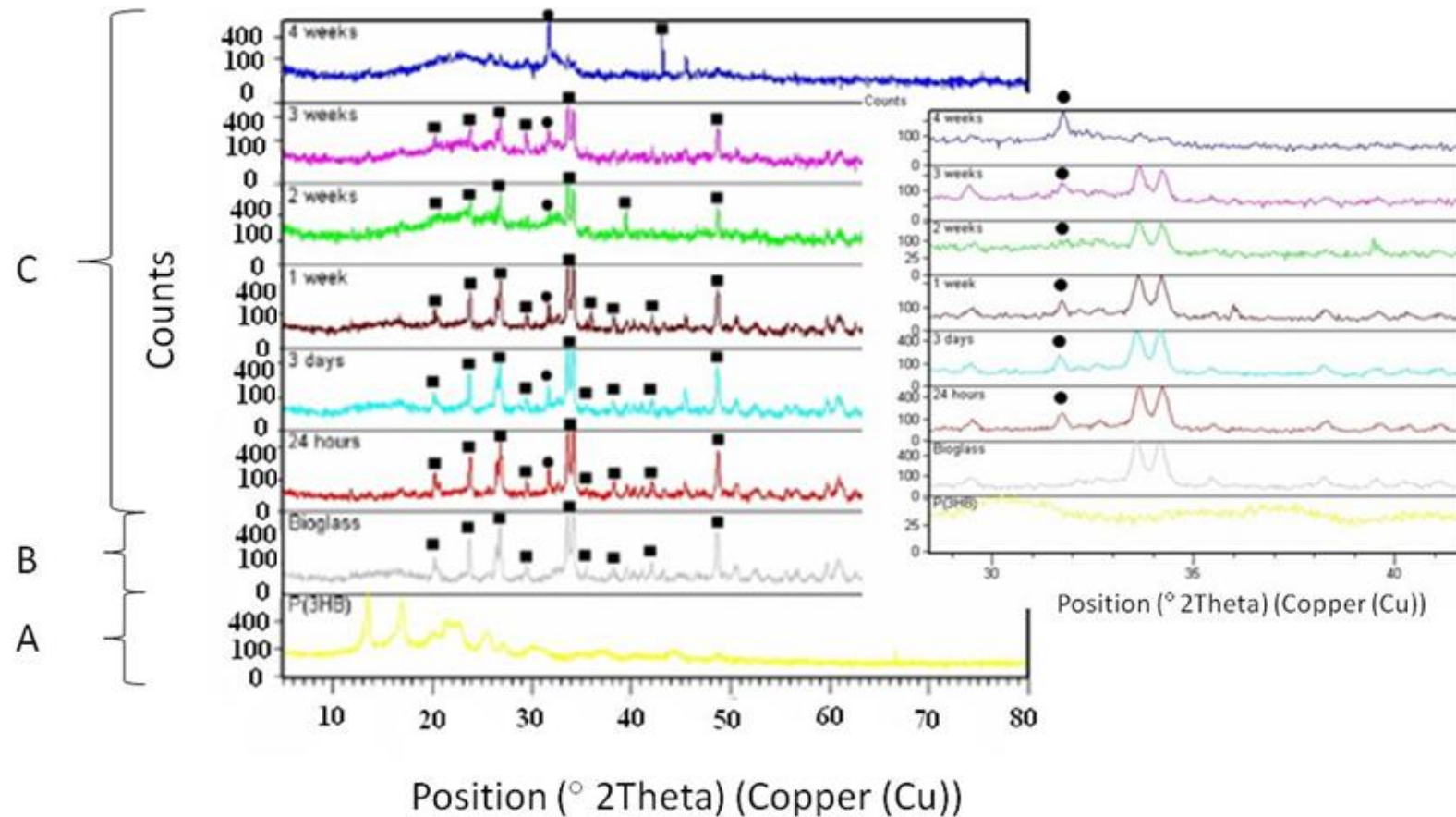
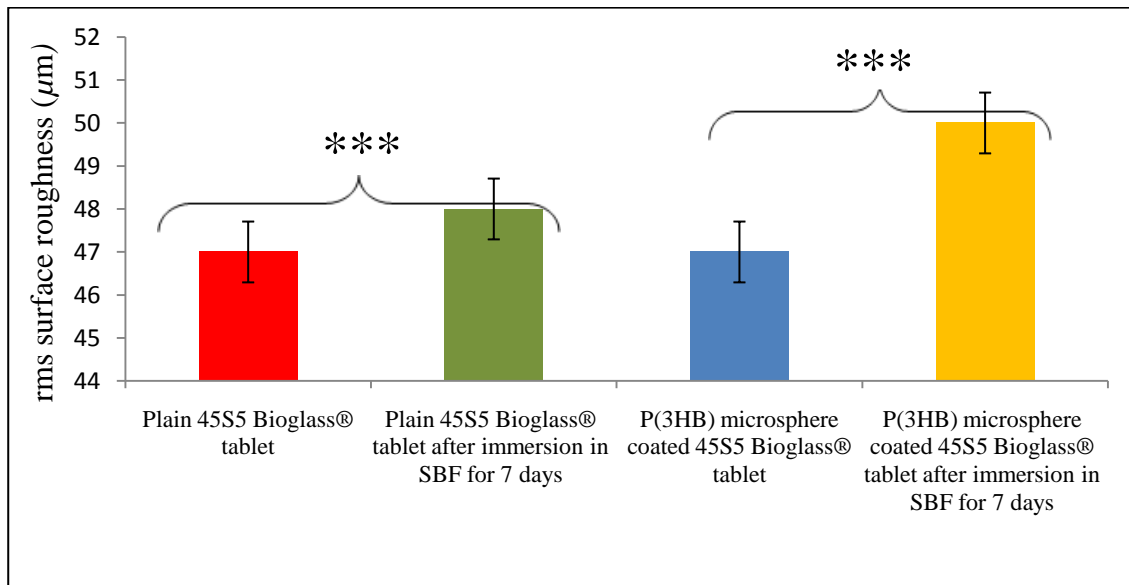


Figure 8:- XRD patterns of A) P(3HB) microspheres only, B) uncoated 45S5Bioglass® scaffold and C) P(3HB) microsphere-coated 45S5Bioglass® scaffolds after immersion in SBF for 24h, 3 days, 7 days, 2 weeks, 3 weeks and 4 weeks. ■HA; ●, Na<sub>2</sub>Ca<sub>2</sub>Si<sub>3</sub>O<sub>6</sub>.

#### 4.2.5 Surface topography studies

In order to study the effect of P(3HB) microspheres on the topography of the scaffold surface, white light interferometry (Zygo<sup>®</sup>) was used. The root mean square (rms) values of all surfaces were measured and the sample coated by microspheres showed a significant increase in RMS value when compared to non-coated specimens as seen in Figure 9. White light interferometry (Zygo<sup>®</sup>) measures the surface roughness of a flat substrate; therefore, sintered 45S5Bioglass<sup>®</sup> cylindrical tablets (diameter=10 mm, thickness =5 mm) were used as the substrate and coated with microspheres following the same procedure used to coat scaffolds. Figures 10A and B show the oblique plots of uncoated tablets before and after immersion in SBF for 7 days, while Figures 10C and d show the corresponding images for coated specimens. Individual P(3HB) microspheres on the coated sample surface were impossible to track by this technique, as the size of individual spheres is very close to the resolution limit of the instrument, which is not sensitive enough to generate the image of each microsphere on the surface; therefore, microspheres cannot be clearly identified in Figure 10C and D.



**Figure 9:- A comparison of the average rms roughness values of the indicated sample surfaces. The data (n = 3; error bars=±SD) were compared using *t*-test and the differences were considered significant at \*\*\* $p < 0.001$ .**

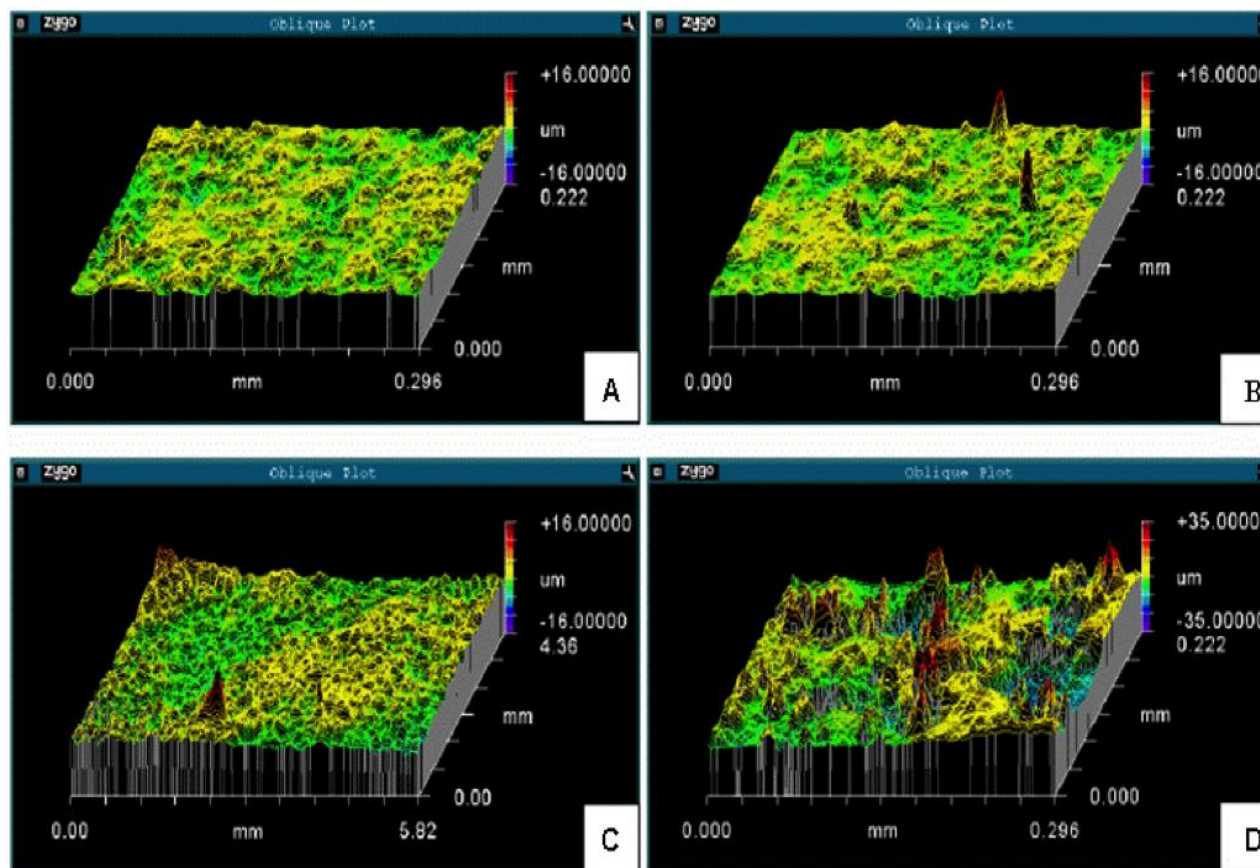


Figure 10:- Schemes showing the oblique plots of the 45S5Bioglass<sup>®</sup> tablet surfaces measured using white light interferometry: (A) plain 45S5Bioglass<sup>®</sup> tablet; (B) plain 45S5Bioglass<sup>®</sup> tablet after immersion in SBF for 7 days; (C) P(3HB) microsphere-coated 45S5Bioglass<sup>®</sup> tablet; (D) microsphere-coated 45S5Bioglass<sup>®</sup> tablet after immersion in SBF for 7 days.

#### 4.2.6 *In vitro* drug release from P(3HB) microsphere-coated 45S5Bioglass<sup>®</sup> composite scaffolds and uncoated 45S5Bioglass<sup>®</sup> scaffolds

Data on drug loading for both uncoated and microsphere coated scaffolds is shown in Table 1. The encapsulation efficiency was determined as described in Chapter 2 section 2.4.1, equation 1.

**Table 1:- Drug loading in uncoated 45S5Bioglass<sup>®</sup> scaffolds and P(3HB) microsphere coated 45S5Bioglass<sup>®</sup> scaffolds.**

<b>Samples</b>	<b>Initial Drug added (mg/g)</b>	<b>Drug loading (mg/g)</b>
Uncoated 45S5Bioglass <sup>®</sup> scaffolds	2mg/g	$1.8 \times 10^{-3}$
45S5Bioglass <sup>®</sup> scaffold coated with P(3HB) microspheres	2mg/g	$1 \times 10^{-2}$

It was found that the encapsulation efficiency of the drug-loaded microspheres with a porosity of approximately 37% was 50%. *In vitro* drug release studies, the drug release profiles from uncoated 45S5Bioglass<sup>®</sup> scaffolds and from free microspheres were used as a control to compare the release kinetics from the P(3HB) microsphere-coated 45S5Bioglass<sup>®</sup> scaffolds. Data of the release profiles of the controls and P(3HB) microsphere-coated 45S5Bioglass<sup>®</sup> scaffolds clearly show their different behaviour, as presented in Figure 11. Compared to the initial burst release of 45% from the uncoated 45S5Bioglass<sup>®</sup> scaffold and from the free microspheres which was 60%, the P(3HB)/45S5Bioglass<sup>®</sup> microspheres coated composite scaffolds showed a much lower initial release of 24%. The percentage cumulative gentamicin release was found to occur in a controlled manner over a period of 30 days from the composite scaffold which was 83.91%, which is a more favourable result when compared to the uncoated scaffold, which exhibited 74.83% release over a period of 15 days and the much faster total drug release of 95.33% over a period of just 24h from the free microspheres, as shown in Figure 11.

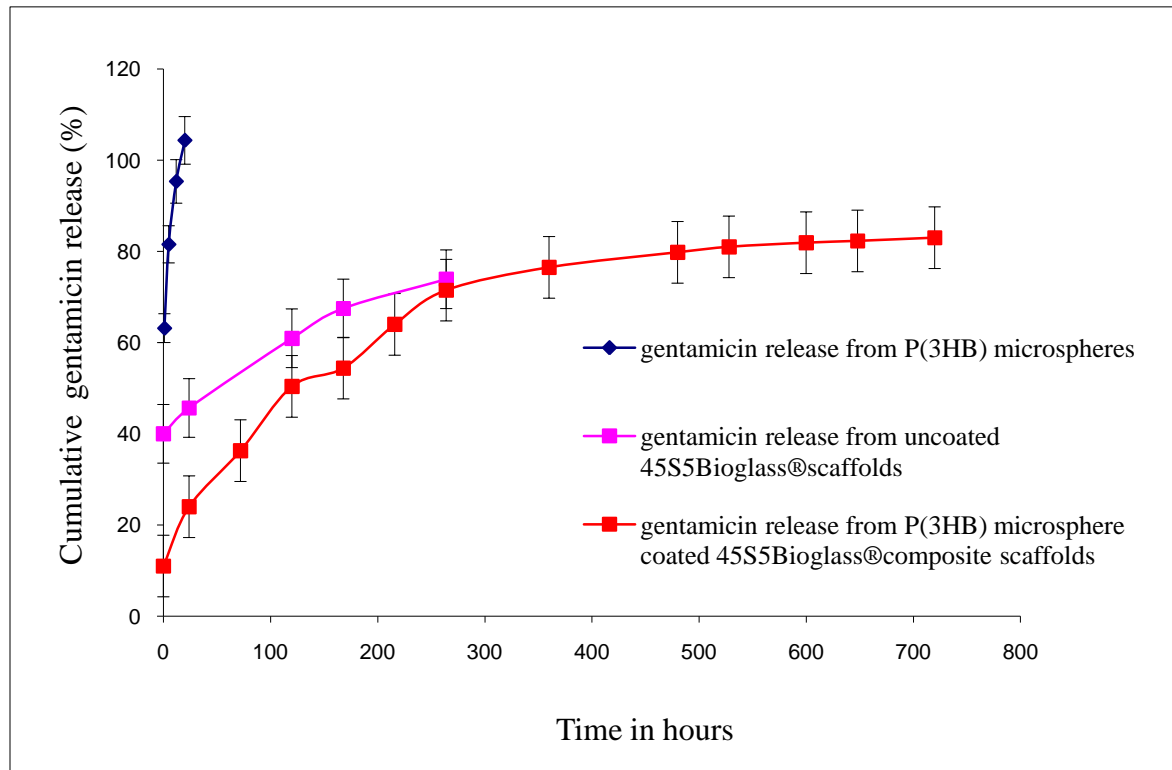


**Figure 11:- Release of gentamicin from free microspheres, uncoated 45S5Bioglass<sup>®</sup> scaffolds and P(3HB) microsphere-coated 45S5Bioglass<sup>®</sup> composite scaffolds (n = 3; error bars= $\pm$ SD).**

#### 4.2.7 *In vitro* degradation studies

The water uptake and weight loss study for the 45S5Bioglass<sup>®</sup> scaffolds (coated and uncoated with P(3HB) microspheres) were carried out using immersion tests in SBF over a period of 30 days. The *in vitro* degradation studies of the 45S5Bioglass<sup>®</sup> scaffolds (coated and uncoated with P(3HB) microspheres) are depicted in Figure 12A and B. The water absorption/uptake (WA) of the 45S5Bioglass<sup>®</sup> scaffolds increased on prolonged immersion in SBF. However, the water uptake of the P(3HB) microsphere-coated 45S5Bioglass<sup>®</sup> composite scaffolds was 650%, which was higher when compared to 483% of the uncoated 45S5Bioglass<sup>®</sup> scaffolds over a period of 30 days. The weight loss (WL) of the P(3HB) microsphere-coated 45S5Bioglass<sup>®</sup> composite scaffolds also increased to 19.3% with the immersion time when compared to the uncoated 45S5Bioglass<sup>®</sup> scaffolds which was only 8.3% over a period of 30 days.

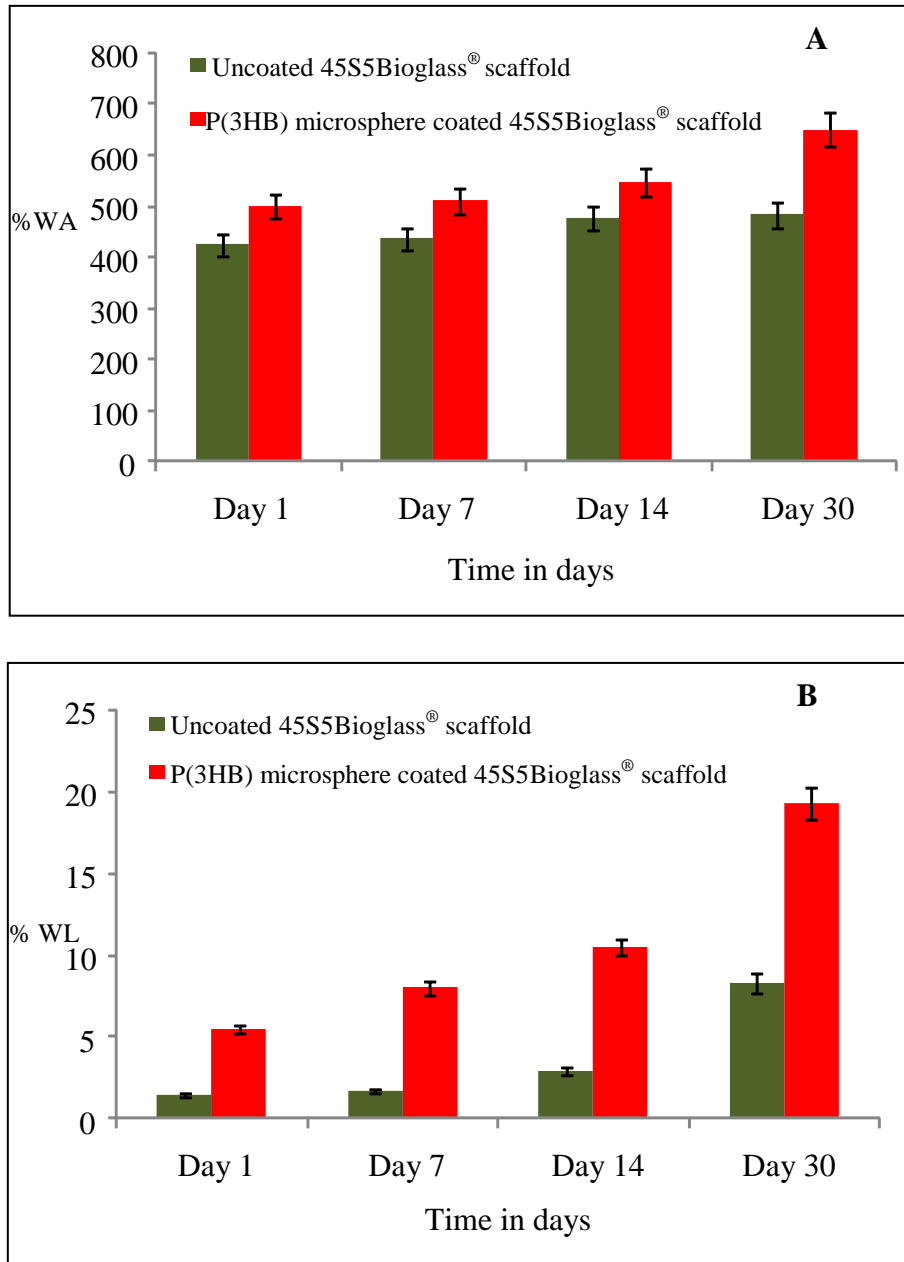
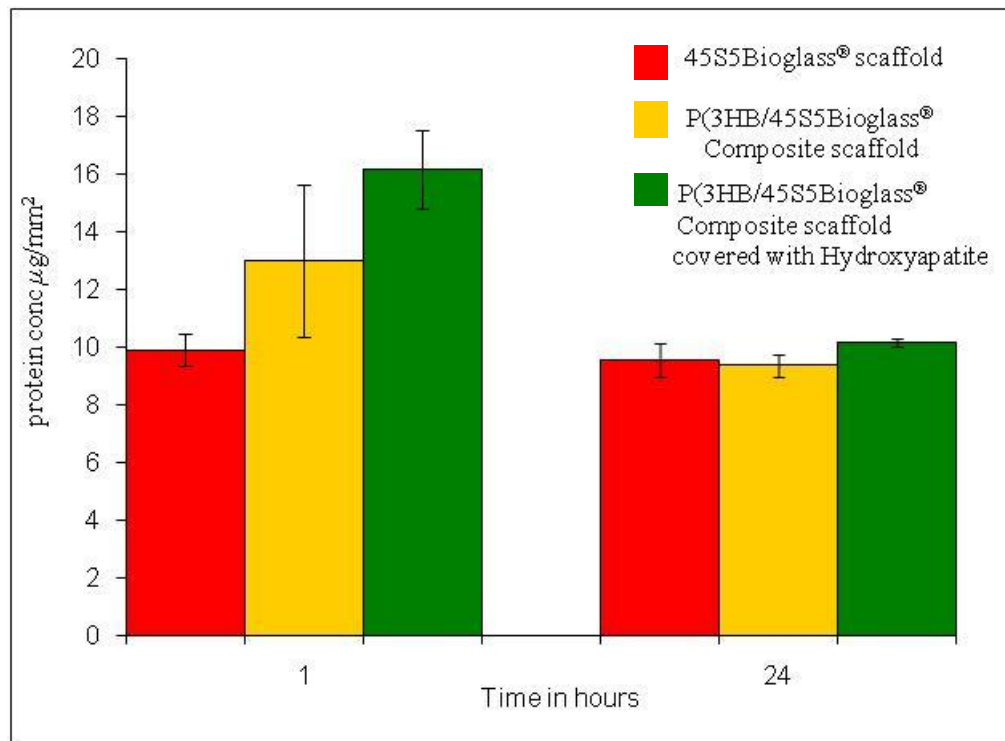


Figure 12:- A) Water absorption and B) weight loss studies of uncoated 45S5Bioglass<sup>®</sup> scaffolds and P(3HB) microsphere coated 45S5Bioglass<sup>®</sup> composite scaffolds (n = 3; error bars=±SD).

#### 4.2.8 Protein adsorption test

The protein adsorption study was carried out on the samples, 45S5Bioglass<sup>®</sup> scaffolds, P(3HB) microspheres coated 45S5Bioglass<sup>®</sup> composite scaffolds and 45S5Bioglass<sup>®</sup> composite scaffolds covered with hydroxyapatite (immersed in SBF for a period of 7 days). From the results, as seen in Figure 13, the total amount of protein adsorbed on the surface was significantly ( $***p<0.001$ ) higher for composites covered with hydroxyapatite which was  $16\mu\text{g}$  when compared to  $12.9\mu\text{g}$  and  $9.9\mu\text{g}$  on the P(3HB) microspheres coated 45S5Bioglass<sup>®</sup> composite scaffolds and 45S5Bioglass<sup>®</sup> scaffolds.



**Figure 13:-** Total protein adsorbed onto to uncoated porous 45S5Bioglass<sup>®</sup> scaffolds, P(3HB) microspheres coated 45S5Bioglass<sup>®</sup> composite scaffolds, P(3HB) microspheres coated 45S5Bioglass<sup>®</sup> composite scaffolds covered with HA after immersion in SBF for 7 days were immersed in tissue culture medium (DMEM) at  $37^\circ\text{C}$  for 1h and 24h. The data compared using ANOVA was significant,  $***p<0.001$ , a Bonferroni Post Hoc was applied and significant differences at  $***p<0.0001$  for 45S5Bioglass<sup>®</sup> composite scaffolds covered with hydroxyapatite was observed when compared to 45S5Bioglass<sup>®</sup> scaffolds, P(3HB) microspheres coated 45S5Bioglass<sup>®</sup> composite scaffolds.

#### 4.2.8.1 Protein profile of the adsorbed proteins observed using SDS-PAGE

After immersion of the samples in the biological medium, Dulbecco's Modified Eagle Medium (DMEM), the protein adsorbed from the medium onto the scaffold was extracted using 1% sodium dodecyl sulphate (SDS) and analysed using polyacrylamide gel electrophoresis (SDS-PAGE) to check for the structural integrity of the proteins adsorbed. As seen from the SDS-PAGE analysis shown in Figure 14, albumin appeared to be the main protein adsorbed onto the scaffolds both at short (1h) and long (24h) exposure times. Again, the relative amount of proteins bound on the P(3HB) microspheres coated 45S5Bioglass<sup>®</sup> composite scaffolds covered with hydroxyapatite both at 1h and 24h were higher when compared to the 45S5Bioglass<sup>®</sup> and P(3HB) microspheres coated 45S5Bioglass<sup>®</sup> composite scaffolds. The SDS-PAGE analysis of the protein eluted from the surface of the scaffolds showed a band at 62 kDa, the molecular weight of albumin. Although the serum protein adsorption was higher on the composite scaffold covered with hydroxyapatite, no difference in the kind of serum proteins adsorbed on the surface of the scaffolds was observed.

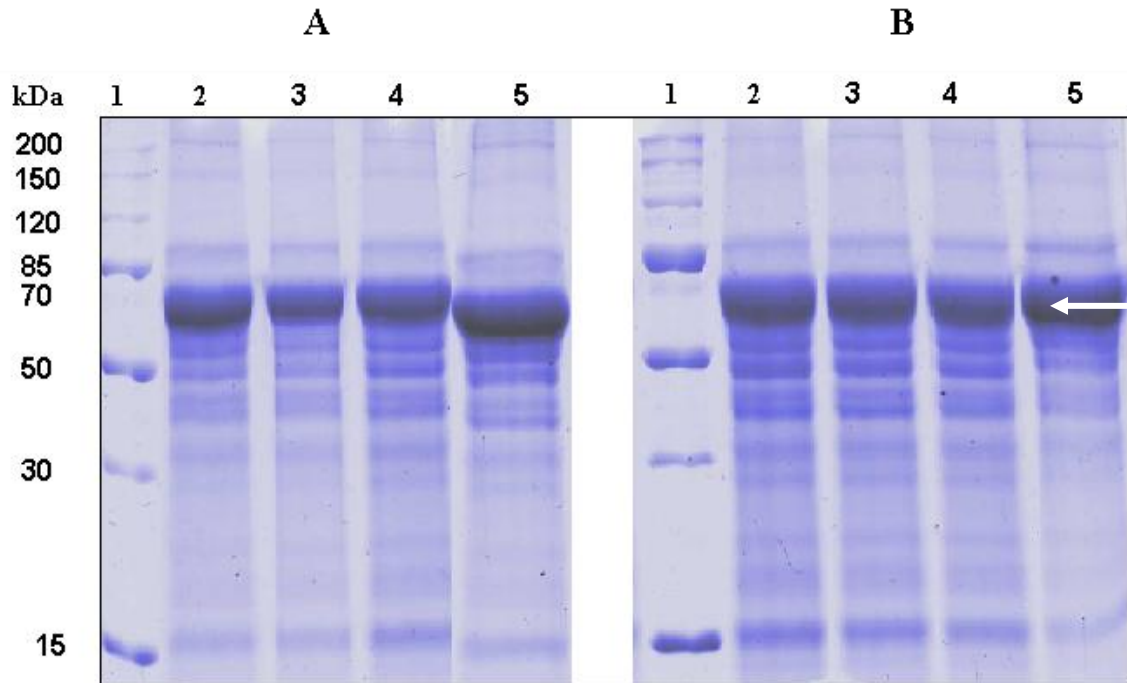


**Figure 14:- A 12% SDS-PAGE showing the integrity of the proteins adsorbed on the 45S5Bioglass<sup>®</sup> samples. Following incubation with tissue culture/biological medium (DMEM) containing foetal calf serum (FCS) for 1h (A) and 24h (B) the protein bands were separated and visualised after staining. Lane 1:- Broad range molecular weight marker (10 kDa-200 kDa) from Lane 2: Protein adsorbed on tissue culture plate, Lane 3:-Proteins extracted from the uncoated porous Bioactive<sup>®</sup> glass, Lane 4:- P(3HB) microspheres coated 45S5Bioglass<sup>®</sup> composite scaffolds, Lane 5:- P(3HB) microspheres coated 45S5Bioglass<sup>®</sup> composite scaffolds covered with HA after immersion in SBF for 7 days. Arrow indicating the presence of albumin (62kDa), the main protein adsorbed onto the scaffold.**

### 4.3 Discussions

#### 4.3.1 45S5Bioglass<sup>®</sup> Scaffold development

In the present study, a drug-encapsulated P(3HB) microsphere coating on 3-D bioactive glass-ceramic scaffold surfaces was developed. A fairly uniform coating throughout the 3-D scaffold structure was achieved by a simple slurry-dipping method, as assessed by SEM. The high level of bioactivity of the scaffolds given by the bioreactivity of 45S5Bioglass<sup>®</sup> was not negatively affected by the polymer coating, as determined by the SBF immersion study. Moreover, the nanoscale surface roughness of the scaffold struts was enhanced due to the presence of the microsphere coating. The coating added a drug delivery function with a controlled release rate to this multi-functional scaffold for bone TE application.

In the present work relative encapsulation efficiency was followed by increasing the viscosity of the aqueous solution, preventing the diffusion of the drug from within the microsphere, thus a 50% encapsulation efficiency was achieved. (Pouton *et al.*, 1996; Naraharisetti *et al.*, 2006). Gentamicin is highly hydrophilic and hence difficult to encapsulate into a hydrophobic polymer from hydrophilic environment (Lecaroz *et al.*, 2006).

In order to achieve a homogeneous and structurally robust coating of P(3HB) microspheres throughout the 3-D structure of the scaffold, a simple slurry-dipping technique was used. In the slurry-dipping technique well-dispersed microsphere suspensions were obtained when compared to the methods of coating agitation and immersion of scaffolds in the final PVA solutions. In addition a slurry of the drug-loaded microspheres was made using the highly non-polar solvent, hexane and then coated onto the 45S5Bioglass<sup>®</sup> scaffolds. In the agitation method a reproducible homogenous coating could not be produced. Similarly when the scaffolds were immersed in the final PVA solution, the microspheres agglomerated on the scaffolds either due to the residual PVA or attractive Van der Waals forces between microspheres. Hence, a homogenous microsphere coating could not be achieved by this method. Therefore, the optimum condition chosen for coating was sonication of 1% wt. aqueous microsphere suspension for 5 min followed by dip-coating for 5 minutes.

### 4.3.2 Scaffold characterization and mechanical properties

Compressive strength tests were carried out to determine the effect of microsphere coating on the mechanical strength of scaffolds. Both scaffolds (coated and uncoated) exhibited a typical failure mode for brittle foams, *i.e.* catastrophic failure after maximum stress and densification stages have been reached (Chen *et al.*, 2006). As expected, the coated scaffold with lower porosity showed a higher maximum strength (0.27 MPa) than the uncoated scaffold (0.11 MPa). However the compression strength could be underestimated due to shearing. Shearing could occur during the compression strength test, mainly caused by the edge effects imposed on the specimen during the test. If the faces of the sample are not aligned well with the loading platen, large stress concentrations can occur, causing local buckling, which in turn can lead to shearing (Chen *et al.*, 2006). Bretcanu *et al.*, fabricated similar 45S5Bioglass<sup>®</sup> scaffolds with 60 pores per inch (ppi) polyurethane foams (PU) foams and sintering at 1100°C for 1h. The compressive strength of those samples was on average 0.22 MPa. When similar scaffolds were coated with polymer by dipping them in a P(3HB) polymer solution, it was observed that the compressive strengths of coated samples were significantly higher than those of the uncoated scaffolds, with values of 0.6 MPa for 45 ppi samples and 1.5 MPa for 60 ppi samples (Bretcanu *et al.*, 2007). This behaviour can be explained considering that the polymer coating acts as a ductile bridge holding the glass particles together as the foam struts start to break during the test (Zhang *et al.*, 2002; Yunos *et al.*, 2008; Bretcanu *et al.*, 2007). Incorporation of a polymer coating thus introduces a toughening effect, as discussed in the literature (Zhang *et al.*, 2002; Miao *et al.*, 2008; Yunos *et al.*, 2008). In the present work, however, the microsphere coating cannot provide such support as a toughening element, since these are individual spheres instead of a continuous polymer layer coating and infiltrating the foam struts. Moreover, the sphere-sphere interaction is weak, hence the spheres cannot act as a structural support during the fracture of foam struts. Nevertheless, a significant increase in the average compression strength was determined (0.27 vs. 0.11 MPa for coated and uncoated scaffolds, respectively), which is related to the reduction of porosity induced by the presence of the microspheres, as described above.

#### 4.3.3 *In vitro* bioactivity study of P(3HB) microsphere-coated 45S5Bioglass<sup>®</sup> scaffolds

The *in vitro* bioactivity of scaffolds was determined in simulated body fluid (SBF). The formation of hydroxyapatite (HA) on the surface of 45S5Bioglass<sup>®</sup> scaffolds after immersion in SBF is normally used as a confirmation for the scaffold's bioactivity (Chen *et al.*, 2006; Hench *et al.*, 1998; Tanahashi *et al.*, 1994). Although 45S5Bioglass<sup>®</sup> is well known for its high bioactivity (Hench *et al.*, 1998), it was important to study here the effect of the presence of biodegradable polymer microspheres on the bioactivity of the Bioglass<sup>®</sup>-derived glass-ceramic scaffolds. Experiments conducted by Chen *et al.*, have shown that, after 3 days of immersion in SBF, the highly crystalline phase of 45S5Bioglass<sup>®</sup>-derived glass-ceramic scaffolds, Na<sub>2</sub>Ca<sub>2</sub>SiO<sub>9</sub>, transforms into an amorphous calcium phosphate phase. Similarly, in the present study the formation of small but prominent X-Ray diffraction (XRD) peaks corresponding to an amorphous calcium phosphate phase was confirmed on the surface of scaffolds coated with P(3HB) microspheres after 3 days of immersion in SBF. The surface morphology of the scaffolds changed after 7 days of immersion in SBF, with a layer of HA particles of average thickness 2–5 μm fully covering the microspheres on the scaffold surface. This fast growth rate of HA in SBF is due to the fact that, even though the scaffolds were coated with microspheres, there was still sufficient bioactive glass-ceramic surface in direct contact with the fluid to facilitate the ion-exchange process leading to HA formation (Bretcanu *et al.*, 2007). It should be noted that, due to the uneven surface of the scaffolds, it is very difficult to produce a microsphere coating that fully covers the entire surface. SEM observations confirmed that some sharp edges of the scaffold had remained uncovered by the microspheres, thus providing sufficient bioactive surface to facilitate ion exchange and induce HA formation instead of preventing it. Moreover, during the process of HA formation, some microspheres could have detached as a consequence of the HA crystals growing on the surface of the scaffold. This effect would expose more surface of the scaffold to the SBF, therefore enhancing the HA formation rate. From the images seen in Figure 7 (e),(e1), it is possible to observe that HA crystals have grown around the microspheres, as indicated by arrows. This observation provides good evidence to conclude that most microspheres were eventually embedded underneath a relatively thick HA layer (Figure 7 (e1). As shown in Figure 7 (e1), a crack (formed when

the scaffold was drying after being extracted from the SBF solution) reveals that microspheres are embedded in the HA layer. The formation of microcracks on both the scaffold and dense tablet surfaces are caused by shrinkage of the surface layer upon drying after scaffolds (or tablets) have been taken out of the SBF solution. This is a common feature in this type of bioactive scaffolds (Bretcanu *et al.*, 2007).

#### 4.3.4 Surface topography studies

Another very important factor determining the success of a TE scaffold is its surface roughness, with rougher surfaces usually providing the ideal topography for cell attachment (Norman *et al.*, 2006; Itala *et al.*, 2002). It has also been shown that nanotopography results in enhanced osteoblast cells attachment, mobility and differentiation, example on nanostructured bioceramics (Webster *et al.*, 1999). In this work, for the first time, we investigated the introduction of desirable nanotopography using the P(3HB) microsphere coating on scaffolds and the subsequent growth of HA crystals upon immersion in SBF (example after 4 weeks of immersion), which provides a desired nanoscaled rough surface, as identified by SEM observation at high magnification. The average of nine rms roughness values obtained from white light interferometry was determined for each sample. The rms roughness values for uncoated and P(3HB) microsphere-coated samples were similar. The similarity of the values for uncoated and P(3HB) microsphere-coated samples could be due to the fact that the related valleys on the surface of the bioactive glass-ceramic tablets investigated which were filled up by the P(3HB) microspheres after the coating process. Therefore, they created a new flat surface and the surface roughness did not change significantly. Overall, the measured roughness value using white light interferometry on the microsphere-coated scaffold, after 7 days of immersion in SBF, was much higher in comparison to that of the uncoated scaffold. This increased roughness plays an important role in enhancing cell attachment, proliferation and bone matrix formation.

In addition to SEM observations, XRD analysis were also carried out to confirm the bioactivity of the 45S5Bioglass<sup>®</sup>/P(3HB) microsphere coated composite scaffolds. XRD analysis as seen in Figure 8 enabled us to identify the presence of HA crystals on the scaffold surface, and also showed the steady decrease in the Na<sub>2</sub>Ca<sub>2</sub>SiO<sub>9</sub> peaks with

increasing immersion time, in agreement with previous studies on similar scaffolds (Chen *et al.*, 2006). XRD analysis indicates that, by week 4, HA has occupied the whole scaffold surface and the peaks corresponding to the sodium calcium silicate phase have almost all disappeared. The characteristic XRD pattern of P(3HB) (from the microspheres) could not be identified because of the relatively small amount present, which thus produced a low intensity diffraction pattern that could not be distinguished from the dominant patterns from the bioactive glass-ceramic scaffold and the newly formed HA. These combined results of SEM, EDX and XRD therefore indicate that P(3HB) microsphere coated 45S5Bioglass<sup>®</sup>-based scaffolds are bioactive, with respect to HA coatings.

#### 4.3.5 *In vitro* drug release from P(3HB) microsphere-coated 45S5Bioglass<sup>®</sup> composite scaffolds and uncoated 45S5Bioglass<sup>®</sup> scaffolds

*In vitro* drug release studies from microsphere-coated scaffolds were carried out using LC-MS, as other derivatization techniques such as fluorimetric and colorimetric assays used by other researchers have been shown to have relatively low specificity and sensitivity (Lecaroz *et al.*, 2006). For the purpose of comparison, the measurement of drug release kinetics from uncoated scaffolds and from P(3HB) microspheres was also carried out. It was observed that gentamicin encapsulated within microspheres fixed on scaffold surfaces was released in a controlled manner, as compared to the rapid release of the drug directly adsorbed onto the 45S5Bioglass<sup>®</sup> scaffold or from P(3HB) microspheres on their own (Figure 11). A rapid burst release of 60% was seen from the free microspheres during the first few hours. This was followed by an almost total drug release of 95.33% over a period of 30h. This result is similar to the release profile observed by Naraharisetti *et al.*, who showed that gentamicin was released from polymer microspheres in less than a day (Naraharisetti *et al.*, 2005). The possible reason for this burst release could be due to the hydrophilic nature of the drug as well as the size of the microspheres used (1–2 $\mu$ m). For the uncoated 45S5Bioglass<sup>®</sup> scaffold, an initial burst release of 45% was followed by a gradual release for a period of 15 days. This dual release profile could be due to the drug being loosely bound to the surface of the scaffold, which should lead to the initial rapid drug release followed by the slower drug release of

the entrapped drug within the micropores present on the scaffold surface. Compared to the initial burst release in the uncoated scaffolds, the microsphere-coated scaffolds exhibited a much lower initial burst of 24% followed by continuous release over a period of 30 days, the appropriate timescale for a tissue engineered graft operation. The release of the drug during the first few hours of immersion could be due to the presence of a given quantity of the surface bonded drug, which diffuses out when in contact with water. The relatively slower gentamicin release from the composite scaffold indicates that the microspheres, once immobilized on the 45S5Bioglass<sup>®</sup> scaffold, exhibit completely different drug release kinetics as compared to P(3HB) microspheres free to move in suspension. This result could be attributed to the decrease in the surface area exposed to the SBF environment in the immobilized microspheres. In addition, the apatite layer formed on the surface of the composite scaffold should also contribute to determining the kinetics of drug release. For example in the coated scaffolds at day 7, the surface of the scaffold was almost fully covered by HA crystals when compared to the uncoated scaffold, which was only unevenly covered by aggregated apatite spheres.

#### 4.3.6 Protein adsorption test

Most mammalian cells adhere to a protein rich surface which promotes cell adhesion, migration and differentiation (Misra *et al.*, 2008). During the first stage of cell adhesion, a layer of water and proteins are known to adhere onto the surface largely mediated by the surface properties of the biomaterial (Soderling *et al.*, 1996). Surface roughness is one of the properties that are known to affect the amount of the proteins adsorbed. Therefore in this study, a higher amount of protein adsorption ( $n=3$  \*\*\* $p<0.001$ ) was observed on the P(3HB) microsphere coated 45S5Bioglass<sup>®</sup> composite scaffolds covered with hydroxyapatite when compared to the 45S5Bioglass<sup>®</sup> and P(3HB) microsphere coated 45S5Bioglass<sup>®</sup> composite scaffolds. This may be attributed to the increased surface roughness of the 45S5Bioglass<sup>®</sup> covered with hydroxyapatite which was confirmed in the surface topography studies when compared to the 45S5Bioglass<sup>®</sup> and P(3HB) microsphere coated 45S5Bioglass<sup>®</sup> composite scaffolds. Bioactive glass such as 45S5Bioglass<sup>®</sup> when immersed in bodily fluids are known to form an apatite or bioactive layer. Due to this bioactive layer an increased surface roughness as well as an increased

surface area is observed (Misra *et al.*, 2008). Thus 45S5Bioglass<sup>®</sup> samples with hydroxyapatite formation in this study also had an increased surface area when compared to the other samples which may have also contributed to an increase in the protein adsorption. In relation to the surface composition of the biomaterials, the surface charge is also known to influence amount of serum proteins adsorbed on the surface (Sahoo *et al.*, 2002). The charged residues of albumin are also known to have a higher affinity to hydroxyapatite. For example the aspartic and glutamic acid residues are known to bind to the calcium site while lysine and arginine are known to bind to the phosphate groups. An increased protein adsorption was observed on the P(3HB) microsphere coated 45S5Bioglass<sup>®</sup> composite scaffolds covered with hydroxyapatite with an increased negative surface charge of -16.30 mV (Lu *et al.*, 2001). 45S5Bioactive glass surface is also known to carry a negative surface charge of -14.72 mV. The surface charge of the major protein (albumin) present in the cell culture media is negative, which is dependent on the pH and ionic strength of the solution (Patil *et al.*, 2007). Since the experiments in this study were carried out in DMEM media, pH 8.0, the surface charge of albumin present in DMEM would be negative. Also, in this study, an increased surface roughness and surface area of the P(3HB)/45S5Bioglass<sup>®</sup> microsphere coated composite scaffolds covered with hydroxyapatite may have also favoured an increased protein adsorption when compared to the other scaffolds. The proteins such as BSA adsorbed on the P(3HB)/45S5Bioglass<sup>®</sup> microsphere coated composite scaffolds covered with hydroxyapatite may have also established a strong molecule-molecule interaction when in contact with the HA surface. Due to the increased non-homogenous surface of the P(3HB)/45S5Bioglass<sup>®</sup> microsphere coated composite scaffolds covered with hydroxyapatite, large aggregates of protein could have also been found on the surface due to which a higher amount of proteins were observed.

A higher amount of protein adsorption was observed during the first hour of immersion on the surface of all the scaffolds after which a considerable decrease was observed with the increase in the immersion time (24h). In general, proteins are known to form monolayers, sub-layers and multilayers and change their native conformation and orientation when they get initially adsorbed onto a surface (Wahlgren *et al.*, 1991). However, over a period of time, protein conformational changes are known to occur

during which time the proteins flatten or spread in an attempt to optimize contact with the sorbent. Similarly the late arriving protein molecules are also observed to adsorb onto the monolayer of the proteins. Thus a structural heterogeneity in the protein adsorbed layer is observed. Proteins are also known to compete with each other for available binding sites on the sorbent, therefore during the time course of adsorption the proteins that were initially adsorbed onto the adsorbent surface could be displaced by the protein molecules that show a higher affinity for the surface. Therefore during the first hour of immersion, protein adsorption could have occurred in multilayers. However with the prolonged immersion (24h) in the biological media, the late-arriving protein molecules which were not bound to the adsorbent surface could have been readily desorbed due to which a lesser amount of proteins were recorded at 24h of immersion (Horbett *et al.*, 1994). The surface composition of the biomaterial surface is also known to affect the binding characteristics as well as the conformation of the attached serum proteins (Gray *et al.*, 2004). Since proteins are often known to denature at the solid-liquid and vapour-liquid interface (Gray *et al.*, 2004), the adsorbed proteins on the sample surfaces in this study were eluted and its stability checked on a SDS-PAGE. From the results, albumin was found to be the main protein that was bound onto the samples. The molecular weight of the albumin adsorbed on the samples which was 62 KDa was comparable to that of the albumin from the serum (used as control). This indicated that the proteins after adsorption on the scaffolds did not undergo any degradation. The 45S5Bioglass<sup>®</sup>/P(3HB) microsphere coated composite scaffolds covered with hydroxyapatite bound the highest amount of total protein when compared to the other samples. Thus apart from the difference in the quantity of the protein adsorbed, in this study there were no differences observed in the kind of proteins adsorbed. Ghannam *et al.*, also similarly observed that there were no significant differences in the kind of serum protein adsorbed on the Bioactive glass surface with and without a HA layer. Thus it was concluded that the Bioactive glass surface with a HA layer had significantly affected the quantity of proteins adsorbed on the surface but the kind of proteins adsorbed remained unchanged (Ghannam *et al.*, 1999).

#### 4.3.7 *In vitro* degradation studies

The P(3HB) microsphere coated 45S5Bioglass<sup>®</sup> composite scaffolds and 45S5Bioglass<sup>®</sup> scaffolds were immersed in SBF and the water uptake and weight loss studies were carried out for a period 30 days. From the results it was observed that the 45S5Bioglass<sup>®</sup> composite scaffolds exhibited an increased rate of degradation when compared to the 45S5Bioglass<sup>®</sup> scaffolds. The presence of the hydroxyapatite on the surface of the P(3HB) microsphere coated 45S5Bioglass<sup>®</sup> composite scaffolds with an increased surface area would have also improved the surface wettability of the scaffolds (data not shown) therefore exhibiting a higher water adsorption. The 45S5Bioglass<sup>®</sup> scaffolds on the other hand however exhibited lower water absorption when compared to the composite scaffolds (coated with microspheres). Thus it could be concluded that a reduced HA formation in the absence of the microsphere coating could have led to a decreased surface area of the scaffolds as well as reduced surface wettability. Thus with added features of increased water adsorption and surface wettability, the P(3HB) microsphere coated 45S5Bioglass<sup>®</sup> composite scaffolds covered with HA exhibited an increased rate of degradation or weight loss when compared to the uncoated 45S5Bioglass<sup>®</sup> scaffolds.

## 4 Conclusions

This work has led to the development of novel multi-functional 45S5Bioglass<sup>®</sup>-based glass–ceramic scaffolds for bone tissue engineering which exhibits topographical features to increase cell attachment and can also act as a carrier for controlled drug delivery *via* the immobilization of P(3HB) microspheres on the scaffold surfaces. Successful P(3HB) microsphere coating on the glass–ceramic scaffold was achieved using an optimized slurry dipping technique. The resulting composite scaffolds had increased compressive strength and ordered surface roughness (given by HA crystal formation on the microspheres in contact with SBF), and maintained the high bioactivity typical of a silicate glass–ceramic derived from Bioglass<sup>®</sup>. *In vitro* degradation studies confirmed that an improved surface wettability of the P(3HB) microsphere coated 45S5Bioglass<sup>®</sup> composite scaffolds due to the HA formation on an increased surface area had significantly increased the water uptake of scaffolds. Thus due to an increased water uptake, a higher weight loss was exhibited by the P(3HB) microsphere coated 45S5Bioglass<sup>®</sup> composite scaffolds. Similarly, the presence of HA on the P(3HB) microsphere coated 45S5Bioglass<sup>®</sup> composite scaffolds also contributed to rough surface morphology which could also be related to an increased surface area available for protein adsorption. Therefore the P(3HB) microsphere coated 45S5Bioglass<sup>®</sup> composite scaffolds exhibited upto 41% increase in protein adsorption when compared to the other scaffolds. The novel scaffolds were successfully tested for their gentamicin delivery capability. The encapsulated drug was released in a slow and sustained manner compared to the burst release of the drug measured from free P(3HB) microspheres and from the uncoated scaffold. Hence, the P(3HB) microsphere coated 45S5Bioglass<sup>®</sup> composite scaffolds developed here is multifunctional in that it provides structural support, adequate surface roughness, bioactivity and controlled drug delivery function, being thus of high interest for bone tissue engineering. The present approach can be extended to other types of tissues due to its high versatility, given by the combination of different biomaterials and processing technologies used.

# Chapter 5

P(3HB/n-BG) composite films for  
wound healing applications

## 5.1 Introduction

Recently a widespread need for the development of new biomaterials that can interface with soft biological tissue/fluid is emerging (Ostomel *et al.*, 2006, Macneil *et al.*, 2007). Several inorganic materials which were previously used only for applications such as bone and dental repair are now being considered for other applications such as wound healing. During a traumatic injury the body's skin barrier is breached which results in haemorrhage (Ostomel *et al.*, 2006, Macneil *et al.*, 2007). The lack of covering of the wound can result in infection leading to further complications. However, traditional dressings are insufficient to control the haemorrhage (Ostomel *et al.*, 2006). Currently zeolite-based granular materials are used on the surface of wounds to induce rapid clotting. Zeolite is a haemostatic agent (HA), which has a high affinity for water; therefore it has a concentrating effect on the plasma by selectively dehydrating the blood. However, as a consequence of the affinity for water, energy release is very high during hydration; due to which they tend to burn the surrounding healthy tissues (Ostomel *et al.*, 2006, Eryilmaz *et al.*, 2009). Therefore, efforts have now been focussed in developing new biocompatible materials to serve as scaffolds with an excellent efficacy for inducing haemostasis as well as promote tissue regeneration. Although bioactive glass ceramics were used largely for dental and bone applications, researchers like Ostomel *et al.*, have focused on the use of these glasses for blood clotting applications. The authors' had formulated a high surface area bioactive glass and then tested

its *in vitro* haemostatic efficacy. Haemostatic bioactive glass (BG) was considered as an ideal material for haemostasis as it is known to release  $\text{Ca}^{2+}$  ions upon hydration, which is required to support thrombosis (Ostomel *et al.*, 2006). In another study Ostomel *et al.*, suggested factors such as porosity, Si/Ca ratio and the spherical morphology of the bioactive glass microspheres (MBGMs) as important properties that affect the biological response required for wound healing scenarios. In addition, during clotting the intrinsic pathway of the blood clotting cascade is activated by the polar surfaces of the glasses. When blood is exposed to a foreign polar surface, blood-clotting factors such as Factors XII, XI, prekallikrein and high molecular weight kininogen are initiated. The activated factors are then responsible for the activation of the thrombin enzyme and polymerization reaction of fibrin. During haemostasis impermeable platelets are formed which act as a

plug at the site of injury, while the procoagulant substances activated in this process are localized at the site of injury (Hoffman *et al.*, 2003). Therefore, haemostatic agents such as bioactive glass are known to produce the fastest haemostatic response by providing  $\text{Ca}^{2+}$  ions that act as cofactors that help in orienting proteins as well as enzymes that are responsible for fibrin production. Ostomel *et al.*, also found that the high surface area of the bioactive glass could provide the support needed for thrombosis as well as provide an optimum ratio of  $\text{SiO}_2$  to  $\text{Ca}^{2+}$  ions required for the clotting cascade. The *in vitro* haemostatic efficacy is assayed using a thromboelastograph (TEG), which monitors the change in the viscoelasticity of blood in the presence of the haemostatic agent (HA) during thrombosis and thrombolysis (Ostomel *et al.*, 2006).

In this work, for applications in wound healing, the nanoscale bioactive glass particles (n-BGs) were incorporated within the P(3HB) matrix. The chemical composition of the n-BGs is not very different from microbioglass (m-BGs), however, they are known to be spherical in shape with a uniform surface morphology as compared to the m-BGs, which are irregular in size with large agglomerates (Misra *et al.*, 2008). The spherical morphology of the ceramic particles with a high specific surface area is crucial for interface effects such as hydroxyapatite formation and contact activated coagulation (Misra *et al.*, 2008; Ostomel *et al.*, 2006). The presence of nanoscale particles have been found to have an effect on the microstructural, mechanical and *in vitro* degradation behaviour of the composite systems used in tissue engineering applications (Pramanik *et al.*, 2006).

Cell response is affected by a number of physicochemical factors such as surface energy, surface charges and chemical composition of the biomaterials. Apart from these above-mentioned factors, cell response is also affected by the surface topography (Teixeira *et al.*, 2004). Surface topography is the most decisive physical cue for the cells, as the topography can be used to guide the cell orientation to achieve a functional tissue such as tendons and nerves. Researchers have focused their efforts on trying to mimic the nanoscale topographical features in the hope that these features can promote cellular functions such as cell adhesion, cell mobility and cell differentiation (Norman 2006).

The nanoscale features are known to have both a direct influence and an indirect influence (an effect on the conformation of the adsorbed extracellular matrix components). The cell adhesion on the nanotopographical substratum is dependent on the integrin adhesion as well as the topographical nanofeatures. During cell adhesion, transmembrane proteins called integrins are recruited and activated. These integrins are known to establish the initial cell-matrix interactions. These integrin receptors are known to form adhesion plaques or focal adhesion sites on the substratum. Following the formation of focal adhesion sites, a series of temporospatial events are known to occur such as integrin clustering. Therefore for an increased cell adhesion, the lateral spacing in the nanofeatures of the matrix must be around 15-30nm (Biggs *et al.*, 2010). Nanofeatures such as height, diameter and edge-edge spacing are also known to affect the integrin clustering. Several polymeric substrates with nanotopographical features have shown an increase in the cell adhesion. For example Poly (L-lactic acid) films with nanofeatures of 500-550 nm in diameter and 250-300 nm in height displayed an increase in human foreskin fibroblast adhesion (Milner *et al.*, 2007). However a disruption in the integrin-substratum is known to occur when spacing between the nanofeatures is between 70-300 nm, the protein recruitment for focal adhesion is disrupted causing a decrease in the cell adhesion (Selhuber *et al.*, 2008). For example a reduced adhesion of human bone marrow stromal cells on polystyrene/poly(n-butyl methacrylate) blend was observed when the nanofeatures displayed dimensions of 0.99  $\mu\text{m}$  in diameter and 90 nm in height (Berry *et al.*, 2006).

Microscale topography is also known to modulate cellular behaviour; however the sub cellular structures of the single cells such as cytoskeletal elements, transmembrane proteins and filipodia of the cells, tend more towards the nanoscale features (Biggs *et al.*, 2010). Several techniques such as electron beam lithography, photolithography have been used for creating ordered features and phase separation and colloidal lithography have been used to create unordered surface patterns. However apart from using these techniques other nanophase materials such as hydroxyapatite nanoparticles, bioactive glass nanoparticles and stimuli-sensitive polymeric nanoparticles have been used to produce nanometer features. These nanophase materials have displayed several advantages such as cell adhesion, proliferation and bioactivity (Webster *et al.*, 1999).

Hence, the presence of nanoscale bioactive glass particles affects the microstructural, mechanical and biological properties of the composite films used for other tissue engineering applications. Therefore, the present study aims to depict the use of P(3HB)/nanoscale bioactive glass (n-BG) microspheres compressed to form films for applications in wound healing. For the first time, n-BG particles have been used to investigate its haemostatic efficacy, in wound healing applications. The reason for using n-BG particles was its spherical morphology, high surface area, increased bioactivity and its haemostatic efficacy higher protein adsorption capacity (Misra *et al.*, 2008). In this chapter, the n-BG particles were mixed with the polymer solution, made into microspheres and compressed into films followed by a series of experimental techniques used to characterize the composite films. The results obtained from the characterization of the microsphere films can be categorized as (i) the effect of n-BG particles on the structural and thermal properties (ii) the effect of n-BG particles on the surface mediated phenomena such as haemostatic activity (iii) A comparative study on the *in vitro* biocompatibility of the P(3HB) and P(3HB)/n-BG microsphere films layer using the HaCaT keratinocyte cell line.

In the second part of this study, the P(3HB)/(n-BG) microsphere films were immersed in SBF for a fixed time period to induce the formation of HA on the surface of the composite films leading to the formation of surface functionalized films. Thus by engineering nanotopography on the biomaterials, the adsorption and functionalities of the biochemical signaling molecules that direct cellular functions were modulated. These P(3HB)/n-BG composite films with HA deposition were also assessed in order to understand the effect of the biomaterial surface properties on the protein adsorption as well as keratinocyte function. The results from this study will give further information to design percutaneous implants with surface properties that can enhance the rate of skin regeneration.

## 5.2 Results

### 5.2.1 Nanoscale bioactive glass and P(3HB)/nBG composite microspheres characterization

The nanoscale bioactive glass (n-BG) particles used in this study had a spherical shape with relatively small agglomerate sizes as seen in Figure 1. These n-BG particles have a specific surface area (SSA) of  $79 \text{ m}^2/\text{g}$  and with a diameter of 29 nm (Misra *et al.*, 2008). SEM images of the P(3HB)/nBG composite microspheres, Figure 1C, revealed the presence of both spherical and smooth surfaces as well as the presence of agglomerations of the n-BG particles present on the surface of the P(3HB) microspheres. SEM/EDX elemental mapping images on the P(3HB) microsphere cross-sections as seen in Figure 2 confirmed the presence of typical elements of bioglass *i.e.*, silica (Si), calcium (Ca), phosphorous (P). This result further indicated that the n-BG particles were distributed throughout the polymeric matrix in addition to being present on the surface of the P(3HB) microspheres.

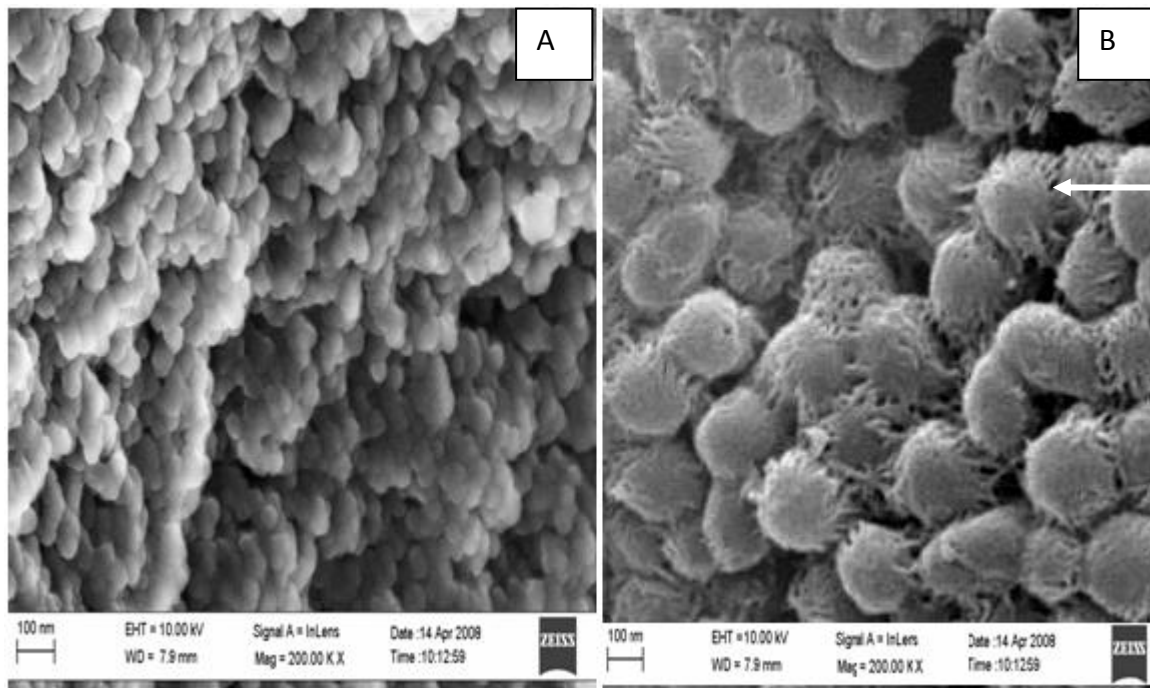


**Figure 1:- (A) SEM image of n-BG particles, (C) P(3HB)/n-BG composite microspheres. (Arrow indicating the presence of n-BG particles on the surface of the microspheres).**

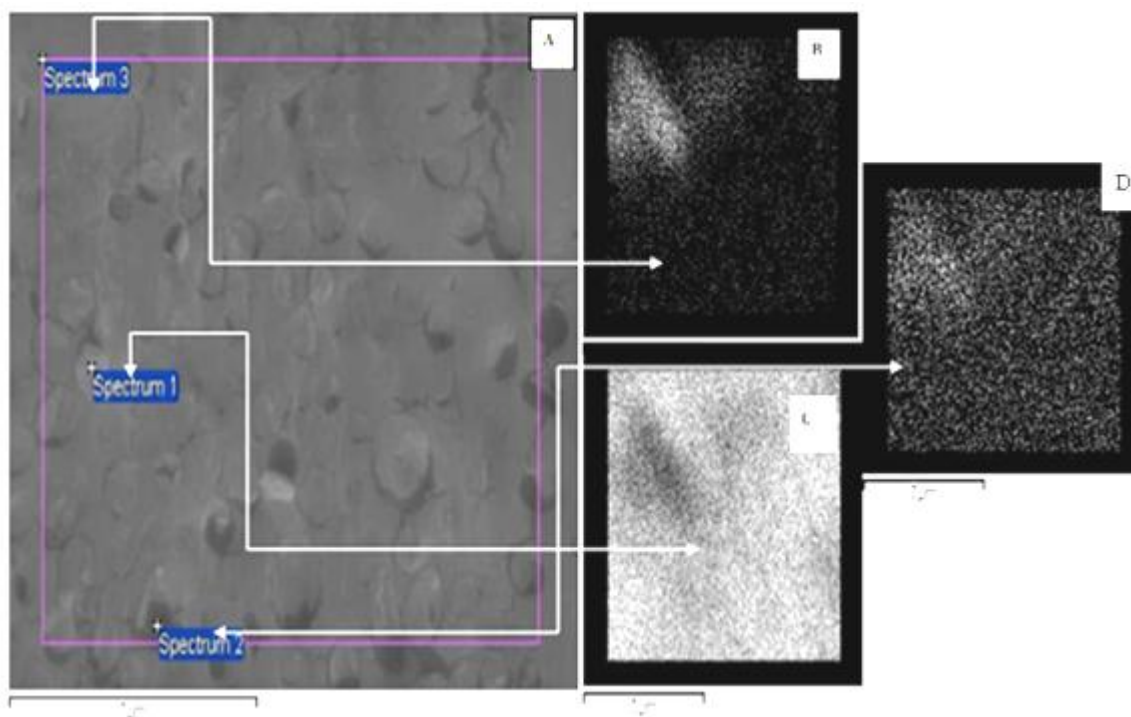


**Figure 2:- An elemental X-Ray mapping of the cross section of the P(3HB)/n-BG microspheres. A) Cross section of the P(3HB)/n-BG composite microspheres. SEM/X-Ray mapping depicting the elements of n-BG, B) Si, C) Ca and D) P.**

#### 5.2.1.1 Fourier Transform Infrared studies (FTIR)

FTIR spectra of the P(3HB) and nanoscale bioactive glass (n-BG) and P(3HB) composite microspheres are represented in Figure 3. The FTIR spectra of the unloaded P(3HB) microspheres is shown in Figure 3A, where the bands with wavenumbers at  $980\text{ cm}^{-1}$ ,  $1226\text{ cm}^{-1}$ ,  $1282\text{ cm}^{-1}$  and  $1782\text{ cm}^{-1}$  were due to the crystalline phase of the polymer and bands at  $1184\text{ cm}^{-1}$  and  $1741\text{ cm}^{-1}$  were due to the amorphous phase of the polymer. The stretching vibrations of the amorphous and crystalline carbonyl groups are seen at  $1741\text{ cm}^{-1}$  and  $1728\text{ cm}^{-1}$  (Vallapil *et al.*, 2007; Shih *et al.*, 2007). FTIR analysis of n-BG particles (Figure 3B) before immersion in SBF revealed bands of silicate with wavenumbers at  $1085\text{ cm}^{-1}$ ,  $802\text{ cm}^{-1}$  and  $472\text{ cm}^{-1}$ . The bands with wavenumbers at  $1085\text{ cm}^{-1}$  corresponded to the vibrational mode of the asymmetric stretch of Si-O-Si, similarly at  $802\text{ cm}^{-1}$  it corresponded to the symmetric stretch of the Si-O and the band at  $472\text{ cm}^{-1}$  corresponded to the vibrational bending of Si-O-Si (Barba *et al.*, 1999). The FTIR spectra of the

P(3HB)/n-BG composite microspheres (Figure 3C) revealed the characteristic bands of P(3HB) with wavenumbers at  $980\text{ cm}^{-1}$ ,  $1282\text{ cm}^{-1}$  and  $1782\text{ cm}^{-1}$ . In addition, the characteristic bands of nanoscale bioactive glass particles with wavenumbers at  $1082\text{ cm}^{-1}$  and  $805\text{ cm}^{-1}$  were also observed.

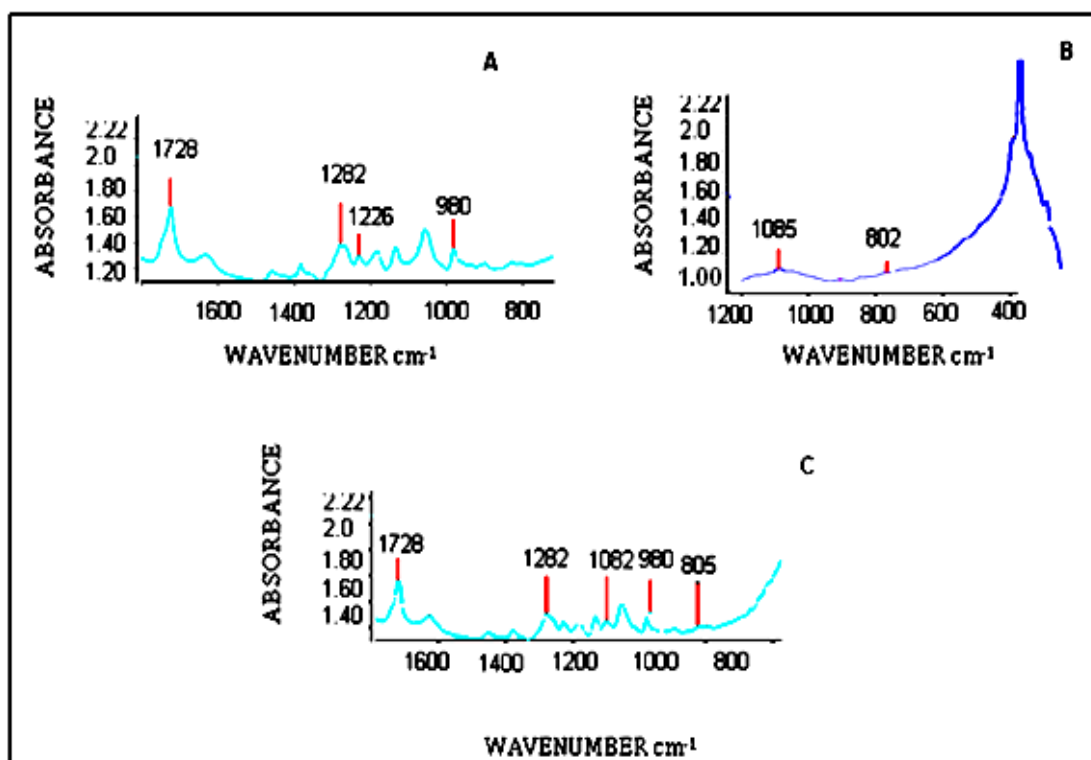


Figure 3:- A) FTIR spectra of the P(3HB) microsphere films revealing the characteristic peak of P(3HB) at wavenumbers  $1728\text{ cm}^{-1}$ ,  $1282\text{ cm}^{-1}$ ,  $1226\text{ cm}^{-1}$  and  $980\text{ cm}^{-1}$ . B) FTIR spectra of the n-BG particles with the characteristic peak at wavenumbers  $1085\text{ cm}^{-1}$  and  $802\text{ cm}^{-1}$ . C) FTIR spectra of the P(3HB)/n-BG composite microsphere films revealing the characteristic peak of P(3HB) at wavenumbers  $1728\text{ cm}^{-1}$  and  $1282\text{ cm}^{-1}$  and the characteristics peaks of n-BG particles at  $1082\text{ cm}^{-1}$  and  $805\text{ cm}^{-1}$ .

### 5.2.1.2 Scanning Electron Micrographs/Energy Dispersive X-Ray (SEM/EDX) of microsphere films

The P(3HB) microsphere films and the P(3HB)/nBG composite microsphere films were analyzed using SEM/EDX analysis (Figure 4 and 5). The P(3HB) microsphere films revealed the presence of carbon and oxygen as shown in Figure 4. The EDX analysis of the P(3HB)/nBG composite microsphere films revealed the presence of silica (Si), calcium (Ca) and phosphorous (P) in addition to C and O (Figure 5).

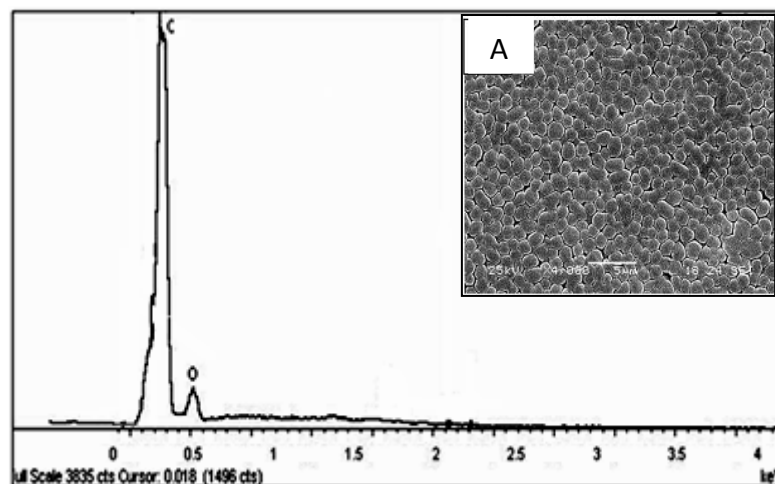


Figure 4:- SEM/EDX micrographs of the P(3HB) microsphere films, revealing the presence of only carbon and oxygen was observed.

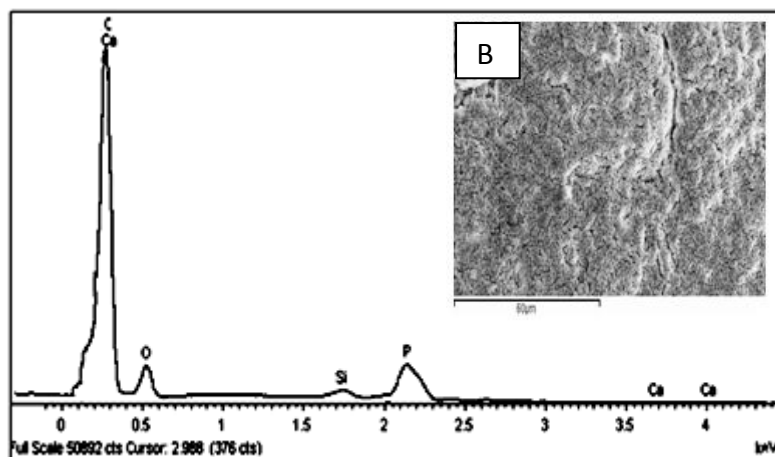


Figure 5:- SEM/EDX micrographs of the P(3HB)/n-BG composite microsphere films depicting the presence of Si, Ca, P in addition to C and O.

### 5.2.1.3 Thermal properties

Differential Scanning Calorimetry (DSC) was used in order to determine the  $T_g$ ,  $\%X_c$  and  $T_m$  values of the P(3HB) microsphere films and P(3HB)/n-BG composite microsphere films. The results of the DSC thermograms are presented in Table 1. The DSC thermograms of the P(3HB) microsphere films and the P(3HB)/n-BG composite microsphere films are shown in Figure 6. There were no significant differences observed between the thermographs of the P(3HB) microsphere films (Figure 6A) and the P(3HB)/n-BG composite microsphere films (Figure 6B) during the first heating run. However, the emergence of a new melting peak in the second heating run was observed in the P(3HB)/n-BG composite microsphere films. The melting temperature and the crystallization temperature of the P(3HB) microsphere films were higher than the P(3HB)/n-BG composite microsphere films as seen in Table 1. The observations made from the thermal measurements for both the P(3HB) films and the P(3HB)/nBG composite microsphere films can be summarized as follows : (i) The % crystallinity was less for the P(3HB)/nBG composite microsphere films as compared to the P(3HB) microsphere films ( $n=3$   $**p<0.01$ ) (ii) The melting temperature ( $T_m$ ) was less for the P(3HB)/nBG composite films as compared to the P(3HB) microsphere films. The P(3HB)/n-BG microsphere films exhibited a decrease of 1.8% in the  $T_m$  values and 5.4% decrease in the  $\%X_c$  values.

**Table 1:- A comparison of the thermal properties of the P(3HB) microsphere films and P(3HB)/n-BG composite microsphere films (n=3).**

<b>Thermal Properties</b>	<b>P(3HB)</b>	<b>P(3HB)/n-BG</b>
$T_m$ (°C)	173.15	170.46
$\% X_c$	47.66	40.03

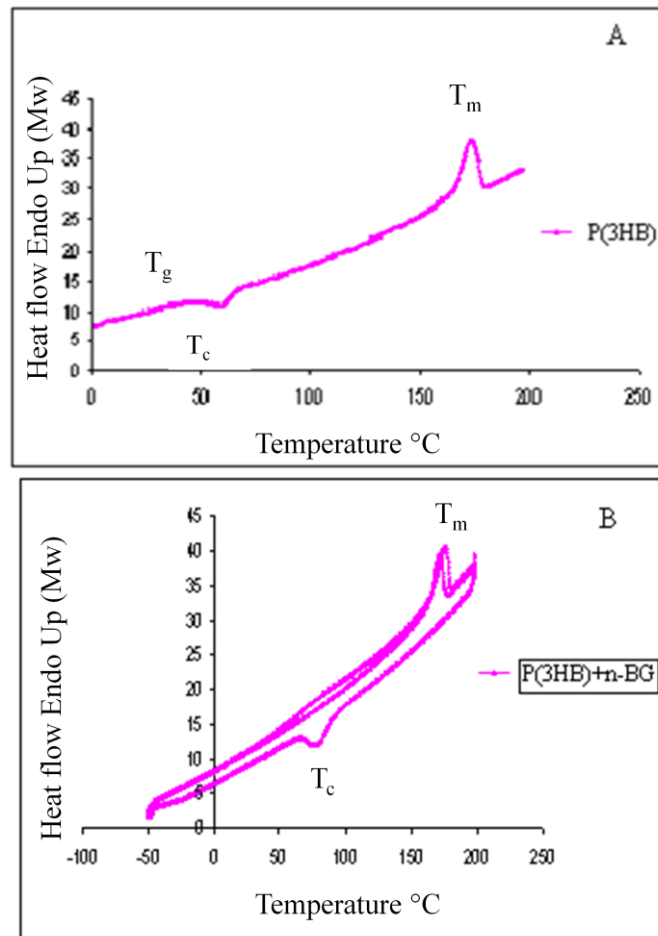
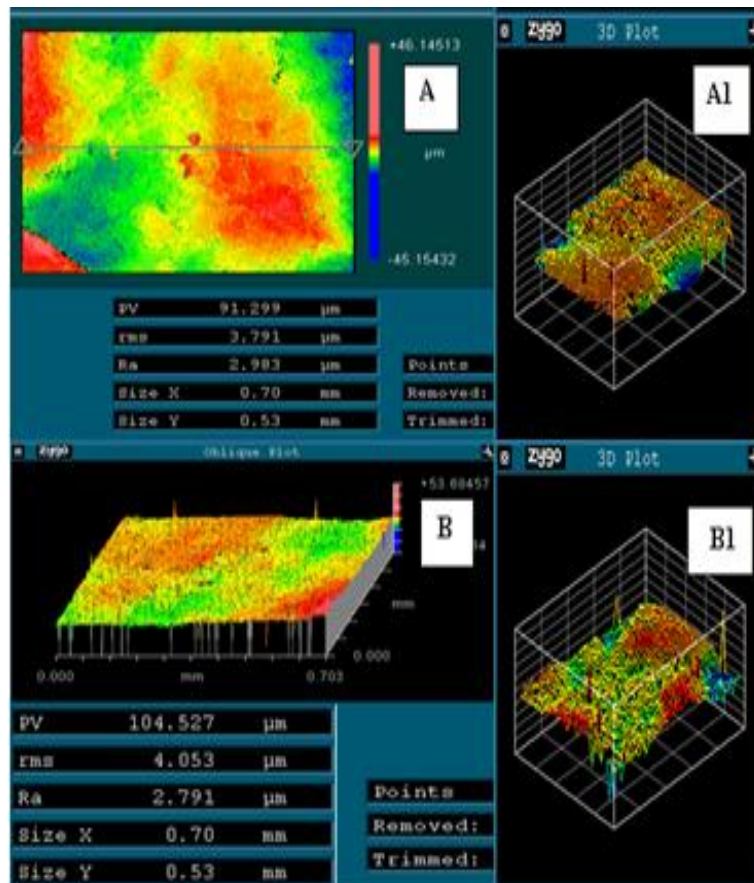


Figure 6:- DSC thermograms of the A) P(3HB) microspheres film and B) P(3HB)/n-BG composite microspheres films.

#### 5.2.1.4 Surface roughness (White light interferometry)

White light interferometry was performed on the samples to analyse the change in the surface roughness induced by the presence of n-BG particles when compared to the P(3HB) microsphere films as seen in Figure 7. This technique measures the surface roughness of a flat substrate; therefore, P(3HB) microsphere films and P(3HB)/n-BG composite microsphere films (diameter = 12.87 mm, thickness = 0.87 mm) were measured for changes in surface roughness. The rms roughness value of the P(3HB)/n-BG composite microsphere films were  $4.00\mu\text{m}$  (Figure 7B) which was significantly ( $n=3$ ,  $**p<0.01$ ) higher than  $3.79\mu\text{m}$  of the P(3HB) microsphere films (Figure 7A).



**Figure 7:-2D and 3D plots of the P(3HB) microsphere film surfaces and P(3HB)/n-BG composite microsphere films as determined by white light interferometry. 2D plot (A) and 3D plot (A1) of the P(3HB) microsphere films. 2D plot (B) and 3D plot (B1) of the P(3HB)/n-BG composite microsphere films.**

## 5.2.1.5 Surface wettability

The static contact angle measurements of the P(3HB) microsphere films and P(3HB)/n-BG composite microsphere films were carried out to measure the surface wettability of the microsphere films as shown in Figure 8. The P(3HB) microsphere films had a contact angle of  $60.9^\circ$  and the composite P(3HB)/nBG microsphere films had a contact angle of  $56.89^\circ$  ( $n=3$  \*\*\* $p<0.001$ ).

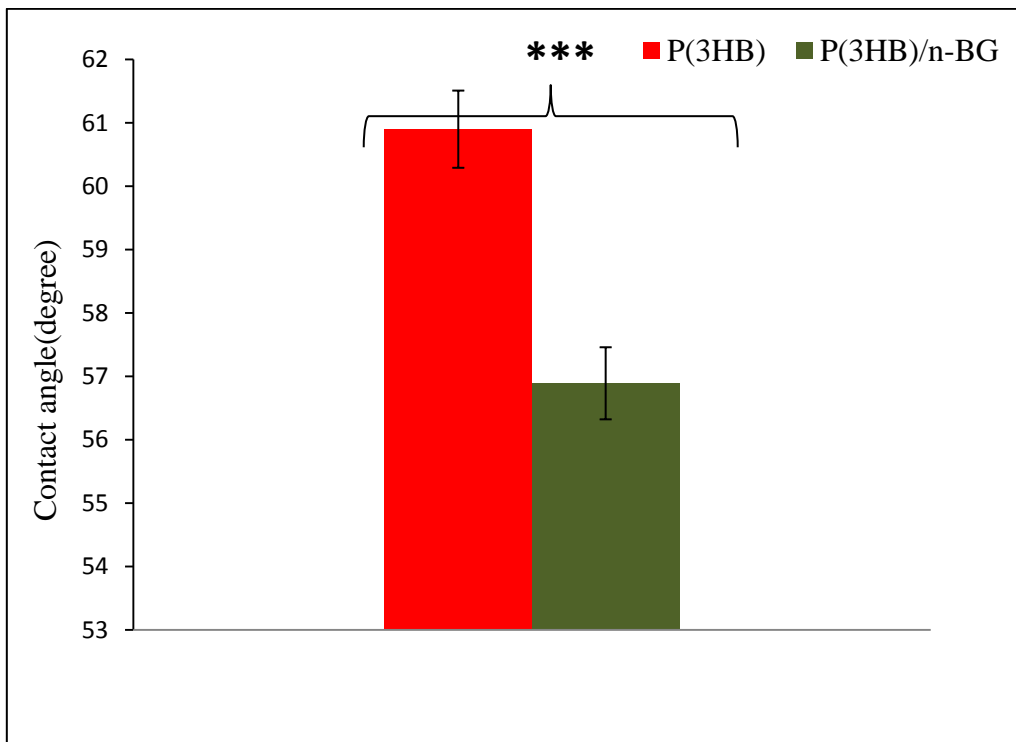


**Figure 8:-** A comparison of the surface wettabilities of the P(3HB) microsphere films and P(3HB)/n-BG composite films. The data ( $n=3$ ; error= $\pm$ s.d) were compared using  $t$ -test and the differences were considered significant when \*\*\* $p < 0.001$ .

## 5.2.1.6 Protein adsorption test

Protein from the DMEM media containing FCS adsorbed on the surface of the P(3HB)/n-BG composite microsphere films before immersion in SBF was  $323.5\mu\text{g}$  which was significantly ( $n=3$   $***p<0.001$ ) higher than  $308\mu\text{g}$  of protein adsorbed on the P(3HB) microsphere films. The presence of the n-BG particles in the composite microsphere films resulted in higher protein binding when compared to the P(3HB) microsphere films, as is evident from the results in Figure 9. Thus, the composite microsphere films exhibited an increase of 4.8% when compared to the P(3HB) microsphere films in total protein adsorption.

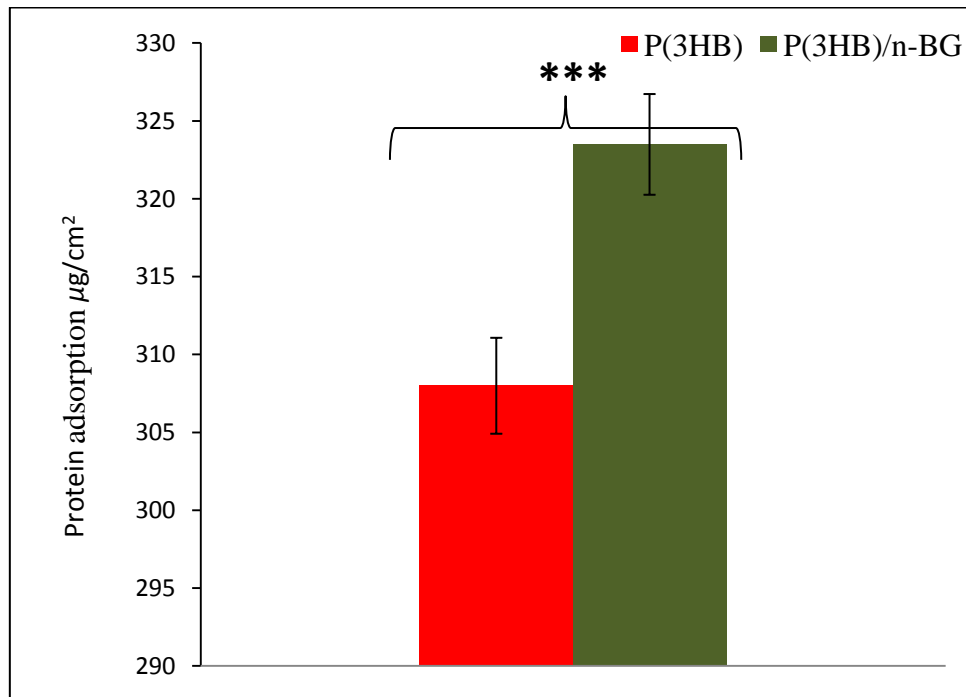


**Figure 9:-Total protein adsorption test carried out on the surface of P(3HB) microsphere films and P(3HB)/n-BG composites microsphere films. The data ( $n=3$ ;error= $\pm$ s.d) were compared using  $t$ -test and the differences were considered significant when  $***p<0.001$ .**

## 5.2.1.7 Cell attachment tests

Cell attachment tests were performed using Neutral red assay upon HaCaT cells grown for a period of three days, the keratinocyte cell line, on P(3HB) and P(3HB)/n-BG composite microsphere films, proved the biocompatibility of the films. The results are presented in Figure 10.

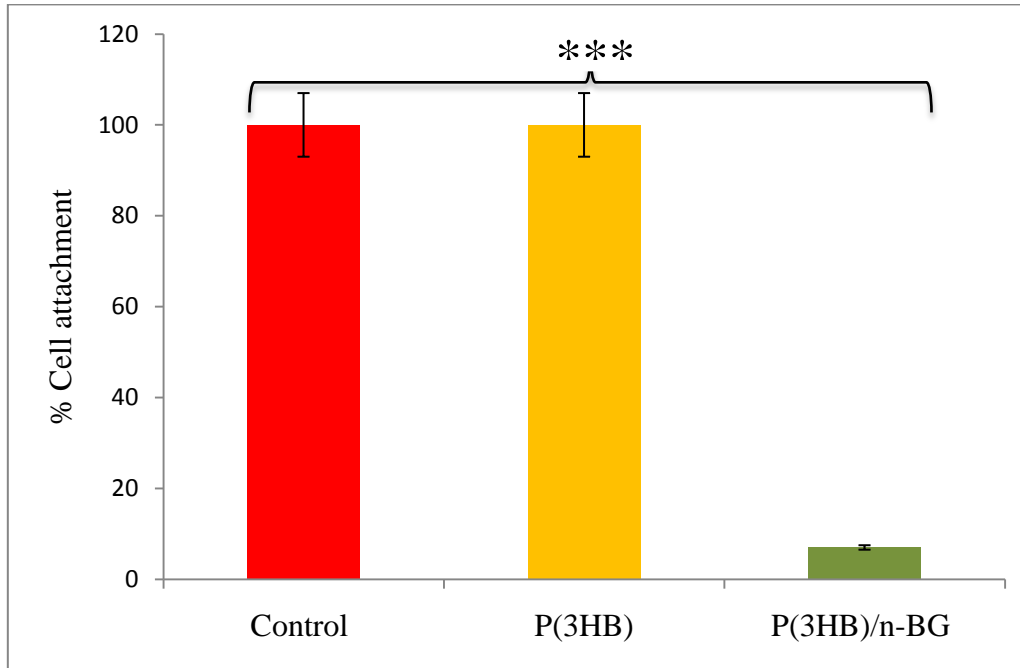


**Figure 10:** - Cell attachment studies performed after 3 days, using Neutral Red assay, on P(3HB) microsphere films and P(3HB)/n-BG composite microsphere films. The cell attachment of all tested samples relative to the control (control set to 100%). The data (n=3; error= $\pm$ s.d) were compared using *t*-test and the differences were considered significant when  $***p < 0.001$ .

The cell viability of the P(3HB)/n-BG composite microsphere films was 100% which was a significant increase ( $n=3$ ,  $***p<0.001$ ) when compared to the cell viability on the P(3HB) microsphere films which was only 7%. SEM images of the cells attached on day 3 on the P(3HB)/n-BG composite microsphere films showed cells appeared to be flat and have confluent layer of cell growth on the surface of the films (Figure 11B). In comparison, the cells attached on the P(3HB) microsphere films were not confluent and continuous as some cells appeared loosely bound as seen in Figure 11A.

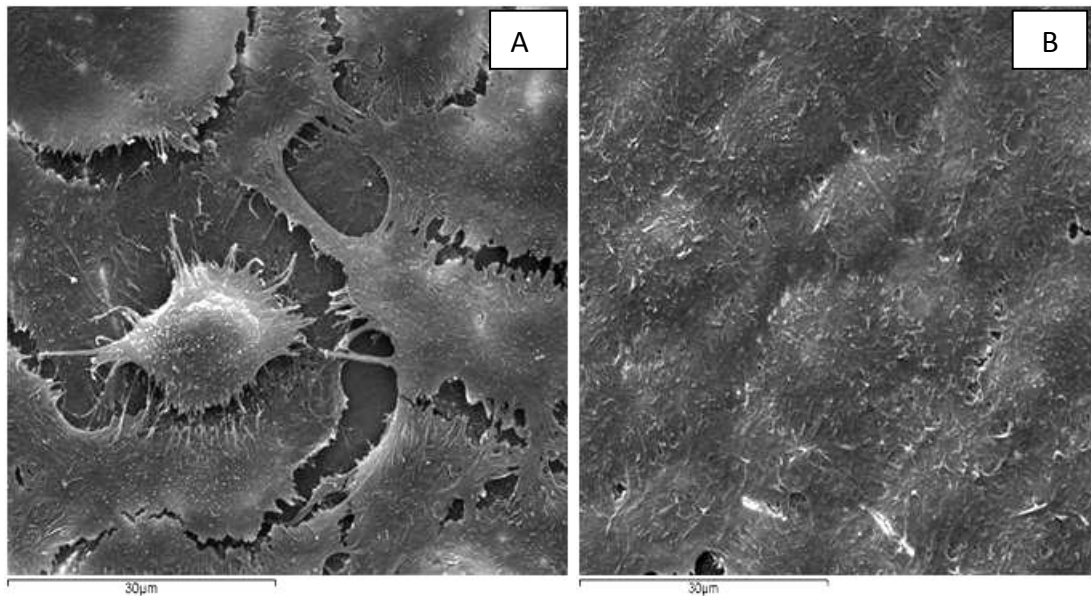


**Figure 11:- SEM images of HaCaT cell attachment seen on day 3, on the surface of A) P(3HB) microsphere films and B) P(3HB)/n-BG composite microsphere films, ( $n=3$ ; error= $\pm$ s.d).**

### 5.2.1.8 Haemostatic activity of n-BG

Nanoscale bioactive glass particles (n-BG) are haemostatically active, promoting the rapid formation of blood clots (Ostomel *et al.*, 2006). Therefore in this study, the *in vitro* haemostatic activity of varying amounts of n-BG particles (1mg, 2mg and 4mg) was evaluated using a thromboelastograph (TEG) which is a clinical instrument that is used to monitor the change in the viscoelasticity of blood during clot formation (Ostomel *et al.*, 2006) (Figure 12). The initial detection of blood clot formation is referred to as R minutes. This is the time when the amplitude of bimodal symmetric viscoelasticity curve is 2mm. For example when 1mg of n-BG particles were used, the R value was 7.7 mins, for 2mg, the R value was 4.2 mins and for 4mg, the R value was 3.8 mins when compared to the control (in the absence of n-BG particles), which was 10.4 mins.

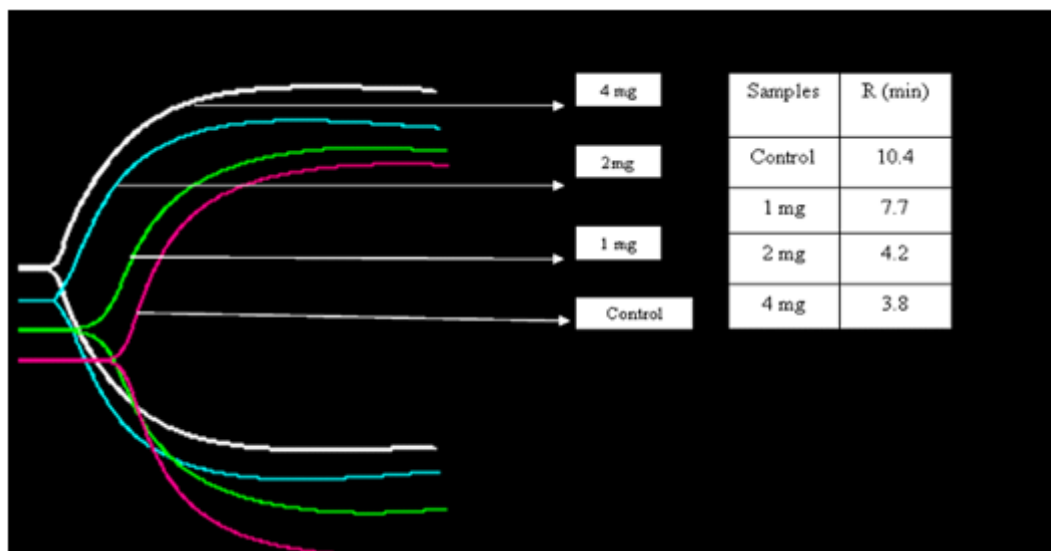


**Figure 12:-** Thromboelastograph plot depicting the haemostatic activity of n-BG particles. The differences in the rate of coagulation in the presence of different amounts of n-BG particles is compared to the rate of coagulation in the control (absence of n-BG particles), (n=3; error= $\pm$ s.d).

## 5.2.2 P(3HB)/n-BG composite microsphere films immersed in SBF

### 5.2.2.1 Surface morphology

In order to further enhance the nanoscale topographical features such as surface roughness on the P(3HB)/n-BG composite microsphere films, they were immersed in SBF for a period of 1, 3 and 7 days to induce the formation of crystalline hydroxyapatite (HA) needles. SEM images of the surface of the P(3HB)/n-BG composite microsphere films immersed in SBF for 1, 3 and 7 days are shown in Figure 13. The surface of the P(3HB)/n-BG composite microsphere films on day 3 and day 7 (Figure 13C and D) revealed rough and uneven surface as compared to the films on day 1 which appeared fairly uniform and smooth (Figure 13B).

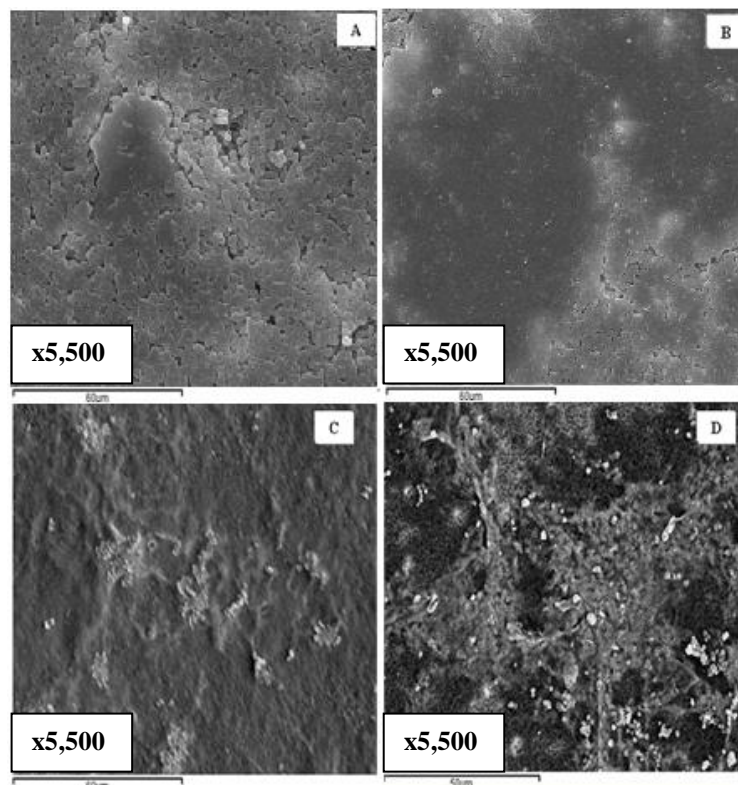


**Figure 13: - SEM images of the P(3HB)/n-BG composite microsphere films before immersion in SBF and after immersion in SBF. A) P(3HB)/n-BG composite microsphere film, B) P(3HB)/n-BG composite microsphere film immersed in SBF for 1 day. C) P(3HB)/n-BG composite microsphere films immersed in SBF for 3 days. D) P(3HB)/n-BG composite microsphere films immersed in SBF for 7 days. Numbers in the insets indicate magnification.**

## 5.2.2.2 Fourier Transform Infrared studies (FTIR)

The FTIR spectra of the nanoscale bioactive glass particles (n-BG) and the P(3HB)/n-BG composite microsphere films after immersion in SBF for a period of 1, 3 and 7 days are represented in Figure 14. FTIR analysis of n-BG particles before immersion in SBF are mentioned in section 5.2.1.1. After immersion on day 1, P(3HB)/n-BG composite microsphere films revealed a P-O bending vibration between  $600\text{ cm}^{-1}$  and  $500\text{ cm}^{-1}$  indicating the presence of a predominantly amorphous calcium phosphate layer. However on day 3 and day 7, the P-O bending band became divided at  $1098\text{ cm}^{-1}$ ,  $1046\text{ cm}^{-1}$ ,  $950\text{ cm}^{-1}$ ,  $606\text{ cm}^{-1}$ , and  $501\text{ cm}^{-1}$  indicating the presence of a crystalline Ca-P layer (Lu *et al.*, 2001).

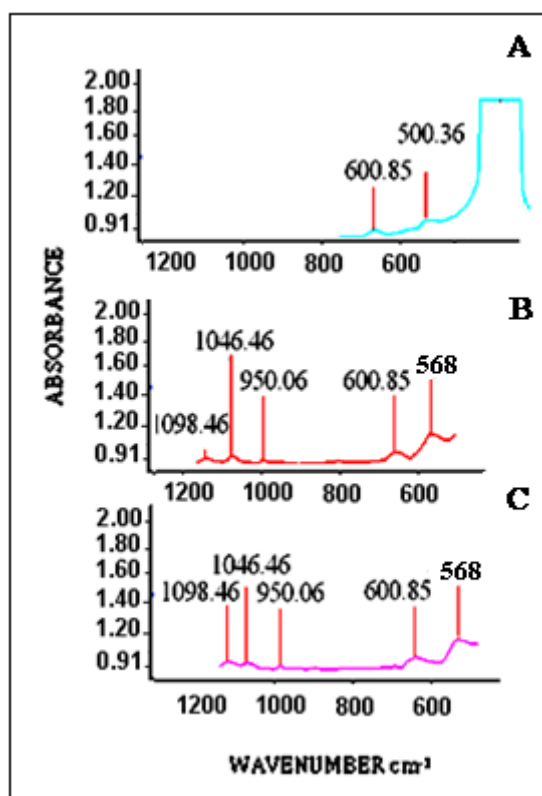
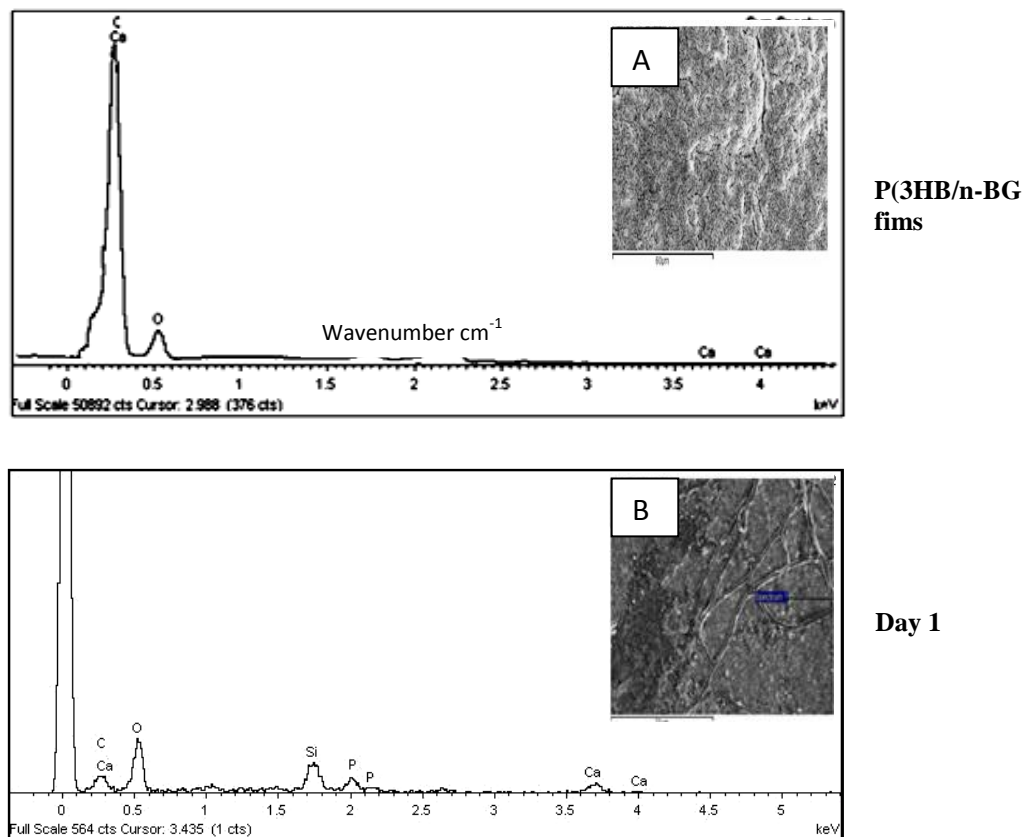
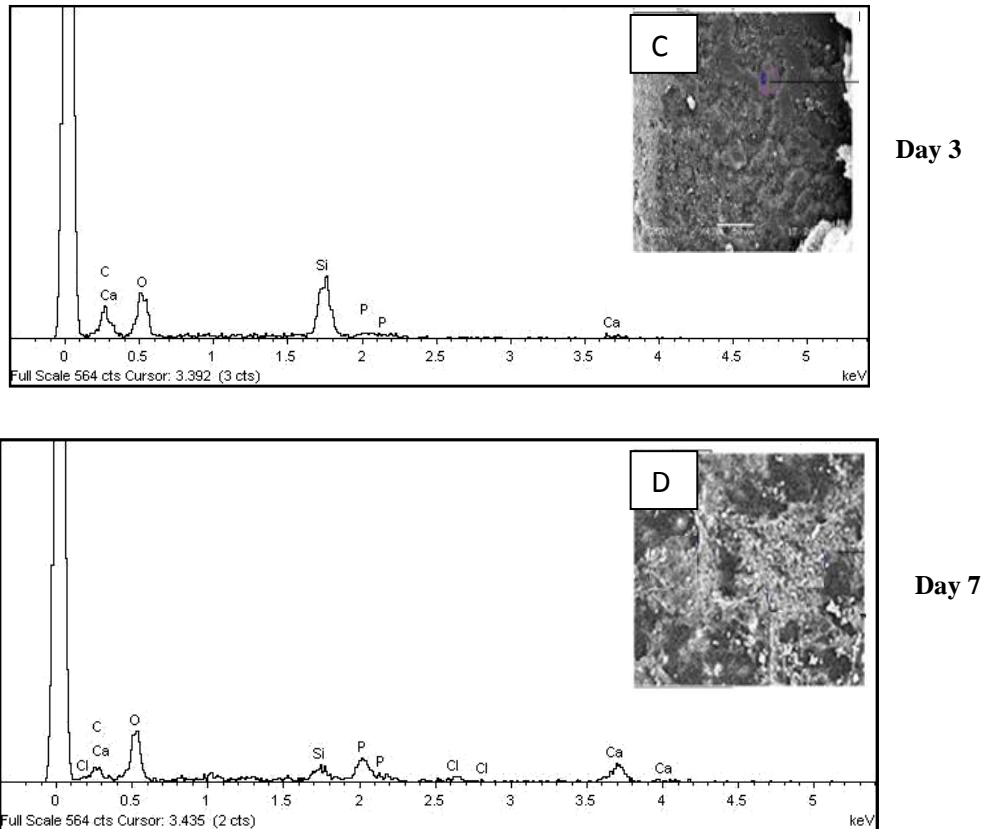


Figure 14:- A) FTIR spectra of P(3HB)/n-BG composite microsphere films immersed in SBF for 1 day, B) P(3HB)/n-BG composite microsphere films immersed in SBF for 3 days, C) P(3HB)/n-BG composite microsphere films immersed in SBF for 7 days.

### 5.2.2.3 Scanning Electron Micrographs/Energy Dispersive X-Ray (SEM/EDX) and X-Ray diffraction (XRD) analysis of P(3HB)/nBG composite microsphere films

The P(3HB)/nBG composite microsphere films when immersed in SBF for a period of 1, 3 and 7 days were analyzed using SEM/EDX analysis to highlight the transition of the nanoscaled bioactive glass particles to a calcium phosphate layer (Figure 15). From the EDX analysis of the composite microsphere films, the presence of Ca and P peaks were observed after immersion in SBF for a period of 1, 3 and 7 days as seen in Figure 15 A, B, and C, although the Si peak was found on all the composite films, the intensity of the peak appeared to diminish after 3 days of immersion in SBF as seen in Figure 15B.





**Figure 15:- SEM/EDX micrographs of the P(3HB)/n-BG composite microspheres films before and after immersion in SBF for a period of 1, 3 and 7 days. A) The P(3HB)/n-BG composite microspheres films before immersion depicting the presence of Si, Ca, P in addition to C and O. B) The presence of Si, Ca and P peaks are observed after immersion in SBF for 1 day. B) The relative intensity of the Si peaks appear increased on the surface of the P(3HB)/n-BG composite films after 3 days of immersion in SBF. C) At day 7, a decrease in the Si peak was observed, followed by an increase in the Ca and P peak on the surface of P(3HB)/n-BG composite microspheres films.**

The X-Ray diffraction peaks of the P(3HB)/n-BG composite microsphere films are represented in Figure 16. The growth of the characteristic crystalline hydroxyapatite peak between  $(2\theta)$   $31^\circ$  and  $33^\circ$  was observed on the P(3HB)/n-BG composite films when immersed in SBF for 1, 3 and 7 days as seen in Figure 16. Thus the observations made from the SEM/EDX and XRD analysis are summarized below (i) characteristic crystalline hydroxyapatite peak between  $(2\theta)$   $31^\circ$  and  $33^\circ$  was observed on the P(3HB)/n-BG composite microsphere films on 1, 3 and 7 days. (ii) the hydroxyapatite peak was shown to increase on prolonging the immersion time, indicating the transformation of amorphous (or weakly crystalline) hydroxyapatite to crystalline hydroxyapatite.

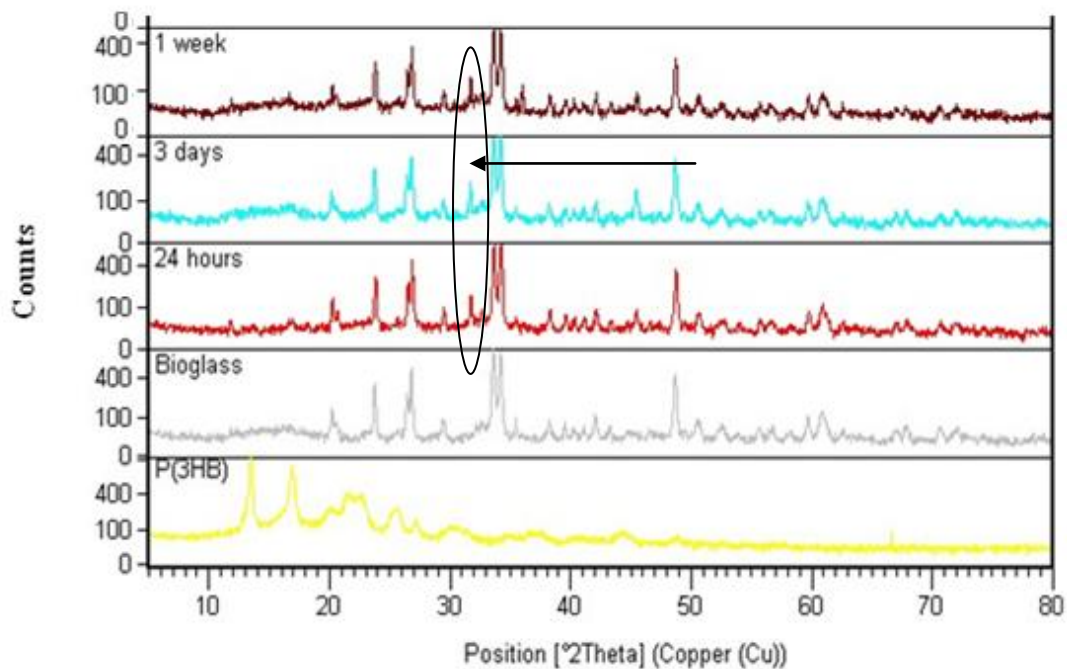


**Figure 16:- X-Ray diffractograms of the P(3HB)/n-BG composite microsphere films after immersion in SBF. The arrow shows the characteristic crystalline hydroxyapatite peak between  $(2\theta)$   $31^\circ$  and  $33^\circ$ .**

#### 5.2.2.4 Thermal properties of P(3HB)/nBG composite microsphere films

Differential Scanning Calorimetry (DSC) was used in order to determine the %  $X_c$  and  $T_m$  values of the P(3HB)/n-BG composite microsphere films. The results of the DSC thermograms are presented in Table 2. The DSC thermograms of the P(3HB)/n-BG composite microsphere films immersed in SBF are shown in Figure 17. There were no significant differences observed between the thermographs of the P(3HB)/n-BG composite microsphere films immersed in SBF for day 1, day 3 and day 7 during the first and second heating run. The emergence of a melting peak in the second heating run was observed in all the P(3HB)/n-BG composite microsphere films immersed in SBF. Thus the observations made from the thermal measurements of the P(3HB)/n-BG composite microsphere films before and after immersion in SBF can be summarized as : (i) insignificant differences ( $n=3$ ,  $p>0.05$ ) in the thermal properties such as melting temperature and % $X_c$  was observed when the P(3HB)/n-BG composite microsphere films were immersed in SBF for a period of 1, 3 and 7 days.

**Table 2:-Thermal properties of the P(3HB)/n-BG composite microsphere films before and after immersion in SBF, (n=3).**

<b>Thermal Properties</b>	<b>P(3HB)/n-BG</b>	<b>Day1</b>	<b>Day3</b>	<b>Day 7</b>
$T_m$ (°C)	170.46	168	168.44	170.17
% $X_c$	40	37.71	36.07	36.00

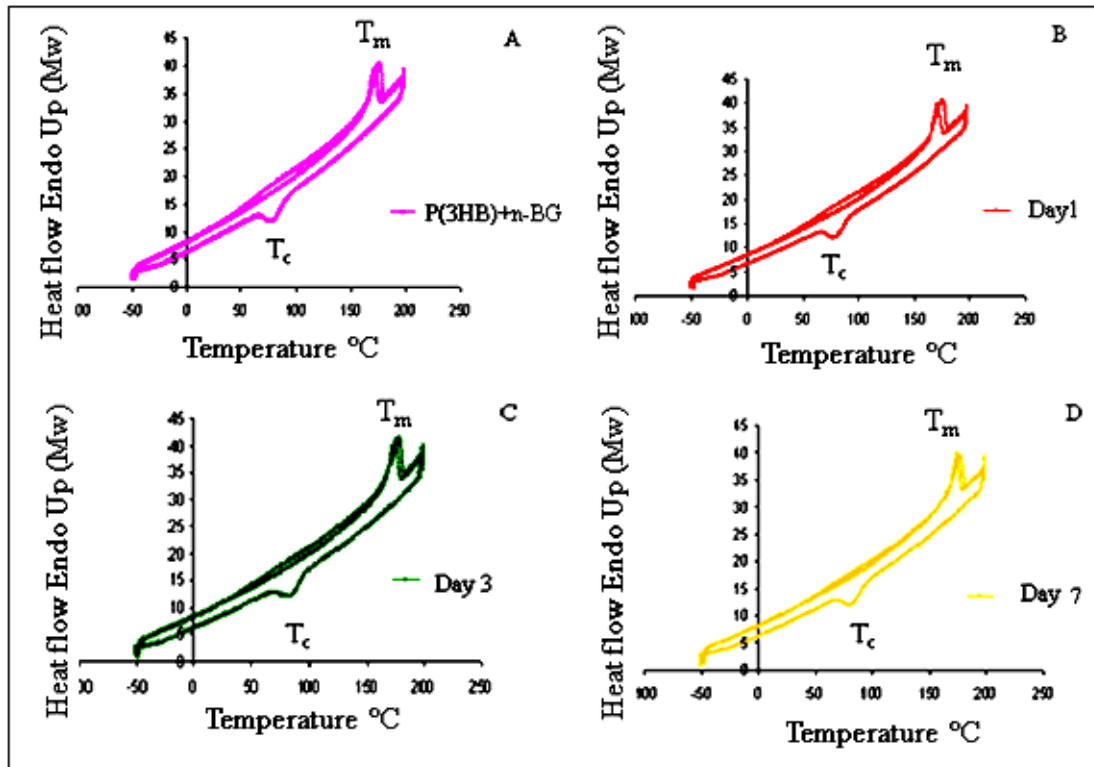
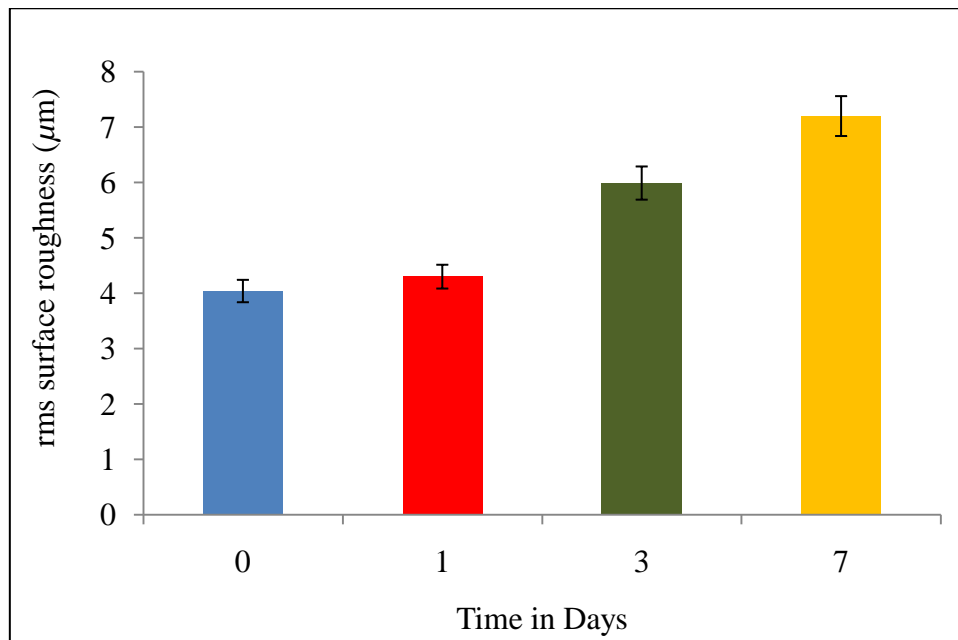


Figure 17:- DSC thermograms of the P(3HB)/nBG composite films (before and after immersion in SBF) A) P(3HB)/n-BG composite microspheres before immersion in SBF used as control, B) P(3HB)/n-BG microspheres immersed in SBF for a period of 1 day, C) P(3HB)/n-BG microspheres immersed in SBF for a period of 3 days and D) P(3HB)/n-BG microspheres immersed in SBF for a period of 7 days,  $n=3$ ; error= $\pm$ s.d.

### 5.2.2.5 Surface roughness (White light interferometry)

White light interferometry was performed on the samples to analyze the change in the surface roughness of the P(3HB)/n-BG composite microsphere films induced by the presence of nanoscaled crystalline hydroxyapatite. The rms roughness value of the P(3HB)/n-BG composite microsphere films on day 1 of immersion in SBF was  $4.3\mu\text{m}$ , on day 3 was  $5.99\mu\text{m}$  and on day 7 was  $7.2\mu\text{m}$  ( $n=3$  \*\*\* $p<0.001$ ) (Figure 18) as compared to much lower rms values of  $4.04\mu\text{m}$  of the P(3HB)/n-BG composite microsphere films before immersion in SBF.



**Figure 18:-** Surface roughness of the P(3HB)/n-BG composite microsphere films after immersion in SBF for 1, 3 and 7 days measured using white light interferometry. The data ( $n=3$ ; error= $\pm$ s.d) compared using ANOVA was significant \*\*\*  $p<0.0001$ . A Bonferroni Post Hoc was applied and significant differences at \*\*\* $p<0.0001$  for P(3HB)/n-BG microsphere films immersed in SBF at day 3 and day 7 were observed when compared to the control and P(3HB) microsphere films immersed for day 1. No significant differences ( $p>1.0$ ) were observed between control and day 1.

A fairly homogenous surface roughness was observed on the P(3HB)/n-BG composite microsphere films immersed for 1 day in SBF as seen in the 2D and 3D plots (Figure 19A and A1) when compared to the surface roughness on the films immersed for 3 days and 7 days where some areas on the films (3 days and 7 days) appeared to have a relatively higher surface roughness as compared to the others (Figure 19 B, B1 and C, C1).

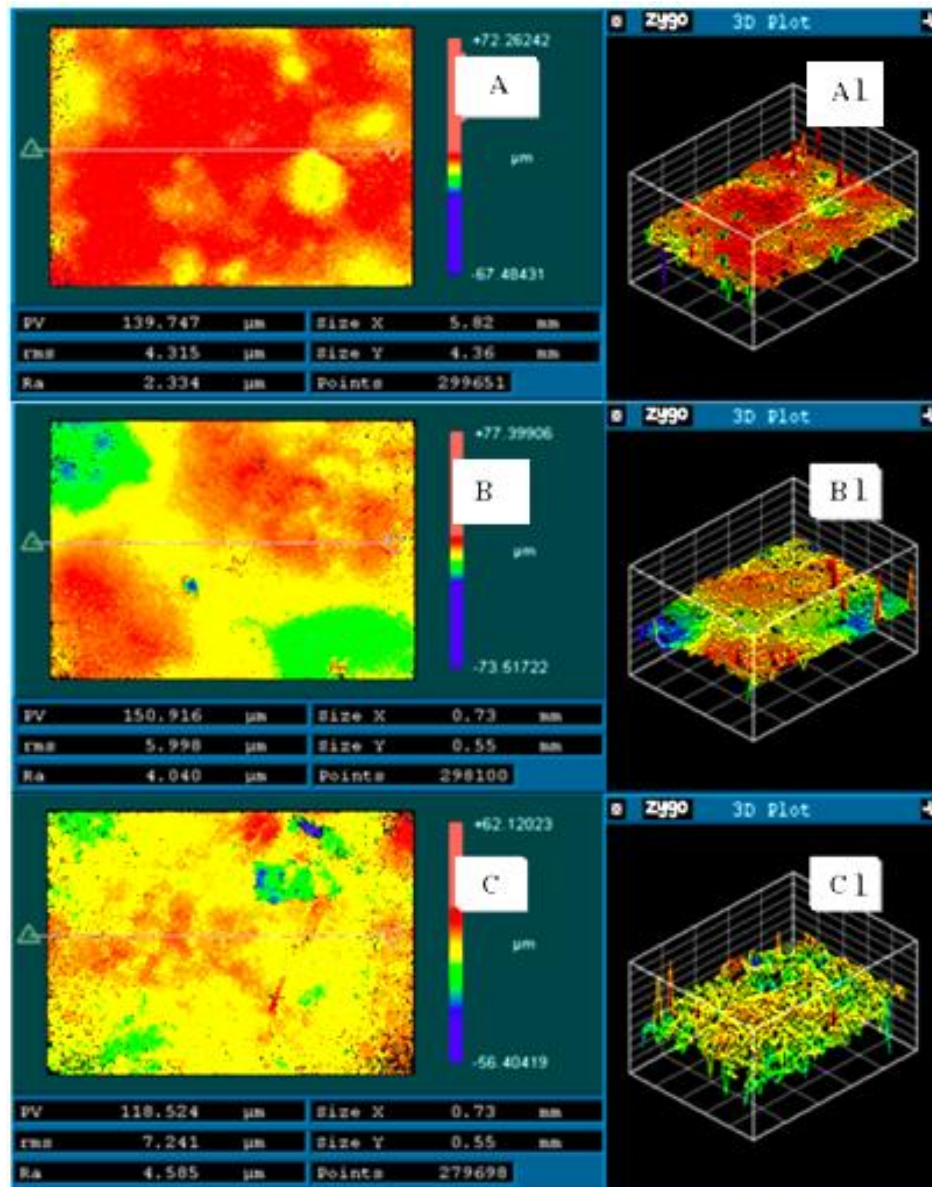
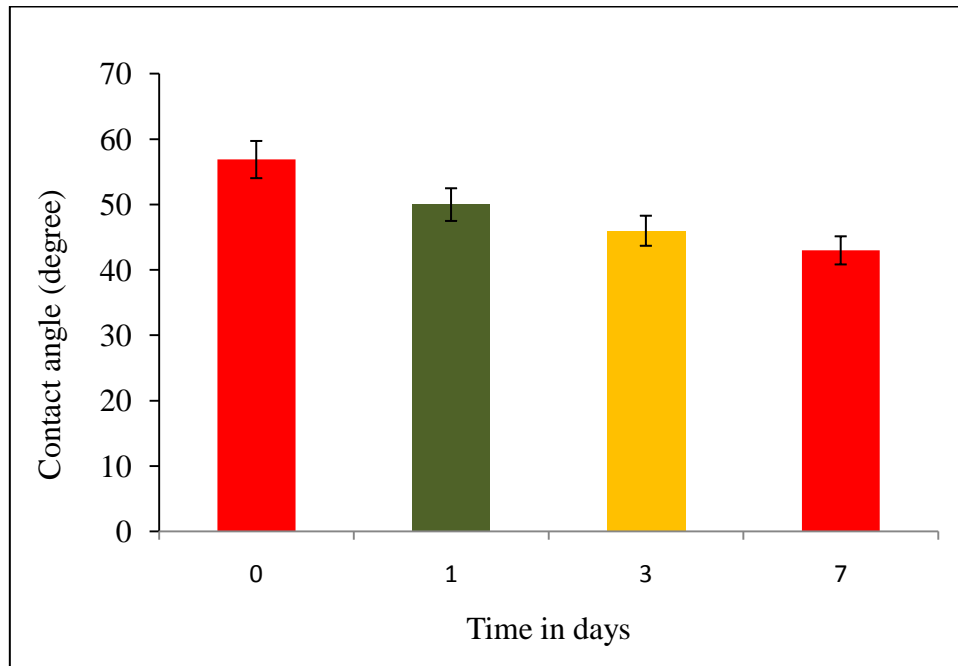


Figure 19:-2D plot (A) and 3D plot (A1) of the P(3HB)/n-BG composite microsphere films after immersion in SBF for 1 day, 2D plot (B) and 3D plot (B1) after immersion in SBF for 3 days. 2D plot (C) and 3D plot (C1) after immersion in SBF for 7 days, (n=3; error= $\pm$ s.d).

### 5.2.2.6 Surface wettability

The static contact angle measurements of the P(3HB)/n-BG composite microsphere films before and after immersion in SBF were compared to monitor the changes in the surface wettability in the presence of the nanoscaled crystalline hydroxyapatite. The surface wettabilities of the P(3HB)/n-BG composite microsphere films after immersion in SBF increased significantly ( $n=3$   $***p<0.001$ ) as compared to the composite microsphere films before immersion as seen in Figure 20. A decrease in the water contact angle of the P(3HB)/n-BG composite microsphere films observed on 1, 3 and 7 days were 12.60%, 19.29%, and 22.62% when compared to the P(3HB)/n-BG composite microsphere films before immersion.



**Figure 20:-** A comparison of the surface wettabilities of the P(3HB)/n-BG composite films before and after immersion in SBF on day 1, day 3 and day 7, data ( $n=3$ ; error= $\pm$ s.d). The P(3HB)/n-BG microsphere films after immersion in SBF had a significant ( $***p<0.0001$ ) effect on surface wettability. Since the data compared using ANOVA was significant, a Bonferroni Post Hoc was applied and significant differences at  $***p<0.0001$  for P(3HB)/n-BG microsphere films immersed in SBF at day 3 and day 7 were observed when compared to the control and P(3HB) microsphere films immersed for day 1. No significant differences ( $p>1.0$ ) were observed between control and day 1.

## 5.2.2.7 Protein adsorption test

In this study, the effect of the nanoscaled crystalline hydroxyapatite and its surface charge on protein adsorption was also investigated. The protein adsorption on the P(3HB)/n-BG composite microsphere films after immersion in SBF exhibited a lower amount of protein adsorption when compared to the composite microsphere films before immersion, as seen in Figure 21. For example the composite microsphere films exhibited a decrease of 28% on day 1. This was followed by a decrease of 90% on day 3 and 88% on day 7 as compared to the P(3HB)/n-BG composite microsphere films before immersion.

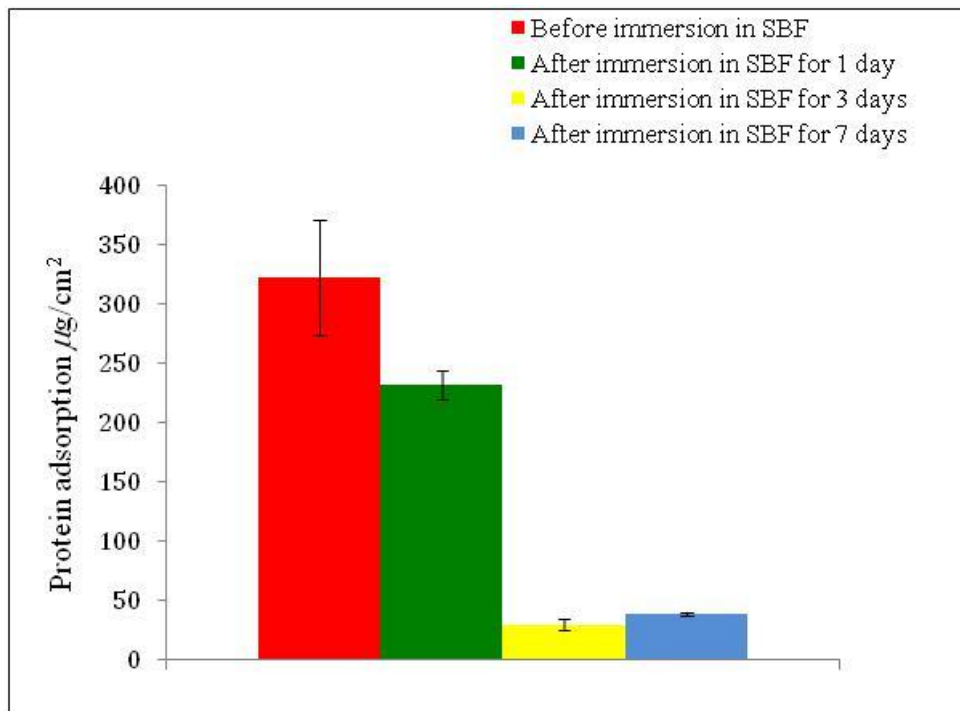
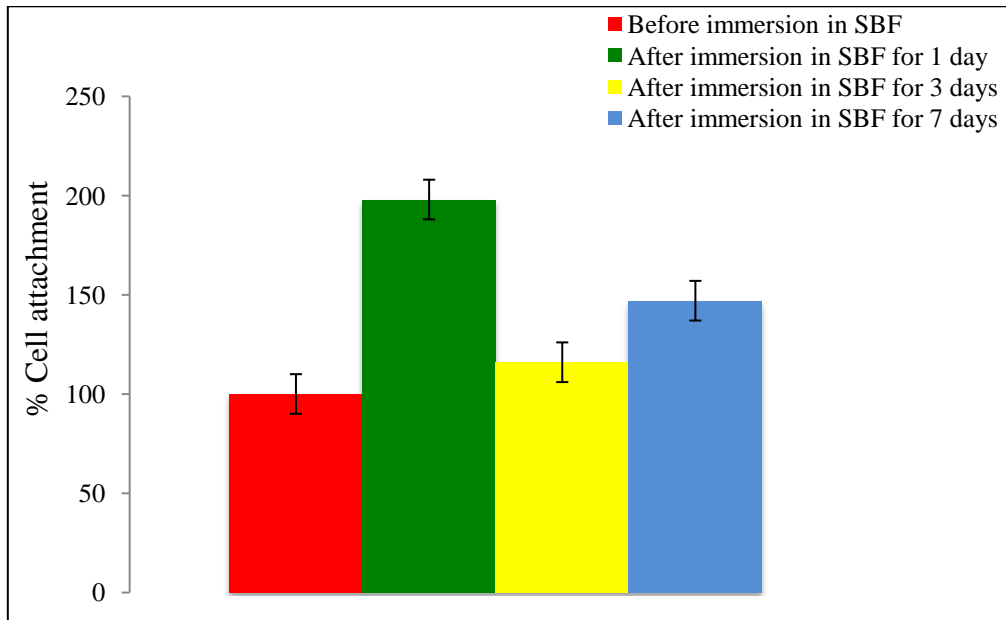


Figure 21:- Total protein adsorption test carried out on the surface of P(3HB)/n-BG composite microsphere films (before and after immersion in SBF), data (n=3; error=±s.d). The P(3HB)/n-BG microsphere films after immersion in SBF had a significant effect ( $***p<0.0001$ ) on protein adsorption. Since the data compared using ANOVA was significant, a Bonferroni Post Hoc was applied and significant differences at  $***p<0.0001$  for P(3HB)/n-BG microsphere films immersed in SBF at day 1 were observed when compared to the control and P(3HB) microsphere films immersed for day 3 and day 7. No significant differences ( $p>1.0$ ) were observed between day 3 and day 7.

## 5.2.2.8 Cell attachment tests

Cell attachment tests performed using HaCaT, the keratinocyte cell line, on P(3HB)/n-BG composite microsphere films before and after immersion in SBF proved the biocompatibility of the films. The results are presented in Figure 22.



**Figure 22:-** Cell attachment studies performed on day 3, using Neutral Red assay, on P(3HB)/n-BG composite films, (n=3; error= $\pm$ s.d). The P(3HB)/n-BG microsphere films after immersion in SBF had a significant ( $***p<0.0001$ ) effect on cell attachment. Since the data compared using ANOVA was significant, a Bonferroni Post Hoc was applied and significant differences at  $***p<0.0001$  for P(3HB)/n-BG microsphere films immersed in SBF at day 1 were observed when compared to the control and P(3HB) microsphere films immersed for day 3 and day 7. No significant differences ( $p>1.0$ ) were observed between day 3 and day 7.

SEM images of the HaCaT cells attached on day 1 of the P(3HB)/n-BG composite microsphere films appeared to have a confluent layer of cell growth on the surface of the films comparable to the morphology of the cells attached on the P(3HB)/n-BG composite microsphere films before immersion in SBF (Figure 23A). Some cells were also seen growing on top of each other exhibiting limited spaces for them to spread. However on day 3 and 7, the cells attached on the films appeared raised due to the formation of the scattered hydroxyapatite crystals on the surface of the composite films as shown in Figure 23B and C. A significant increase in the cell viability, expressed as a percentage of cell growth on tissue culture plastics, was observed on

the P(3HB)/n-BG composite microsphere films after immersion in SBF when compared to the P(3HB)/n-BG composite microsphere films before immersion. The cell viability of the films immersed in SBF for day 1 had increased to 198% followed by a decrease of 116% on films immersed for 3 days and a 147% on films immersed for 7 days.

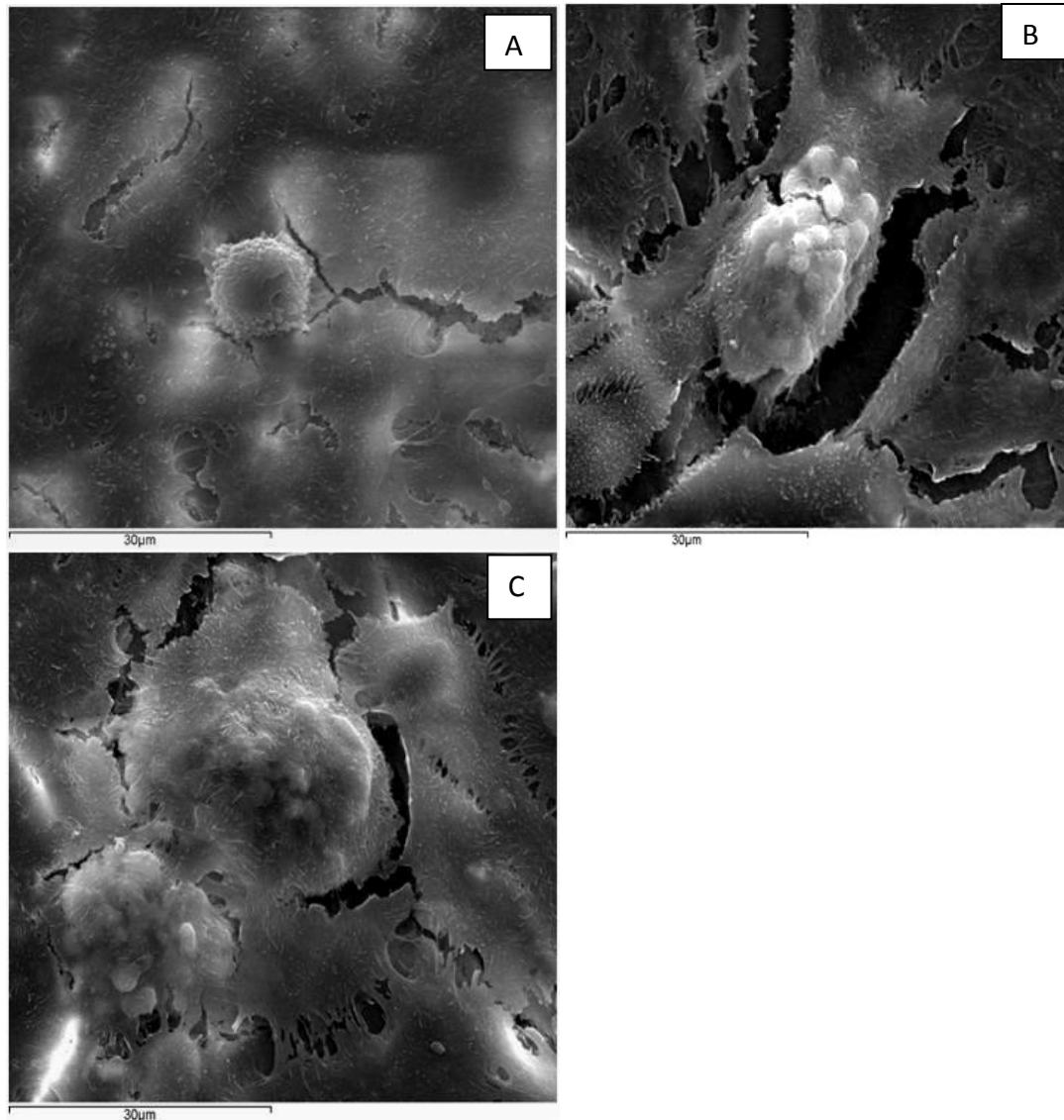


**Figure 23:-** A) SEM images of HaCaT cell attachment seen on the surface of P(3HB)/n-BG composite microsphere films after immersion in SBF for 1 day. Similarly the HaCaT cell attachment is seen on the P(3HB)/n-BG microsphere films immersed in SBF on day 3 and day 7 are represented in Figures B and C. (The arrow shows growth of HaCaT cells on the calcium/phosphate aggregates subsequent to NR assay).

### 5.3 Discussions

In this study nanoscale bioactive glass particles were used in combination with P(3HB) due to the haemostatic efficacy. In addition this study allowed the investigation of the effect of the surface mediated phenomena such as *in vitro* hydroxyapatite deposition on cell attachment. The P(3HB)/n-BG composite microsphere films after immersion in SBF was also investigated in relation to microstructural, thermal properties, protein adsorption and the influence of varying surface properties such as nanotopography, surface chemistry and surface charge on the biocompatibility of the P(3HB)/n-BG composite microsphere films were also highlighted.

#### 5.3.1 Nanoscale bioactive glass and P(3HB)/nBG composite microsphere characterization

##### 5.3.1.1 Surface morphology of the n-BG particles and the P(3HB)/n-BG composite microspheres

For this study nanoscale bioactive glass (n-BG) particles with a specific surface area of  $79 \text{ m}^2\text{g}^{-1}$  were used, which was much higher than that of microbio glass (m-BG) ( $<1\text{m}^2\text{g}^{-1}$ ) (Misra *et al.*, 2008). These particles were also smooth, spherical in shape and relatively small when compared to the irregularly shaped m-BG particles. The spherical morphology, with smooth regular shaped agglomerate sizes of the bioactive glass particles have been found to influence the rates of hydroxyapatite deposition as well as to improve its haemostatic efficacy (Ostomel *et al.*, 2006). The spherical morphology, large pore volume and a higher surface area are thought to facilitate the cation release required for both hydroxyapatite depositions as well as contact activated coagulation (Ostomel *et al.*, 2006). Ostomel *et al.*, have also demonstrated the accelerated deposition rates of hydroxyapatite formation when mesoporous bioactive glass (MBGMs) particles with a high surface area were used (Ostomel *et al.*, 2006; Shih *et al.*, 2006). The SEM images of the P(3HB)/n-BG composite microspheres revealed the presence of n-BG particles attached on the surface of the microspheres. In a similar study, Qiu *et al.*, also encapsulated modified bioactive glass (MBG) powders into polylactic acid (PLA) microspheres using a solid-oil-in-water (s/o/w) technique. The surface morphology of the composite microspheres when analysed using SEM revealed the presence of MBG on the polymeric matrix (Qiu *et*

*al.*, 2000). Thus apart from identifying the presence of n-BG particles on the surface of the microspheres, other characterization techniques such as FTIR and SEM/EDX analysis were employed to identify the presence of n-BG particles within the microspheres.

#### 5.3.1.2 FTIR analysis

After the fabricating the P(3HB)/n-BG composite microspheres, FTIR analysis was done to detect the presence of the n-BG particles in the composite microspheres. The characteristic peaks representative of P(3HB) and n-BG particles were detected in the FTIR spectra indicating the presence of n-BG particles in the P(3HB)/n-BG composite microspheres. In another relevant study Wang *et al.*, incorporated hydroxyapatite nanoparticles (HA) within poly(3-hydrobutyrate-co-hydroxyvalerte) P(3HB-co-3HV) microspheres encapsulating gentamicin. In order to detect the presence of HA particles within the P(3HB-co-3HV) microspheres and on the surface, the authors' used characterization techniques such as FTIR. The FTIR spectra revealed sharp peaks with wavenumbers at  $3570\text{ cm}^{-1}$  and  $630\text{ cm}^{-1}$  characteristic of the HA molecules (Wang *et al.*, 2007).

#### 5.3.1.3 Scanning electron microscopy /Energy dispersive X-Ray (SEM/EDX)

A cross-section of the P(3HB)/n-BG composite microspheres was analysed using SEM/EDX analysis to identify the presence of n-BG particles embedded within the microspheres. An elemental surface mapping of silica, calcium and phosphorous, the main components of n-BG in a fixed area on the cross-section of the P(3HB) microspheres, highlighted the presence of n-BG particles within the microspheres. This indicated that n-BG particles were successfully encapsulated within the P(3HB) microspheres during the microsphere preparation process. In another similar experiment Qiu *et al.*, examined the cross-section of polylactic acid/modified mesoporous Bioglass composites (PLA/MBG) using SEM/EDX analysis. The presence of typical elements of MBG such as silica, calcium and phosphorous were detected in the EDX analysis which confirmed the presence of MBG within the composite microspheres (Qiu *et al.*, 2000).

#### 5.3.1.4 Effect of n-BG particles on the thermal properties of the P(3HB) microsphere films

From the results of the thermal analysis it was observed that in the presence of n-BG particles, % crystallinity and the melting temperature of the P(3HB)/n-BG composite microsphere films were reduced when compared to the P(3HB) microsphere films. In the presence of n-BG particles, the crystallinity of the P(3HB)/n-BG composite films were reduced. The n-BG particles are known to hinder the growth of primary crystallites in P(3HB) due to which the crystallinity of the composite microspheres films are reduced. In this study the melting temperature of the P(3HB)/n-BG composite films reduced when compared to the P(3HB) films. The DSC thermograms of the P(3HB)/n-BG composite microsphere films in this study had also revealed the presence of a melting peak in the second heating run which was a significant observation. This indicated that the n-BG particles present in the P(3HB)/n-BG composite microsphere films did not retard the re-crystallization of P(3HB) during the cooling stage. Due to this, the presence of a crystallization peak in the P(3HB)/n-BG composite microsphere films was also observed. This observation was in agreement with the results obtained by Misra *et al.*, where, in the presence of n-BG particles in the (3HB)/n-BG composite solvent cast films, the heat of fusion, an indicator of crystallinity was reduced to 55 J/g when compared to the P(3HB) solvent cast films which was 73 J/g. Here the presence of n-BG particles was observed to hinder the growth of the crystallites in the polymer (Misra *et al.*, 2008). In the study conducted by Misra *et al.*, the increasing concentrations of microbioglass (m-BG) particles in the P(3HB)/m-BG composite films have been observed to prevent the re-crystallization of the polymer during the cooling stage. Due to this the prominent crystallization peak as well as a melting peak in the second heating run is not observed. However, the appearance of a small melting peak is also noticed when low concentrations of m-BG particles were used, indicating that the polymer was able to re-crystallize (Misra *et al.*, 2008). Thus from the above observation made by Misra *et al.*, it can be concluded that the concentration of the n-BG particles used in this study was probably relatively low and hence did not prohibit the recrystallization of the polymer due to which a melting peak in second heating run was observed. The DSC thermograms of the P(3HB) microsphere films exhibited prominent melting peaks both in the first and second

heating run. Misra *et al.*, also observed no changes in the melting peaks of the P(3HB) microsphere films both in the first and second heating runs (Misra *et al.* , 2008).

#### 5.3.1.5 Surface morphology and roughness of the P(3HB) and P(3HB)/n-BG composite microsphere films

The surface morphology of the P(3HB)/n-BG composite microsphere films when viewed under SEM revealed a fairly uniform surface morphology when compared to the P(3HB) microsphere films. However, when analysed for surface roughness using white light interferometry, the roughness of the P(3HB)/n-BG composite microsphere films was much higher than the P(3HB) microsphere films. A fairly homogenous distribution of surface roughness was observed for the P(3HB)/n-BG composite microsphere films. A possible reason for the increase in the surface roughness of the P(3HB)/n-BG composite microsphere films could also be due to the presence of n-BG agglomerations on the surface of the microspheres. After the fabrication of the P(3HB)/n-BG composite microspheres, some amount of n-BG particles that were not encapsulated within the microspheres could have possibly settled down on the fabricated microspheres. These n-BG particles would have then bound to the surface of the composite microspheres due to the physical interlocking. In another relevant study Misra *et al.*, examined the surface morphology of P(3HB)/n-BG composite solvent cast films using SEM. The presence of the n-BG particles had changed the surface morphology of the P(3HB)/n-BG composite solvent cast films inducing a rough topography to the films. The authors' had observed that despite sonicating the P(3HB)/n-BG mixture, the agglomerations of n-BG particles were evident. Thus a rapid solvent evaporation procedure was suggested (Misra *et al.*, 2009). For wound healing applications the presence of the n-BG particles on the surface would be advantageous as both biomineralization and blood clotting are surface-mediated phenomenon. Also, the presence of the n-BG particles on the surface of the microspheres would induce nanoscale topographies which can guide the cells required for wound healing.

### 5.3.1.6 Factors affecting the biocompatibility of the microsphere films

The water contact angle measurements (also an indication of surface wettability) was carried out to study the influence of the n-BG particles on surface wettability of the P(3HB)/n-BG composite microsphere films. From the results, the surface wettability of the films had increased in the P(3HB)/n-BG composite microsphere films when compared to the P(3HB) microsphere films. The presence of the n-BG particles on the surface had increased the hydrophilicity the P(3HB)/n-BG composite microsphere films due to which the water adsorption of the films had also increased (Misra *et al.*, 2008). In a similar observation made by Misra *et al.*, the presence of n-BG particles in the P(3HB)/n-BG composite microsphere films had improved the surface wettability of the films considerably due to its hydrophilicity (Misra *et al.*, 2008). The P(3HB) microsphere films on the other hand exhibited a higher water contact angle as compared to the P(3HB)/n-BG composite microsphere films, due to its lower water adsorption, further confirming the hydrophobic nature of the polymer. The water contact angle determined in this study for the P(3HB) films was however lower than the reported value of  $70 \pm 5^\circ$  (Wang *et al.*, 2006), here the presence of the hydrophilic PVA used to fabricate the microspheres would have made them relatively hydrophilic, hence influencing the surface wettability of the P(3HB) films.

The adsorption of proteins on the surface of biomaterials is important as this will permit the cells to attach, spread, proliferate and differentiate (Misra *et al.*, 2010). In the present study, the total serum protein adsorbed on the P(3HB)/n-BG composite microsphere films was significantly ( $n=3$ ,  $***p<0.001$ ) higher, when compared to the P(3HB) microsphere films before immersion in SBF. This difference was attributed to the effect of surface roughness on the P(3HB)/n-BG composite microsphere films caused by the presence of n-BG particles when compared to the P(3HB) microsphere films. This result was in agreement with the observation made by Misra *et al.*, where the total protein adsorption was significantly higher ( $171\mu\text{g}$ ) on P(3HB/n-BG) composite films when compared to the neat P(3HB) films. This difference in the protein adsorption was attributed to the marked differences in surface morphology and surface area available for protein adsorption (Misra *et al.*, 2008).

The presence of proteins on the surface of a biomaterial is also known to promote the subsequent adhesion of cells on the biomaterial surface (Ghannam *et al.*, 1999).

The % cell viability results in this study revealed a higher cell attachment on the P(3HB)/n-BG composite microsphere films when compared to the P(3HB) microsphere films. In this study, the presence of a nanotopography induced by the presence of n-BG particles as well as an increased protein adsorption had contributed to the higher cell attachment on the P(3HB)/n-BG microsphere films as compared to the P(3HB) microsphere films. Misra *et al.*, observed an increase of 65% in the proliferation rate of MG-63 osteoblast cell line when compared to the control (tissue culture plastic) (Misra *et al.*, 2008). The nanoprotusions formed on the P(3HB)/n-BG composite microsphere films in this study had also increased the surface area for cell-substratum contact and at this protrusion height, the focal adhesion was not perturbed, as they were also able to trap the proteins that were necessary to increase cell adhesion. This also establishes the fact that the height of the nanotopographical feature is very critical; as this determined whether the adherent cells were exclusively located on the apex of the nanotopographical feature or if they were able to establish contact with the basal substrate and the other cells (Biggs *et al.*, 2010). Thus the protein adsorption results along with the cell proliferation data indicated that the P(3HB)/n-BG composite microsphere films exhibited good biocompatibility. The P(3HB) microsphere films on the other hand exhibited a hydrophobic surface with reduced protein adsorption due to which the cell adhesion was lower. Generally the cells when added to a hydrophobic surface form few filaments due to which they do not adhere onto the surface, thus resulting in a loose attachment (Peschel *et al.*, 2007).

#### 5.3.1.7 Haemostatic activity

Apart from favouring the formation of silanol groups on the surface of Bioglass<sup>®</sup> and inducing the formation of hydroxyapatite, Ca<sup>2+</sup> ions are responsible for a cascade of reactions that lead to fibrin polymerization and clot stabilization (Hoffman *et al.*, 2003). Bioactive glasses are also known to be a rapid acting haemostatic agent as they release Ca<sup>2+</sup> ions upon hydration (Ostomel *et al.*, 2006). Therefore in order to investigate the haemostatic efficacy of n-BG particles and determine its suitability as a wound healing agent, a thromboelastograph test was done to measure the change in the viscoelasticity of blood during clot formation in the presence of the n-BG particles. From the results it was observed that the time for clot detection had decreased linearly with the increase in the concentration of n-BG particles. These results were similar to the observation made by Ostomel *et al.*, where a decrease in the clot detection time

had decreased linearly when the concentration of mesoporous bioactive glass (MBGM 80) was increased. In this study, the time for the clot formation, in the presence of n-BG particles, was much less when compared to those of the m-BG particles. The n-BG particles as mentioned earlier have a higher specific surface area of  $79 \text{ m}^2\text{g}^{-1}$  when compared to m-BG  $<1\text{m}^2\text{g}^{-1}$ . Hence, a reduced time for clot detection was observed in the presence of nBG.

### 5.3.2 P(3HB)/n-BG composite microsphere films immersed in SBF

A composite film containing bioactive glass is considered to be bioactive largely due to its ability to nucleate new layers of hydroxyapatite (HA) at the implant-tissue interface (Misra *et al.*, 2008). The presence of an apatite layer on a biomaterial is also known to induce nanotopography. In addition, the surface chemistry of the apatite layer immersed for different time periods is known to vary. These variations in the biomaterial surface properties are known to have a significant effect on protein adsorption and the subsequent cellular interactions. Therefore for this study, the P(3HB)/n-BG composite microsphere films were immersed in SBF for a period of 1, 3 and 7 days to induce the formation of an apatite layer. The *in vitro* bioactivity tests were performed in a simulated body fluid, SBF, which is known to have an ionic composition similar to that of blood plasma. This bioactive layer was characterized using a range of techniques such as FTIR, SEM/EDX and XRD analysis. Finally, the total protein adsorption on the surface of these composite films and the effect of this nanotopography on the keratinocyte attachment, morphology and proliferation was investigated. In another relevant study Ostomel *et al.*, immersed mesoporous bioactive glass microspheres (MBGMs) in SBF to monitor the formation of hydroxyapatite on the surface of the microspheres. Since Ca is an important parameter to accelerate coagulation response, the authors' wanted to determine the bioavailability of these Ca ions for coagulation (Ostomel *et al.*, 2006).

### 5.3.2.1 Surface morphology of the P(3HB)/n-BG composite microsphere films

As seen from the SEM images in Figure 13, the surface morphology of the P(3HB)/n-BG composite microsphere films before immersion in SBF was fairly uniform in appearance. The surface morphology of the films immersed in SBF for 1 day was also comparable to films before immersion. However the nucleation of hydroxyapatite from the n-BG particles was evident from the SEM micrographs of the films immersed for 3 and 7 days. The presence of spherical nodules scattered over the surface was observed on the films immersed for 3 days. However, a more or less homogenous layer of HA crystals were observed on day 7. In a study conducted by Misra *et al.*, the formation of scattered HA crystals were observed on the P(3HB)/n-BG composite films only after 5 days of immersion and a homogenous distribution of HA crystals were observed on the entire surface after 30 days of immersion in SBF. The formation of HA crystals is qualitatively proportional to the concentration of n-BG particles used to fabricate the films and its availability on the surface of the films. Therefore the formation of HA crystals was much earlier in this study, at 3 days when compared to 7 days as observed by Misra *et al.*, probably due to the presence of higher amount of n-BG particles on the surface (Misra *et al.*, 2008).

### 5.3.2.2 FTIR analysis

The P(3HB)/n-BG composite microsphere films after immersion in SBF for a period of 1, 3 and 7 days were characterized using FTIR to detect the presence of Ca and P formation on the surface. In the FTIR spectrum of the P(3HB)/n-BG composite microsphere films before soaking in SBF, the absorption bands of silica were observed. The P(3HB)/n-BG composite microsphere films after 1 day of immersion revealed the presence of two new absorption bands with wavenumbers at  $500\text{ cm}^{-1}$  and  $600\text{ cm}^{-1}$  corresponding to the formation of an amorphous calcium phosphate layer. The FTIR spectra of the P(3HB)/n-BG composite microsphere films after 3 and 7 days of immersion in SBF revealed bands that were analogous to that of apatite. The presence of absorption bands with wavenumbers at  $601\text{ cm}^{-1}$  and  $568\text{ cm}^{-1}$  further confirmed the formation of a crystalline calcium phosphate layer. When the biomaterial is immersed in SBF a sequence of reactions are involved in the formation of hydroxyapatite. Initially there is a rapid exchange of  $\text{Na}^+$  and  $\text{Ca}^+$  ions followed by an increase in the hydroxide ion concentration and the loss of soluble silica ( $\text{Si}^+$ ) due

to the formation of SiOH. The formation of a Si-O-Si group is observed after the condensation and repolymerisation of a SiO<sub>2</sub> rich layer. Finally, the absorption of Ca<sup>2+</sup> ions and PO<sub>4</sub><sup>2-</sup> takes place, leading to the formation of an amorphous calcium phosphate layer. This amorphous layer further undergoes crystallization leading to the formation of a hydroxyapatite layer. The results obtained in this study were also in agreement with the above observations where on day 1, two new absorption bands corresponding to the formation of an amorphous calcium phosphate layer was observed. With the increase in the immersion time the transformation of these bands to a crystalline HA layer was observed. These results were similar to the observations made Lu *et al.*, when 45S5Bioglass particles were immersed in an electrolyte solution for 1, 3 and 7 days and then analysed using FTIR. The presence of an amorphous calcium phosphate layer was observed on day 1 of immersion which was followed by the appearance of P-O bending vibration band between 500 cm<sup>-1</sup> and 600 cm<sup>-1</sup>, indicating the formation of an amorphous calcium phosphate layer. The crystallization of this Ca-P layer was observed on day 3 and day 7 when the P-O bending band became divided (Lu *et al.*, 2001).

#### 5.3.2.3 SEM/EDX and XRD analysis

SEM/EDX analysis of the P(3HB)/n-BG composite microsphere films immersed in SBF were carried out to highlight the transition of the bioactive glass particles to calcium phosphate layer. The results of the EDX analysis of this study revealed the presence of Ca and P deposits on the films on day 1. These surface deposits contained high concentrations of Ca and Si initially but were low in P concentrations. All the samples were initially high in Si concentrations but began to diminish after 3 days. Similarly an increase in the P concentrations were also observed with the increase in the immersion time. These results were also similar to observation made by Lu *et al.*, where the results of the EDX analysis revealed the presence of Ca, P and Si initially on day 1 of immersion followed by decrease in the Si concentrations and an increase in the P concentrations with prolonged immersion time (Lu *et al.*, 2001). The early levels of bioactivity although confirmed using FTIR and SEM/EDX analysis, the X-Ray diffraction studies were carried out to identify the presence of a prominent hydroxyapatite peak. The results of the XRD studies in this study, confirmed the presence of HA where the corresponding peaks at 2θ of 32° was found to increase

with the immersion time. Misra *et al.*, also observed an increase in the HA peaks at  $2\theta$  of  $32^\circ$  in the X-Ray diffractograms of P(3HB)/n-BG composite films with the increase in the immersion time (Misra *et al.*, 2008). Thus from the results of the characterizations (FTIR, SEM/EDX and FTIR) done in this study it can be concluded that the P(3HB)/n-BG composite microsphere films when immersed in SBF exhibited bioactivity. These immersion experiments in SBF showed that the n-BG particles had significantly enhanced the surface reactivity of the P(3HB)/n-BG composite microsphere films. The higher exposure of the n-BG particles on the film surface could have also contributed towards the bioactivity of the P(3HB)/n-BG composite microsphere films thus transforming the polymeric surface into a highly bioactive surface.

#### 5.3.2.4 Thermal properties

The thermal properties of the P(3HB)/n-BG microsphere films such as melting temperature and  $\%X_c$  after immersion in SBF for 1, 3 and 7 days did not exhibit significant changes when compared to the films before immersion. The thermal properties of a biomaterial are known to have an effect on the *in vitro* degradation rate. For example polymer films with a combination of high molecular weight, high crystallinity and relatively hydrophobic nature prevents any appreciable water uptake. However initial degradation in biomaterials which are not highly crystalline exhibit initial degradation in the amorphous regions followed by a second round of degradation through a chain scission in the crystalline domains, thus exhibiting an overall reduction in the crystallinity of the matrix with the increase in the water uptake. P(3HB)/n-BG films have been observed to exhibit a rapid increase in the water uptake (33%) within the first 10 days of immersion in SBF (Misra *et al.*, 2008), However in this study, the increased water uptake in the presence of the n-BG particles as well the formation of HA did not seem to have a significant effect on the thermal properties. Since the thermal properties were measured only for a period of 7 days, significant changes in the thermal properties would have probably occurred on prolonged immersion.

### 5.3.2.5 Surface roughness

The surface roughness of the P(3HB)/n-BG composite microspheres immersed in SBF for 1, 3 and 7 days were analysed using white light interferometry to study the changes induced in the roughness due to the formation of crystalline hydroxyapatite (HA). The surface roughness of the films on day 1 was comparable to the rms roughness values of the films before immersion in SBF. SEM images also verify this observation where fairly uniform and smooth surfaces were observed. However, films immersed in SBF for 3 and 7 days, revealed an increasing surface roughness when compared to the films before immersion. As observed from the SEM images, the presence of the spherical nodules on day 3 and a non-uniform layer of HA on day 7 had contributed to the changes in the surface roughness. The surface roughness maps along with the 2D plots of P(3HB)/n-BG composite microspheres films immersed in SBF for 3 days and 7 days did not reveal a homogenous roughness and there were some areas which exhibited higher relative roughness than the others. This non-homogenous surface roughness was again contributed by the lack of a uniform HA layer formed on day 3 and day 7. Similar results were observed in a study conducted previously, where the measured surface roughness values on day 7 for bioactive glass-ceramic tablets coated with microspheres after immersion in SBF was much higher as compared to just the bioactive glass-ceramic tablets. The growth of HA crystals upon immersion in SBF was known to be responsible for inducing changes in the surface roughness of the bioactive glass-ceramic tablets coated with microspheres (Francis *et al.*, 2010).

### 5.3.2.6 Surface wettability

Static contact angle measurements were done to study the effect of HA crystals on the surface wettability of the P(3HB)/n-BG microsphere films. The presence of the HA crystals on the surface of the P(3HB)/n-BG composite microsphere films led to a significant increase in the wettability of the composite films by lowering the water contact angle. The presence of the amorphous calcium phosphate deposition on day 1 and nanoscale sized HA crystals on day 3 and day 7 of the P(3HB)/n-BG composite microsphere films had improved the surface wettability of the films due to the increased hydrophilicity.

### 5.3.2.7 Protein adsorption

P(3HB)/n-BG composite microsphere films with enhanced surface roughness induced by the formation of HA were tested for their biocompatibility. Surface roughness is known to increase the potential surface area for cell attachment and biomaterial-cell interactions (Itala *et al.*, 2002). Thus for this study, the influence of HA formation on the total protein adsorption were investigated. From the results, the P(3HB)/n-BG composite microsphere films before immersion in SBF had exhibited the highest amount of protein adsorption as compared to the films after adsorption. The total protein adsorption on the P(3HB)/n-BG composite microsphere films after adsorption was recorded highest on day 1 and a small amount of protein adsorption was observed on day 7 and on day 3. This difference in the protein adsorption between the P(3HB)/n-BG composite microsphere films before and after immersion in SBF could be attributed to the surface charge, surface area, surface roughness and hydrophilicity variations induced by the formation of HA on the surface composite microsphere films. Bioactive glass surface is known to carry an intrinsically negative surface charge (Lu *et al.*, 2001). However, after immersion in SBF, the negative charge of the bioactive glass surface is neutralized by the adsorbed proteins (Lu *et al.*, 2001). On day 1 of immersion in SBF, the formation of an amorphous Ca-P layer is observed to induce a charge reversal from a negative to a positive surface charge (Lu *et al.*, 2001). However, when an amorphous Ca-P layer is converted to a crystalline Ca-P layer with a prolonged immersion in SBF (3 days and 7 days), a second charge reversal from a positive to negative charge between -13 mV to -16.30 mV is observed to occur. This second sign reversal from a positive to negative charge occurs due to the precipitation of phosphate ions from the solution (Lu *et al.*, 2001). The nature of the zeta-potential charge of a material surface affects both the amount as well as the orientation of the proteins adsorbed (Lu *et al.*, 2001). Thus based on these observations, on day 1 of immersion in SBF the amorphous calcium phosphate layer carries a positive surface charge of 7.47 mV, therefore negatively charged protein molecules such as albumin, fibronectin and vitronectin present in Dulbecco's Modified Eagle medium (DMEM) bound to the surface, hence a higher amount of protein adsorption was observed when compared to the P(3HB)/n-BG composite films immersed in SBF for 3 and 7 days. On day 3 of immersion in SBF, the crystalline HA layer exhibited a surface charge of -13mV, which was higher than the negative charge of the P(3HB)/n-BG composite

microsphere films before immersion, due to which less protein adsorption was observed. On day 7 of immersion in SBF, the films exhibited a higher negative surface charge of -16.30 mV when compared to the films on day 3. Nevertheless a small amount of protein adsorption was also observed. Ghannam *et al.*, also observed a significant decrease from 1000 $\mu$ g to 800 $\mu$ g in the serum protein adsorbed onto bioactive glass when the negativity of the material increased. The negatively charged serum proteins were inhibited from adsorbing onto the surface due to which a decrease in the protein adsorption was observed (Ghannam *et al.*, 1999). BSA carries a negative charge at neutral pH; however the net charges of three domains of BSA (I, II, III) are not uniformly distributed. For example the net charge of domain I and II are -16.8mV whereas the domain III carries a net charge of -1.3mV at pH 7. An imbalanced charge distribution is also observed where some amino acids are negatively charged at pH 7 and some amino acids are hydrophobic with no charge at any pH. As a result only 36% of the negatively charged groups of the BSA molecule are neutralised in an electrostatic interaction with a positively charged surface (Rezwan *et al.*, 2004). Therefore in this study other factors such as increased surface roughness and surface area would have contributed to the protein adsorption on the negatively charged surfaces, where an increasing surface roughness as well a higher surface area is known to affect the amount of proteins adsorbed on the scaffolds (Misra *et al.*, 2008).

#### 5.3.2.8 Cell adhesion

The presence of proteins on the surface of a biomaterial is known to promote the subsequent adhesion of cells on the biomaterial surface (Ghannam *et al.*, 1999). Similarly a rough surface of a biomaterial is also known to not only provide an optimal surface topography for cell attachment but it could also provide a larger surface area for biomaterial-cell interactions (Itala *et al.*, 2002). Thus in the present study, the effect of biomaterial surface properties and protein adsorption on the subsequent cellular attachments was evaluated. The biocompatibility of the P(3HB)/n-BG composite microsphere films after immersion in SBF was demonstrated using the HaCaT keratinocyte cell line, the cell proliferation rate was determined using Neutral Red assay and the cell attachment and distribution of HaCaT on the P(3HB)/n-BG composite microsphere films were examined through SEM. From the results obtained,

highest % cell viability was observed on the P(3HB)/n-BG composite microsphere films immersed in SBF for 1 day when compared to the % cell viability on the P(3HB)/n-BG composite microsphere films before immersion. The enhanced surface topography as well as an increased amount of protein adsorption might be one of the reasons why a significant increase in the % cell viability on the P(3HB)/n-BG composite microsphere films after immersion in SBF was observed. These results were similar to the observations made by Ghannam *et al.*, where the highest adhesion of osteoblast (MC3T3-E1) cells were observed on the bioactive glass surface covered both by a layer of amorphous Ca/P and adsorbed serum protein when compared to other surfaces such as (hydroxyapatite (HA) and bioactive glass (BG) with only protein and no amorphous Ca/P layer (Ghannam *et al.*, 1999). In this study the films immersed in SBF for 3 days and 7 days also exhibited a significant increase in the % cell viability when compared to the % cell viability observed on the P(3HB)/n-BG composite microsphere films before immersion in SBF. The enhanced surface roughness as well as available surface area may have contributed to an increase in the protein adsorption. In another relevant study Itala *et al.*, compared the osteoblast cell surface response on a microroughened bioactive glass surface with a surface roughness of  $0.35\mu\text{m}$  and  $0.52\mu\text{m}$  and a smooth surface with a surface roughness between  $0.1\mu\text{m}$  to  $0.15\mu\text{m}$ . The cell proliferation assay analysed using a non-radioactive cell proliferation assay and *in situ* staining and laser confocal microscopy revealed an enhanced cell attachment on the microrough surface when compared to the smooth surface (Itala *et al.*, 2002).

When the % cell viability of the P(3HB)/n-BG composite microsphere films after immersion in SBF were compared, the highest % cell viability were observed on the films immersed in SBF for 1 day when compared to the films immersed for 3 and 7 days. Although a small-scale surface roughness between 10 nm to  $10\mu\text{m}$  is known to influence biomaterial-cell interactions, an increase in the surface roughness beyond an optimum point is known to affect the cell interactions (Itala *et al.*, 2002). Thus the increased surface roughness of the films on day 3 and day 7 might have affected the % cell viability. The lesser amount of proteins adsorbed as well as the changes in the conformation of the adsorbed proteins on different surface roughness observed on the day 3 and day 7 films may have contributed to the lower cell adhesion when compared to the cell adhesion on day 1.

A qualitative analysis of cell adhesion and distribution on the P(3HB)/n-BG composite microsphere films were carried out using SEM. The SEM images of the cells attached on the films immersed in SBF on day 1 revealed a well-spread uniform surface morphology comparable to the cell attachment on the P(3HB)/n-BG microsphere films before immersion in SBF. The morphology of the cells attached on the P(3HB)/n-BG composite microsphere films immersed for 3 days and 7 days appeared raised due to the presence of HA crystals present beneath. The cells appeared to spread and form a non-uniform layer on the films. The surface irregularities of the films also seem to interfere with the cell attachment where a continuous uniform layer was not observed. Therefore, these results indicated that due to increased surface roughness or nanotopography, the cell attachment was affected due to which lower cell viability was recorded. Although nanoscale protrusions act as mediators for cellular adhesions, protein kinetics and cellular differentiation, an increase in the nanoprotrusion height such as 90 nm for some cells such as human bone marrow stromal cells is known to cause a reduction in cellular adhesion (Biggs *et al.*, 2010). The cytoskeletal organization and the filipodia formation initially increase in the presence of an increased nanoscale protrusion when compared to the cells on a flat substrate. However, this attachment phase does not last for long and the cells adhered on this protrusion undergo dedifferentiation or adhesion mediated apoptosis. Due to this a reduced cell adhesion or cell spreading is observed. Thus the results in this study were indicative of an increased nanoscaled protrusion (diameter and height) seen on the films immersed in SBF for 3 days and 7 days. Thus it can also be inferred that the nanoscaled feature of the films immersed in SBF for 1 day was probably less than 60-70 nm in pillar height, which facilitated integrin clustering, and focal adhesion formation due to which a higher cell adhesion and enhanced cellular spreading by providing tactile stimuli. Thus from these results of the cell viability tests, the P(3HB)/n-BG composite microsphere films immersed in SBF exhibited biocompatibility and no measureable toxicity towards the HaCaT keratinocyte cell line. However, this study also revealed that there is an optimal point for increased surface roughness beyond which a negative effect on the cell-biomaterial interaction would be observed. The influence of varying surface properties such as surface chemistry and surface charge on the biocompatibility of the P(3HB)/n-BG composite microsphere films were also highlighted.

## 5.4 Conclusions

In this chapter P(3HB)/n-BG composite microspheres were studied as potential wound healing patches. Detailed structural, thermal and biocompatibility studies were carried out. The nanoscaled bioactive glass with a high surface area was also tested for its *in vitro* haemostatic efficacy and was able to successfully reduce the clot detection time. This feature would add an additional desirable property to the wound healing patches.

The presence of n-BG particles in the P(3HB)/nBG composite microspheres films resulted in a uniform surface roughness on the P(3HB)/n-BG composite microsphere films which increased by 5% when compared to the P(3HB) microsphere films. Similarly, an increase of 6.5% was observed in the surface wettability of the P(3HB)/n-BG composite microsphere films when compared to the P(3HB) microsphere films. The presence of the n-BG particles on the surface had increased the hydrophilicity of the P(3HB)/n-BG composite microsphere films due to which the water adsorption of the films had also increased. The effects of nanotopography on the biocompatibility such as protein adsorption and HaCaT keratinocyte cell attachment were also highlighted. The total serum protein adsorbed and the cell proliferation rate on the P(3HB)/n-BG composite microsphere films was significantly ( $n=3$ ,  $***p<0.001$ ) higher, when compared to the P(3HB) microsphere films. This difference can most likely be attributed to the effect of surface roughness. The addition of the n-BG particles had also affected the thermal properties of the P(3HB)/n-BG composite microsphere films, where the heat of fusion was significantly ( $n=3$   $***p<0.001$ ) reduced when compared to the P(3HB) microsphere films. However, the presence of the n-BG particles had not completely prevented the re-crystallization of the polymer, as was evident by the presence of the melting peak in the second heating run.

For the second part of this study, the surface roughness of the P(3HB)/n-BG composite microsphere films were further enhanced by immersion in SBF for a period of 1, 3 and 7 days. The films were immersed in SBF, in an effort to study the effect of the roughness induced by the formation of HA on the cellular functions such as cell adhesion. From the SEM images the surface of the P(3HB)/n-BG composite microsphere films appeared fairly uniform and smooth on day 1, however on day 3 and day 7 a rough and uneven surface was observed. The presence of HA on the

P(3HB)/n-BG composite microsphere films on day 3 and day 7 had increased the surface roughness of the films. HA formation on the surface of the P(3HB)/n-BG composite microsphere films was confirmed using FT-IR, SEM/EDX and XRD analysis.

The presence of the amorphous calcium phosphate deposition on day 1 and nanoscale sized HA crystals on day 3 and day 7 of the P(3HB)/n-BG composite microsphere films had also improved the surface wettability of the films due to an increased hydrophilicity. The total protein adsorption on the P(3HB)/n-BG composite microsphere films after adsorption was recorded highest on day 1 and a small amount of protein adsorption was observed on day 3 and day 7. Similarly, the highest % cell viability was observed on the P(3HB)/n-BG composite microsphere films immersed in SBF for 1 day. The morphology of the cells attached on the P(3HB)/n-BG composite microsphere films after immersion in SBF for 1 day appeared well-spread with a flattened morphology. On the other hand, the cell morphology on the films immersed for day 3 and day 7 did not reveal a flattened morphology, the cells appeared raised due to the presence of the crystalline calcium-phosphate layer found beneath. Thus the rough surface morphology of the films on day 3 and day 7 appeared to interfere with cell adhesion where the cells appeared scattered without the formation of a continuous thick layer.

Thus from this study, the advantages of incorporating n-BG particles in the P(3HB) microsphere films were understood. The presence of n-BG in the P(3HB) microsphere films was able to induce a nanotopography, which in turn had an effect on the surface wettability of the films as well protein adsorption. The %cell viability was also significantly increased in the presence of the n-BG particles. However when the P(3HB)/n-BG composite microsphere with enhanced surface roughness were tested for biocompatibility, reduced amount of protein adsorption and cell adhesion were observed. This study further indicated that there is an optimal surface roughness for increased cell adhesion beyond which it would be deleterious for cell adhesion.

# Chapter 6

Tetracycline encapsulated poly(3-hydroxybutyrate) for wound healing

## 6.1 Introduction

The skin is the largest organ of the body which represents one-tenth of the body mass. It is composed of three layers, the epidermis, dermis and the hypodermis (Metcalf *et al.*, 2007). The main function of these layers is to protect the skin from any mechanical damage such as wounding. The epidermis, a thin and cellular layer is known primarily to provide vital barrier function and maintain homeostasis by constant recycling of the basal layer. The common cell type forming a barrier layer in the epidermis is the keratinocytes (Metcalf *et al.*, 2007). Since the skin contributes to the major part of the body, any damage due to injury, burns and disease can have a major consequence. Therefore, several tissue engineered skin substitutes are being designed to treat acute and chronic and skin wounds (Metcalf *et al.*, 2007). In tissue engineering, a biomaterial is designed that can be used to replace the damaged organ or tissue. However, for skin tissue regeneration or wound healing the biomaterial should possess the strength to promote the growth of skin cells such as keratinocytes, melanocytes and fibroblasts. They should be non-toxic, non-antigenic and facilitate angiogenesis while being incorporated with minimal scarring and pain. In addition to this, biomaterials are also required to act as an artificial extracellular matrix (ECM) for the cells to attach.

Apart from providing adequate mechanical stability and providing a desired cellular response, there is a growing need to functionalise these biodegradable polymeric scaffolds by adding either growth factors or drugs. Thus biodegradable scaffolds can be multi-facteted where, the improved surface characteristics can promote cell attachment, while acting as a drug delivery vehicle for a controlled release of drugs or growth factors. In the present chapter compressed P(3HB) microsphere films encapsulating tetracycline were developed for wound healing applications. Tetracycline is one of the most abundantly used drug, since it is a broad spectrum antibiotic. It is also known to exhibit anti-inflammatory action and the ability to promote fibroblast attachment (Domingues *et al.*, 2004).

In previous studies, films made of polysaccharides;  $\alpha$ -hydroxy acids and their copolymers have been used as dermal tissue patches. However, due to some disadvantages such as prolonged healing times and limited tissue functionality, alternative biodegradable polymers have been considered (Metcalf *et al.*, 2007).

Although polyhydroxyalkanoates (PHAs) have been used for a number of biomedical applications, polymers such as P(3HB), P(3HB-co-HV) and P(3HB-co-3HHx) have not yet been fully investigated for skin tissue engineering due to their crystallinity and poor flexibility, which have been considered limiting (Peschel *et al.*, 2008; Luo *et al.*, 2009). Nevertheless, P(3HB-co-4HB-co-3HHx) films were made in an attempt to improve the mechanical and biocompatible properties of the films for use as an implant for wound healing applications. L929 mouse fibroblasts and human keratinocytes, (HaCaT) cells were seeded on these films to test their biocompatibility in comparison to films made of poly(lactic acid)(PLA), P(3HB-co-3HHx) films and polylysine-coated plates used as a control (Liu *et al.*, 2008). From the SEM images a well spread cell shape with large number of pseudopods indicating strong cell-to-cell and cell to material interactions were identified. Thus from this study it was proven that films made of P(3HB-co-4HB-co-3HHx) exhibited favourable biocompatible and biodegradable properties when compared to poly(lactic acid)(PLA) and P(3HB-co-3HHx) films (Liu *et al.*, 2008). Other novel terpolyesters of poly(3-hydroxybutyrate-co-3-hydroxyvalerate-co- hydroxyhexanoate),(P(3HB-co-3HV-co-3HHx), produced from recombinant microorganisms were made into films and tested for their mechanical and biocompatible properties for possible use in skin tissue engineering (Ji *et al.*, 2008). These films exhibited the flexibility that was required for skin tissue engineering. Similarly, P(3HB-co-3HV-co-3HHx) films seeded with HaCaT cells exhibited the highest cell density and viability when compared to films made of other polyhydroxyalkanoates such as P(3HB), P(3HB-co-3HV), P(3HB-co-4HB), P(3HB-co-3HHx) (Ji *et al.*, 2008).

For research related to skin graft or wound healing one of the most commonly used cell types is the HaCaT cell line. These cell lines were isolated from the periphery of a melanoma of human adult skin (Metcalf *et al.*, 2007). These differentiated keratinocytes appear to be similar to normal human keratinocytes. When the skin is subjected to injury, the keratinocytes present near the wound site respond to the biochemical signalling by migrating and adhering to the site. The adherence of the cells is mediated by integrins. These integrins have receptor sites, which exhibit domains for the specific proteins in the extracellular matrix (ECM) to bind (Wozniak *et al.*, 2004). After adhering, the cells aggregate to form clusters or focal adhesion (FA) sites/complexes. Following this, a series of multiple signalling complexes are

formed which initiate the re-epithelisation of a wound site (Miyamoto *et al.*, 1995; Wozniak *et al.*, 2004). The adherence of keratinocytes onto PHAs depends on a number of factors such as the adsorption of proteins on the surface the surface chemistry which influences the hydrophobicity or hydrophilicity, surface energy and the pH (Nebe *et al.*, 2002, Patil *et al.*, 2007). The extent and quality of protein adsorption on the biomaterial/scaffold is dependent on the nano/microstructural morphology and on the wettability of the films. Wang *et al.*, have demonstrated the preference of different cell lines on various surfaces and observed that with the changes in the topography and roughness of the surfaces, the protein conformation also changes. Due to this, the ligand binding for specific cells is affected (Wang *et al.*, 2007). Misra *et al.*, 2009 incorporated vitamin E in P(3HB) films and studied the effect of vitamin E incorporation on the hydrophilicity and total protein adsorption on the films. The incorporation of vitamin E introduced some nano/microstructural changes on the surface, which, in addition to increasing the hydrophilicity of the surface, also increased the protein adsorption (Misra *et al.*, 2009).

This chapter describes work related to the combined applications of PHAs for scaffolds and drug delivery. The chosen drug for this work was tetracycline. Tetracycline were encapsulated in P(3HB) microspheres which was then compressed to form films. The effect of tetracycline addition on the surface roughness, wettability, thermal and crystalline properties of P(3HB) microsphere films were studied in detail.

## 6.2 Results

### 6.2.1 Tetracycline loaded P(3HB) microsphere films characterizations

#### 6.2.1.1 Surface morphology of the P(3HB) microsphere films

SEM images of the surface of the tetracycline loaded and unloaded P(3HB) microsphere films are shown in Figures 1 and 2. The surface of the unloaded P(3HB) microsphere films appear fairly uniform and smooth as seen in Figure 1A when compared to the tetracycline loaded films which were rough and uneven in appearance. The films with the highest drug loading of 4wt% appeared increasingly uneven and rough as seen in Figure 2 A3 when compared to the films with lower amount of the drug (0.5 wt% and 2 wt%) as seen in Figure 1 A1 and Figure 2 A2. The former also had an increased number of pores on the surface. Although the microspheres on the surface of the tetracycline loaded and unloaded films lost their identity when compressed into discs as seen in Figures 1B, 1B1, 2B2 and 2B3, the microspheres within the disc remained unaffected by the pressure applied and retained their shape, as seen in the cross-section images seen in Figures 1C, 1C1, 2C2 and 2C3.

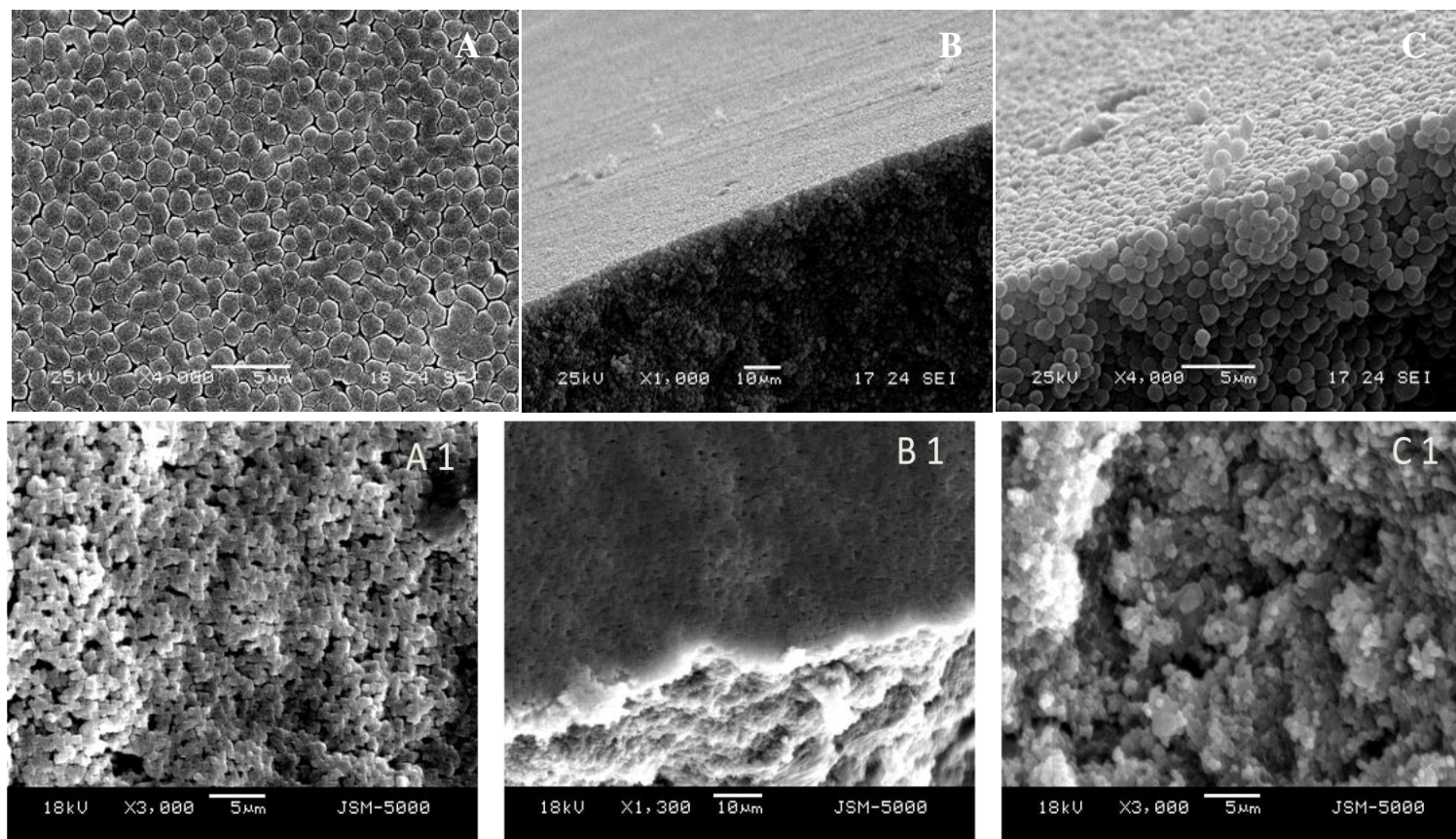


**Figure 1:- Scanning electron micrographs of the surface of the P(3HB) microsphere films A) unloaded/blank P(3HB) microsphere films A1) P(3HB) microsphere films loaded with 0.5 wt% of tetracycline, B) Cross-section view of unloaded P(3HB) microsphere films, B1) cross-section view of 0.5 wt% tetracycline loaded microsphere films and Side view of the C) unloaded P(3HB) microsphere films and C1) 0.5 wt% tetracycline loaded microsphere films.**

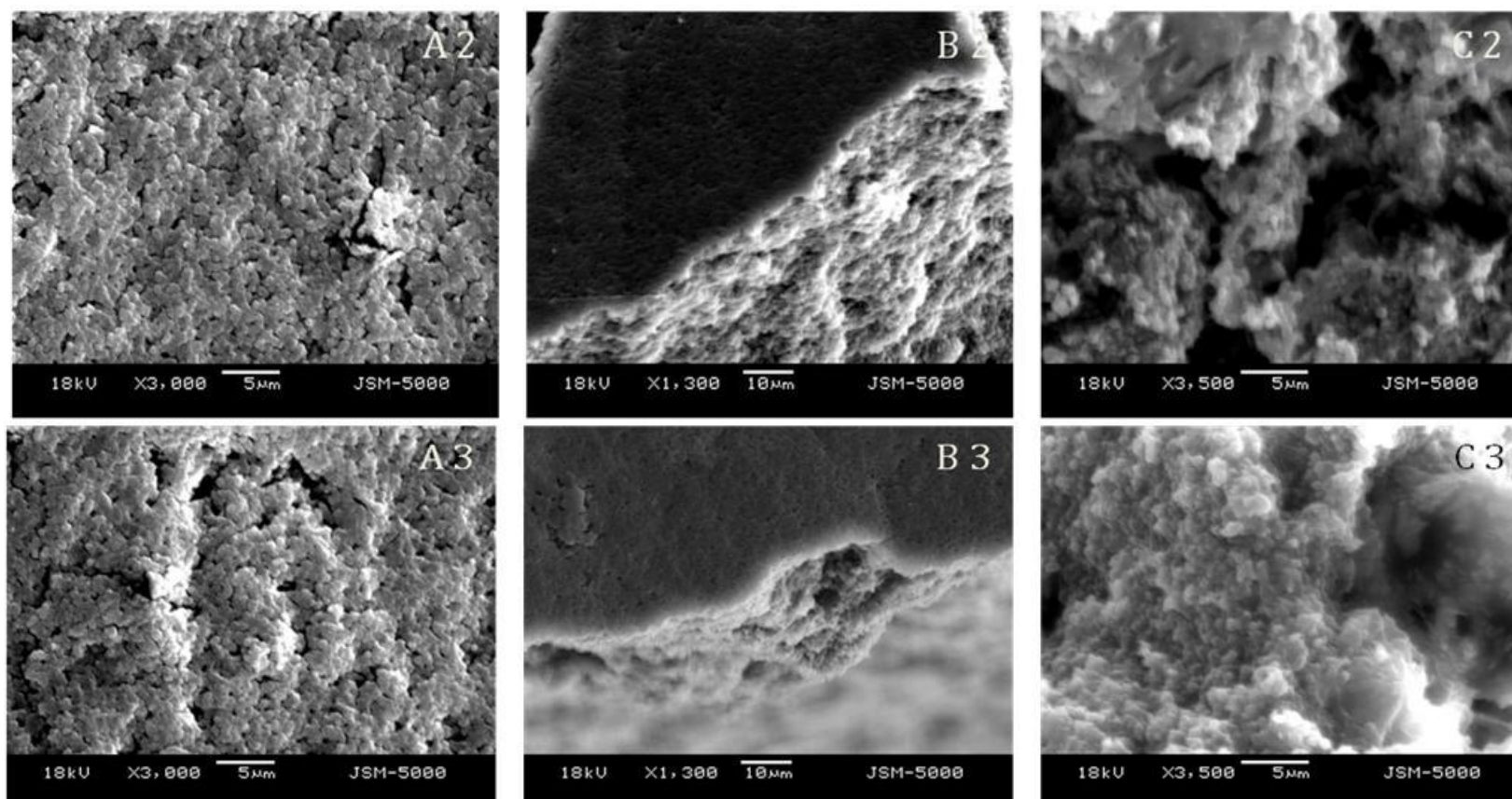


Figure 2:- Scanning electron micrographs of the surface of the P(3HB) microsphere films with tetracycline loadings of A2) 2 wt%, A3) 4 wt%. Cross-section view P(3HB) microsphere films with tetracycline loadings of B2) 2 wt%, B3) 4 wt% and Side view of the P(3HB) microsphere films with tetracycline loadings of C2) 2wt% and C3) 4wt%.

## 6.2.1.2 XPS evaluation

The surface chemistry of the microspheres was analysed using XPS, enabling the examination of carbon, nitrogen and oxygen content using a soft X-Ray excitation, as shown in Figure 3 A, B, C. Since nitrogen species is unique to the drug and absent in the P(3HB) microspheres it was used to estimate the amount of drug entrapped during the microsphere fabrication procedure. The surface chemical composition of the tested samples listed in Table 1 showed an increase in the nitrogen content with the increase in the tetracycline loading ratio. The binding energy of nitrogen (N) was 399.5eV which corresponds to the single bonded nitrogen. The binding energy of the tetracycline loaded microspheres was found to be 402.2 eV, quite close to the value for singly bonded nitrogen.

**Table 1: XPS data for the P(3HB) microspheres loaded with different amounts of tetracycline 0.5 wt%, 2wt% and 4wt%. The relative mass percentages of each compound are presented (n=3).**

Tetracycline loaded P(3HB) microsphere films	% Carbon	% Oxygen	% Nitrogen
0.5 wt%	70.69	26.76	2.56
2 wt%	71.53	25.46	2.60
4 wt%	72.36	23.39	4.08

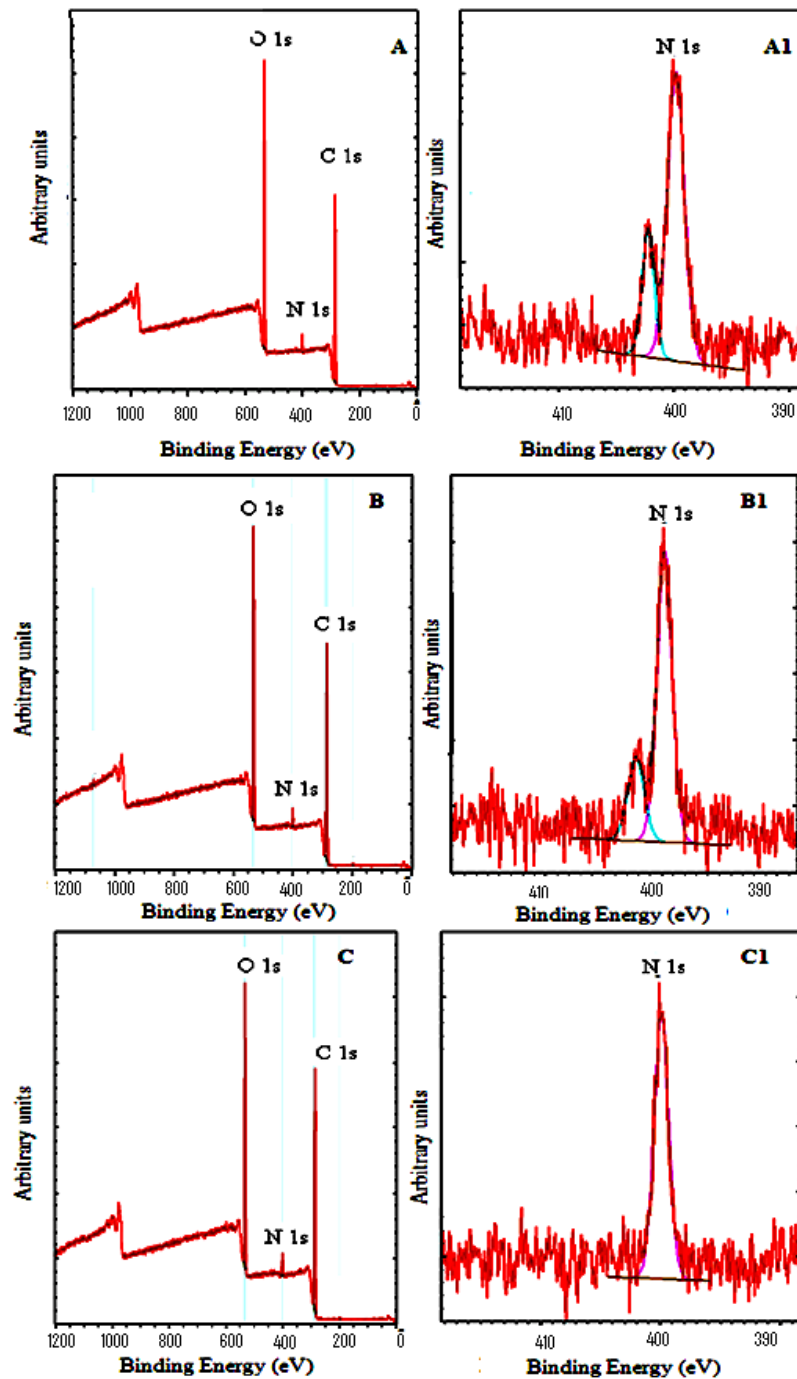


**Figure 3:-** The surface chemistry of the microspheres was analysed using XPS as nitrogen species is unique to the drug and absent in the P(3HB) microspheres A) Nitrogen (N1s) XPS spectra of P(3HB) microsphere film B) The nitrogen peak with a binding energy of 402.2 eV with a tetracycline loading of 0.5 wt%. B) Nitrogen (N1s) XPS spectra of P(3HB) microsphere film with a tetracycline loading of 2wt% B1) The nitrogen peak with a binding energy of 402.2 eV. C) Nitrogen (N1s) XPS spectra of P(3HB) microsphere film with a tetracycline loading of 4wt% C1) The nitrogen peak with a binding energy of 402.2 eV.

## 6.2.1.3 Surface topography studies

In order to study the effect of tetracycline loading on the compressed P(3HB) microsphere film surface roughness, white light interferometry was used as shown in Figure 4. A comparison of the surface roughness quantified as rms of roughness (for the unloaded and loaded P(3HB) microsphere films represented in Figure 4 revealed that the maximum surface roughness was exhibited by the surface of the P(3HB) microsphere films with the highest drug loading.

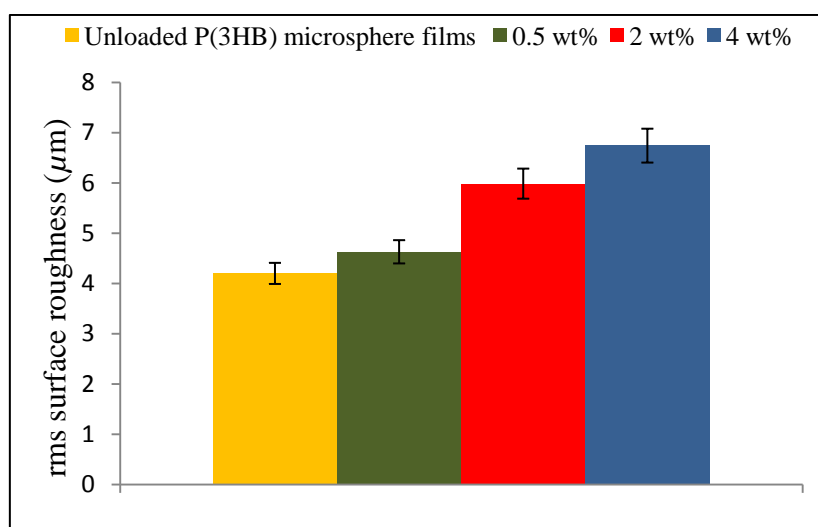


**Figure 4:-** A comparison of the surface roughness quantified as root mean square of roughness (rms), for the unloaded and loaded microsphere films, data ( $n=3$ ; error= $\pm$ s.d). The tetracycline loaded P(3HB) microsphere films had a significant ( $***p<0.0001$ ) effect on the surface roughness. Since the data compared using ANOVA was significant, a Bonferroni Post Hoc test was applied and significantly greater effect at  $***p<0.0001$  on the surface roughness for 4wt% tetracycline loaded P(3HB) microsphere films were observed when compared to the control and other tetracycline loaded films.

The rms roughness value of the unloaded P(3HB) microsphere film of  $4.2\mu\text{m}$  (Figure 5A) was slightly lower than the film with a drug loading of 0.5 wt% as seen in Figure 5B, thus indicating no significant difference in the surface roughness in the presence of the lower amount of drug. However, significant increases ( $n=3$ ,  $***p<0.001$ ), in the rms roughness values were observed when the drug loading in the films were increased. The P(3HB) microsphere films with 2 wt% of the drug had a rms roughness value of  $5.98\mu\text{m}$ , Figure 5C and films with 4 wt% had a rms roughness value of  $6.74\mu\text{m}$  ( $n=3$ ,  $***p<0.001$ ), Figure 5D, thus indicating a higher surface roughness with an increase in the drug loading.

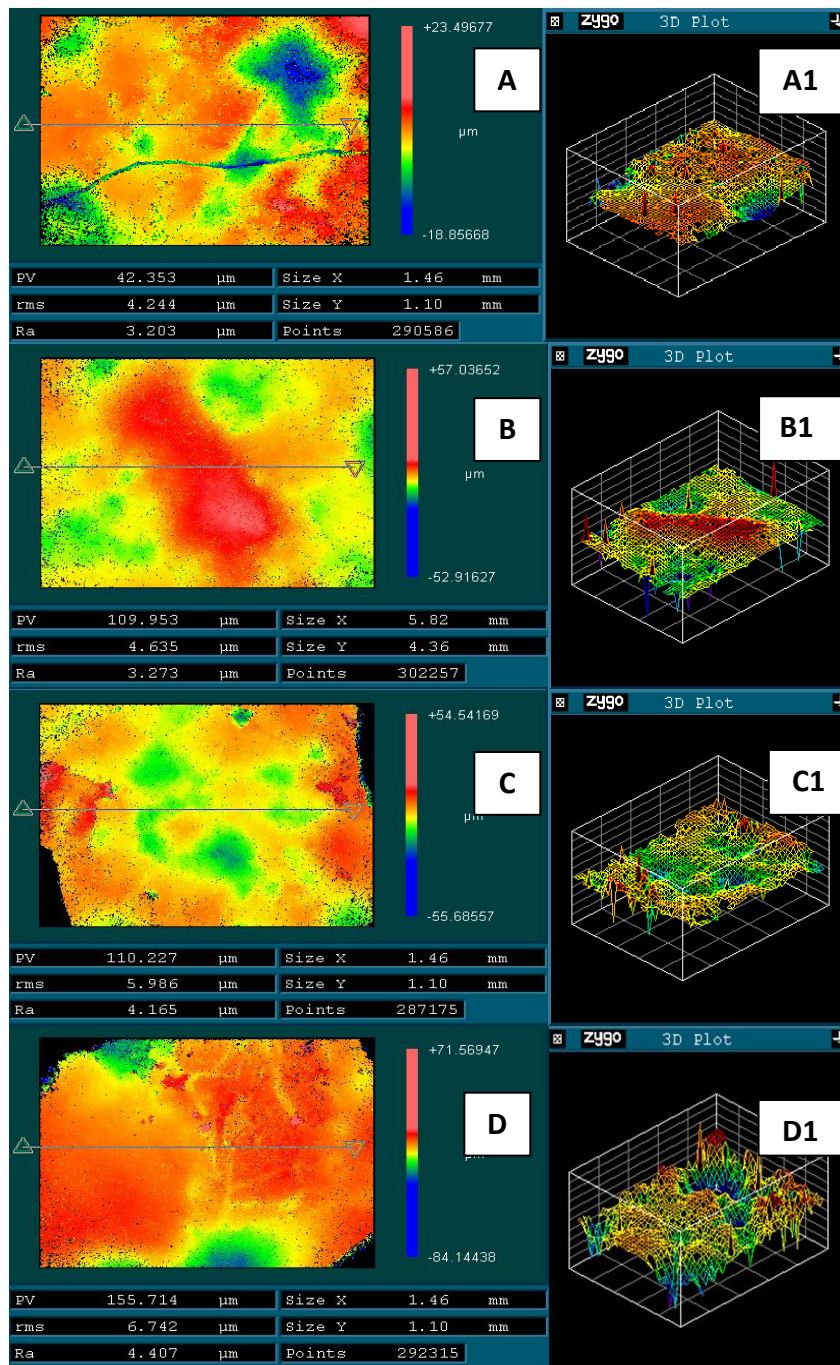


**Figure 5:** The 2D and 3D plots of the P(3HB) microsphere film surfaces (with and without the drug) as determined by white light interferometry. 2D plot (A) and 3D plot (A1) of the unloaded P(3HB) microsphere films. 2D plot (B) and 3D plot (B1) of the P(3HB) microsphere films with 0.5 wt% of tetracycline loading. 2D plot (C) and 3D plot (C1) of the P(3HB) microsphere films with 2 wt% of tetracycline loading. 2D plot (D) and 3D plot (D1) of the P(3HB) microsphere films with 4 wt% of tetracycline loading, ( $n=3$ ; error= $\pm$ s.d).

#### 6.2.1.4 Fourier Transform Infrared studies (FTIR)

FTIR spectra of the unloaded P(3HB) microsphere films and tetracycline loaded P(3HB) microsphere films with different tetracycline loadings were carried out to identify any possible chemical drug-polymer interaction. The FTIR spectra of the tetracycline loaded P(3HB) microspheres as shown in Figure 6 revealed absorption bands with characteristic wavenumbers at  $980\text{ cm}^{-1}$ ,  $1230\text{ cm}^{-1}$ ,  $1282\text{ cm}^{-1}$  and  $1782\text{ cm}^{-1}$  due to the crystalline phase of P(3HB) and wavenumbers at  $1184\text{ cm}^{-1}$  and  $1741\text{ cm}^{-1}$  due to the amorphous phase of P(3HB). The stretching vibrations of the amorphous and crystalline carbonyl groups are seen at  $1741\text{ cm}^{-1}$  and  $1728\text{ cm}^{-1}$  respectively (Vallapil *et al.*, 2007; Shih *et al.*, 2006). The characteristic peaks for the tetracycline hydrochloride is seen between the wavenumbers  $1200\text{ cm}^{-1}$  and  $1800\text{ cm}^{-1}$  as shown in Figure 6A. The carbonyl and amino groups of the amide group in ring A are assigned at wavenumbers  $1673\text{ cm}^{-1}$  and  $1537\text{ cm}^{-1}$  and the carbonyl groups were assigned to the wavenumbers at  $1619\text{ cm}^{-1}$  and  $1586\text{ cm}^{-1}$  (Gu *et al.*, 2005). The tetracycline loaded P(3HB) microsphere films with different drug loadings showed no additional chemical shifts in the FTIR spectra.

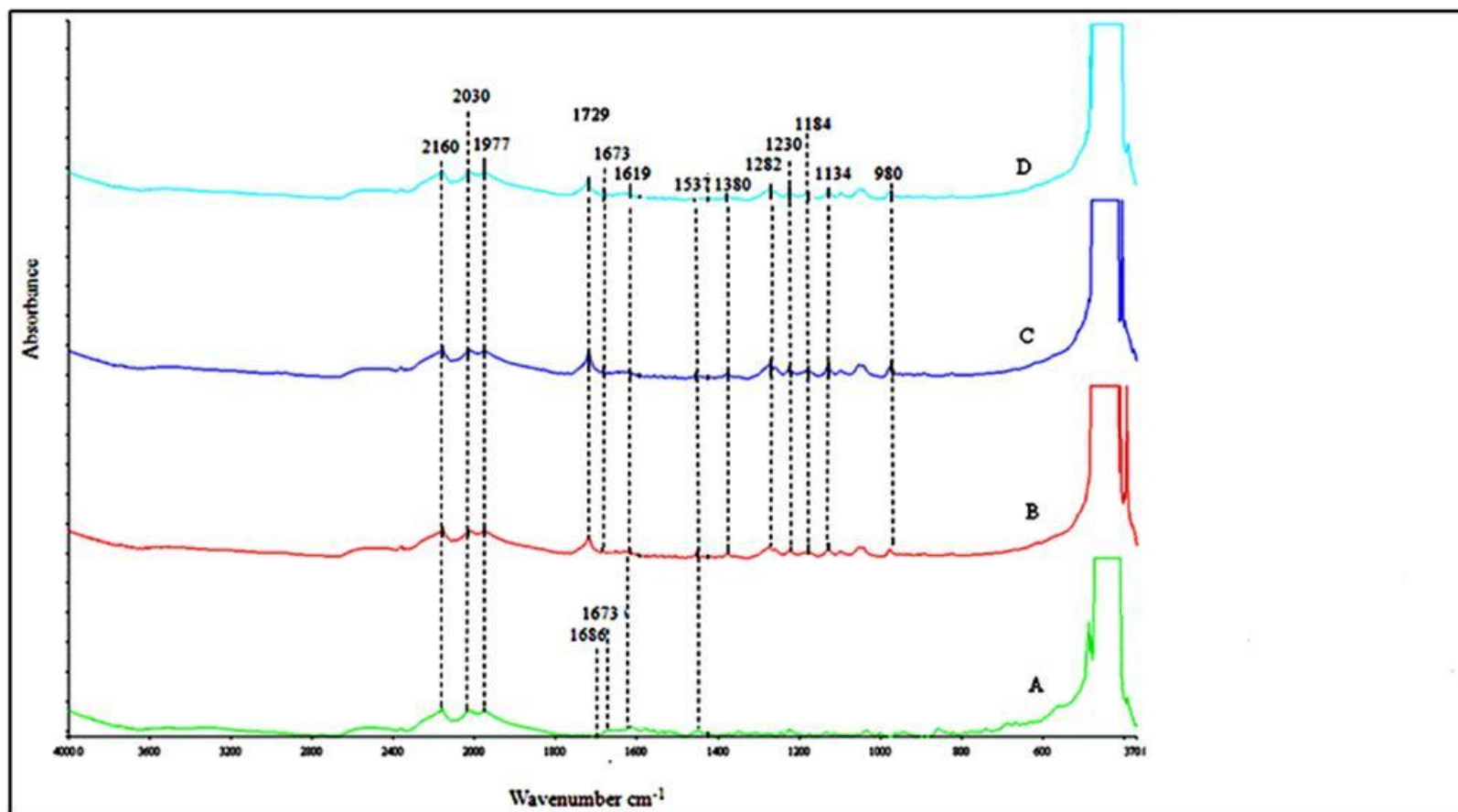


Figure 6:- FTIR spectrum of the P(3HB) microspheres films (with and without tetracycline). (A) Tetracycline, P(3HB) microspheres films loaded with 0.5wt% (B), 2 wt% (C) and 4wt% (D)

#### 6.2.1.5 X-Ray diffraction analysis (XRD)

X-ray diffraction analysis was carried out to evaluate the effect of tetracycline on the crystallinity of P(3HB). The X-ray diffraction pattern of tetracycline hydrochloride could be observed at diffraction angles of  $2\theta$  with characteristic peaks at  $11.2^\circ$ ,  $13.88^\circ$ ,  $16.04^\circ$ ,  $20^\circ$ ,  $24.48^\circ$  and  $28.76^\circ$ , as seen in Figure 7A. The X-ray diffraction peaks obtained for P(3HB) at  $2\theta$  were  $13.48^\circ$ ,  $16.88^\circ$ ,  $21.72^\circ$ ,  $22.64^\circ$  and  $25.64^\circ$  as shown in Figure 7E, which are comparable to those, observed in literature (Bidone *et al.*, 2009), thus reflecting its semi-crystalline nature. The X-ray diffraction patterns of the P(3HB) microspheres loaded with tetracycline such as 0.5 wt%; 2wt%; 4wt% are represented in the diffractograms 7C, D and E. The intensity of the X-ray diffraction peaks of the tetracycline loaded P(3HB) microsphere films with different drug loading ratios were not significantly changed in comparison to the unloaded P(3HB) microspheres.

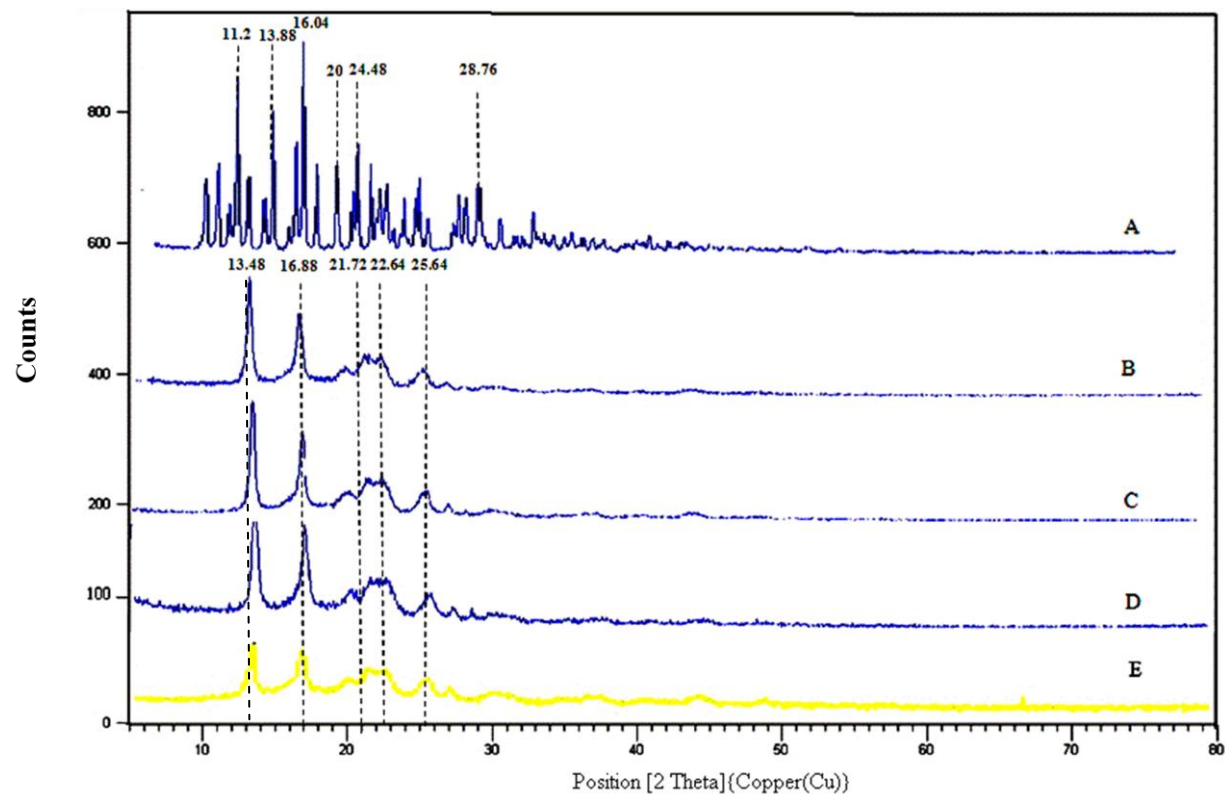


Figure 7:- X-Ray diffractograms of the P(3HB) microsphere films (with and without the drug). X-Ray diffractogram of A) Tetracycline. B) Unloaded P(3HB) microsphere films and P(3HB) microsphere films loaded C) with 0.5 wt% of tetracycline, D) with 2 wt% of tetracycline and E) with 4 wt% of tetracycline.

## 6.2.1.6 Thermal analysis

Differential scanning calorimetry (DSC) was used to determine the changes in the thermal behaviour of the P(3HB) microspheres during solvent evaporation, as well as to determine the possible interaction between the drug and the polymer (Figure 8). The  $T_m$  of the unloaded P(3HB) microspheres and the drug loaded P(3HB) microspheres were lower than that of the crude polymer. A decrease in the degree of crystallinity ( $\%X_c$ ) of the P(3HB) loaded microspheres with 0.5wt%, 2wt% and 4wt% of tetracycline was observed when compared to the crude and unloaded P(3HB) microspheres (Figure 8). However, the glass transition temperature ( $T_g$ ) of the tetracycline loaded P(3HB) microspheres were higher than that of the crude polymer and the unloaded P(3HB) microspheres, where the highest  $T_g$  value was exhibited by the microspheres with highest tetracycline loading (Figure 9).

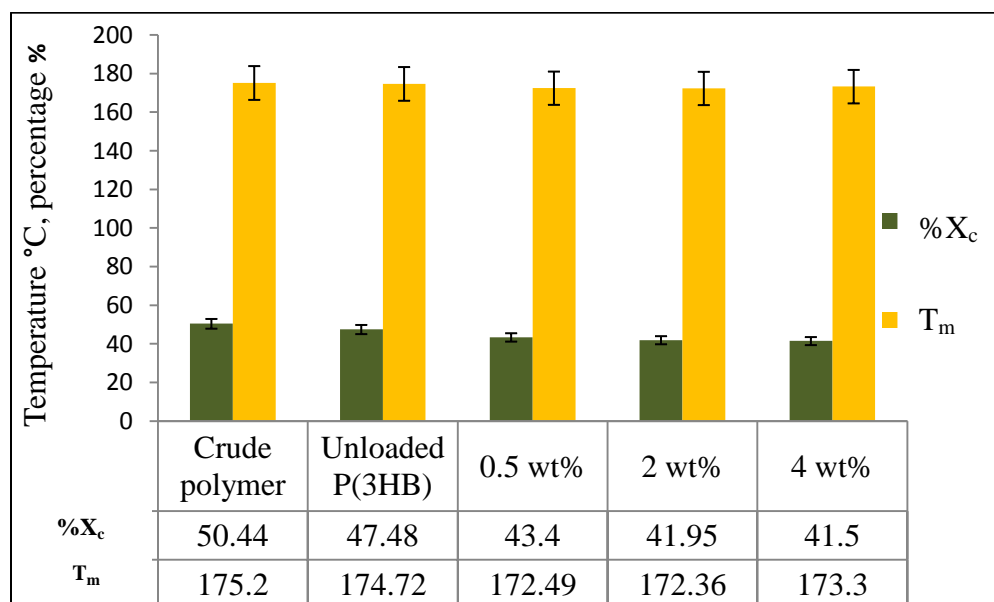
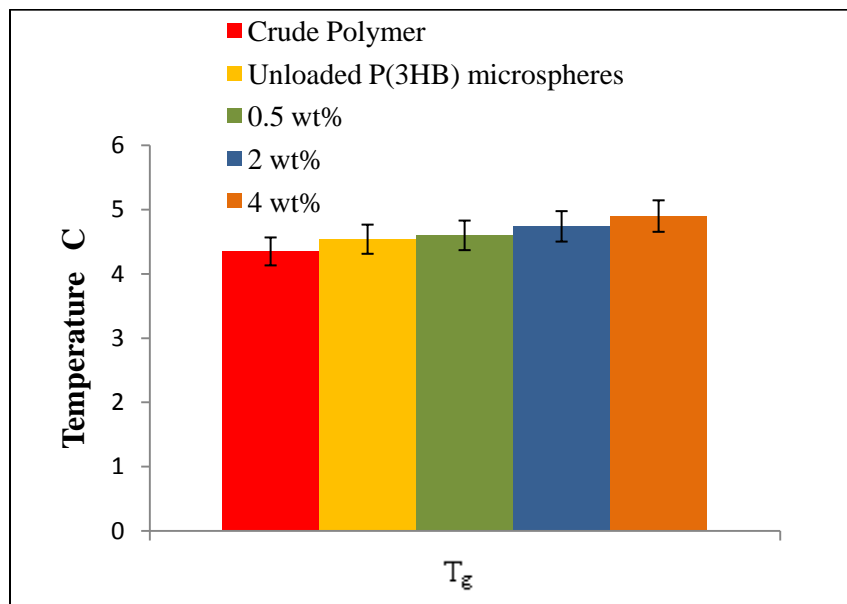


Figure 8:- A comparison of the  $\%X_c$  and  $T_m$  of the crude polymer and the P(3HB) microspheres (with and without the drug), data ( $n=3$ ; error= $\pm$ s.d). The tetracycline loaded P(3HB) microsphere films had a significant ( $*** p<0.0001$ ) effect on the  $\%X_c$ . Since the data compared using ANOVA was significant, a Bonferroni Post Hoc test was applied and significantly greater effect at  $***p<0.0001$  on the  $\%X_c$  values for 4wt% tetracycline loaded P(3HB) microsphere films were observed when compared to the control and 0.5 wt% tetracycline loaded films. No significant differences ( $p>1.0$ ) were observed in the  $T_m$  values of the tetracycline loaded P(3HB) microsphere films when compared to the control.



**Figure 9:-** A comparison of the  $T_g$  values of the crude polymer and the P(3HB) microspheres (with and without the drug), ( $n=3$ ; error= $\pm$ s.d). The tetracycline loaded P(3HB) microsphere films had a significant ( $***p<0.0001$ ) effect on  $T_g$ . Since the data compared using ANOVA was significant, a Bonferroni Post Hoc test was applied and significantly greater effect at  $***p<0.0001$  on the  $T_g$  values for 4wt% tetracycline loaded P(3HB) microsphere films were observed when compared to the control and other tetracycline loaded films.

### 6.2.2 *In vitro* degradation studies of the tetracycline loaded P(3HB) microsphere films

The water uptake (WA) and weight loss (WL) study for the tetracycline loaded microsphere films with different drug loadings such as 0.5 wt%, 2wt%, 4wt%, were conducted using immersion tests in 0.1M phosphate buffered saline solution (PBS) for a period of 30 days. The results from the *in vitro* degradation studies are depicted in Figure 10.

The unloaded P(3HB) microsphere films exhibited a %WA of 180% to 250% over a period of 30 days. The %WL was 5% to 8% over a period of 30 days.

Tetracycline loaded P(3HB) films with 0.5 wt% of the drug showed an increase in the %WA from 237% to 300% from day 1 to day 30, where insignificant differences ( $n=3$ ,

$p>0.5$ ) were observed on day 1 when compared to the %WA of the unloaded P(3HB) microsphere films but significant changes ( $n=3$ ,  $***p<0.001$ ) in the %WA were observed from 15 days to 30 days when compared to the unloaded P(3HB) microsphere films. The %WL was 12% over a period of 30 days. This change in the %WL was significant ( $n=3$ ,  $**p<0.01$ ) when compared to the unloaded P(3HB) microspheres films which exhibited a %WL of 8% over a period of 30 days. No significant differences ( $n=3$ ,  $p>0.2$ ) in the %WL were observed from day 1 to day 15 when compared to the unloaded P(3HB) microsphere films.

Films with 2 wt% of tetracycline also showed no significant increase ( $n=3$ ,  $p>0.2$ ) in the %WA on day 1 when compared to the unloaded P(3HB) microsphere films. However with an increase in the immersion time from day 15 day 30, a significant ( $n=3$ ,  $***p<0.001$ ) increase in the %WA of 388% (a 25% increase) was observed when compared to the %WA of the unloaded P(3HB) microsphere films. The P(3HB) microsphere films with 2wt% of tetracycline exhibited a significant( $n=3$ ,  $***p<0.001$ ) in %WL of 9% to 33% when compared to the unloaded P(3HB) microsphere films which was 5% to 8% over a period of 30 days.

Finally, the %WA for the tetracycline loaded films with the highest drug loading of 4 wt% was 488% over a period of 30 days which was higher than that of the other tetracycline loaded films. When compared to the %WA of the unloaded P(3HB) microsphere films, a significant ( $n=3$ ,  $***p<0.001$ ) increase of 49% was observed. As expected, the highest %WL from day 1 to day 30, of 13% to 35%, was exhibited by these microsphere films when compared to the unloaded P(3HB) microsphere films ( $n=3$ ,  $***p<0.001$ ).

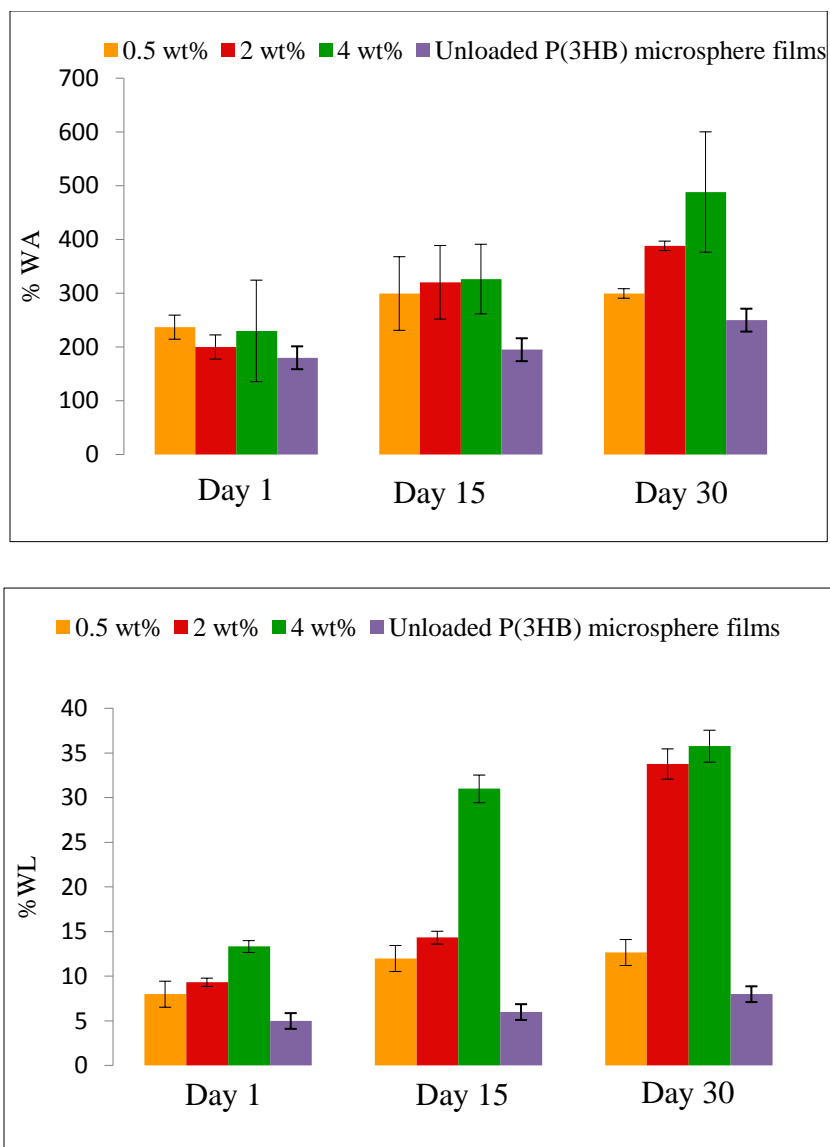


**Figure 10:** - *In vitro* degradation study of the P(3HB) microsphere films (with and without tetracycline) in phosphate buffered saline solution (PBS). The tetracycline loaded P(3HB) microsphere films had a significant ( $*** p < 0.0001$ ) effect on A) % water absorption (WA) and B) % weight loss (WL). A Bonferroni Post Hoc was applied and significant differences at  $*** p < 0.0001$  for 2wt% and 4wt% tetracycline loaded P(3HB) microsphere films were observed when compared to the control and 0.5wt% tetracycline loaded P(3HB) microsphere films on day 15 and day 30. No significant ( $p > 2.0$ ) differences in the %WA and %WL of the tetracycline loaded P(3HB) microspheres films on day 1 when compared to the control.

A gradual change in the pH of PBS (7.4) with the increase in the immersion time of the unloaded and tetracycline loaded P(3HB) microsphere films were also observed, as shown in Figure 11. The pH of the unloaded P(3HB) microsphere films changed from 7.25 to 7.24 over a period of 30 days. The pH of the media with 0.5 wt% tetracycline loaded films remained also from 7.24 to 7.23 over a period of 30 days. The pH of the media with the 2 wt% tetracycline loaded P(3HB) microsphere films changed from 7.24 to 7.22 over a period of 30 days but no significant changes were observed when compared to the pH of the unloaded P(3HB) microsphere films. However a significant ( $n=3$ ,  $***p<0.0001$ ) and ( $n=3$ ,  $**p<0.001$ ) pH change from 7.24 to 7.19, occurred from day 15 to day 30 in media with the films loaded with the highest drug loading 4 wt% tetracycline when compared to the control and other tetracycline loaded microsphere films as seen in Figure 11.

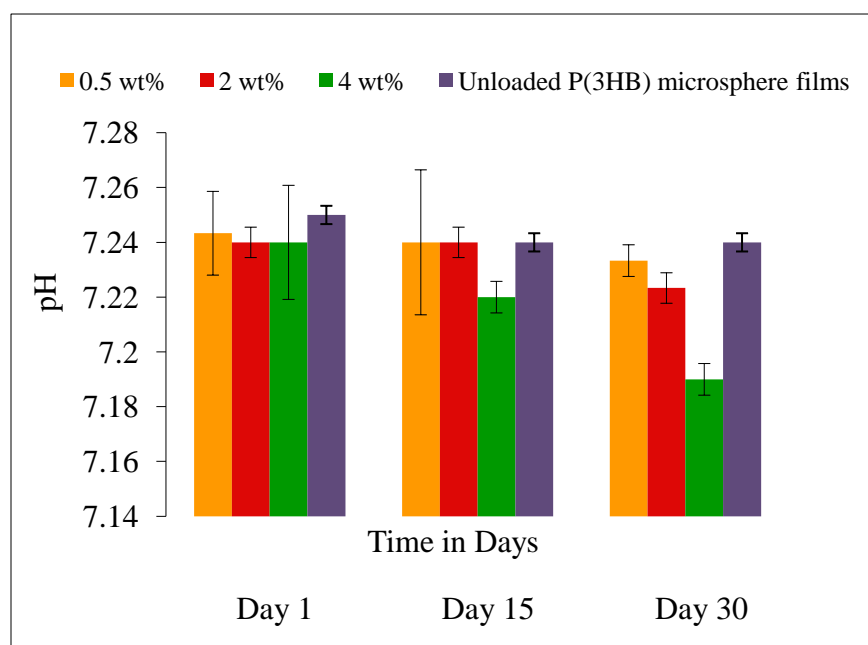


**Figure 11:-** Changes in the pH of the 0.1 M PBS solution over a period of 30 days in the presence of the tetracycline loaded P(3HB) microspheres films is represented, ( $n=3$ ; error= $\pm$ s.d). Tetracycline loaded P(3HB) microsphere films had a significant ( $**p<0.001$ ) effect on pH . Since the data compared using ANOVA was significant, a Bonferroni Post Hoc was applied and significant differences at  $***p<0.0001$  for 4wt% tetracycline loaded P(3HB) microsphere films were observed when compared to the control and 0.5 wt%, 2 wt% tetracycline loaded films on day 15 and day 30. No significant ( $p>2.0$ ) differences between 0.5 wt% and 2 wt% tetracycline loaded films were observed.

### 6.2.2.1 Thermal analysis after *in vitro* degradation studies of the P(3HB) microsphere films (with and without the drug)

Thermal analysis of the P(3HB) microsphere films (with and without the drug) were carried out to identify the possible changes in the thermal properties after *in vitro* degradation studies (Figure 12).

The  $T_m$  and  $\%X_c$  values of the 0.5wt% tetracycline loaded P(3HB) microsphere films, when compared to the unloaded P(3HB) microsphere films, did not exhibit any significant changes over a period of 30 days (Figure 11A). However, the  $T_g$  values on day 15 and day 30 were significantly reduced ( $n=3$ ,  $***p<0.001$ ) when compared to the  $T_g$  values of  $4.56^\circ\text{C}$  and  $4.41^\circ\text{C}$  on day 15 and day 30 of the unloaded P(3HB) microsphere films (Figure 13).

The  $T_m$  and the  $\% X_c$  values of the P(3HB) microsphere films loaded with 2wt% tetracycline, after immersion in PBS, continued to remain insignificantly different ( $n=3$ ,  $p>0.2$ ) when compared to unloaded P(3HB) microsphere films immersed in PBS over a period of 30 days (Figure 12B), but a significant reduction ( $n=3$ ,  $***p<0.001$ ) in the  $T_g$  values of  $3.75^\circ\text{C}$  and  $3.54^\circ\text{C}$  on day 15 and day 30 were observed when compared to the  $T_g$  values of the unloaded P(3HB) microsphere films on day 15 and day 30 (Figure 13).

The  $T_m$  of the P(3HB) microsphere films loaded with 4wt% tetracycline after immersion in PBS, continued to remain insignificant ( $n=3$ ,  $p>0.2$ ) when compared to unloaded P(3HB) microsphere films over a period of 30 days (Figure 12C), but significant reduction ( $n=3$ ,  $***p<0.01$ ) in the  $\% X_c$  and  $T_g$  values were observed when compared to the unloaded P(3HB) microsphere films on day 1, day 15 and day 30 (Figure 13).

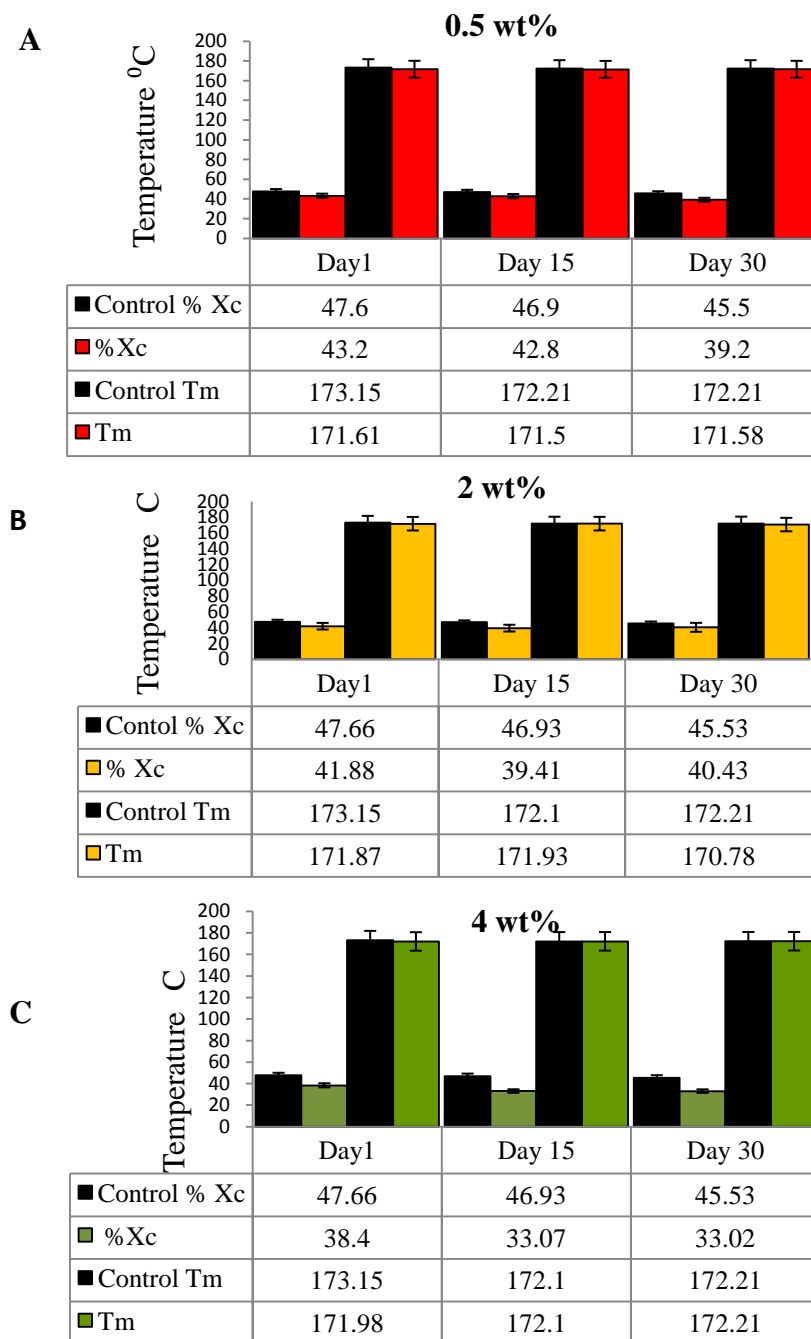
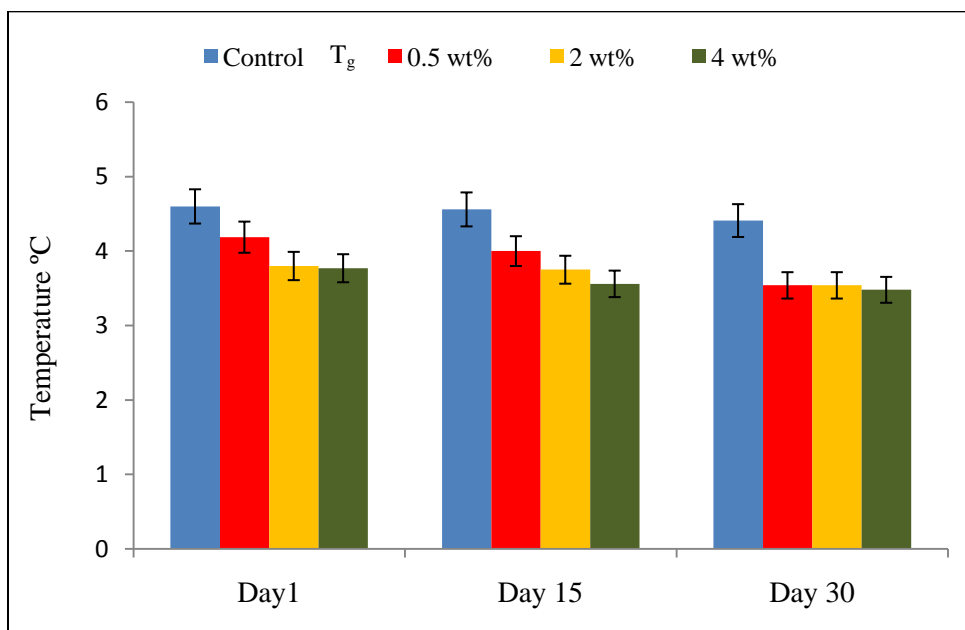


Figure 12:- A comparison of the thermal properties of the P(3HB) microsphere films (with and without the drug) measured on day1, day 15 and day 30 using DSC. A) The thermal properties of the P(3HB) microsphere films loaded with 0.5 wt% of tetracycline. B) The thermal properties of the P(3HB) microsphere films loaded with 2 wt% of tetracycline and C) the thermal properties of the P(3HB) microsphere films loaded with 4 wt% of tetracycline. The tetracycline loaded P(3HB) microsphere films had a significant ( $***p < 0.001$ ) effect on the %X<sub>c</sub>. Since the data compared using ANOVA was significant, a Bonferroni Post Hoc was applied and significant differences at  $***p < 0.0001$  for 4wt% tetracycline loaded P(3HB) microsphere films were observed when compared to the control and other tetracycline loaded films on day1, 15 and day 30. No significant differences ( $p > 2.0$ ) were observed in the T<sub>m</sub> values of the tetracycline loaded P(3HB) microsphere films when compared to the control.



**Figure 13:-** A comparison of the glass transition properties ( $T_g$ ) of the P(3HB) microsphere films (with and without the drug) measured on day 1, day 15 and day 30 using DSC. The tetracycline loaded P(3HB) microsphere films had a significant ( $*** p < 0.0001$ ) effect on the  $T_g$  values. Since the data compared using ANOVA was significant, a Bonferroni Post Hoc was applied and significant differences at  $*** p < 0.0001$  for 2 wt% and 4wt% tetracycline loaded P(3HB) microsphere films were observed when compared to the control and 0.5wt% tetracycline loaded films on day 15 and day 30.

The DSC thermograms of P(3HB) microsphere films (with and without the drug) after the *in vitro* degradation studies in PBS over a period of 30 days are shown in Figure 14. The DSC thermograms of the tetracycline loaded microsphere films as seen on day 1, day 15 and day 30 showed no characteristic endothermic peak at 234°C for tetracycline (Govender *et al.*, 2005). The thermograms also appeared similar to those of unloaded P(3HB) microsphere films.

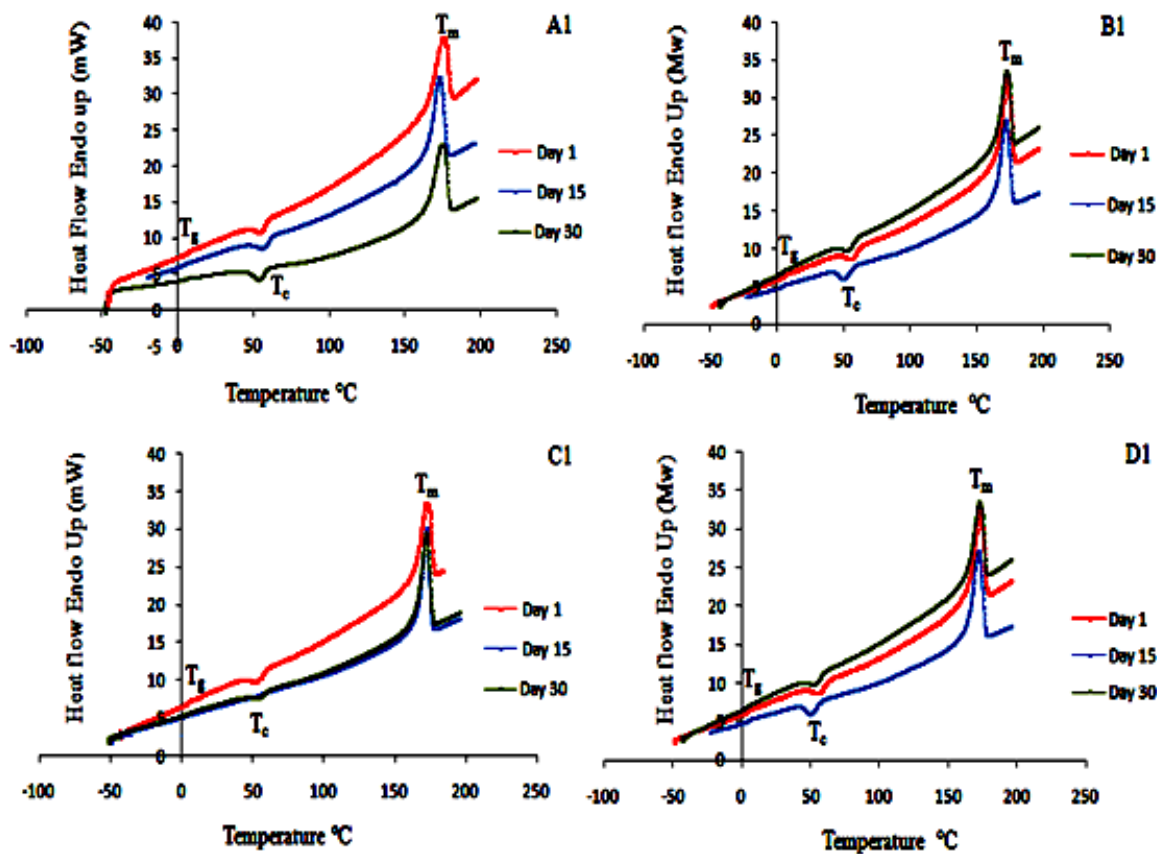


Figure 14:- A comparison of the DSC thermograms of the P(3HB) microspheres films (with and without the drug) measured at day 1, day 15 and day 30 to identify the possible drug-polymer interaction. A1) The DSC thermograms of the unloaded P(3HB) microspheres films and the P(3HB) microspheres loaded B1) with 0.5 wt% of tetracycline, C1) with 2 wt% of tetracycline and D1) with 4 wt% of tetracycline. ( $n=3$ ; error= $\pm$ s.d).

### 6.2.3 *In vitro* drug release studies

The cumulative *in vitro* release of tetracycline from microsphere films with different drug loading ratios 0.5 wt%, 2 wt% and 4 wt% are represented in Figure 15. The encapsulation efficiencies of the tetracycline loaded microsphere films were determined as described in Chapter 2 section 8.1.1, shown in Table 2. The tetracycline loaded microspheres with the lowest drug loading ratio of 0.5 wt% exhibited the highest encapsulation efficiency of 25% when compared to the P(3HB) microspheres with 15% and 11% for 2wt% and 4 wt% of tetracycline respectively.

**Table 2:- The encapsulation efficiency of the P(3HB) microspheres loaded with different drug loadings (n=3).**

Sample	Initial Drug Loading (w/w)	(%) Encapsulation Efficiency
0.5 wt%	0.5 mg drug/100 mg P(3HB)	25%
2 wt%	2 mg drug /100 mg P(3HB)	15%
4 wt%	4 mg drug /100 mg P(3HB)	11%

From the results a biphasic release profile was observed, an initial burst release followed by a sustained release in the medium. The tetracycline loaded film with 0.5 wt% of the drug exhibited an initial burst release of 13.49% from 0 to 1 hour of the actual drug loading. Similarly, microsphere films with 2 wt% and 4 wt% tetracycline exhibited a burst release of 6.4% and 14% of the actual drug loading of from 0 to 1 h of immersion in the release buffer.

Following the initial phase of burst release, 48% of sustained phase of controlled drug release was observed in films loaded with 0.5 wt% tetracycline between 24 h to 48 h. Similarly, tetracycline films loaded with 2 wt% of the drug exhibited a controlled release of 33% the drug between 24 h and 168 h. Finally, the tetracycline film loaded with 4 wt% of the drug exhibited a controlled release of 31% between 24 h and 48 h. As expected, the highest % cumulative release of 100% was observed from the films with the highest drug loading when compared to 99% from films with 2 wt% and 99% from films with 0.5 wt%

of tetracycline. Although a cumulative release of 100% was achieved by all the films the intermediate drug release rates were different due to the different drug loadings.

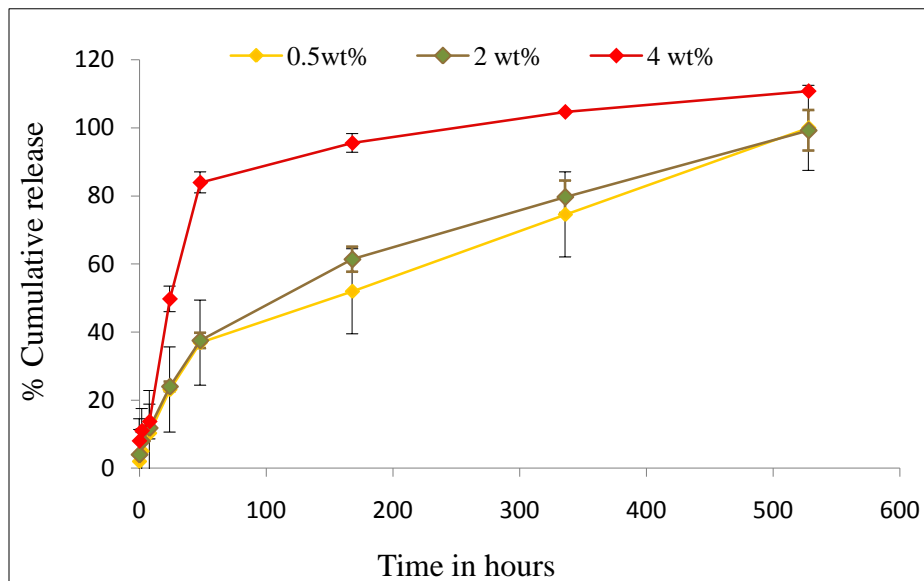


**Figure 15:- *In vitro* kinetic profiles of tetracycline release from P(3HB) microsphere films containing microspheres with different drug loading ratios of 0.5 wt%, 2 wt% and 4 wt% in phosphate buffer at 37°C, ( $n=3$ ; error= $\pm$ s.d).**

## 6.2.4 Factors affecting the biocompatibility of the biodegradable polymers used as scaffolds

### 6.2.4.1 Surface wettability (before protein adsorption)

The effect of drug loading on the surface wettability of films was investigated. The water contact angle values of both the tetracycline loaded and unloaded microsphere films are shown in Figure 16. The water contact angle of the tetracycline loaded film with 4 wt% was reduced to 54.39° from 64.67° (16% decrease), 2 wt% was reduced to 57.13° (11.65% decrease) and 0.5 wt% the water contact angle was reduced to 62.13° (not significant) when compared to the control value of 64.67°. The surface wettability of tetracycline films loaded with 2wt% and 4 wt% was significantly reduced ( $*** p < 0.0001$ ) when compared to the control and 0.5 wt% tetracycline loaded films.

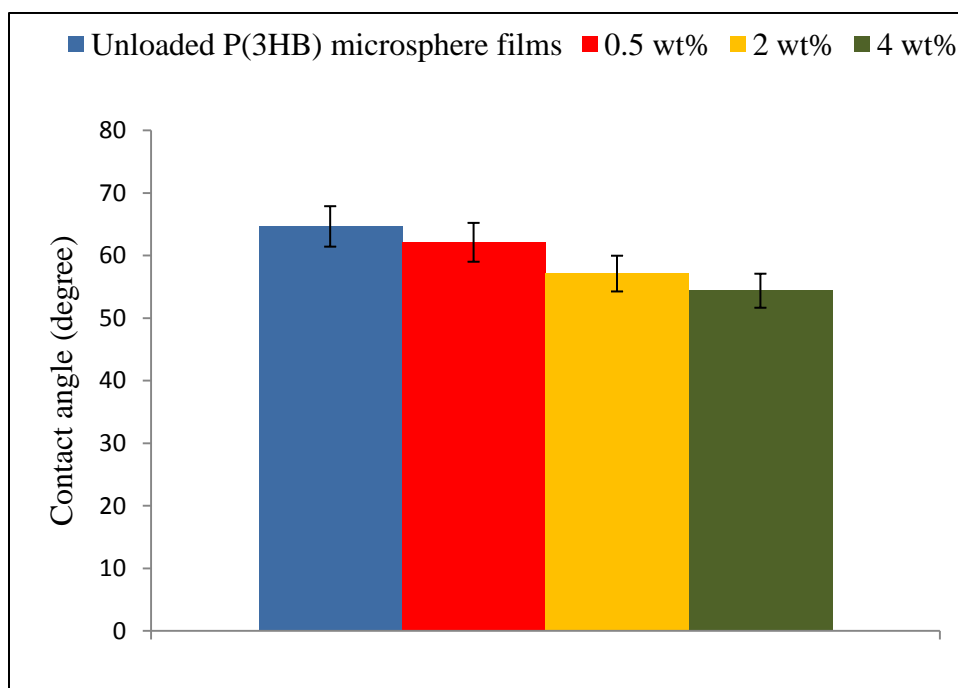


**Figure 16:- A comparison of the surface wettabilities of the P(3HB) microsphere films (with and without the drug). The P(3HB) microsphere films tetracycline loadings had a significant ( $*** p < 0.0001$ ) effect on the surface wettability. Since the data compared using ANOVA was significant, a Bonferroni Post Hoc was applied and significant differences at  $***p < 0.0001$  for 2 wt% and 4wt% tetracycline loaded P(3HB) microsphere films were observed when compared to the control and 0.5wt% tetracycline loaded films.**

## 6.2.4.2 Protein adsorption study in DMEM media

The protein adsorption test carried out after a period of 3 days on the tetracycline loaded P(3HB) microsphere films with different drug loadings were compared to the unloaded P(3HB) films. As shown in Figure 17, a higher adsorption of protein was observed on the drug loaded P(3HB) microsphere films when compared to the unloaded P(3HB) microsphere films. As expected, a higher adsorption of protein was observed on the P(3HB) microsphere films with the highest drug loading ratio of 4 wt% when compared to the films with a drug loading ratio of 2wt% and 0.5%. The unloaded P(3HB) films had  $308.5\mu\text{g}/\text{cm}^2$  of adsorbed protein where as the tetracycline loaded P(3HB) films with 0.5wt% of tetracycline had  $331.4\mu\text{g}/\text{cm}^2$  of adsorbed protein, those with 2wt% tetracycline had  $385.6\mu\text{g}/\text{cm}^2$  and with 4wt% of drug had  $581.4\mu\text{g}/\text{cm}^2$  of adsorbed protein. Hence, in the presence of the highest concentration of tetracycline (4 wt%), a significant increase ( $n=3$ ,  $***p<0.001$ ) of 88% in the protein adsorption was observed, when compared to 25% of 2 wt% and 7.5% of 0.5 wt% tetracycline loaded microsphere P(3HB) films, with respect to the unloaded P(3HB) films.

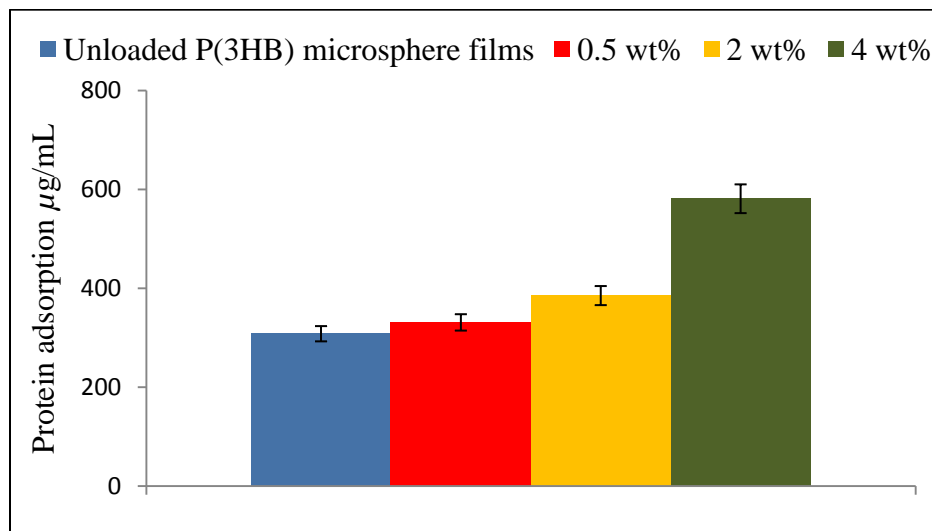


**Figure 17:- Total protein adsorption carried out on the surface of the P(3HB) microsphere films (with and without the drug) ( $n=3$ ; data= $\pm$ s.d). The P(3HB) microsphere films with tetracycline loadings has a significant  $*** p<0.0001$  effect on protein adsorption. Since the data compared using ANOVA was significant, a Bonferroni Post Hoc was applied and a significantly greater difference at  $***p<0.0001$  for 4wt% tetracycline loaded P(3HB) microsphere films were observed when compared to the control and other tetracycline loaded films.**

## 6.2.4.3 Surface wettability tests (after protein adsorption)

The water contact angle of the tetracycline loaded and unloaded P(3HB) microsphere films after the protein adsorption test for a period of 3 days were compared as shown in Figure 18. It was observed that with higher protein adsorption, there was an increase in the wettability of the samples. The water contact angle of the unloaded P(3HB) microsphere films reduced from  $64.67^\circ$  to  $58.94^\circ$ , a decrease of 9%, ( $n=3$   $**p<0.01$ ). In the 4wt% tetracycline loaded film, after protein adsorption, the water contact angle reduced from  $54.39^\circ$  to  $52.6^\circ$ , a 3% reduction, ( $n=3$ ,  $**p<0.01$ ). Similarly, a reduction in the water contact angle from  $57.13^\circ$  to  $56.1^\circ$  a decrease of 2% ( $n=3$ ,  $**p<0.01$ ) was observed with tetracycline films loaded with 2 wt% and that of films with 0.5 wt% of tetracycline reduced from  $62.13^\circ$  to  $57.4^\circ$ , a decrease of 7% ( $n=3$ ,  $**p<0.01$ ).

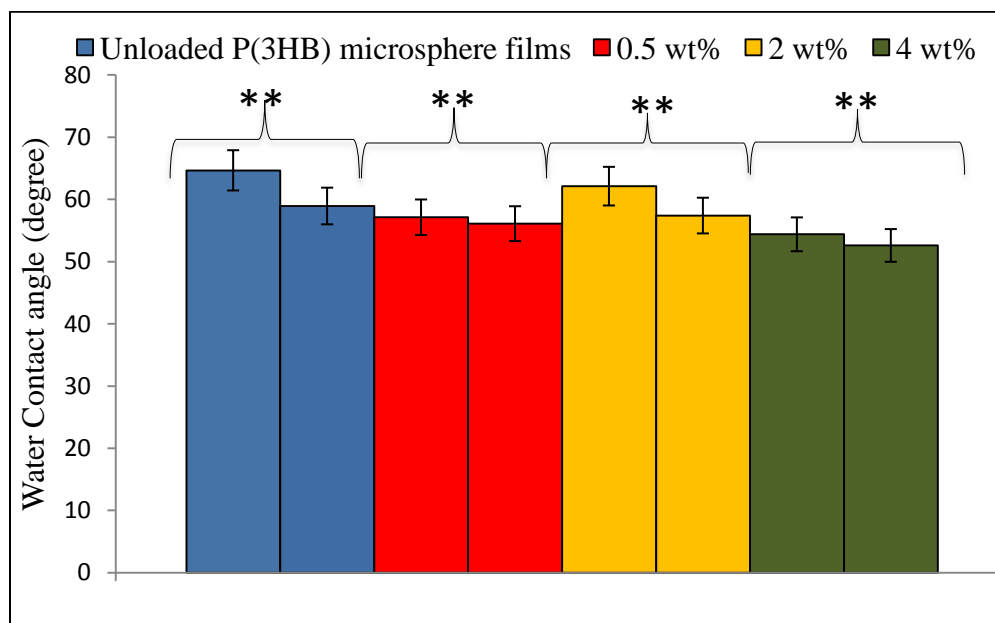


**Figure 18:-** A comparison of the surface wettabilities of the P(3HB) microsphere films (with and without the drug) after protein adsorption (after 3 days). The data ( $n=3$ ; error= $\pm$ s.d) were compared using  $t$ -test and the differences were considered significant when,  $**p < 0.001$ .

## 6.2.4.4 Cell attachment tests

Cell attachment tests performed using HaCaT cells, the keratinocyte cell line, on both unloaded and drug loaded P(3HB) films, proved the biocompatibility of the films. A significant increase in the cell viability, expressed as a percentage of cell growth on tissue culture plastics (Figure 19), was observed on the tetracycline loaded P(3HB) films containing 0.5 wt% of the drug, 48% ( $n=3$ ,  $***p<0.0001$ ) when compared to the films with 2 wt%, 32 % ( $n=3$ ,  $***p<0.0001$ ), 4 wt%, 24%, ( $n=3$ ,  $***p<0.0001$ ) and even the unloaded films 5.99%, ( $n=3$ ,  $***p<0.0001$ ).

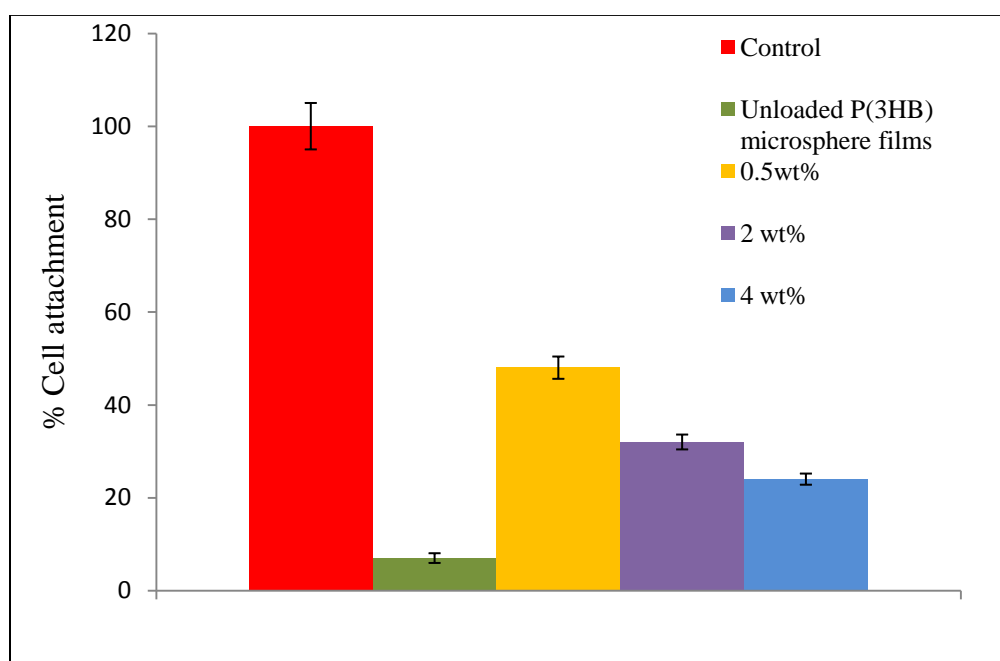


**Figure 19:-** Cell attachment study performed on day 3, using Neutral Red assay, on P(3HB) microsphere films (with and without the drug). All tested samples were relative to the control expressed as a percentage of cell growth on tissue culture plastics. The P(3HB) microsphere films with tetracycline loadings has a significant effect on cell attachment. Since the data ( $n=3$ ; data= $\pm$ s.d) compared using ANOVA was significant  $*** p<0.0001$ , a Bonferroni Post Hoc was applied and a significant differences at  $***p<0.0001$  for 2 wt% and 4wt% tetracycline loaded P(3HB) microsphere films were observed when compared to the control and 0.5wt% tetracycline loaded films.

SEM images of the cells attached on day 1 of the tetracycline loaded microsphere films containing 0.5 wt% and 2 wt% of the drug appeared flat and uniformly spread (Figure 20 A2, A3). Whereas the cells attached on the tetracycline films with 4wt% of the drug appeared rounded in morphology and less confluent (Figure 21A4). After 3 days of incubation in the cell culture media, all the tetracycline loaded films appeared to have a confluent layer of cell growth on the surface (Figure 21B2, B3, B4) when compared to the cell growth on the unloaded films where the growth was less confluent (Figure 20B1).

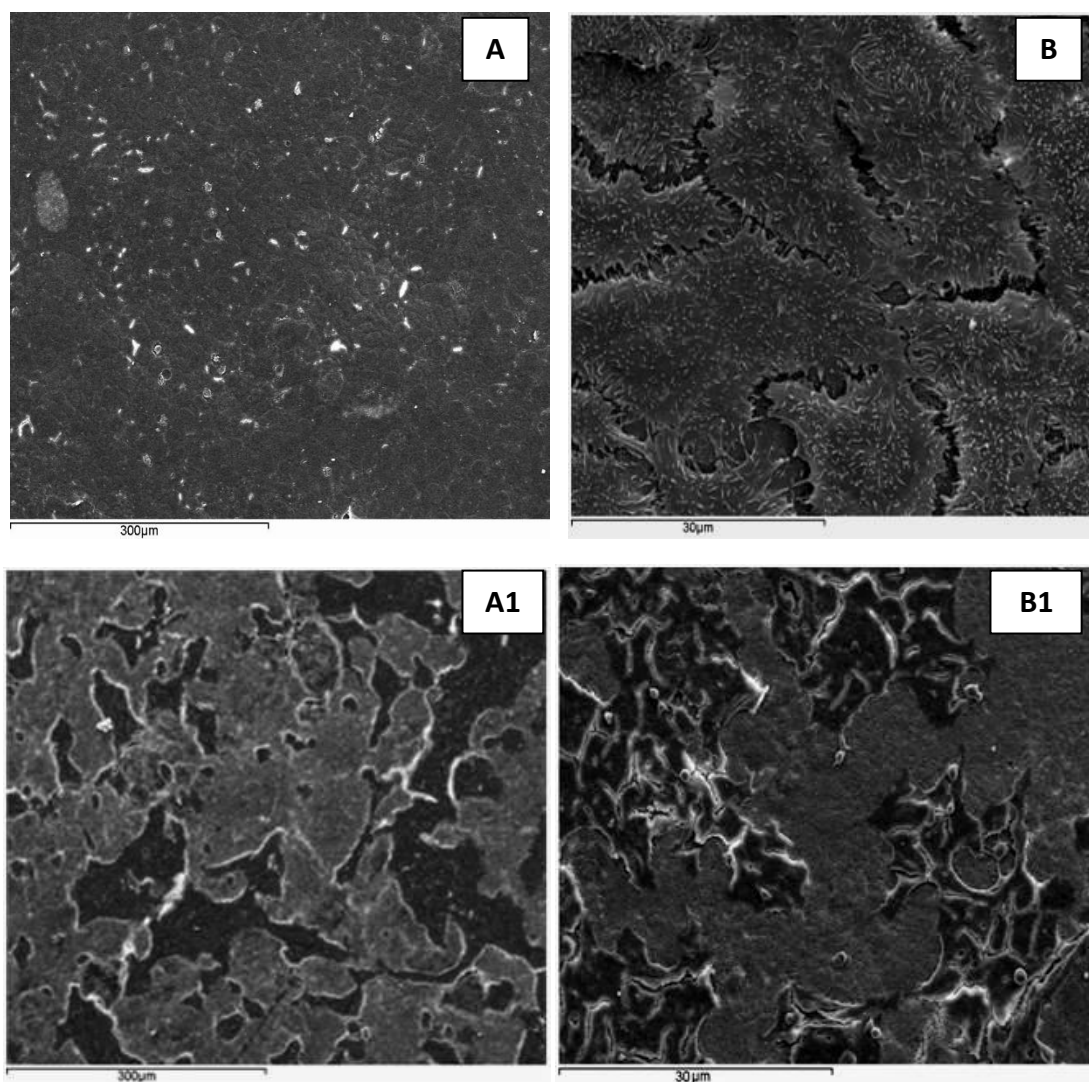


**Figure 20: - Scanning electron micrographs (SEM) of HaCaT cell attachment on day 1 and day 3 on the surface of the control (tissue culture plastic) A and B respectively. Unloaded P(3HB) microsphere films A1 and B1 respectively.**

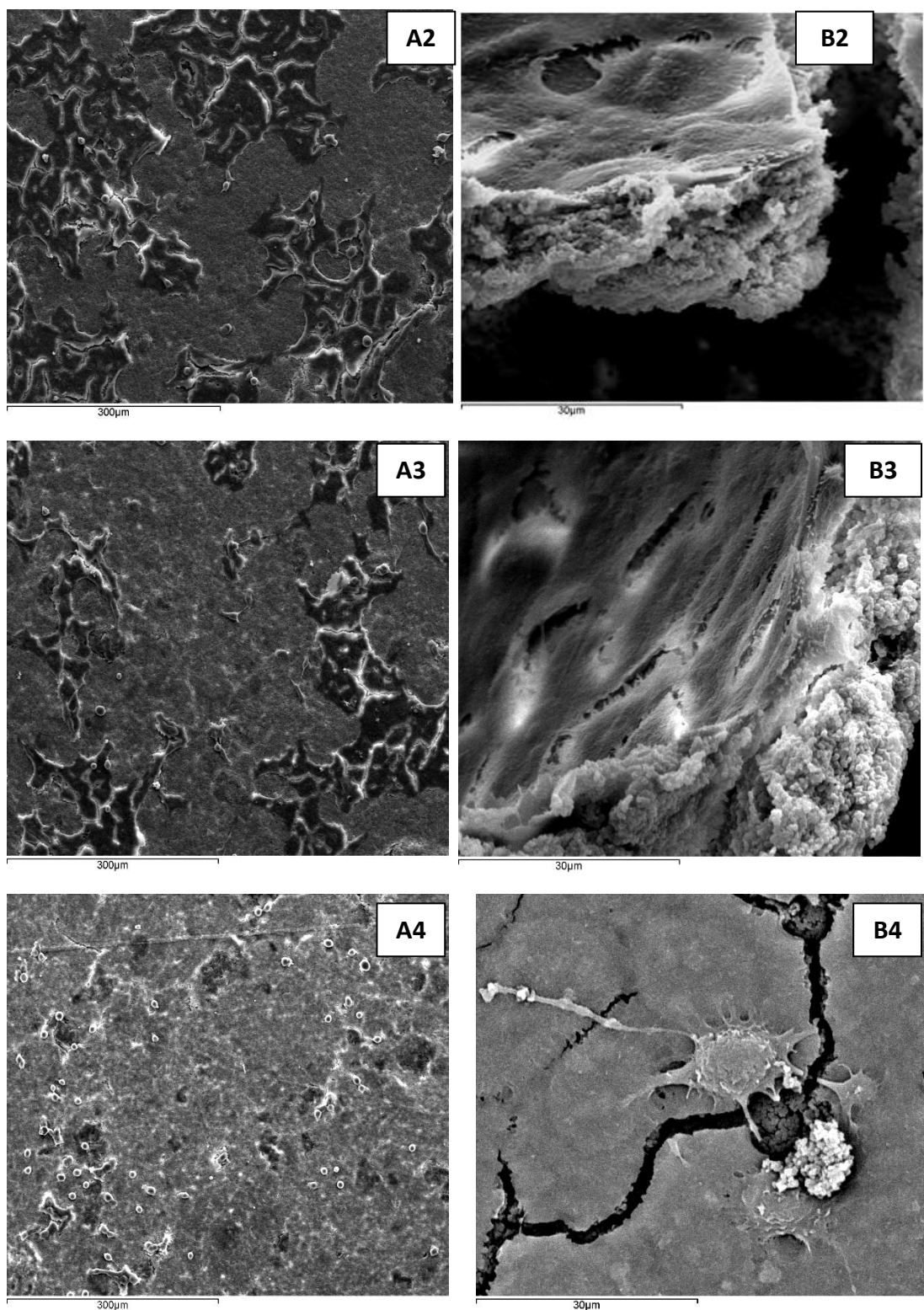


**Figure 21:-** The HaCaT cell attachment seen on day 1 and day 3 on the P(3HB) microspheres films loaded with 0.5 wt% tetracycline (A2 and B2), 2 wt% tetracycline (A3 and B3) and 4 wt% tetracycline (A4 and B4).

## 6.3 Discussions

### 6.3.1 Tetracycline loaded P(3HB) microsphere films characterizations

In this study tetracycline was incorporated in the newly developed and novel P(3HB) microsphere films in order to serve a dual purpose, improving surface properties and biocompatibility and as a source of the antibiotic in order to prevent bacterial infection. With the incorporation of tetracycline, the surface roughness, surface wettability and surface morphology/topography were all improved significantly.

#### 6.3.1.1 Surface morphology

The surface morphology of the tetracycline loaded compressed microsphere films with different drug loadings were compared to the surface morphology of the unloaded P(3HB) microsphere films used as controls. The SEM images of the P(3HB) microsphere films after drug loading appeared to have a porous structure and an uneven surface morphology when compared to the smooth surface of the unloaded P(3HB) microsphere films. The microsphere films with the highest tetracycline loading of 4 wt% appeared more irregular and rougher when compared to the films loaded with lower tetracycline such as 0.5wt% and 2 wt%. The rough surface of the microsphere films is most likely to be due to the presence of the drug molecules adsorbed on the surface of the microsphere and the change in the surface morphology of the microspheres when formed in the presence of the drug. Thus, with the increase in drug loading the surface morphology of the films appeared uneven and irregular. In a study conducted by Misra *et al.*, a smooth surface morphology of the P(3HB) solvent cast films were observed after the incorporation of vitamin E. The vitamin E added to the polymer solution was incorporated within the microstructure of the film during the solvent cast film synthesis, due to which a homogenous distribution of the vitamin E was achieved (Misra *et al.*, 2006). However, in another relevant study Chee *et al.*, used a similar technique as in Misra *et al.*, 2006, for the incorporation of the Mitragynine in poly(3-hydroxybutyrate-co-4-hydroxybutyrate), P(3HB-co-4HB) solvent cast films. The drug and the polymer were dissolved in the chloroform solution and then cast into films. The surface morphology of the films initially appeared smooth and even, however, with the increase in the drug concentration from 10 wt% to 40 wt% a coarse and rough surface morphology

was observed (Chee *et al.*, 2008). Thus apart from the different techniques used to fabricate the films, the increasing concentrations of the drug are also known to influence the surface morphology of the films.

Due to the encapsulation and adsorption of the drug, a topographical change on the surface was observed leading to an increased roughness of the P(3HB) microsphere films. The quantification of surface roughness using white light interferometry confirmed that the drug loaded microsphere films had a rougher surface when compared to the unloaded microsphere films. The tetracycline loaded P(3HB) microsphere films with the highest drug loading exhibited a surface roughness of  $6.74\mu\text{m}$  which was significantly higher than those with a lower drug loading. Thus it can be concluded that with the increase in the concentration of the drug loading an increase in the surface roughness of the microsphere films were also observed. Researchers like Lu *et al.*, have also made similar observations with the emergence of a rougher surface morphology in the presence of an increasing concentration of the drug (Lu *et al.*, 2001). Bazzo *et al.*, also confirmed that the presence of the drug crystals on the surface of the P(3HB) microspheres contributed to the rough morphology of the drug loaded microspheres. SEM images had revealed the presence of crystalline needles of the drug piroxicam (PXC) on the surface of the P(3HB) microspheres (Bazzo *et al.*, 2008).

#### 6.3.1.2 X-Ray photoelectron spectroscopy (XPS)

The assessment of the tetracycline adsorption on the microsphere surface was done on the basis of nitrogen content present on the samples since the nitrogen species is unique to the drug and is absent in the P(3HB) microspheres. From the XPS data, a significant increase in the nitrogen content of the drug loaded samples was observed when compared to the unloaded P(3HB) microsphere films, where, as expected, only carbon and oxygen were seen. Similarly, with an increase in the tetracycline loading, an increase in the nitrogen species on the surface of the microspheres was observed. Therefore, from this data it was deduced that in addition to being encapsulated within the microspheres, tetracycline was also adsorbed on the surface. Studies by Gangrade *et al.*, also revealed an increase of drug crystals on the surface of poly(hydroxybutyrate) P(3HB) and poly(3-hydroxybutyrate-co-3-hydroxyvalerate),P(3HB-co-3HV), microspheres when the

concentration of the drug progesterone was increased from 1 wt% to 5 wt% (Gangrade *et al.*, 1991).

It has been observed by Bazzo *et al.*, that in the solid-oil-water emulsion technique used to fabricate the drug loaded microspheres, the aqueous solution of the drug added into the polymer solution in addition to being encapsulated within the P(3HB) microspheres could also diffuse out and remain on the outer surface of the microspheres during solvent evaporation. The increasing viscosity of the second emulsion phase prevents the drug from diffusing out into the aqueous phase; as a result they get adsorbed on the surface of the microspheres (Bazzo *et al.*, 2008). Thus in this study due to the increasing viscosity of the second emulsion in the presence of the increasing concentration of the drug, tetracycline could have got adsorbed on the surface of the microspheres.

#### 6.3.1.3 Thermal analysis of the P(3HB) microspheres (with and without the drug)

The  $T_g$  values of the microspheres with different tetracycline loadings before immersion in PBS and fabrication into films were carried out in order to investigate the changes in the thermal properties of the polymer, in the presence of the drug as well as the fabrication techniques used. From the results it was observed that the  $T_g$  values of the unloaded microspheres after fabrication was slightly higher than those compared to the crude polymer. This increase in the  $T_g$  value could indicate that the mobility of the polymer chains in the microspheres after the fabrication was restricted. Similarly the  $T_g$  values of the P(3HB) microspheres loaded with tetracycline also increased further when compared to the crude polymer and the unloaded P(3HB) microspheres. The microspheres with the highest drug loading of 4 wt% exhibited an increased  $T_g$  value of 4.9°C when compared to the films with lower loading of tetracycline. Numerous factors like structural change in molecules, cooling rate and incorporation of additives alter the  $T_g$ . For example the insertion of bulky, inflexible side group increases  $T_g$  of the polymer due to decrease in mobility of the polymer chains. Thus in this study the presence of the drug could have acted as an impurity thus affecting the  $T_g$  of P(3HB) microspheres.

### 6.3.2 In vitro degradation studies of the P(3HB) microsphere films (with and without the drug) in PBS

The degradation rates of the microsphere films (with and without the drug) were evaluated based on the water absorption and weight loss studies after time bound degradation in PBS (pH 7.4) at 37°C. The results of the 30 day degradation study indicated that the tetracycline films with the highest drug loading underwent a maximum weight loss over a period of 30 days when compared to the films with a lower drug loading. This result suggested that the tetracycline films with the highest drug loading were more sensitive to degradation when compared to the other films. This increase in the degradation rate was most likely due to the presence of a higher amount of the hydrophilic drug (tetracycline) present both on the surface and encapsulated within the P(3HB) matrix, allowing access to water from the PBS, leading to faster degradation *via* hydrolytic cleavage. The surface morphology of all the tetracycline loaded films appeared uneven and exhibited porosity. However, the tetracycline films with the highest drug loading appeared to have an increased porosity when compared to the films with lower tetracycline loading and the tetracycline particles were found entrapped within the pores. The initial dissolution of the drugs, upon immersion in the PBS buffer, leads to the formation of aqueous channels on the surfaces which were filled with the aqueous medium. Water penetration in the polymer matrix results in hydrolytic scission of the ester linkages in the polymer backbone, thus accelerating the polymer degradation due to which the drug mobility and the release rates are also affected (Chee *et al.*, 2008). A similar observation was made by Chee *et al.*, where the P(3HB-co-4HB) films exhibited higher pore size and porosity when the concentration of the drug was increased from 10 wt% to 40 wt%. The authors' observed that before drug loading the polymer pores were present closer to each other, however after drug loading the pores got entrapped with the drug therefore increasing in size. Films with a higher drug loading also appeared coarser with the increased drug entrapment within the pores. As a result, the large amount of drugs present on the surface and entrapped within the pores underwent rapid dissolution when immersed in the release buffer thereby increasing the water channels in the films. Due to this, the polymer degradation rate by hydrolytic scission was accelerated (Chee *et al.*, 2008). The crystallinity of the tetracycline loaded and unloaded P(3HB) microsphere

films are also shown to influence the rate of *in vitro* degradation. In this study, the tetracycline loaded films with a lower %  $X_c$  exhibited an increased degradation rate when compared to the films with a higher degree of crystallinity. As suggested in literature, with the prolonged immersion in the aqueous medium, the  $T_g$  value also decreases, causing an increase in the polymer chain mobility, thus allowing more water to penetrate, hence increasing hydrolytic degradation (Chee *et al.*, 2008).

### 6.3.3 Differential Scanning Calorimetry (DSC) and X-Ray Diffraction (XRD) analysis

DSC and XRD analysis were carried out to verify the changes in the thermal properties and crystallinity of the drug loaded microspheres during the *in vitro* degradation study. The representative DSC thermograms of the tetracycline loaded and unloaded P(3HB) microsphere films at different time points were analysed to study the possible changes in the melting temperature ( $T_m$ ), the glass transition temperature ( $T_g$ ) and the degree of crystallinity (%  $X_c$ ) in the presence of the drug tetracycline.

In this study the endothermic events corresponding to the melting temperature ( $T_m$ ) of all the tetracycline loaded microsphere films at day 1, day 15 and day 30 exhibited only one melting peak in the range of 171°C to 173°C when compared the unloaded P(3HB) microsphere films. Similarly, no separate peak for tetracycline was seen in the tetracycline loaded microsphere films, this indicated that the peak corresponding to the melting of the drug was probably not revealed, as it melted with the polymer while heating. The DSC thermograms of the poly(3-hydroxybutyrate), P(3HB) and poly(3-hydroxybutyrate-co-3-hydroxyvalerate) P(3HB-co-3HV) microspheres loaded with the 5 wt% of the drug progesterone also did not reveal a separate peak in a study conducted by Gangrade *et al.* The authors' also observed that the peak corresponding to the melting of the drug had merged with the polymer melting peak (Gangrade *et al.*, 1991).

The tetracycline films with the highest drug loading also exhibited significant changes ( $n=3$ ,  $***p<0.001$ ) both in the %  $X_c$  and  $T_g$  over a period of 30 days when compared to the unloaded P(3HB) microsphere films. However the films with a lower loading of tetracycline such as 0.5 wt% and 2wt% exhibited no such changes in the % $X_c$  over a period of 30 days when compared to the unloaded P(3HB) microspheres. The change in

the %X<sub>c</sub> of the tetracycline loaded microsphere films with the highest drug loading indicated that the tetracycline might have acted as an impurity thereby hindering the crystallization of the polymer. Due to this, a reduction in the %X<sub>c</sub> values of the highest drug loaded films were observed when compared to the films with lower drug loadings. In the P(3HB) microsphere films with the lower drug loading, the amount of drug present was too low to have an effect on the crystalline properties of the polymer, due to which no changes were observed in the %X<sub>c</sub> values. Freiberg *et al.*, have also observed that at higher concentrations, the drugs are known to exist in a particulate form rather than a dispersion within the microspheres possibly due to its lack of solubility in the polymer matrix thereby affecting the crystallinity of the polymer (Freiberg *et al.*, 2004).

Palau *et al.*, also observed similar changes in the crystallinity of the two new copolyesters consisting of an alternating disposition of glycolic acid units and 4-hydroxybutyric or 6-hydroxyhexanoic acid, named as poly(4HB-alt-Glc) and poly(6HHx-alt-Glc) in the presence of the drug triclosan. The crystallinity of the drug loaded polymer reduced to 13% when compared to the crystallinity of the unloaded polymer which was 17%. This indicated that triclosan hindered the crystallization of the polymer and that some amount of drug molecules were incorporated into the crystalline phase (Palau *et al.*, 2008). Significant changes in the T<sub>g</sub> values of all the drug loaded microsphere films over a period of time indicated that an increase in the polymer chain mobility over time allowed the PBS solution to penetrate within the films, thereby increasing the degradation process. Although, in this study the DSC thermograms indicated that the presence of the drug may have hindered the crystallinity of the polymer more reliable measurements can however be obtained from X-ray diffraction analysis.

X-ray diffraction (XRD) analysis of tetracycline loaded microspheres were carried out to confirm the dispersion of the tetracycline particles within the P(3HB) microspheres. The diffraction patterns of both tetracycline and P(3HB) measured separately and used as controls exhibited intense peaks confirming their high crystallinity. However, the diffraction patterns of the tetracycline loaded microspheres with 0.5 wt%, 2 wt% and 4 wt% were identical to those of the unloaded P(3HB) microspheres. Although tetracycline rendered a well-defined diffraction pattern with intense peaks, they could not

be detected in the tetracycline loaded microspheres. This result could possibly suggest that tetracycline was too low in concentration to be detected, due to which no separate diffraction peaks of tetracycline could be detected. However other analysis such as small-angle diffraction analysis (SAXD) could be carried out to get additional information on the lamellar structures such as the thickness, the organization between the crystalline and amorphous domains in the presence and the absence of the drug (Palau *et al.*, 2008).

#### 6.3.4 Factors affecting the *in vitro* drug release

A number of factors are known to affect the drug release rate such as the microsphere size, drug distribution within the microsphere and porosity, which are all related to the matrix processing condition used to fabricate the microspheres. In this study the microsphere films with the highest drug loading (4wt%) exhibited the lowest encapsulation efficiency of 11% when compared to 15% and 25% of the films loaded with 2 wt% and 0.5 wt% of tetracycline. Often factors such as drug/polymer ratio, affinity of the drug for the aqueous or organic phase and the microsphere size play an important role in the affecting the encapsulation efficiency of the microspheres (Wang *et al.*, 2007). In this study the polymer ratio was kept constant and the drug concentration in the drug/polymer ratio varied. Thus, with the increase in the drug loading, the viscosity of the emulsion phase appeared to increase due to which the diffusion of the drug back into the emulsion phase was prevented, hence getting adsorbed onto the microsphere surface. This was further confirmed in the XPS analysis by the increase in the nitrogen species on the surface with the increase in the tetracycline loading. Another possible reason for the low encapsulation efficiency in the microspheres with a high drug loading is the presence of insufficient amount of polymer to encapsulate drug completely (Wang *et al.*, 2007). Since in this study the polymer ratio in the drug/polymer ratio was kept constant and as the drug concentration increased lower encapsulation efficiency was observed due to the increased leakage of the drug into the buffer. Wang *et al.*, also observed a decrease in the encapsulation efficiency from 59% to 45% in P(3HB-co-3HV) microspheres when the drug loading (ibuprofen) was increased from 9.8 wt% to 16.9 wt% (Wang *et al.*, 2007).

The average microsphere size is also found to have an effect on the encapsulation efficiency and the drug distribution within the microspheres (Sahoo *et al.*, 2002; Bidone *et al.*, 2009). However, in this study, all the microspheres appeared similar in size. Therefore, from the *in vitro* release profile a biphasic release was seen where all the films exhibited an initial burst release followed a slow sustained release of the drug. As expected, the films with the highest drug loading ratio exhibited a higher burst release within the first hour when compared to the other films. Wang *et al.*, also made similar observations, when the drug/polymer ratio was increased from 10/50 (mg/mg) to 30/50 (mg/mg) where a burst release of 70%, 84% and 88% were observed in the first 2 hours of immersion (Wang *et al.*, 2007). Therefore, in this study, once the films were immersed in the release buffer the drug particles present close to the surface underwent a rapid dissolution thus creating large openings/pores for the faster buffer penetration into the microsphere films.

SEM analysis demonstrated the difference in the surface morphology and porosity of the films with different drug concentrations. The films with the highest drug loading ratio appeared less porous in appearance before immersion in the release buffer. After immersion in the release buffer the dissolution of the drugs created a diffusion path, which was filled with water and this facilitated the drug release initially from amorphous region. Chee *et al.*, also made a similar observation in porous structures of the amorphous films when the drug (Mitragynine) loading was increased from (10 wt% to 40 wt%). The drug appeared to be entrapped within the polymer pores due to which a higher initial release was observed (Chee *et al.*, 2008). Similarly, the number of pores on the polymer matrix also appeared to increase after drug dissolution. This had further created a number of open water filled channels for the drugs to diffuse (Chee *et al.*, 2008).

Often polymeric matrices are known to swell and expand in size when the water uptake within the microspheres/films increases (Naraharisetti *et al.*, 2006). Following the initial diffusion of the drugs, a slower release or lag phase is observed in films with different drug loadings. During the lag phase the remaining drug entrapped deep within the microsphere films was released gradually. In the films with the lowest drug loading such as 0.5 wt% of tetracycline, the lag phase was observed only for a period of 48 hours when

compared to 48 hours and 168 hours of the films with 2 wt% and 4 wt% of tetracycline respectively. The films with lower drug loading had less surface associated drugs, the drug release from the microspheres was attributed to a small-scale diffusion from the surface of the microspheres. Thus, with an increase in the drug loading the dissolution of a large amount of surface associated drugs continued for a period of 48 hours followed by a considerably longer lag phase. With the increase in the water uptake a simultaneous decrease in the  $T_g$  value was also observed. A decrease in the  $T_g$  value, as mentioned earlier, indicated that the polymer chain mobility was more restricted, as a result an increase in the drug release from deep within the films were observed with rapid uptake of water.

#### 6.3.5 Factors affecting the biocompatibility of the tetracycline loaded microsphere films

In this study the change in the wettability of the films in the presence of tetracycline and the adsorbed proteins were measured. The surface wettability of the tetracycline loaded films with different drug loading ratios were measured and compared with the unloaded P(3HB) films used as controls. With the increase in the tetracycline concentration a significant increase in the wettability of films was observed when compared to the controls. A significant increase in the wettability of P(3HB) films was also observed by Misra *et al.*, when vitamin E was incorporated in the films (a decrease of 27%). In another relevant study, poly(3-hydroxybutyrate-co-3-hydroxyvalerate) solvent cast films were treated by exposing the films to oxygen plasma glow discharge and polymerised using acrylic acid and then coupled with insulin (Kang *et al.*, 2001). The presence of insulin on the surface significantly decreased the water contact angle of the P(3HB-co-3HV) microsphere films from  $75^\circ$  to  $31^\circ$  (Kang *et al.*, 2001).

The role of the extracellular matrix proteins (ECM) is to direct the function of the cells (such as keratinocytes) attached on the surface of a biomaterial towards re-epithelialisation phase of wound healing. Other factors such as the biomaterial surface properties also play an important role in protein adhesion, conformation and subsequent protein mediated keratinocyte functions (Bush *et al.*, 2008). In the present study, a statistically higher level of protein adsorption was observed on the surface of the tetracycline loaded microsphere films in comparison to the unloaded P(3HB) microsphere

film. Similarly, the tetracycline loaded film of 4 wt% exhibited the highest amount of protein adsorbed on the surface when compared to the films with lower tetracycline loading. Often, the most abundant protein that binds to the biomaterial surface when exposed to serum is albumin. Albumin adsorption particularly increases when there is an increase in the surface wettability and surface roughness of the sample. This observation correlates with the results obtained in this work, where the increase of hydrophilicity and surface roughness of the tetracycline loaded films led to a higher level of protein adsorption when compared to the unloaded P(3HB) microsphere films. Similarly an increase in the tetracycline loading also contributed an increase in hydrophilicity and surface roughness due to which an increased protein adsorption was observed. For example 4 wt% tetracycline loaded P(3HB) microsphere films exhibited higher hydrophilicity and surface roughness and increased protein adsorption when compared to the 0.5 wt% and 2 wt% tetracycline loaded P(3HB) microsphere films. This result was in agreement with the observation made by Misra *et al.*, where the total protein adsorption was significantly higher ( $171\mu\text{g}$ ) on P(3HB/n-BG) composite films when compared to the neat P(3HB) films. This difference in the protein adsorption was attributed to the marked differences in surface morphology and surface area available for protein adsorption (Misra *et al.*, 2008).

Cell adhesion on the surface of biomaterials are initiated in two stages, where in at the first stage the water and a layer of proteins are selectively adsorbed on the surface this is followed by the adhesion of the cells on the layer of proteins which is mediated by the ECM, cell membrane and the cytoskeletal proteins (Misra *et al.*, 2009). Thus, the surface properties of the biomaterial such as wettability, roughness, and porosity influence cell adhesion and cell proliferation (Peschel *et al.*, 2007; Liu *et al.*, 2008). In this study the effect of the hydrophilic drug and the layer of adsorbed protein on cell adhesion were studied. SEM images of the cells adherence after 3 days of incubation in biological media such as Dulbecco's Modified Eagle Medium (DMEM) appeared to have a difference in cell morphology, shape and degree of attachment on all the films. The tetracycline loaded films with a lower drug loading of 0.5 wt% and 2 wt% appeared to have layers of cells as seen from the cross section images when compared to the unloaded P(3HB) films and the P(3HB) films loaded with 4 wt% of tetracycline where a less confluent single layer was

formed indicating loose attachment or poor adherence. The unloaded P(3HB) films exhibited poor cell adherence and proliferation kinetics due to their higher surface hydrophobicity when compared to the tetracycline loaded P(3HB) microsphere films. Peschel *et al.*, have also observed loose adherence of keratinocytes (HaCaT) on P(3HB) films. It was observed that the cells grew in the form of clusters on the surface of the films with few filaments that resulted in a loose attachment when compared to films made of other PHAs such as P(4HB) where the maximum cell number amounted to about 50% of the control (Peschel *et al.*, 2007). Similarly in this study, the rounded morphology and the less confluent growth of the cells on the P(3HB) loaded films with 4 wt% of tetracycline was due to the high concentration of the drug that was released from the films which affected the cell viability and growth. Although the films with the highest tetracycline loading had exhibited increased surface wettability and protein adsorption, the higher drug concentration appeared to have a profound effect on the cell viability and morphology on the surface of materials thereby affecting the cell growth. Chee *et al.*, also observed a decrease in the cell growth (L929 fibroblast) from 12% to 9.4% when the drug loading (mitragynine) was increased from 10 wt% to 40 wt% in the poly(3-hydroxybutyrate-co-45%-4hydroxybutyrate) P(3HB-co- 45% 4HB) films. In this study, the effects of high concentrations of the drug and surface morphology were studied (Chee *et al.*, 2008).

#### **6.4 Conclusions**

The efficacy of using films made from compressed P(3HB) microspheres encapsulating tetracycline as a patch for drug delivery and wound healing purposes was studied. In this study the incorporation of the drug successfully improved the surface properties of the biomaterial such as surface morphology, wettability, and roughness thereby promoting cell adhesion on the microsphere films. The presence of tetracycline on the surface of the microspheres, as detected by XPS, and possible structural changes within the microsphere, in the presence of tetracycline, resulted in changes in the surface properties of these films. The results from the water contact angle study showed a significant improvement in the hydrophilicity of the microsphere films with the addition of tetracycline which was further complemented by the increase in the total protein adsorption. These alterations in film surface properties resulted in an improved patch for keratinocyte adhesion and growth as indicated by the increased numbers of viable cells on the drug loaded microsphere films compared to those on the unloaded microsphere films.

# Chapter 7

Polyhydroxyalkanoate microsphere-  
based protein encapsulation for  
biomedical applications

## 7.1 Introduction

Proteins constitute very important therapeutic drugs in the recent years. They have been used in the form of vaccines, cytokines, enzymes, hormones and growth factors, for example proteins such as human growth hormone, erythropoietin, interferon, and lysozymes have been increasingly used for a number of different biomedical applications (Morita *et al.*, 2000). However the major disadvantage faced in using proteins is the requirement of recurrent injections in order to maintain adequate therapeutic concentrations due to short half-lives *in vivo*. Some proteins are also not completely absorbed in the gastrointestinal tract due to their high molecular weight. Thus efforts are now being focussed on the use of successful long term controlled release devices (Morita *et al.*, 2000). In the recent years implantable biodegradable polymers such as poly(lactide-co-glycolide), poly(vinyl alcohols) and polyanhydrides have been used as an alternative to the traditional methods of protein delivery (Morita *et al.*, 2000). The protein stability is however known to be preserved when other techniques such as microencapsulation are used. For example a solid-in-oil-water (s/o/w) double emulsion has been known to be suitable for protein drugs as the activity of the proteins can sometimes be retained in organic solutions. Thus microencapsulation techniques have now been commonly used for the encapsulation of proteins and peptide based drugs into the polymeric microspheres. Yang *et al.*, successfully used the double emulsion solvent/evaporation method for the encapsulation of BSA into PCL (polycaprolactone) and PLGA (poly(DL-lactic-co-glycolic acid)) 65 : 35 microspheres (Yang *et al.*, 2001). Microspheres can also be used to target specific sites in the body thereby optimising the therapeutic response and eliminating the inconvenience of repeated injections. Integrins, lipoproteins and monoclonal antibodies have been encapsulated within microspheres for targeted protein release. However, drug release in target specific sites will depend on the microsphere size (Yang *et al.*, 2001). For example microspheres used to deliver drugs in the lungs should be around 10 $\mu$ m as this will allow the lung's capillaries to capture the microspheres. Ophthalmic drug delivery is also another application where the microspheres encapsulated with the drug can be used for the slow/gradual release of the drug, owing to their small size. Macular degeneration is often age related and the most common cause for vision loss. This condition occurs when the arteries that supply oxygen

and nutrients to the retina harden. As a result, the central vision of the affected individual deteriorates. There are two main types of macular degeneration, dry and wet. The dry form occurs by the deposition of yellow spots in the macula and does not cause any loss of vision. Wet macular degeneration is a more serious condition causing permanent central vision loss. In this condition the newly formed blood vessels under the macula become thin and tend to rupture causing bleeding and damage to the surrounding tissues. It causes significant vision problems in the affected eye and can progress very rapidly, causing permanent central vision loss. Currently the most common treatment for the wet macular degeneration is the drug Lucentis<sup>®</sup>, produced by Genentech, USA. Lucentis<sup>®</sup> contains a protein ranibizumab, a humanised monoclonal antibody fragment which is produced in *Escherichia coli*. This antibody is targeted against human vascular endothelial growth factor A (VEGF A) which is responsible for endothelial cell proliferation, neovascularisation and vascular leaks. The binding of ranibizumab to VEGF A prevents the interaction of VEGF A to its receptors, vascular endothelial growth factor receptor 1 and 2 (VEGFR 1 and 2) thereby preventing the progression of wet form of age-related macular degeneration (Sanharawi *et al.*, 2010). Lucentis<sup>®</sup> however needs to be administered through monthly intraocular injections, a requirement extremely distressing to the patient. In addition, it can lead to conjunctival haemorrhage, inflammation of the eye, retinal tear, traumatic cataract and retinal detachment. Also, the cost of Lucentis<sup>®</sup>, used every month *i.e.* 12 injections per year is £14,000 at the currently proposed selling price. Hence, there is a need for the development of improved methods of delivery of this drug. An ideal solution would be the introduction of the drug in such a manner that it is released slowly over a long period of time (for example 6 months), hence decreasing the number of intraocular injections required by the patients.

PHAs are biocompatible and degrade in the human body. In work described in this chapter we aimed to produce PHA microspheres and to use them as drug delivery vehicles in the intraocular environment. Bovine serum albumin (BSA) with a molecular mass of 66,200 Da was used as the model protein to study the *in vitro* release rate in phosphate buffer saline and contact lens solution (representative of an intraocular environment). The stability of BSA within the P(3HB) microspheres and in the *in vitro*

release medium was studied using sodium dodecyl sulphate polyacrylamide gel electrophoresis (SDS-PAGE). The results obtained from this study were then used for planning the encapsulation of the expensive drug Lucentis<sup>®</sup> in P(3HB) microspheres. These microspheres can then be injected into the patient's eye leading to a gradual release of the drug, hence eliminating the need for monthly injections. The *in vitro* release rate in phosphate buffer saline and contact lens solution (representative of an intraocular environment) was carried out.

In order to enhance the tissue development, tissue-engineering scaffolds are loaded with growth factors. Often the simplest method of incorporating the growth factors is by the direct addition of growth factors in the scaffolds (Sokolsky *et al.*, 2007). Both natural and synthetic scaffolds have been used for the delivery of these growth factors. One of the major challenges faced in the direct incorporation of the growth factor in the scaffold, is the denaturation of these growth factors during the fabrication process. Hydrogels used to encapsulate bone morphogenic proteins (rh-BMP) during the fabrication process have proven to be effective in promoting bone and cartilage formation; however the main disadvantage is the inhibition of complete release of proteins from the hydrogels. The release kinetics from hydrogels is largely diffusion controlled through numerous aqueous channels within the hydrogel, as a result the extended release of the proteins do not occur (Sokolsky *et al.*, 2007). Microencapsulation is another common method for the delivery of growth factors. Both double emulsion and single emulsion techniques have been used for the encapsulation of the growth factors, where the growth factors have been dissolved in the organic polymer solution during microsphere fabrication. Patrick *et al.*, successfully encapsulated vascular endothelial growth factor (VEGF) within poly(DL-lactic-co-glycolic acid)/poly(ethylene glycol) microspheres. These microspheres were used to stimulate angiogenesis of the tissues by a slow and sustained release of VEGF over a period of 28 days (Patrick *et al.*, 1999). Platelet derived growth factors have also been successfully encapsulated within microspheres and loaded onto 3-D nano fibrous materials leading to a sustained release of this growth factor for days to months (Wei *et al.*, 2004). However, during microencapsulation of proteins into biodegradable microspheres, the exposure of protein molecule to the organic solvents and physical

stresses such as agitation can cause undesirable changes to the three-dimensional structure of the protein leading to loss of its activity (Nellore *et al.*, 1996). Therefore Ribonuclease A (RNase A), a monomeric enzyme with a molecular mass of 13,700 Da, similar in size to that of BMP-2 growth factor (too expensive to be used for initial experiments) was chosen as a model protein to study the effects of microencapsulation on the structural integrity and activity of the protein. The primary, secondary and tertiary structures of RNase A have been well characterized and it is also easy to monitor for bioactivity. Therefore the aim of this study was to identify whether the RNaseA activity and structural integrity is maintained during the encapsulation process. The results could then be extrapolated to BMP-2.

## 7.2 Results

### 7.2.1 Characterization of Bovine serum albumin (BSA) encapsulated P(3HB) microspheres

#### 7.2.1.1 Production of BSA encapsulated P(3HB) microspheres

A solid-oil-in-water encapsulation method was optimised to entrap different concentrations of BSA within the P(3HB) microspheres as shown in Table 1.

**Table 1:-The different BSA loadings entrapped within P(3HB) microspheres**

Sample	Initial Drug Loading (w/w)
0.75 wt%	0.75mg BSA/100 mg P3HB
1.5 wt%	1.5mg BSA/100 mg P3HB
5 wt%	5mg BSA//100 mg P3HB

The optical micrographs of the first emulsion ( $w_1/o$ ) (mentioned in Chapter 2, section 2.2.2) and second emulsion ( $w_1/o/w_2$ ) (mentioned in Chapter 2, section 2.2.2) are shown in Figure 1A and 1B respectively. The formation of microdroplets of water within the microspheres is observed in the second emulsion. After solvent evaporation the microspheres formed were washed with water and dried.

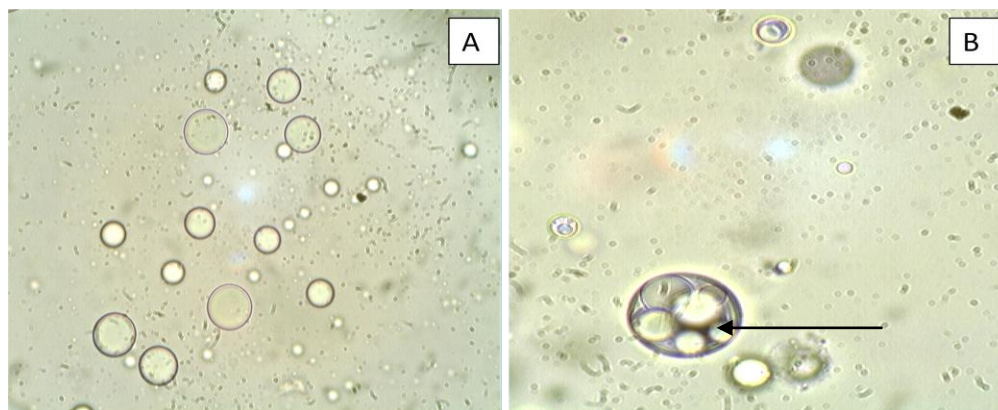


**Figure 1:- The optical micrographs of the A) first emulsion ( $w_1/o$ ) and B) second emulsion ( $w_1/o/w_2$ ) during the P(3HB) microsphere formation loaded with 0.75 wt%, 1.5 wt% and 5 wt% of BSA. Arrow indicating the formation of microdroplets of the water within the P(3HB) microspheres.**

## 7.2.1.2 Bulk shape and structure of the BSA loaded P(3HB) microspheres

The bulk shape and structure of the BSA loaded microspheres were observed using scanning electron microscopy (SEM), Figure 2. The surface morphology of P(3HB) microspheres loaded with 0.75 wt% of BSA appeared smooth and more or less spherical. The P(3HB) microspheres loaded with 1.5wt% and 5wt% of BSA also appeared spherical but the surface morphology of the microspheres were less smooth.

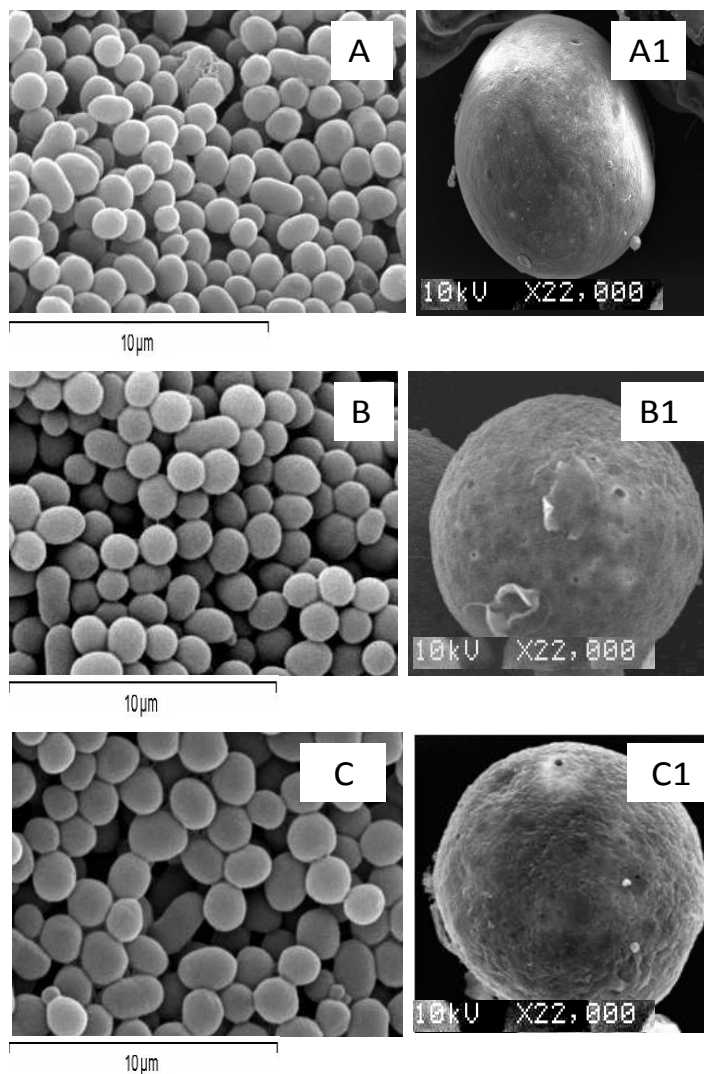


**Figure 2:- SEM image of P(3HB) microspheres loaded with A) 0.75 wt%, B) 1.5 wt% and C) 5 wt% of BSA. SEM images of the surface morphology of BSA-loaded P(3HB) microspheres at high magnification (x22,000) A1) 0.75wt%, B1) 1.5 wt% and C1) 5 wt% of BSA.**

### 7.2.1.3 Microsphere size and its distribution

The particle size distribution curve of the P(3HB) microspheres loaded with 0.75 wt%, 1.5 wt% and 5 wt% of BSA are shown in Figure 3A, B and C respectively. The particle size distribution curve of the P(3HB) microspheres loaded with 0.75 wt% of BSA shown in Figure 3A revealed that more than 50% of the measured particles had a mean particle size ranging from 1.5 $\mu$ m-2 $\mu$ m and 90% were below 5 $\mu$ m in size range. Figure 3B shows that the size range for the microspheres loaded with 1.5 wt% of BSA were around 1-15 $\mu$ m, where 50% of the measured particles had a mean particle size ranging from 1.5  $\mu$ m to 2.0 $\mu$ m and 90% of the microspheres had diameters below 5 $\mu$ m. Figure 3C shows that the size range for the microspheres loaded with 5 wt% of BSA which were around 1-10 $\mu$ m, where 90% of the measured particles had a mean particle size ranging from 1.5 $\mu$ m to 2.0 $\mu$ m and 80% of the microspheres had diameters below 5 $\mu$ m.

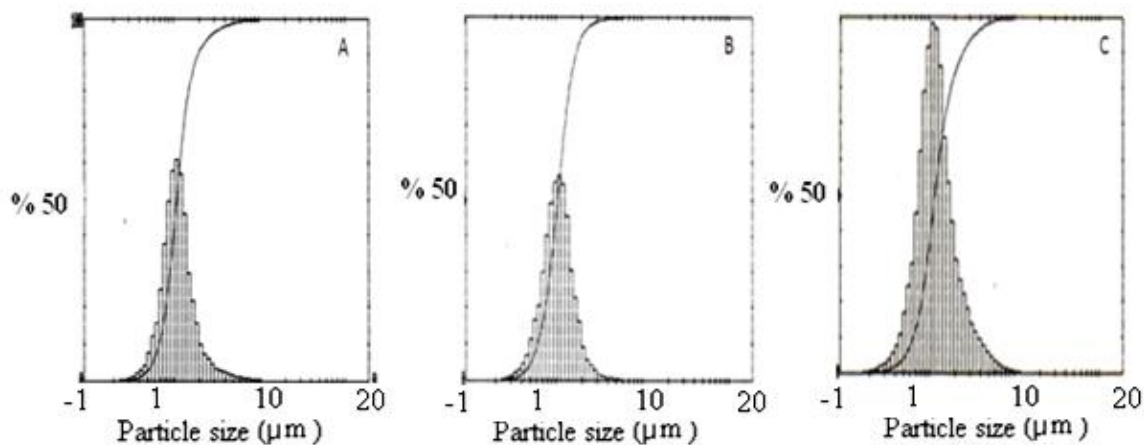


**Figure 3:- Size distribution analysis of P(3HB) microspheres loaded with A) 0.75 wt%, B) 1.5 wt% C) 5 wt% of BSA.**

The % porosity of the microspheres loaded with 0.75 wt%, 1.5 wt% and 5 wt% BSA was calculated using equation 6 from Chapter 2, section 2.8.1.3, and found to be 32%, 39% and 24%. The % residual PVA of 0.28%, 0.39% and 0.54% were found bound on the surface of the microspheres loaded with 0.75 wt%, 1.5 wt% and 5 wt% of BSA.

## 7.2.1.4 Encapsulation efficiency

The encapsulation efficiencies, surface associated proteins and the total amount of BSA remaining in the PVA solution for the different loadings of BSA in the microspheres are represented in Figure 4. The encapsulation efficiencies were calculated using equation 1, Chapter 2, section 2.4.1. The encapsulation efficiency of the P(3HB) microspheres loaded with 0.75 wt%, 1.5 wt% and 5 wt% of BSA were 58.1%, 50% and 69.4% respectively. The surface associated proteins bound onto the microspheres were 9%, 13.93% and 8.36% for 0.75 wt%, 1.5 wt% and 5 wt% of BSA respectively. The total amount of BSA remaining in the final PVA solution of the microspheres fabricated with 0.75 wt%, 1.5 wt% and 5 wt% were 32.58%, 29.63% and 18.64% respectively.

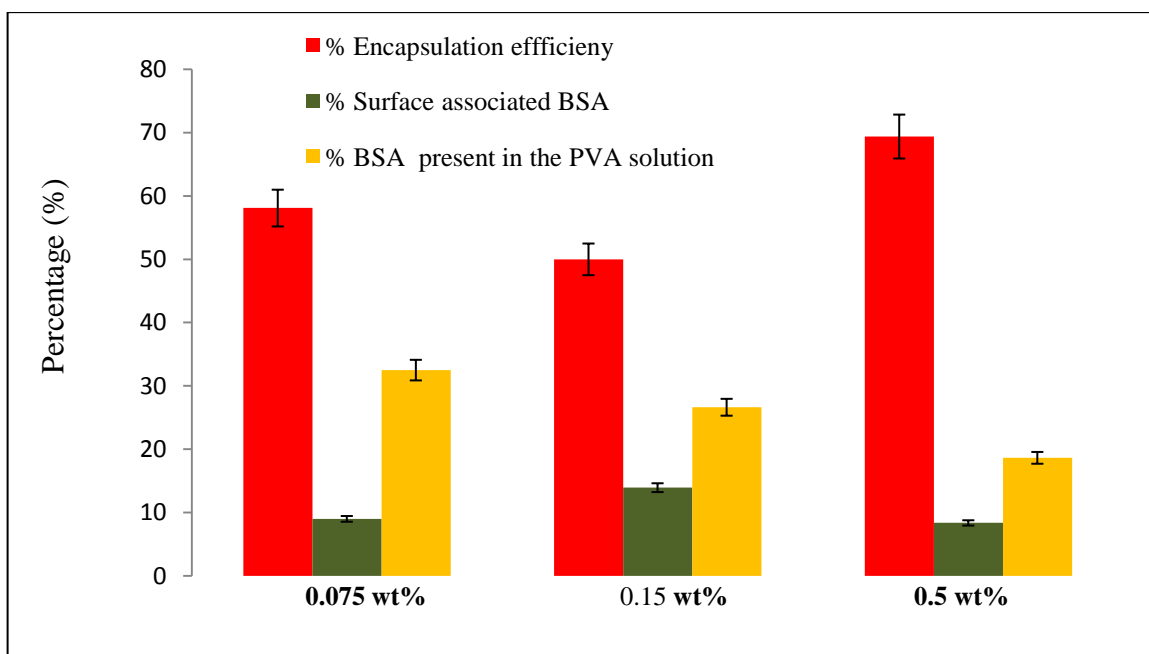


**Figure 4:- Encapsulation efficiency, % of surface associated BSA and % of BSA present in the PVA solution for different BSA loadings, ( $n=3$ ; error= $\pm$ s.d).**

7.2.1.5 *In vitro* release kinetics of BSA

*In vitro* BSA release from the P(3HB) microspheres with different BSA loadings were carried out in PBS solution and contact lens solution. The contact lens solution was used to mimic the ocular environment. A biphasic release profile was observed, as shown in Figure 5. The BSA loaded P(3HB) microspheres in the PBS solution exhibited a higher initial burst release of the actual BSA loading when compared to the P(3HB) microspheres in contact lens solution (Figure 6).

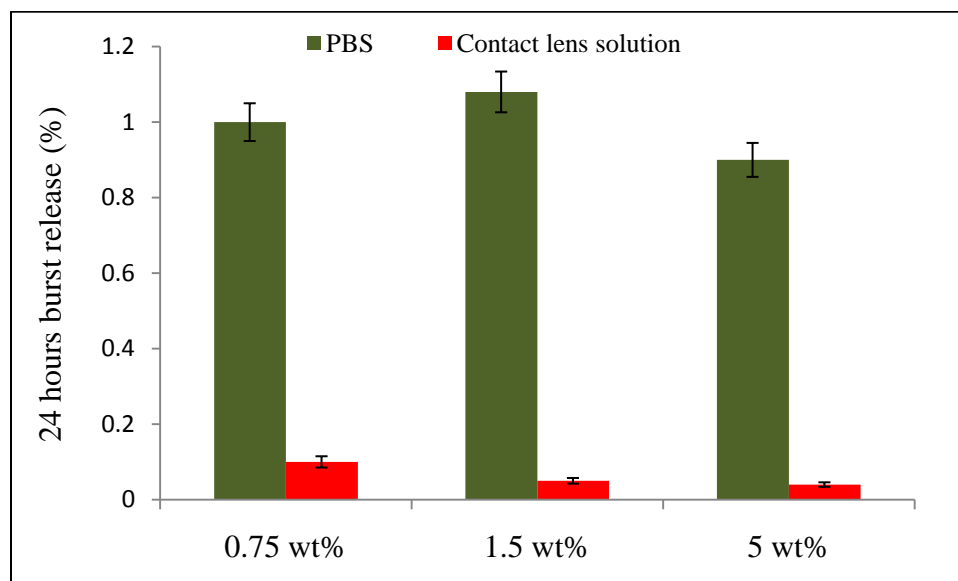


**Figure 5:-The 24 hour burst release of BSA in PBS and contact lens solution, ( $n=3$ ; error= $\pm$ s.d).**

The P(3HB) microspheres loaded with 0.75 wt%, 1.5 wt% and 5 wt% of BSA exhibited an initial burst release of 1%, 1.08% and 0.9% whereas the initial burst exhibited by the BSA loaded P(3HB) microspheres in contact lens solution was 0.1%, 0.05% and 0.04% respectively. A maximum cumulative percentage release observed for the 0.75 wt%, 1.5 wt% and 5 wt% BSA loaded microspheres in PBS, were 15.87%, 59.83%, and slightly higher than 100% (indicating slight overestimation of the protein) BSA respectively, as shown in Figure 6A. Similarly a maximum cumulative percentage release of 5.4%, 14.60%, and 52.46% was observed for the 0.75 wt%, 1.5 wt% and 5 wt% BSA loaded microspheres in the contact lens solution as shown in Figure 6B.

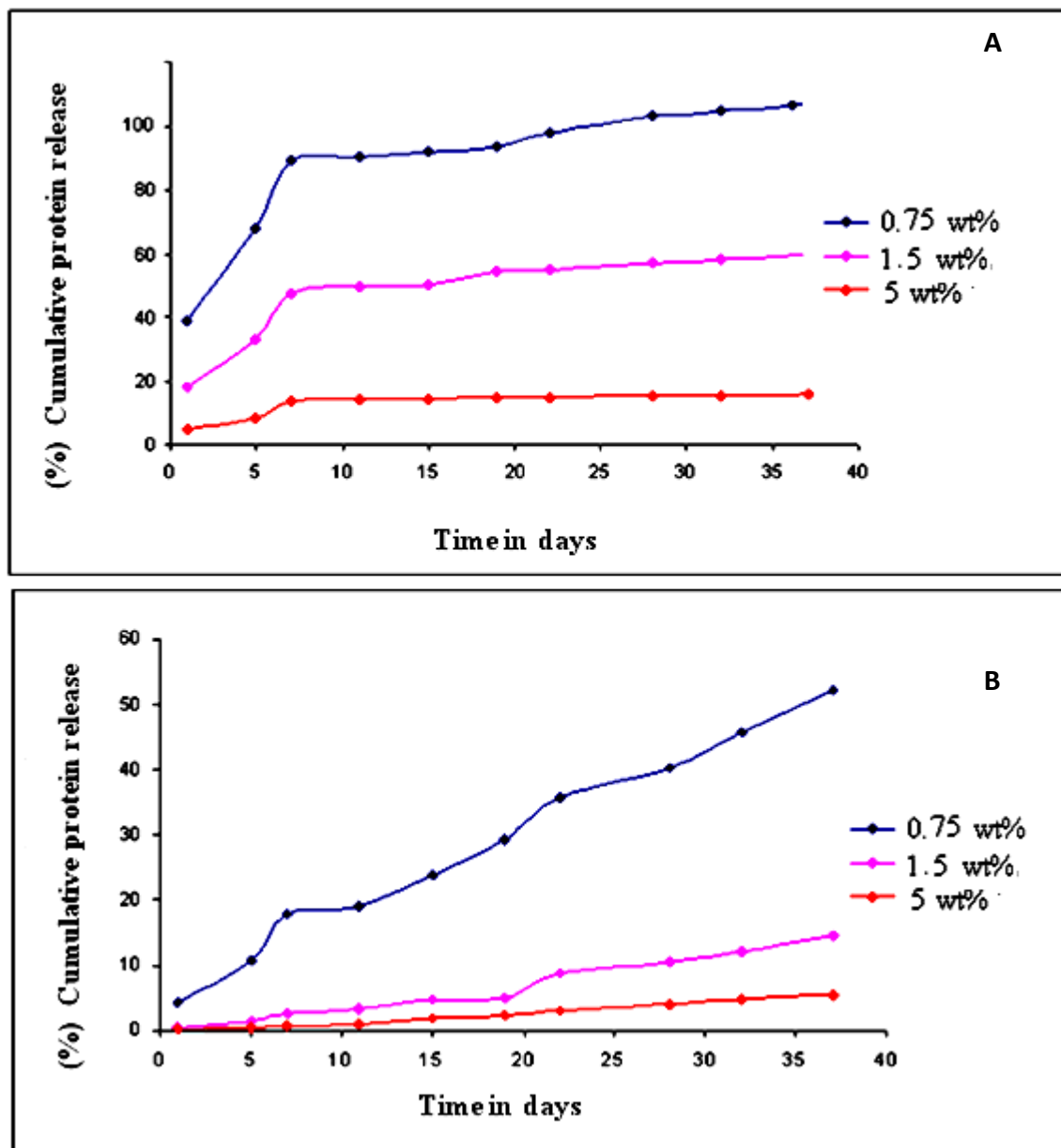


Figure 6:-A) *In vitro* cumulative release profiles of BSA loaded P(3HB) microspheres in PBS and B) contact lens solution (the initial amount of BSA loaded is indicated on the graph), ( $n=3$ ; error= $\pm$ s.d).

7.2.1.6 *In vitro* degradation studies

The *in vitro* degradation of the P(3HB) microspheres were carried out in contact lens solution and PBS solution at 37°C under static conditions for a period of 30 days. The parameters measured in order to assess the degradation behaviour of P(3HB) microspheres were, the water uptake (%WA) and weight loss (%WL) studies, pH changes and SEM to observe changes in the surface morphology. As seen in Figure 7A, the %WA of the P(3HB) microspheres in the PBS solution increased from 148.4% on day 1 to 250% over a period of 30 days. The %WL of the P(3HB) microspheres on day 1 was 13% followed by an increase to 45.16% over a period of 30 days. The %WA of the P(3HB) microspheres in the contact lens solution from day 1 to day 30 increased from 105% to 156.9%. Similarly, an increase in the %WL of the P(3HB) microspheres from 8% to 30.23% from day 1 to day 30 was observed (Figure 7B).

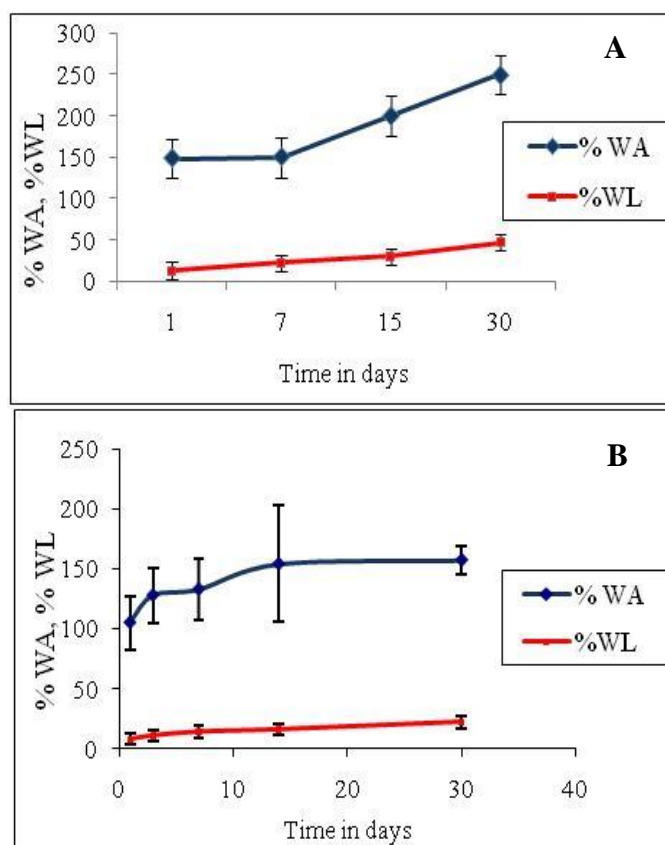
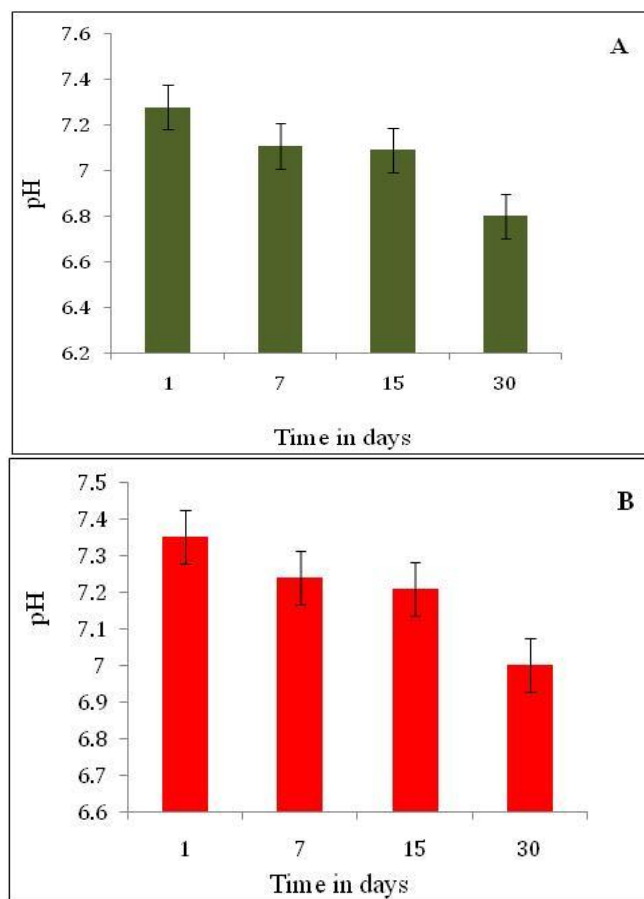


Figure 7:- Water adsorption and weight loss measurements after immersion in A) PBS and B) contact lens solution, ( $n=3$ ; error= $\pm$ s.d).

## 7.2.1.6.1 Changes in pH

The pH of PBS solution as well the contact lens solution was monitored for a period of 30 days to analyse the changes in the surrounding medium induced by the immersion of P(3HB) microspheres. The pH of the PBS solution exhibited a gradual decrease in the pH of the solution from 7.28 to 6.8, from day 1 to day 30, as seen in Figure 8A. Similarly the pH of the contact lens solution also exhibited a gradual decrease from 7.35 to 7.0 over a period of 30 days (Figure 8B).



**Figure 8:-** A) Changes in the pH of PBS over a period of 30 days was significant ( $F(2,6)=3.23$ ),  $**p<0.001$ . A Bonferroni Post Hoc was applied and significant differences at  $***p<0.0001$  on day 30 was observed when compared to day 1, day 7 and day 15. No significant differences between day 1, day 7 and day 15 were observed. B) Changes in the pH of the Contact lens solution containing P(3HB) microspheres was significant  $*** p<0.0001$ . ( $n=3$ ; error= $\pm$ s.d). A Bonferroni Post Hoc was applied and significant differences at  $***p<0.0001$  on day 30 was observed when compared to day 1, day 7 and day 15. No significant differences between day 1, day 7 and day 15 were observed.

### 7.2.1.6.2 Examination of surface morphology after *in vitro* degradation

The surface morphology of the P(3HB) microspheres after *in vitro* degradation studies carried out both in PBS (Figure 9A) and contact lens solution (Figure 9B) for a period of 30 days, as examined by SEM, remained smooth and spherical with no changes to its surface morphology. However in the contact lens solution traces of degradation was observed in the 30 day sample. The contact lens solution should be more representative of the intraocular environment.

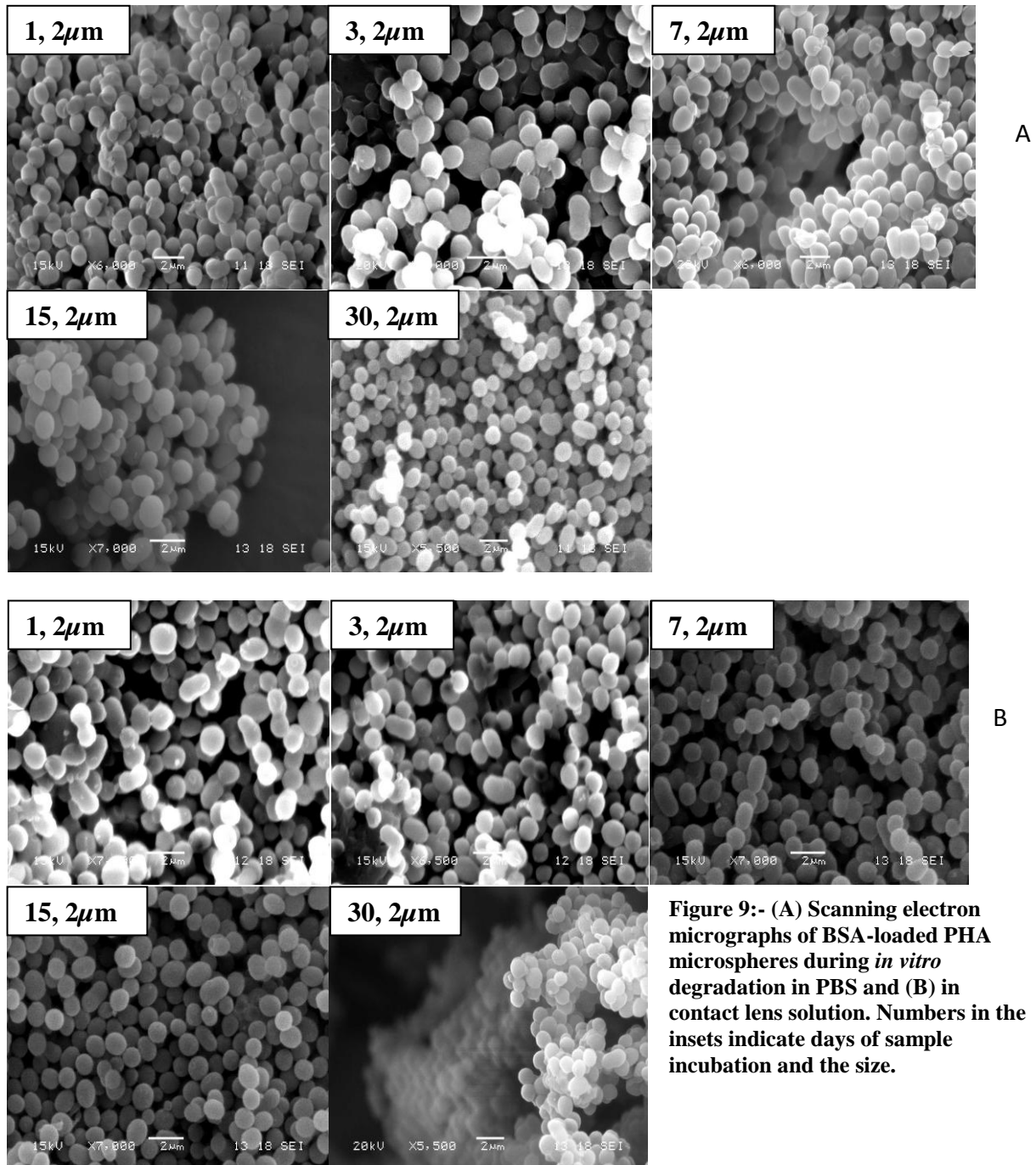


**Figure 9:- (A) Scanning electron micrographs of BSA-loaded PHA microspheres during *in vitro* degradation in PBS and (B) in contact lens solution. Numbers in the insets indicate days of sample incubation and the size.**

### 7.2.1.7 Protein profile of the BSA entrapped in the microspheres and released into PBS and contact lens solution observed using SDS-PAGE

The protein profile of the microsphere entrapped BSA and released was studied using SDS-PAGE as shown in Figure 10. From the gel, a single band corresponding to the  $M_w$  of BSA (66,200 Da), identical to that found in the control lanes were observed at all time points.

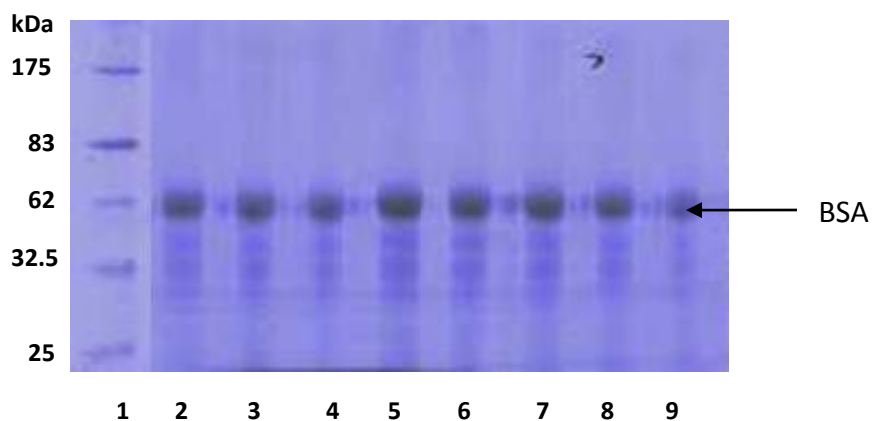


**Figure 10:- SDS-PAGE results of BSA samples taken after different time points.**

Lane 1,  $M_w$  marker, Lane 2, 5, normal BSA solution used as controls. Lanes 3&4, BSA released from microspheres into PBS and contact lens solution respectively, on day 1. Lanes 6&7, BSA released from microspheres into PBS and contact lens solution respectively, on day 14 and Lane 8 & 9, BSA released from microspheres into PBS and contact lens solution on day 28 of the *in vitro* release study.

## 7.2.2 Lucentis<sup>®</sup> encapsulation studies

### 7.2.2.1 Characterization of P(3HB) microspheres entrapped with Lucentis<sup>®</sup>

The bulk shape and structure of the 5 wt% Lucentis<sup>®</sup> loaded microspheres were observed using scanning electron microscopy (SEM) (Figure 11A). Figure 11B shows spherical microspheres with a more or less uniform shape and structure. From the particle size distribution curve as shown in Figure 11C, revealed that more than 50% of the measured particles had a mean particle size ranging from 1.5 $\mu\text{m}$ -2 $\mu\text{m}$  and 90% were below 5 $\mu\text{m}$  in size range. The measured sizes were compared with the SEM photomicrographs to verify accuracy. The % porosity calculated using equation 6 from Chapter 2, section 2.8.1.3 was 17.4% and the % residual PVA bound onto the surface of the P(3HB) microspheres was 0.56%.

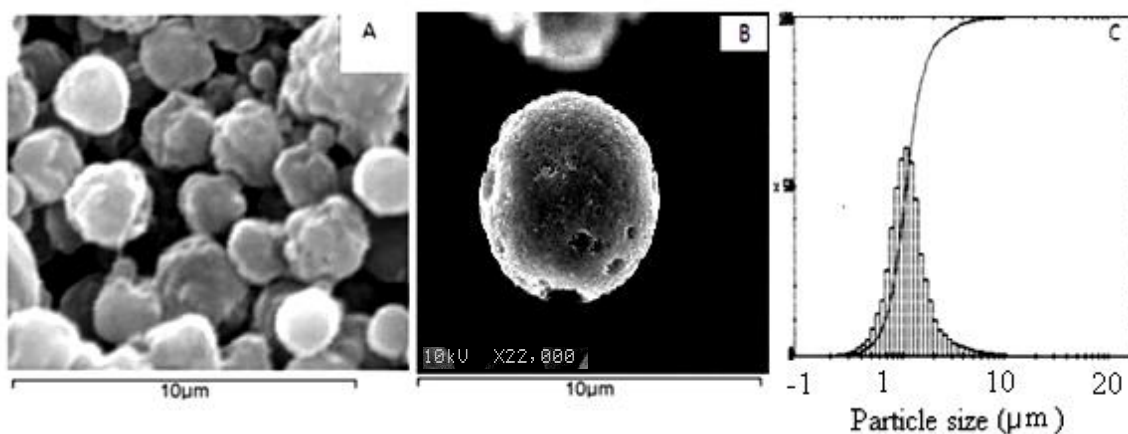


**Figure 11:- A) SEM image of Lucentis<sup>®</sup> loaded P(3HB) microspheres. B) SEM images of the surface morphology of Lucentis<sup>®</sup> loaded P(3HB) microspheres at high magnification (x22,000) C) Particle size distribution analysis of P(3HB) microspheres loaded with Lucentis<sup>®</sup>.**

## 7.2.2.2 Encapsulation efficiency

The encapsulation efficiencies (%EE), surface associated Lucentis<sup>®</sup> and the total amount Lucentis<sup>®</sup> present in the PVA solution is represented in Figure 12. The encapsulation efficiency (%EE) of the P(3HB) microspheres loaded with Lucentis<sup>®</sup> were calculated using equation 1, Chapter 2, section 2.4.1. The % EE of the P(3HB) microspheres loaded with 5 wt% (5mg/100mg) of Lucentis<sup>®</sup> was 48%. The total amount of Lucentis<sup>®</sup> present in the final PVA solution was 38% and the surface associated proteins bound to the microspheres were 13%

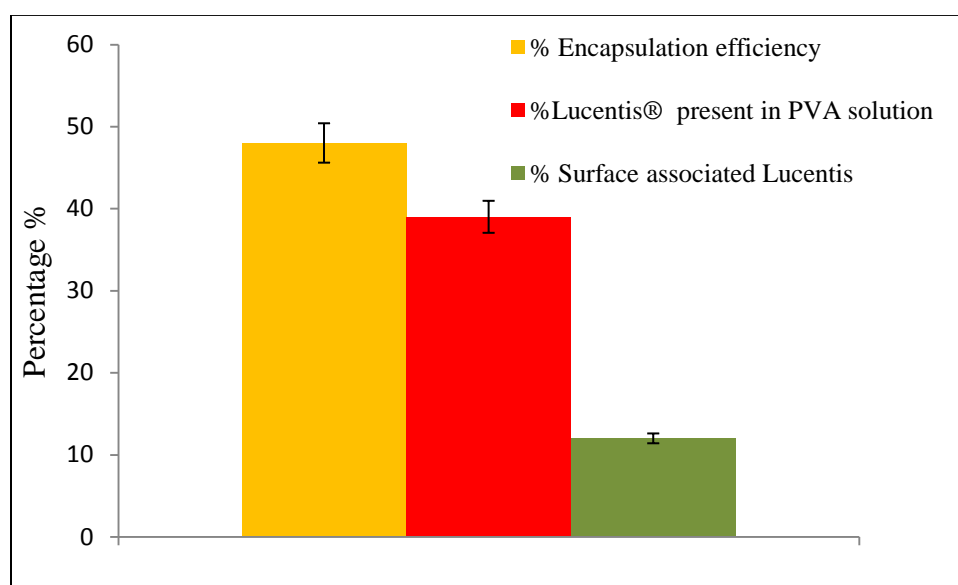


**Figure 12:-** The percentage encapsulation efficiency, percentage of surface associated protein and percentage of Lucentis<sup>®</sup> present in the PVA solution of the Lucentis<sup>®</sup> loaded microspheres, ( $n=3$ ; error= $\pm$ s.d).

### 7.2.2.3 *In vitro* release kinetics of Lucentis<sup>®</sup>

*In vitro* Lucentis<sup>®</sup> release from the P(3HB) microspheres were carried out in PBS solution and contact lens solution. The contact lens solution was used to mimic the ocular environment. A triphasic release profile was observed, as shown in Figure 13. The Lucentis<sup>®</sup> loaded P(3HB) microspheres in the PBS solution exhibited a higher initial burst release of 12% when compared to 9% in the contact lens solution after 24 hours of immersion. Following an initial burst release, a gradual increase in the release was observed until 40 days after which a steady sustained release was observed for a period of 75 days. A maximum cumulative percentage release of 57% was observed for the Lucentis<sup>®</sup> loaded microspheres in PBS and a maximum cumulative percentage release of 39% was observed for the Lucentis<sup>®</sup> loaded microspheres in contact lens solution after a period of 75 days, as shown in Figure 13.

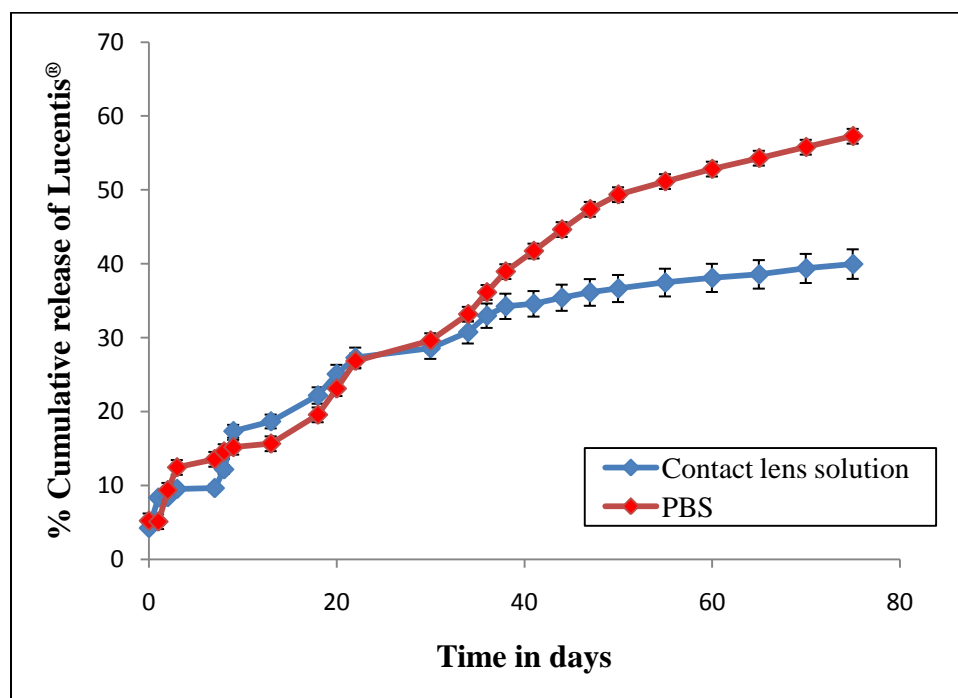
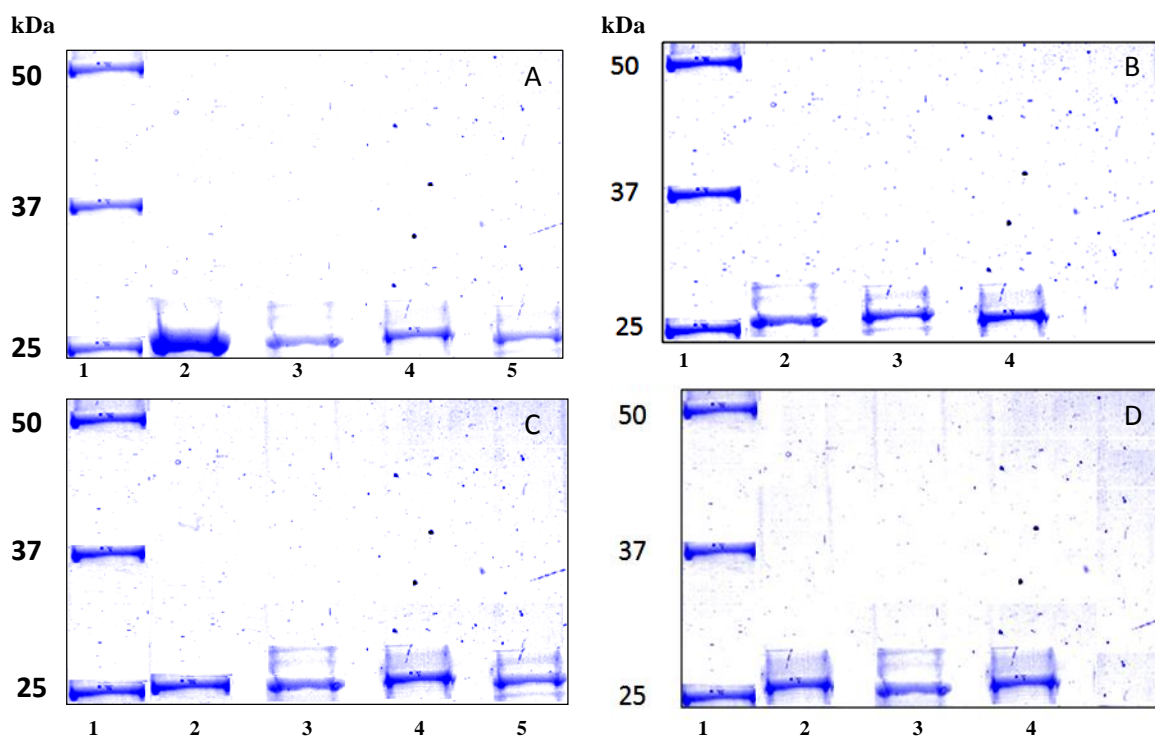


Figure 13:-*In vitro* release profile of Lucentis<sup>®</sup> from P(3HB) microspheres, ( $n=3$ ; error= $\pm$ s.d).

#### 7.2.2.4 Protein profile of Lucentis<sup>®</sup> entrapped in the P(3HB) microspheres and released into PBS and contact lens solution observed using SDS-PAGE

The protein profile of the microsphere entrapped Lucentis<sup>®</sup> and released was studied using SDS-PAGE as shown in Figure 14. From the gel, a single band corresponding to the heavy and light chain of Lucentis<sup>®</sup> (23,00 Da and 25,000 Da), identical to that found in the control lanes were observed at all time points.



**Figure 14:- SDS-PAGE results of Lucentis<sup>®</sup> samples released from P(3HB) microspheres after different time points.**

- A) Lane 1,  $M_w$  marker, Lane 2, Lucentis<sup>®</sup> solution used as control, Lanes 3, 4, & 5, Lucentis<sup>®</sup> released from microspheres into PBS on day 1, day 15 and day 30 respectively of the *in vitro* release study.
- B) Lane 1,  $M_w$  marker, Lane 2, 3, & 4 Lucentis<sup>®</sup> released from microspheres into PBS on day 45, day 60 and day 75 respectively of the *in vitro* release study.
- C) Lane 1,  $M_w$  marker, Lane 2 Lucentis<sup>®</sup> solution used as control. Lanes 3, 4, & 5 Lucentis<sup>®</sup> released from microspheres into contact lens solution on day 1, day 15 and day 30 respectively of the *in vitro* release study.
- D) Lane 1,  $M_w$  marker, Lane 2, 3, & 4 Lucentis<sup>®</sup> released from microspheres into contact lens solution on day 45, day 60 and day 75 of the *in vitro* release study.

### 7.2.3 RNase A encapsulation studies

#### 7.2.3.1 Characterization of P(3HB) microspheres entrapped with RNase A

The bulk shape and structure of the 50 wt% RNase A loaded microspheres were observed using scanning electron microscopy (SEM) (Figure 15A). Figure 15B shows spherical microspheres with a more or less uniform shape and structure.

#### 7.2.3.2 Microsphere size and size distribution

From the particle size distribution curve as shown in Figure 15C, more than 80% of the measured particles had a mean particle size ranging from  $1.5\mu\text{m}$ - $2\mu\text{m}$  and 20% were below  $5\mu\text{m}$  in size range. The measured sizes were compared with the SEM photomicrographs to verify accuracy. The average % porosity calculated using equation 6 from Chapter 2, section 2.8.1.3 was 12.34% was and the % residual PVA bound onto the surface of the P(3HB) microspheres was 0.6%.

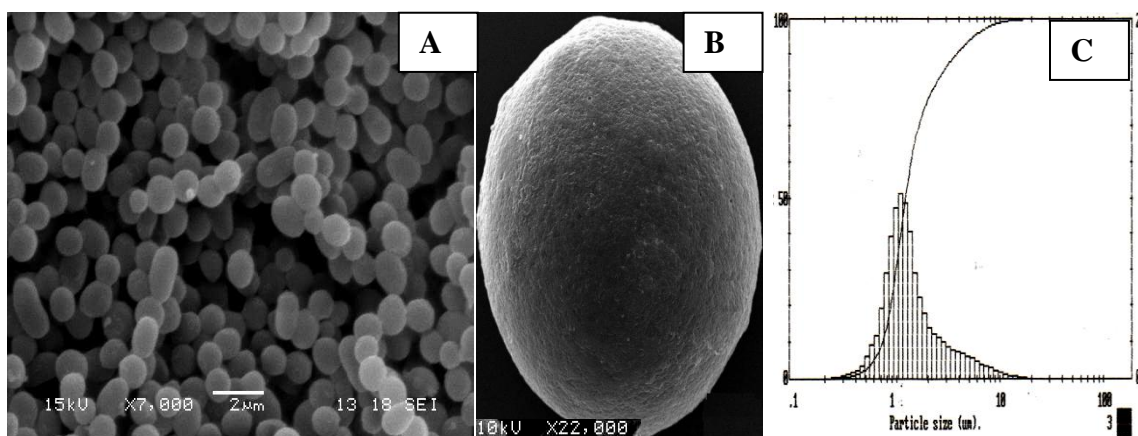


**Figure 15:- A) SEM image of P(3HB) microspheres. B) SEM images of the surface morphology of RNase A loaded P(3HB) microspheres at high magnification (x22,000) C) Particle size distribution analysis of P(3HB) microspheres.**

## 7.2.3.3 Encapsulation efficiency

The encapsulation efficiencies (%EE), surface associated RNase A and the total amount of RNase A present in the PVA solution is represented in Figure 16. The encapsulation efficiencies of the P(3HB) microspheres loaded with RNase A were calculated using equation 1, Chapter 2, section 2.4.1. The % EE of the P(3HB) microspheres loaded with 50 mg of RNase A was 48%. The surface associated proteins bound to the microspheres were 8.6% and the total amount of RNase A present in the final PVA solution was 43%.

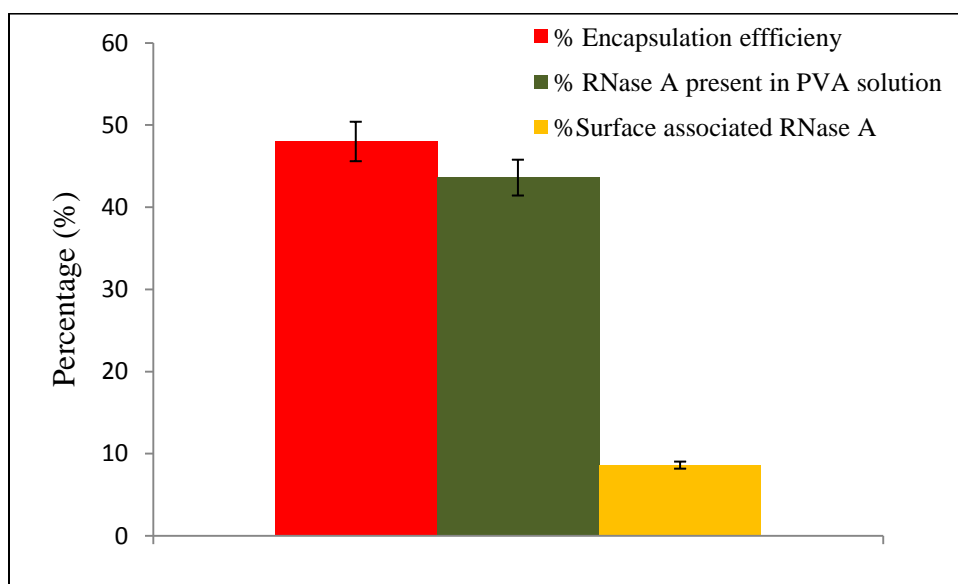


**Figure 16:-** The percentage encapsulation efficiency, percentage of surface associated protein and percentage of protein present in the PVA solution of the RNase A loaded microspheres, ( $n=3$ ; error= $\pm$ s.d).

#### 7.2.3.4 *In vitro* release kinetics of RNase A

*In vitro* release studies were performed by monitoring the release of RNase A in pH 7.4, PBS solution at 37°C. The amount of RNase A released at each sampling point, determined by the BCA assay, was plotted as a function of time in Figure 17. The *in vitro* release was characterised by an initial burst release of 8.4% in 24 hours followed by a slower release profile. The % cumulative release achieved at the end of 30 days was 68.7%.

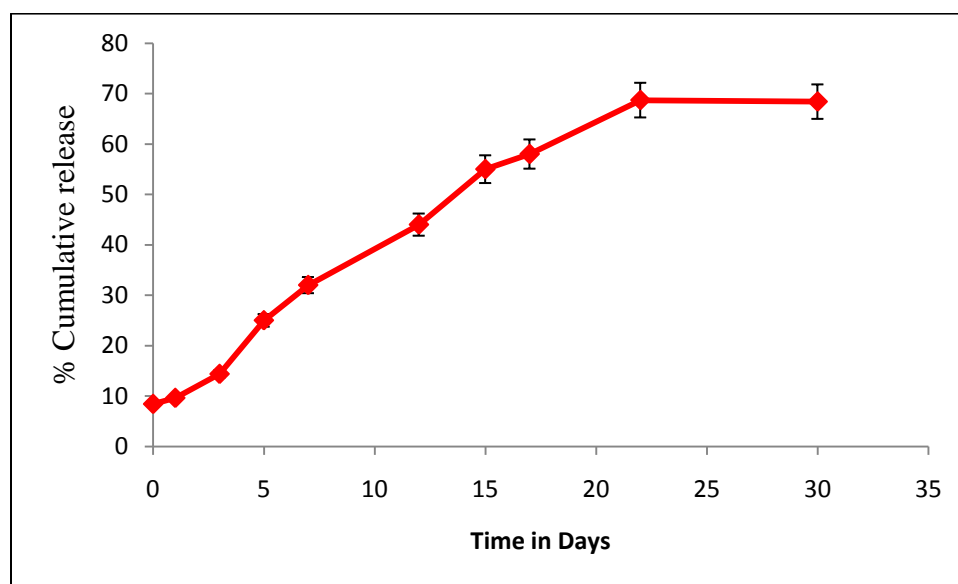


Figure 17:-*In vitro* release profile of RNase A from P(3HB) microspheres, ( $n=3$ ; error= $\pm$ s.d).

### 7.2.3.5 Stability of RNase A entrapped in the microspheres

#### 7.2.3.5.1 Fluorescence studies

Fluorescence emission scans were used to determine the changes in tyrosine residues present in the RNase A structure, which has a maximum emission spectra around 303 nm. The fluorescence emission scans of the control and RNase A entrapped within the P(3HB) microspheres after chloroform treatment is represented in Figure 18. From the results both the spectra appear to be super imposable with maximum emission observed at 303 nm.

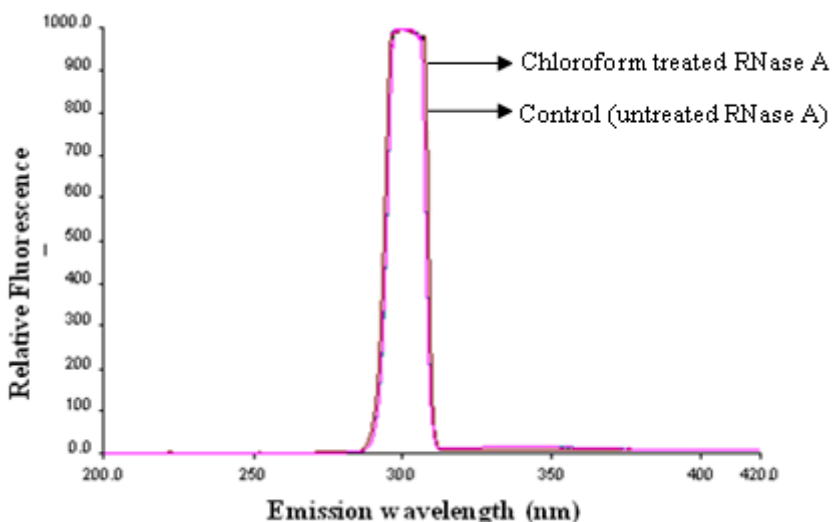
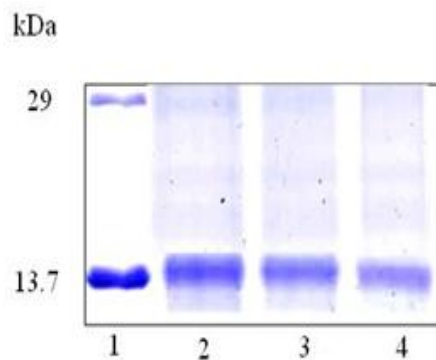


Figure 18:-Fluorescence spectra of chloroform-treated RNase A as compared to the untreated RNase A.

### 7.2.3.5.2 Protein profile of the RNase A entrapped microspheres observed using SDS-PAGE

The protein profile of the solvent treated RNase A entrapped within P(3HB) microspheres was determined using a 15% gel, (Figure 19). From the gel, the band corresponding to the  $M_w$  of RNase A (13,700 Da) was found to be identical to that found in the control lanes 2, lane 3 (free RNase A placed in contact with unloaded microspheres and subjected to the same release medium and temperature) and lane 4 (chloroform treated RNase A). Thus the structural integrity of RNase A was confirmed during the extended release periods.



**Figure 19:- SDS-PAGE results of RNase A samples.**

**Lane 1,  $M_w$  marker, Lane 2, Control, Lane 3, free RNase A placed in contact with the placebo microspheres and subjected to the same release medium and temperature and Lane 4, chloroform treated RNase A.**

## 7.2.3.6 Enzyme activity of RNase A using methylene blue assay

The Ribonuclease (RNase A) released from the P(3HB) microspheres and the RNase A (used as a control not subjected to the microsphere fabrication conditions) were assayed for a period of 30 days by monitoring the shift in the absorbance maximum of methylene blue (688 nm) upon intercalation into intact RNA. From the results, the specific enzyme activity of RNase A released from the P(3HB) microspheres was 12 EU/mg on day 0 when compared to 24.4 EU/ $\mu$ g of the RNase A not subjected to the microsphere fabrication conditions. The enzyme activity continued to decrease from day 1 to day 30. For example on day 30 the specific enzyme activity of RNase A released from the P(3HB) microspheres had reduced to 0.13 EU/ $\mu$ g when compared to the control which had reduced to 0.22 EU/ $\mu$ g (Figure 20). % decline in the enzyme activity of the control and release samples expressed over a period of 30 days is represented in Figure 21.

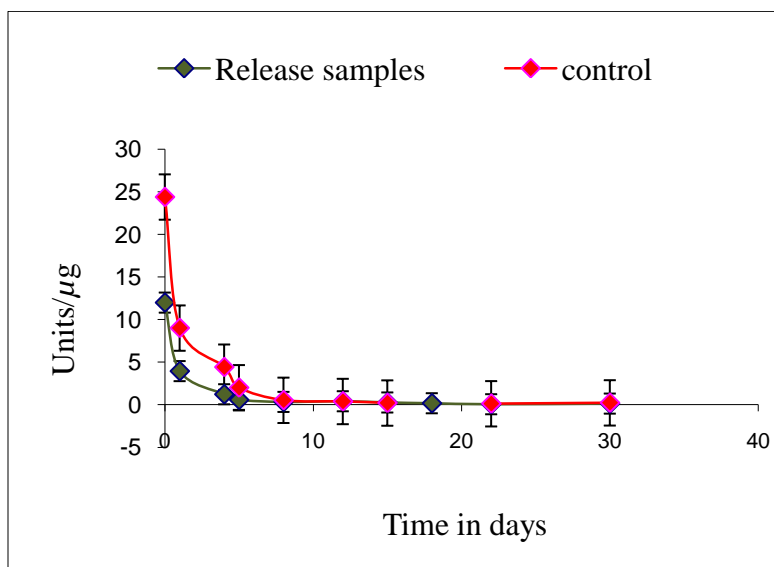


**Figure 20:- A decline in the intercalation of methylene blue by RNase A was observed over a period of 30 days, ( $n=3$ ; error= $\pm$ s.d).**

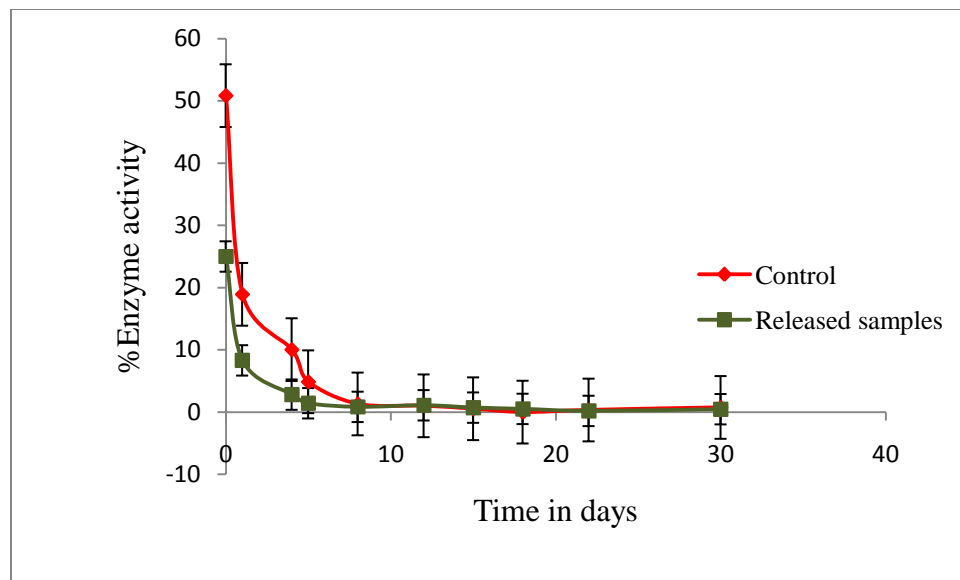


Figure 21:- % enzyme activity of the control and release samples expressed over a period of 30 days, ( $n=3$ ;error= $\pm$ s.d).

## 7.3 Discussions

### 7.3.1 Protein loaded P(3HB) microsphere characterizations

#### 7.3.1.1 Bulk shape and structure of the protein loaded microspheres

The bulk shape and structure of the bovine serum albumin (BSA), Lucentis<sup>®</sup> and ribonuclease A (RNase A) loaded microspheres when observed under SEM appeared more or less spherical with uniform shape and structure and did not appear to be aggregated. The results from the optical micrographs revealed microspheres with a hollow inner core during the first emulsion phase (w/o). However, in the second emulsion phase, micro droplets of water with a honeycomb structure within the emulsion droplets were observed. The volume of the oil-phase, *i.e* 50mL and the solvent evaporation rate used in this study had a significant effect on the internal morphology of microspheres. At a lower oil-phase volume, the polymer is known to be concentrated and viscous; as a result it is difficult to break the internal water into smaller droplets during the first emulsion phase. Thus at a rapid solvent evaporation rate and polymer precipitation, large hollow spaces are formed. However, at a higher oil phase volume and rapid solvent evaporation rate the microspheres solidify quickly. As a result the water droplets that diffuses into the microspheres forming honeycomb structures. These solidified microspheres then prevent further influx of water into the microspheres thereby preventing them from coalescing together and forming large hollow spaces (Jayanthi *et al.*, 1996). In a similar study conducted by Yang *et al.*, uniform honeycomb structures within the PLGA microspheres were observed when 250 mL of the second oil phase volume was used. However when 9 mL was used in the first oil phase, microspheres with a hollow inner core was observed (Yang *et al.*, 2001). Thus in this study the second oil phase volume of 250 mL during microsphere fabrication could have contributed to the formation of small spherical porous microspheres. This is desirable for controlled drug delivery applications as the drugs can be entrapped within these porous structures, thereby contributing to a controlled release

### 7.3.1.2 Particle size analysis

For controlled release applications microsphere particle size plays an important role. For example for ophthalmic delivery, an increase in size to  $10\mu\text{m}$  is known to cause patient discomfort and blurring of vision. In this study, the size of the P(3HB) microspheres encapsulating BSA, as revealed by the particle size analyser, was of an average size of  $1.5\mu\text{m}$  to  $2.0\mu\text{m}$ . Similarly the Lucentis<sup>®</sup> loaded P(3HB) microspheres were also of an average size of  $1.5\mu\text{m}$  to  $2.0\mu\text{m}$  which is ideal for use in intraocular drug delivery. The RNase A loaded P(3HB) microspheres also exhibited 80% of the mean particle size ranging from  $1.5\mu\text{m}$ - $2\mu\text{m}$  and 20% below  $5\mu\text{m}$  in size range. Although the molecular weights of the proteins encapsulated, *i.e.* BSA (66.2 kDa) Lucentis<sup>®</sup> (48 kDa) and RNaseA (13.7 kDa), were different, the microsphere size was not affected by this. Sandor *et al.*, made similar observations, where no differences in the average poly(lactic-co-glycolic acid), PLGA, microsphere size was seen when encapsulated with different molecular weight proteins such as BSA (66.2kDa) and lysozyme (14.3kDa). The average sizes of the microspheres observed were in the range of  $2.23\mu\text{m}$  (Sandor *et al.*, 2001). The size of the microspheres is known to be affected by a number of processing factors such as viscosity of the polymer solution, stirrer speed and the PVA concentration used in the external phase, as mentioned in Chapter 3, section 3.3.1. For BSA, Lucentis<sup>®</sup> and RNase A encapsulation, in this study, the stirrer speed could have contributed to the formation of  $2\mu\text{m}$  sized microspheres. The stirrer speed of 800 rpm was probably high enough to disperse the second emulsion into small droplets due to which smaller sized microspheres were produced. Igartua *et al.*, observed the formation of uniform sized PLGA microspheres with an average size of  $1.32\mu\text{m}$  when a stirrer speed of 9500 rpm was used (Igartua *et al.*, 1998). As mentioned in earlier in Chapter 3, section 3.3.1 and 3.3.2, an increase in the PVA and polymer concentration is known to increase the viscosity in the emulsion phase, which in turn leads to the production of larger sized microspheres. However there is a maximum PVA and polymer concentration which influences the size of the microsphere beyond which an increase in the viscosity does not have any further influence on the size of the microspheres and the stirrer speed dominates (Lee *et al.*, 1999). For example Lee *et al.*, observed that at a polymer concentration of 6 wt%, an increase in the PVA concentration from 0.1% w/v to 1% w/v

and an increase in the stirrer speed from 2500 rpm to 5000 rpm, the microspheres sizes appeared similar at  $2.0\mu\text{m}$  and  $2.1\mu\text{m}$ . The authors' observed that although the PVA and polymer concentration is important up to maximum concentration, the stirrer speed had dominated leading to the formation of small sized microspheres (Lee *et al.*, 1999). The results from this study also further indicate that microspheres sizes were influenced by the stirrer speed which had contributed to the formation of small sized microspheres.

#### 7.3.1.3 Surface morphology

The BSA, Lucentis<sup>®</sup> and RNase A loaded P(3HB) microspheres when examined under SEM appeared smooth and spherical. The type of protein loading did not affect the morphology of the microspheres. However the P(3HB) microspheres with the higher BSA loading of 1.5wt% and 5wt% and the Lucentis<sup>®</sup> loaded microspheres appeared slightly rough due to the presence of surface associated proteins. In a study conducted by Bouissou *et al.*, the surface morphologies of the poly(lactic-co-glycolic acid) PLGA microspheres encapsulated with fibronectin prepared using different surfactants such as PVA, Igepal and Triton X-100 were compared. The PLGA microspheres prepared using PVA appeared smooth and uniform when compared to the rough surface morphology of the microspheres prepared with other surfactants such as Igepal and Triton X-100. The authors' had observed that the reduced surfactant viscosity while using PVA was responsible for the production of a smooth surface morphology when compared to the other surfactants used (Bouissou *et al.*, 2004). In this study PVA used as surfactant in the emulsion could have also contributed to the formation of a smooth microsphere surface. The microsphere wall is also known to vary in both thickness and porosity depending on the varying temperatures during solvent evaporation (Yang *et al.*, 2001). At higher temperatures, microspheres with highly porous outer walls are formed due to the rapid solvent evaporation. Since the solvent evaporation was carried out at room temperature in this study, smooth surfaced microspheres were produced in most cases.

#### 7.3.1.4 Porosity

The BSA (66.2kDa) loaded P(3HB) microspheres with different loadings exhibited an internal porosity of 32%, 39% and 24%, while Lucentis<sup>®</sup> (48kDa) and RNase A

(13.7kDa) loaded microspheres had exhibited a lower internal porosity of 17% and 12%. Thus the % porosity of the P(3HB) microspheres in this study varied with the type of protein encapsulated. Often the microspheres encapsulating smaller molecular weight proteins are known to have reduced number of pores within the microspheres. On the other hand, the microspheres encapsulating larger molecular weight proteins such as BSA are known to have an increased number of pores (Sandor *et al.*, 2001). These observations correlated with the results obtained in this study where P(3HB) microspheres encapsulating the high molecular weight proteins such as BSA and Lucentis<sup>®</sup> exhibited higher porosity when compared to the microspheres encapsulating lower molecular weight protein such as RNase A.

#### 7.3.1.5 Protein encapsulation efficiency

The highest encapsulation efficiency of 70% was observed in microspheres that were loaded with 5 wt% of BSA when compared to the microspheres loaded with lower concentrations of BSA. As expected, in this case the amount of microsphere surface associated protein was relatively low and the amount of protein that was lost in the PVA solution was also the lowest. The viscosity of the outer emulsion phase with the increasing BSA concentration would have increased, which would have further inhibited the BSA diffusion from the microspheres into the outer oily phase comprising of PVA, solvent and water. As a result, a higher BSA distribution within the microspheres with 5 wt% BSA was observed when compared to the P(3HB) microspheres with lower BSA loadings.

P(3HB) microspheres loaded with 5wt% of Lucentis<sup>®</sup> exhibited an encapsulation efficiency of 48% and a surface associated protein of 13%. The average microsphere pore size is affected by the molecular weight of the proteins. Therefore, with an increase in the molecular weight of the proteins, an increase in the average pore size of the microsphere is observed. For example Sandor *et al.*, observed an average pore size of 40nm for microspheres encapsulating larger proteins such as BSA (66.2kDa) and an average pore size of 20nm for microspheres encapsulating lysozyme (13.4kDa) (Sandor *et al.*, 2001). The molecular weight of Lucentis<sup>®</sup> (48kDa) encapsulated within P(3HB) microspheres in this study was slightly smaller than the molecular weight of BSA,

therefore the average pore size of the microspheres may be similar. However, a non-denaturing PAGE, which is known to preserve the covalently and non-covalently bonded aggregates, should be carried out in the future to confirm the absence of protein aggregates. Higher molecular weight proteins are known to be compact in nature thus getting entangled within the polymeric device and affecting the *in vitro* drug release kinetics (Pouton *et al.*, 1996). Nevertheless during microsphere fabrication, Lucentis<sup>®</sup> may have diffused from within the microspheres due to its lower molecular weight in comparison to the molecular weight of BSA and got bound onto the surface of the microspheres. This could probably explain the higher percentage of surface associated protein (13%) and lower encapsulation efficiency (48%) when compared to 8% of surface associated protein and 70% encapsulation efficiency on the 5wt% BSA loaded P(3HB) microspheres.

RNase A loaded P(3HB) microspheres in this study exhibited an encapsulation efficiency of 48%. The encapsulation efficiency is also influenced by the distribution of pores within the microspheres, which in turn is affected by the molecular weight of the proteins. For example microspheres encapsulating larger molecular proteins are known to exhibit large open pores at the surface of the microspheres and dense layers within the microspheres. Due to this the encapsulation of the large molecular weight proteins within the microspheres is reduced. However, by increasing the microsphere size a higher encapsulation of larger molecular weight proteins could be achieved, as these proteins will largely be present within the core of the microspheres. On the other hand microspheres encapsulating proteins with smaller molecular weight have a uniform pore distribution where the proteins are entrapped largely within the microspheres thus exhibiting higher encapsulation efficiency. For example Sandor *et al.*, observed that microspheres encapsulating smaller molecular weight proteins such as Lysozyme (13.4kDa) exhibited uniformly distributed open branched network of pores within the microspheres. These microspheres exhibited a higher encapsulation efficiency of 80% when compared to the lower encapsulation efficiency of 45% when BSA (66.2 kDa) used which exhibited large open pores at the surface of the microspheres. Thus in this study an encapsulation efficiency of 48% of RNase A (13.7 kDa) was observed probably due to the encapsulation of the protein within the core of the microspheres. In another relevant

study Murata *et al.*, also observed an encapsulation efficiency of 48% of small interfering RNA (siRNA) within PLGA microspheres with an average size of 35-45 $\mu$ m. However, in order to increase the encapsulation efficiencies, they used carriers such as arginine. Due to the ionic interaction between the terminal carboxylic anions of PLGA and the basic amino acid groups of the arginine, a rigid structure of the PLGA microspheres were formed resulting in an increased encapsulation efficiency of 64.3% (Murata *et al.*, 2008).

### 7.3.2 In vitro release studies

#### 7.3.2.1 BSA *in vitro* release studies

*In vitro* release studies of BSA were conducted both in contact lens solution as well PBS solution to measure the amount of BSA that was released from the microspheres with different BSA loadings. An *in vitro* release study in contact lens solution was chosen, as it was more representative of the intraocular environment. From the results, a relatively higher initial burst release was observed, after 24 hours, in the microspheres immersed in PBS solution, when compared to those immersed in contact lens solution. The very small burst release observed in the contact lens solution was a positive result as this could indicate that there will be minimal burst release of the drug when the microspheres are used for intraocular delivery.

Within the first few hours, the BSA that was bound loosely to the surface of the microspheres could have contributed to the initial burst release. The initial burst release was however not dependent on the BSA loadings. The P(3HB) microspheres with a higher BSA loading exhibited a lower burst release due to the lower surface associated proteins when compared to the microspheres with a lower BSA loading and higher surface associated proteins. Following the initial burst release of BSA, a diffusion controlled release phase for microspheres with different BSA loading conditions both in PBS and contact lens were observed. However the microspheres loaded with 5 wt% of BSA exhibited a higher diffusion controlled release both in PBS as well in the contact lens solution when compared to the microspheres with lower BSA loadings. Due to the higher amount of BSA encapsulated in the 5 wt% microspheres, the concentration gradient between the microspheres and the outer emulsion phase would have been higher

when compared to the microspheres with lower BSA loadings. This difference in the concentration gradient would have initiated the higher release of protein from within the microspheres. The solvation of the protein molecules would have further created interconnecting channels and pores providing increased access for the surrounding medium. As a result, the additional protein molecules embedded within the microspheres would have migrated and a faster release rate would have occurred when compared to the microspheres with lower BSA loadings. Similarly researchers like Yang *et al.*, have also observed that PLGA microspheres with the highest BSA loading of 2.64% had exhibited a higher release rate when compared to the microspheres loaded with 0.66% and 0.45% of BSA.(Yang *et al.*, 2001).

#### 7.3.2.2 Lucentis<sup>®</sup> *in vitro* release studies

*In vitro* release study of Lucentis<sup>®</sup> (48kDa) was also conducted both in contact lens solution as well PBS solution to measure the amount of Lucentis<sup>®</sup> that was released from the microspheres. From the results, as seen a relatively higher initial burst release of 12% was observed after 24 hours in the microspheres immersed in PBS solution, when compared to 9% of those immersed in contact lens solution. This difference in the initial burst release observed between PBS and contact lens solution could be due to the higher solubility of Lucentis<sup>®</sup> in PBS when compared to the contact lens solution. Following an initial burst release, again a higher diffusion controlled release rate was observed in PBS when compared to the contact lens solution. This was due to the initial solvation of the protein molecules on the surface of the microspheres into the PBS solution. This could have created interconnecting channels providing access to the surrounding medium. The buffer penetration into the microspheres would have further initiated subsequent dissolution of Lucentis<sup>®</sup> embedded within the matrix. The % cumulative release of Lucentis<sup>®</sup> from both PBS and contact lens solution was 57% and 39% respectively for an extended period of 75 days. This slow release of Lucentis<sup>®</sup> could be attributed to the low porosity of the microspheres. For example Lucentis<sup>®</sup> loaded P(3HB) microspheres exhibited a porosity of 17% when compared to 24% porosity exhibited by the 5wt% BSA loaded microspheres which contributed to a release rate of 100% and 52% in PBS and contact lens solution respectively, within a period of 30 days.

### 7.3.2.3 RNase A *in vitro* release studies

The RNase A *in vitro* release profiles were also characterised by a biphasic release profile. An initial burst release of 8.45% was observed in 24 hours followed by a slower release over a period 30 days. The burst release from the microspheres was attributed to the surface associated proteins. Nellore *et al.*, observed a burst release of 50-70% in PBS solution due to the presence of surface associated RNase A. Following an initial burst release a gradual increase in the release rate was observed due to the higher amount of protein that is entrapped within the uniform open branched network of pores within microspheres. Sandor *et al.*, also observed a higher initial phase of release from PLGA microspheres encapsulating proteins such as lysozyme, which was followed by a gradual increase in the release phase. The authors' also observed a small amount of protein release in the final stages (4 weeks) which was largely attributed to the degradation of the PLGA microspheres (Sandor *et al.*, 2001). Although polymer erosion is known to contribute to final stages of drug delivery, in this study however it is probable that the RNase A release was complete before the polymer erosion could play a significant role. This is the major difference between PLGA and PHAs; the latter are very slow degrading, so in this study the degradation would contribute really minimally to drug elution.

### 7.3.3 *In vitro* microsphere degradation study of P(3HB) microspheres

In order to study the *in vitro* degradation of the P(3HB) microspheres; they were immersed in PBS and contact lens solution for different time periods. The water uptake (%WA) and weight loss (%WL) exhibited by the P(3HB) microspheres in the PBS solution were higher when compared to that of the contact lens solution. This indicated that the P(3HB) microspheres exhibited a much slower degradation rate in contact lens solution when compared to the degradation rate in PBS. The different rates of BSA release in PBS and contact lens solution from the P(3HB) microspheres could also influence the %WA of the P(3HB) microspheres. Since the BSA release rate was higher in PBS when compared to the release rate in contact lens solution, the empty voids steadily forming in the P(3HB) microsphere due to BSA release may increase the network of water channels for water penetration, thereby accelerating the weight loss of

the P(3HB) microspheres in PBS. P(3HB) undergoes random chain scission by ester hydrolysis, auto-catalysed by the generation of carboxylic acid end groups (Knowles *et al.*, 1992). The surface morphology of the P(3HB) microspheres after *in vitro* degradation studies carried out both in PBS and contact lens solution for a period of 30 days, remained smooth and spherical. This indicated minimal surface degradation. *In vitro* degradation of P(3HB) in buffer solutions is observed to show no visible bulk mass loss after 180 days indicating that P(3HB) undergoes slow *in vitro* degradation. However, a decrease in the molecular weight of the polymer is observed after 80 days of incubation (Doi *et al.*, 1989). The degradation of P(3HB) is observed to take place through random scission in both the amorphous and crystalline regions of the polymer matrix (Freier *et al.*, 2002b).

#### 7.3.4 Protein stability tests

##### 7.3.4.1 Protein profile of the BSA entrapped in the microspheres and released in to PBS and contact lens solution

From the gel, a single band corresponding to the  $M_w$  of BSA (66, 200Da), identical to that found in the control lanes was observed at all time points. Proteins are known to possess a complex internal structure, which provides its unique biological activity. These proteins can become inactive by denaturation and aggregation when exposed to surfactants or elevated temperatures. Similarly, reduction in the pH during incubation in the release medium is known to cause protein inactivation. Thus, in order to develop a successful protein-microsphere based delivery system; the structural integrity of the protein needs to be retained throughout the encapsulation and release period. However this result does not completely rule out the presence of protein aggregates linked by either covalent or non-covalent bonding. Therefore a non-denaturing PAGE, which is known to preserve the covalently and non-covalently bonded aggregates, should be carried out in the future to confirm the absence of protein aggregates. In another relevant study, Igartua *et al.*, confirmed the structural integrity of BSA using SDS-PAGE analysis which encapsulated in PLGA microspheres prepared using a w/o/w technique. The structural integrity of the protein released in phosphate buffered saline (PBS) during the *in vitro* assays was confirmed with a single band that corresponded to its molecular weight. The authors'

had also carried out a non-denaturing PAGE which did not reveal any aggregates of the protein further confirming that the structural integrity of BSA was retained even under the unfavourable encapsulation conditions (Igartua *et al.*, 1998).

#### 7.3.4.2 Protein profile of the Lucentis<sup>®</sup> entrapped in the microspheres and released into PBS and contact lens solution

From the gel, a single band identical to that found in the control lanes (25,000Da) was observed at all time points. The molecular weight of Lucentis<sup>®</sup> is 48,000Da (23,000Da and 25,000Da for the light and heavy chain, respectively). The reducing agent  $\beta$ -mercaptoethanol is known to break all disulphide bonded aggregates and the surfactant SDS is known to cause the complete unfolding of the native protein structure by binding to the hydrophobic residues and to the peptide backbone. Therefore, during SDS-PAGE analysis both the short and long chains (23 kDa, 25kDa) would have appeared as a single band after reduction of the disulphide linkage. A non-denaturing PAGE could also be carried out in future to preserve the covalently and non-covalently bonded aggregates.

#### 7.3.4.3 RNase A stability evaluation

Damaging effects on the enzymatic activity of the protein is known to occur when they come in contact with organic solutions (Nellore *et al.*, 1996). In order to monitor the stability of RNase A before and after *in vitro* release studies, fluorescence tests, SDS-PAGE and Methylene blue activity tests were performed.

##### 7.3.4.3.1 Fluorescence tests

The fluorescence emission spectra for RNase A placed in contact with the microsphere solution and not subjected to agitation was used as a control. Chloroform treated RNase A were conducted to investigate the possible changes in the three-dimensional structure of the protein in the presence of the organic solvent. From the results, the fluorescence emission spectra of the control and chloroform treated microspheres were super imposable with a maximum emission spectra at 303nm. A slight difference in the fluorescence intensity was observed which could be due to the difference in the protein concentration of the samples. During denaturation, the hydrogen bonds of RNase A are

disrupted leading to changes in the tryptophan fluorescence, leading to an increase in the fluorescence emission (Nellore *et al.*,1996). Unfolding of the tryptophan and tyrosine containing proteins such as RNase A is known to shift the fluorescence maximum to longer wavelengths such as 350 nm. Since the maximum fluorescence emission spectra of the control and chloroform treated RNase A were at 303nm in this study, this indicated that the RNase A loaded in the microspheres, after chloroform treatment, was not affected by the microsphere fabrication methods used (Nellore *et al.*,1996). In a similar study conducted by Nellore *et al.*, the fluorescence emission spectra of the acetonitrile treated RNase A, seen at 303 nm was super imposable with the emission spectra of the control, thus confirming that the acetonitrile treatment did not lead to any significant changes in the tyrosine and tryptophan residues of the RNase A molecules (Nellore *et al.*, 1996).

#### 7.3.4.3.2 Protein profile of the RNase A entrapped in the microspheres and released into PBS solution

In the SDS-PAGE, a single band corresponding to the  $M_w$  of RNase A (13,700 Da), identical to that found in the control lanes were observed with the solvent treated RNase A. This treatment should be analogous to the conditions used during microsphere manufacture. However a non-denaturing PAGE, which is known to preserve the covalently and non-covalently bonded aggregates, should be carried out in the future to confirm the absence of protein aggregates. Nellore *et al.*, also observed no changes in the molecular weight of the RNase A after solvent treatment. They observed that the relative mobility ( $R_f$ ), a function of the logarithm of the molecular weight, was similar to that of the untreated RNase A, used as a control, indicating that there was no gross aggregation (Nellore *et al.*, 1996).

#### 7.3.4.3.3 Methylene Blue RNase Enzyme Assay

The enzyme activities of the control RNase A (free RNase A placed in contact with the placebo microspheres and subjected to the same release medium and temperature) was compared with the specific activity of the RNase A released in the PBS solution. From the results it was observed that about 56% of the initial activity of the microencapsulated

RNase A was retained when compared to the control RNase A on day1. Nellore *et al.*, also observed loss of enzymatic activity when RNase A encapsulated within PLGA microspheres was compared with RNase A placed in contact with the placebo microspheres (controls) at 37°C and pH 7.4. The authors' observed a loss of 17% of the RNase A enzyme activity of the controls over a period of 7 days when compared to 70% loss of enzyme activity of the *in vitro* released samples. During microencapsulation the protein comes in contact with the organic solvent and then is released into the medium when the buffer penetrates further into the microspheres. This process may be unfavourable for the protein due to which it gets inactivated. A change in pH, such as reduction in the pH during incubation in the release medium would have also caused protein inactivation.

## 7.4 Conclusions

Protein delivery using biodegradable polymers is becoming increasingly common. The conventional method of encapsulating drugs in microspheres has also been applied to proteins. Often during microencapsulation, the surface and internal morphology, protein distribution and release kinetics are affected by a number of factors such as the type of protein encapsulated, polymer used and the methods of microsphere fabrication used. In this study an initial development of a microsphere-based protein delivery system using the biodegradable and biocompatible polyhydroxyalkanoates was developed. The microspheres were encapsulated with three model proteins BSA, Lucentis<sup>®</sup> and RNase A to understand the effect of morphology, drug distribution on the *in vitro* release profiles. The effects of solvent treatment and physical stresses encountered during microencapsulation into polymeric matrices were also examined using SDS-PAGE and fluorometric analysis. The microspheres produced were of an average size of 2 $\mu$ m. For the first part of this study where microsphere-based intraocular drug delivery was developed, this size would be advantageous, as it will allow their use in an ophthalmic context. Once injected intraocularly, they would allow the gradual release of the relevant drug in the intraocular chamber. The microspheres were encapsulated with different BSA loadings, 0.75wt%, 1.5wt% and 5wt%. The microspheres with the highest BSA loading yielded a larger concentration gradient between the emulsion droplet and the continuous phase, due to which a higher amount of BSA was released when compared to the microspheres with a lower BSA loading. The initial burst release was attributed to the surface associated BSA rather than the actual loadings, nevertheless the microspheres with the highest BSA loading exhibited a higher burst release due to the higher amount of surface associated BSA. The microencapsulation process also did not lead to any degradation of BSA and hence can be assumed to be equally gentle to any protein drug. The microspheres encapsulated with 5wt% of the second model protein Lucentis<sup>®</sup> exhibited an encapsulation efficiency of 48% and a surface associated protein of 13%. A higher percentage of surface associated protein (13%) was observed when compared to 8% of the 5 wt% BSA loaded microspheres. The lower molecular weight of Lucentis<sup>®</sup> may have diffused from within the microspheres and got bound onto the surface of the microspheres thereby increasing the percentage of surface associated proteins.

A relatively higher initial burst release was observed after 24 hours in the microspheres immersed in PBS solution, when compared to those immersed in contact lens solution. The initial burst release was attributed to the surface associated Lucentis<sup>®</sup> on the microsphere surface as well as the higher solubility of Lucentis<sup>®</sup> in PBS when compared to the contact lens solution may have contributed to the initial burst release. The % cumulative release of Lucentis<sup>®</sup> from both PBS and contact lens solution was slower for an extended period of 75 days when compared to the higher release exhibited by the 5 wt% BSA loaded microspheres within a period of 30 days. This slow release of Lucentis<sup>®</sup> could be attributed to its lower porosity when compared to the porosity exhibited by the 5wt% BSA loaded microspheres. The microencapsulation process also did not lead to any degradation of Lucentis<sup>®</sup>. However a non-denaturing PAGE, which is known to preserve the covalently and non-covalently bonded aggregates, should be carried out in the future to confirm the absence of protein aggregates. Hence in the context of wet macular degeneration, this drug delivery system would work very well as a controlled delivery can be achieved. Its use would decrease the frequency of injections required by the patients, a major achievement both in terms of the cost of treatment (for NHS in the UK) and the physical and emotional well being of the patients.

The third model protein used in this study was RNase A. RNase A has the same molecular weight as other functional agents such as bone morphogenic proteins (BMP-2). Therefore, the aim of this study was to identify whether the RNase A activity and structural integrity is maintained during the encapsulation process. The *in vitro* release study of RNase A in PBS revealed an initial burst release within the first 24 hours followed by a gradual increase a period of 30 days. The stability of RNase A following exposure to organic solvents was evaluated using a variety of analytical techniques such as fluorescence emission spectra, SDS-PAGE and methylene blue enzyme activity test. The fluorescence emission spectra revealed that the solvent treatment did not perturb the structure of RNase A. In the SDS-PAGE, a single band corresponding to the  $M_w$  of RNase A (13,700 Da), identical to that found in the control lanes were observed with the solvent treated RNase A. This treatment should be analogous to the conditions used during microsphere manufacture. As mentioned above a non-denaturing PAGE, which is known to preserve the covalently and non-covalently bonded aggregates, should be

carried out in the future to confirm the absence of protein aggregates. During microencapsulation the protein comes in contact with the organic solvent and then is released into the medium when the buffer penetrates further into the microspheres. This process may be unfavourable for the protein due to which it gets inactivated. As a result a gradual decrease in the enzyme activity of RNase A was observed over a period of time.

# Chapter 8

## Conclusions

## 8.1 Conclusions

The biodegradable P(3HB) microspheres system developed in this research has shown the potential to be used in various biomedical applications. Poly(3-hydroxybutyrate) P(3HB), was used to produce microspheres using a solid-in-oil-water (s/o/w) technique. For this study, several parameters namely as polymer concentration, surfactant and stirring rates were considered. The average dimensions of the microspheres were  $2\mu\text{m}$  to  $1.54\mu\text{m}$  with specific surface areas from  $9.60\text{ m}^2/\text{g}$  to  $6.05\text{ m}^2/\text{g}$  was produced. The microspheres produced using low stirring speed of 300 rpm produced slightly larger microspheres when compared to the smaller microspheres produced when the stirring rate was increased to 800 rpm. The surface morphology of the microspheres after solvent evaporation appeared smooth when observed under SEM. Gentamicin was also encapsulated within these P(3HB) microspheres and the release kinetics of the microspheres exhibiting the highest encapsulation efficiency, 48%, was investigated. The DSC analysis showed that the microsphere preparation process as well as the drug had influenced the thermal behaviour of the microspheres. The hydrophilic nature of the drug also had an influence on the polymeric degradation as well as the drug release behaviour. The *in vitro* release of gentamicin was biphasic where an initial burst release was observed followed by a diffusion mediated sustained release.

P(3HB) microspheres have been used in combination with 45S5Bioglass<sup>®</sup> (micro and nanoscale bioactive glass). The P(3HB) microspheres were coated onto the 3-D 45S5Bioglass<sup>®</sup> scaffolds. Successful microsphere coating on the 45S5Bioglass<sup>®</sup> scaffold was achieved using an optimized oil/water emulsion. The resultant composite scaffold had increased compressive strength, surface nanotopography and high bioactivity. The multifunctional scaffold was also successfully used as a drug delivery vehicle. The encapsulated drug within the coated scaffolds was released in a slow and sustained manner compared to the burst release of the drug from the P(3HB) microspheres on their own and the uncoated scaffold. Hence, this multifunctional scaffold can potentially be used to deliver drugs, proteins or growth factors to treat bone related diseases.

P(3HB) compositions were also used to prepare composite films with a combination of nanoscale bioactive glass (n-BG) (10 wt%) for wound healing applications. With the incorporation of n-BG particles, the changes in the thermal and surface properties such as surface roughness and protein adsorption were investigated. The various analyses performed/undertaken showed that the addition of n-BG particles had increased the surface roughness of the films, improved the surface wettability and reduced the heat of fusion by 19%. Surface mediated reactions such as clot formation was also investigated. By using n-BG particles the time until clot detection was found to decrease linearly with the increase in the amount of n-BG particles. An increase in the rate of coagulation was also observed when the amounts of n-BG particles were increased. Although 45S5Bioglass<sup>®</sup> has been previously reported as a haemostatic agent, this is the first time that n-BG particles have been reported for its applicability as a haemostatic agent. For the second part of this study, P(3HB)/n-BG composite microsphere films were immersed in SBF for a period of 1, 3 and 7 days and the effect of surface roughness of the cell adhesion was studied. The presence of the amorphous calcium phosphate deposition on day 1 and nanoscale sized HA crystals on day 3 and day 7 of the composite microsphere films had improved the surface wettability of the films due to its increased hydrophilicity. However due to the variations in the surface charge of the films after immersion in SBF, the protein adsorption was affected. This difference in the protein adsorption was attributed to the variations in the surface charge of the HA. The % cell viabilities on the composite microsphere films after immersion in SBF for 3 and 7 days were however affected by the rough surface morphology of the films. The cells on these films appeared scattered without the formation of a continuous thick layer due to which a lower cell adhesion was observed. Thus, in this study an optimal surface roughness for increased cell adhesion was observed beyond which it would be deleterious for cell adhesion and differentiation.

The efficacy of using films made from compressed P(3HB) microspheres encapsulating tetracycline as a scaffold for drug delivery and wound healing purposes was also studied. In this study the incorporation of the drug successfully improved the surface properties of the biomaterial such as surface morphology, wettability, roughness and porosity thereby promoting cell adhesion on the microsphere films. The presence of tetracycline on the

surface of the microspheres, as detected by XPS, resulted in changes in the surface properties of these films. The results from the water contact angle study showed a significant improvement in the hydrophilicity of the microsphere films with the addition of tetracycline that was further complemented by the increase in the total protein adsorption. These alterations in film surface properties resulted in an improved scaffold for keratinocyte adhesion and growth as indicated by the increased numbers of viable cells on the drug loaded microsphere films compared to those on the unloaded microsphere films. Finally the P(3HB) degradation was dependant on the crystallinity, thermal properties and water permeability. The different drug loading ratio, which led to, surface morphology changes also had an effect on polymer degradation.

P(3HB) microspheres were also investigated for use as drug delivery vehicles in the intraocular environment. These drug-loaded microspheres would then be injected into the vitreous humor of the patient's eye leading to gradual release of the drug, hence eliminating the need for monthly injections. Thus for this study the P(3HB) microspheres were entrapped with BSA and the release kinetics of BSA from the loaded microspheres were investigated. Finally, the degradation studies on the BSA loaded P(3HB) microspheres were carried out. The results from this preliminary study had confirmed that the BSA entrapped in the microspheres was released slowly and thus this system, when optimised, has the potential to be used for long-term intraocular drug delivery. The release rate of the drug, after optimisation, should allow release of the relevant drug for at least six months. The process did not lead to any degradation of BSA and hence can be assumed to be equally gentle to any protein drug. This is in fact the most positive result obtained in this project indicating the feasibility of the use of this system in the context of wet macular degeneration.

The results obtained from BSA encapsulation were then used for planning the encapsulation of the Lucentis<sup>®</sup>, currently the most common treatment for the wet macular degeneration produced by Genentech USA. These microspheres can then be injected into the patient's eye leading to gradual release of the drug, hence eliminating the need for monthly injections. The *in vitro* release rate in phosphate buffered saline and contact lens

solution (representative of an intraocular environment) was carried out. The % cumulative release of Lucentis<sup>®</sup> from both PBS and contact lens solution was slower for an extended period of 75 days when compared to the higher release exhibited by the 5 wt% BSA loaded microspheres within a period of 30 days. This slow release of Lucentis<sup>®</sup> could be attributed to its lower porosity when compared to the porosity exhibited by the 5wt% BSA loaded microspheres. The microencapsulation process also did not lead to any degradation of Lucentis<sup>®</sup>. However a non-denaturing PAGE, which is known to preserve the covalently and non-covalently bonded aggregates, should be carried out in the future to confirm the absence of protein aggregates.

Finally the effects of solvent treatment encountered by the model protein Ribonuclease A (RNase A) during microencapsulation in P(3HB) microspheres were investigated. Thus from these preliminary results the same encapsulation technique can be used for the encapsulation of BMP-2 and the typical response of cells C2C12 in the presence of BMP-2 from the release media can be studied. The stability of RNase A during the microencapsulation procedure was monitored using fluorspectrophometric studies and SDS-PAGE. The biological activity of the protein present in the release samples was determined by the Methylene Blue assay. The microspheres were characterised for surface morphology and encapsulation efficiency protein release profiles and protein activity. From the results, structural integrity of RNase A was maintained. Uniformly spherical sized microspheres in the size range of 2  $\mu\text{m}$  were prepared. The fluorescence emission spectra revealed that the solvent treatment did not perturb the structure of RNase A. In the SDS-PAGE, a single band corresponding to the  $M_w$  of RNase A (13,700 Da), identical to that found in the control lanes were observed with the solvent treated RNase A. During microencapsulation the protein comes in contact with the organic solvent and then is released into the medium when the buffer penetrates further into the microspheres. This process may be unfavourable for the protein due to which it gets inactivated. As a result, a gradual decrease in the enzyme activity of RNase A was observed over a period of time.

# Chapter 9

## Future work

## 9.1 Future work

On the basis of the results achieved there are potential areas of further research that will provide a better understanding of the applicability of P(3HB) and P(3HB)/n-BG composite systems

- P(3HB) microsphere production:- Surface properties of the microspheres have been known to have a significant influence on the host response system. The cells of the mononuclear phagocyte system rapidly clear most of the microspheres once injected in the body. However if the microspheres are internalised it could be advantageous, as these microspheres can be targeted to specific locations such as the spleen, liver and bone marrow to achieve a sustained release of the drug. Therefore drugs that would become effective only after internalization by the phagocytic cells should be chosen. The physico-chemical properties of the microspheres such as surface charge, surface hydrophobicity and size should be controlled and the intracellular microspheres uptake should be carried. The *in vitro* experiments can provide useful information of the fate of the drugs once injected into the body.
- The P(3HB) microspheres coated 45S5Bioglass<sup>®</sup> composite scaffolds:- GFP transfected MG63 cells can be used to assess cell viability/proliferation in order to measure biocompatibility and bioactivity, the number of cells will be determined by means of Cyquant and Alamar Blue assays, both of which are quantitative, reproducible assays. It can also be determined if osteoblastic growth is indeed induced and maintained by these composites by evaluating the expression of important bone-associated proteins namely, core binding factor 1 (cbfa1), alkaline phosphatase (AP), osteopontin (OP), osteocalcin (OC) and type I collagen (Col I) using a combination of biochemical assays, immunocytochemistry and quantitative Real Time Polymerase chain reaction (RT-PCR). Furthermore, bone mineralization; a strong indicator of bioactivity, on these composites will be assessed using Alizarin Red staining. Implantation of these scaffolds in bone defects and the bone formation and effects on angiogenesis and vascularization of these scaffolds can be monitored.

- P(3HB) microspheres/n-BG (10 wt%) composite microsphere films :- These films could be further characterised with respect to porosity and mechanical properties. The surface energy of the composite microsphere films and its effect on cell proliferation should be identified. Foreign body reactions should also be monitored when used as subcutaneous implants for *in vivo* experiments. Based on several factors of the microsphere films such as surface hydrophobicity, surface morphology and crystallinity the platelet adhesion and activation tests such as a lactate dehydrogenase (LDH) assay should be carried out to characterize the haemostasis of the materials and further confirm their applicability in wound healing.
- Polyhydroxyalkanoate microsphere-based systems for intraocular drug delivery: - Since the preliminary data from this study indicated that the BSA and Lucentis<sup>®</sup> entrapped in the microspheres was released slowly, this system can now be used for long-term intraocular drug delivery of other drugs such as Avastin, produced by Genentech USA. The drug needs to be administered through monthly intraocular injections Hence, P(3HB) microspheres can be used to encapsulate the drugs and it's *in vitro* release kinetics measured over a long period of time (for example 3 months). The degradation studies of Lucentis<sup>®</sup> and Avastin as well as the structural integrity of the drug using non-denaturing PAGE should be monitored. The release of Lucentis<sup>®</sup> and Avastin from the P(3HB) microspheres should be studied *in vitro*.
- Polyhydroxyalkanoate microsphere-based systems for encapsulating Bone morphogenic proteins (BMP-2):- The use of solid-oil-in-water emulsion technique for the encapsulation of BMP-2 should be carried out. The growth factor encapsulated microspheres can be incorporated into the 3-D scaffolds and the *in vitro* release of BMP-2 can be assayed using alkaline phosphatase (AP) assay. The cell line C2C12 cells which when stimulated with BMP-2 is known to induce an increase in alkaline phosphatase activity. This can be measured by staining. Therefore, the typical response of cells C2C12 in the presence of BMP-2 from the release media should be studied. Further studies on cell attachment, cytoskeleton/focal contacts and signal transduction should be investigated. This

long term *in vitro* release system of BMP-2 could be used to induce bone formation.

# References

Akhtar S, Pouton CW and Notarianni LJ Gould PL (1989). "A study of the mechanism of drug release from solvent evaporated carrier systems of biodegradable P(HB-HV) polyesters". *J Pharm Pharmacol* 41:694-699.

Akhtar S, Pouton CW and Notarianni LJ Gould PL(1992). "Crystallization behaviour and drug release from bacterial polyhydroxyalkanoates". *Polymer* 33:117-126.

Ali SAM, Doherty PJ and Williams DF (1994). "The mechanisms of oxidative degradation of biomedical polymers by free radicals". *J Appl Poly Sci* 51:1389-1398.

Ameer GA, Mahmood TA and Langer R (2002). "A biodegradable composite scaffold for cell transplantation". *J Ortho Res* 20:16.

Anderson AJ and Dawes EA (1990). "Occurrence, metabolism, metabolic role and industrial uses of bacterial polyhydroxyalkanoates". *Microbiol Rev* 54:450-472.

Asrar J, Valentin HE, Berger PA, TranM, Padgett S R and Garbow JR (2002). "Biosynthesis and Properties of Poly(3-hydroxybutyrate-co-3-hydroxyhexanoate) Polymers". *Biomacromol* 3:1006-1012.

- M (1999). "In vitro calcium phosphate layer formation on sol-gel glasses of the CaO-SiO<sub>2</sub> system". *J Biomed Mater Res* 47:243-250.

Bazzo GC, Lemos-Senna E, Gonçalves MC and Pires ATN (2008). "Effect of Preparation Conditions on Morphology, Drug Content and Release Profiles of Poly(hydroxybutyrate) Microparticles Containing Piroxicam". *J Braz Chem Soc* 19:914-921.

Berkland C, Kim K and Pack DW (2002). "PLG Microsphere Size Controls Drug Release Rate through Several Competing Factors". *Pharma Res* 20:1055-1062.

Berry CC, Dalby MJ, Oreffo RO, McCloy D, Affrossman S, Curtis AS (2006). "The interaction of human bone marrow cells with nanotopographical features in three dimensional constructs". *J Biomed Mater Res A* 79:431-439.

Bidone J, Paula APM, Bazzo GC, Carmignan F, Soldi MS, Pires ATN, Lemos-Senna E (2009). "Preparation and characterization of ibuprofen-loaded microspheres consisting of poly (3-hydroxybutyrate) and methoxy poly (ethylene glycol)- $\beta$ -poly (D, L-lactide) blends or poly(3-hydroxybutyrate) and gelatin composites for controlled drug release". *Mat Sci and Eng* 29:588-593.

Biggs MJP, Richards GR, McFarlane S, Wilkinson CD, Oreffo RO, Dalby MJ (2008). "Adhesion formation of primary human osteoblasts and the functional response of mesenchymal stem cells to 330 nm deep microgrooves". *J R Soc Interface* 5:1231-1242.

Biggs MJP, Richards GR and Dalby MJ (2010). "Nanotopographical modification: a regulator of cellular function through focal adhesions". *Nanomed Nanotech, Biol and Med* 6:619-633.

Bissery MC, Valeriote FA, Thies C (1985). "Therapeutic efficacy of CCNU-loaded microspheres prepared from poly (D, L) lactide (PLA) or poly-hydroxybutyrate (PHB) against Lewis Lung (LL) carcinoma". *Proc Ame Assoc Cancer Res* 26:355.

Bluhm, TL, Hamer GK, Marchessault RH, Fyfe CA and Veregin RP (1986). "Isodimorphism in bacterial poly(3-hydroxybutyrate-co-3-hydroxyvalerate)". *Macromol* 19:2871-2876.

Boeree NR, Dove J, Cooper JJ, Knowles J and Hastings GW (1993). "Development of a degradable composite for orthopaedic use: mechanical evaluation of a hydroxyapatite-

polyhydroxybutyrate composite material”. *Biomaterials* 14:793-796.

Bonfield W, Grynblas MD, Trully AE, Bowman J and Abram J (1981). “Hydroxyapatite reinforced polyethylene-a mechanically compatible implant material for bone replacement”. *Biomaterials* 2:185-187.

Bonartsev AP, Livshits VA, Makhina TA, Myshkina VL, Bonartseva GA, Iordanskii AL (2007). “Controlled release profiles of dipyridamole from biodegradable microspheres on the base of poly(3-hydroxybutyrate)”. *Poly Lett* 1:797-803.

Bouissou C, Potter U, Altroff H, Mardon H, Van der Walle C (2004). “Controlled release of the fibronectin central cell binding domain from polymeric microspheres”. *J Control Rel* 95:557-566.

Bretcanu O, Chen QZ, Misra SK, Roy I, Verne E, Vitale C, Brovarone, Boccaccini AR (2007). “Biodegradable polymer coated 45S5 Bioglass-derived glass ceramic scaffolds for bone tissue engineering”. *Glass Technol-Eur J Glass Sci Technol A* 48:227-234.

Bretcanu O, Misra SK, Roy I, Renghini C, Fiori F, Boccaccini AR, (2009) “*In vitro* biocompatibility of 45S5Bioglass-derived glass ceramic scaffolds coated with poly(3-hydroxybutyrate)”. *J Tissue Eng Reg Med* 3:139-148.

Brin YS, Golenser J, Mizrahi B, Maoz G, Domb AJ, Peddada S, Tuvia S, Nyska A, Nyska M (2008). “Treatment of osteomyelitis in rats by injection of degradable polymer releasing gentamicin”. *J Control Rel* 131:121-127.

Brophy MR and Deasy PB (1986). “*In vitro* and *in vivo* studies on biodegradable polyester microparticles containing sulphamethiazole”. *Int J Pharm* 29:223-231.

Bush KA, Driscoll PF, Soto ER, Lambert CR, McGimpsey WG, Pins GD (2008). “Designing tailored biomaterial surfaces to direct keratinocytes morphology, attachment

and differentiation". *J Biomed Mater Res* 90A:999-1009.

Caballero KP, Karel SF, Register RA (1995). "Biosynthesis and characterization of hydroxybutyrate-hydroxycaproate copolymers". *Int J Biol Macromol* 17:86-92.

Collins AEM, Deasy PB, MacCarthy DJ and Shanley DB (1989). "Evaluation of a controlled release compact containing tetracycline hydrochloride bonded to tooth for the treatment of periodontal disease". *Int J Pharm* 5:103-114.

Chang H, Perrie IY, Coombes AGA (2006). "Delivery of the antibiotic gentamicin sulphate from precipitation cast matrices of polycaprolactone". *J Control Rel* 110:414-421.

Chan BP and Leong KW (2008). "Scaffolding in tissue engineering: general approaches and tissue-specific considerations". *Eur Spine J* 17:467-479.

Chaput C, Yahia L, Selman A and Rivard C (1995). "Natural poly(hydroxybutyratehydroxyvalerate) polymers as degradable biomaterials". *Mater Res Soc Symp Proc* 385:49-51.

Chee J-W, Amirul AA, Majid MIA, Mansor SM (2008). "Factors influencing the release of *Mitragyna speciosa* crude extracts from biodegradable P(3HB-co-4HB)". *Int J Pharm.* 361:1-6.

Chen LJ and Wang M (2002). "Production and evaluation of biodegradable composite based on PHB-PHV copolymer". *Biomaterials* 23:2631-2639.

Chen GQ, Wu Q (2005). "The application of polyhydroxyalkanoates as tissue engineering materials". *Biomaterials* 226:6565-6578.

Chen Q, Thompson DI, Boccaccini AR (2006). "45S5Bioglass-derived glass-ceramic scaffolds for bone tissue engineering". *Biomaterials* 27:2414-2425.

Dash AK, Suryanarayanan R (1992). "An implantable dosage form for the treatment of bone infections". *Pharm Res* 9:993-1002.

Dass C R. and Peter F C (2007). "GFP Expression Alters Osteosarcoma Cell Biology". *DNA and Cell Biology* 26:599-601.

Dang JM and Leong KW (2006). "Natural polymers for gene delivery and tissue engineering". *Adv Drug Deliv Rev.* 58:487-499.

Deng Y, Zhao K, Zhang XF, Hu P and Chen GQ (2002). "Study on the three-dimensional proliferation of rabbit articular cartilage-derived chondrocytes on polyhydroxyalkanoate scaffolds". *Biomaterials* 23:4049-4056.

Deasy PB, Collins AEM, MacCarthy DJ and Russell RJ (1989). "Use of strips containing tetracycline hydrochloride for the treatment of advanced periodontal disease". *J Pharm Pharmacol.* 41:694-699.

Doi Y, Kanesawa Y, Kawaguchi Y and Kunioka M (1989a). "Hydrolytic degradation of microbial poly(hydroxyalkanoates)". *Macromol Rapid Commun.* 10:227-230.

Doi Y, Kitamura S and Abe H (1995). "Microbial synthesis and characterization of Poly(3-hydroxybutyrate-co-3-hydroxyhexanoate)". *Macromol* 28:4822-4828.

Domingues ZR, Cortés M E, Gomes TA, Diniz HF, Freitas CS, Gomes JB, Faria AMC, Sinisterra RD (2004). "Bioactive glass as a drug delivery system of tetracycline and tetracycline associated with  $\beta$ -cyclodextrin". *Biomaterials* 25:327-333.

Dufresne A and Vincendon M (2000). "Poly (3-hydroxybutyrate) and Poly (3 - hydroxyoctanoate) Blends: Morphology and Mechanical Behavior". *Macromol* 33:2998-3008.

Dupeyron D, Gonzalez M, Saez V, Ramon J and Rieumont J (2005). "Nano-encapsulation of protein using an enteric polymer as carrier". *IEE Proc.-Nanobiotechnol* 152:165-168.

Dyson JA, Paul GG, Kenneth W, Dalgrano and David JW (2007). "Development of Custom-Built Bone Scaffolds Using Mesenchymal Stem Cells and Apatite-Wollastonite Glass-Ceramics". *Tissue Eng* 13:2891-2901.

Edlund U, Albertsson AC (2002). "Degradable polymer microspheres for controlled drug delivery". *Adv Polym Sci* 157:67-112.

Eldridge JH, Hammond CJ, Meulbrook JA, Staas JK, Gilley RM and Tice TR (1990). "Controlled vaccine release in the gut-associated lymphoid tissues, I: Orally administered biodegradable microspheres target the Payer's patches". *J Control Rel* 11:205-214.

Eryilmaz M, Ozer T, Menteş O, Torer N, Durusu M, Günal A, Uzar AI (2009). "Is the zeolite hemostatic agent beneficial in reducing blood loss during arterial injury". *Ulus Travma Acil Cerrahi Derg* 15(1):7-11.

Francis L, Meng D, Knowles JC, Roy I, Boccaccini A R (2010). "Multi-functional P(3HB) microsphere/45S5 Bioglass-based composite scaffolds for bone tissue engineering". *Acta Biomater* 6:2773-2786.

Frank A, Rath SK, Venkatraman SS (2005). "Controlled release from bioerodible polymers: effect of drug type and polymer composition". *J Control Rel* 102:333-344.

Freier T, Kunze C, Nischan C, Kramer S, Sternberg K *et al.*, (2002a). "In vitro and In vivo degradation studies for development hydroxybutyrate)". *Biomaterials* 23:2649-2657.

Freier S and Zhu (2004). "Polymer microspheres for controlled drug release". *Int J of Pharma* 282:1-18.

Gangrade N and Price JC (1991). "Poly(hydroxybutyrate-hydroxyvalerate) microspheres containing progesterone: Preparation, morphology and release properties". *J Microencapsul* 8:185-202.

Gagnon D, Lenz RW, Farris RJ and Fuller RC (1992). "Crystallization behaviour and its influence on the mechanical-properties of a thermoplastic elastomer produced by *Pseudomonas oleovorans*". *Macromol* 25:3723-3728.

Galego N, Rozsa C, Sanchez R, Fung J, Vazquez A et al. (2000). "Characterization and application of Poly( $\beta$ -hydroxyalkanoates) family as composite biomaterials". *Polym Test* 19:485-492.

Ghannam EA, Ducheyne P and Shapiro M (1999). "Effect of serum proteins on osteoblasts adhesion to surface-modified Bioactive glass and Hydroxyapatite". *J Ortho Res* 17:340-345.

Gittens SA and Uludag H (2001). "Growth factor delivery for bone tissue Engineering". *J Drug Target* 9:407-429.

Gursel I, Yagmurlu F, Korkusuz F, Hasirci V (2002). "In vitro antibiotic release from poly(3-hydroxybutyrate-co-3-hydroxyvalerate) rods". *J Microencapsul* 19:153-64.

Gu C and Karthikeyan KG (2005). "Interaction of Tetracycline with Aluminum and Iron Hydrous Oxides". *Environ Sci Technol.* 39:2660-2667.

Giannuzzi LA, Stevie FA (2005). "Introduction to Focused Ion Beams: Instrumentation, Theory, Techniques, and Practice". Springer, New York.

Goldberg VM and Stevenson S (1987). "Natural history of autografts and allografts". *Clin Orthop. Relat Res* 225:7-16.

Gomes ME and Reis RL (2004). "Tissue engineering: some key elements and some trends". *Macromol Biosci* 4:737-742.

Gould PL, Holland SJ and Tighe BJ (1987). "Polymers for biodegradable medical devices IV Hydroxybutyrate- hydroxyvalerate copolymers as non-disintegrating matrices for controlled release oral dosage forms". *Int J Pharm* 38:231-237.

Govender S , Pillay V., Chetty DJ, Essack SY, Dangor CM and Govender T (2005). "Optimisation and characterisation of bioadhesive controlled release tetracycline microspheres". *Int J Pharm* 306:24-40.

Gross R A, DeMello C, Lenz R W, Brandl H, Fuller RC (1989). "The biosynthesis and characterization of poly( $\beta$ -hydroxyalkanoates) produced by *Pseudomonas oleovorans*". *Macromol* 22:1106-1115.

Gray JJ (2004). "The interaction of proteins with solid surfaces". *Current Opinion in structural biology* 14:110-115.

Habraken WJ, Wolke JG and Jansen JA (2007). "Ceramic composites as matrices and scaffolds for drug delivery in tissue engineering". *Adv Drug Deliv Rev* 59:234-248.

Hasırcı V, Lewondrowski K, Gresser JD, Wise DL, Trantolo DJ (2000). "Versatility of biodegradable biopolymers: degradability and *in vivo* application". *J Biotech* 86:135-150.

Hench LL (1998). "Bioceramics". *J Am Ceram Soc* 81(7):1705-28.

Hench LL (1998b). "Biomaterials: a forecast for the future". *Biomaterials* 19:1419-1423.

Hoffman M (2003). "Remodelling the blood coagulation cascade". *J Thromb Thrombolysis* 16:17-20.

Horbett TA (1994). "The role of adsorbed proteins in animal cell adhesion". *Colloids and Surfaces B: Biointerfaces* 2:225-240.

Huang J and Best S (2008). Ceramic Biomaterials. Tissue engineering using ceramics and polymers. Boccaccini AR and Gough JE. Cambridge, England, Woodhead Publishing Ltd.

Huang W, Wang Y, Ren L, Du C, X Shi (2009). "A novel PHBV/HA microsphere releasing system loaded with alendronate". *Mat Sci and Eng C* 29:2221-2225.

Huang YY and Chung TW (2001). "Microencapsulation of gentamicin in biodegradable PLA and/or PLA/PEG copolymer". *J Microencapsul* 18:457-465.

Hutmacher DW (2000). "Polymeric scaffolds in tissue engineering bone and cartilage". *Biomaterials* 21:2529-2543.

, Esquisabel A, Gascon AR, Calvo MB, and Pedraz JL (1998). "Stability of BSA encapsulated into PLGA microspheres using PAGE and capillary electrophoresis". *Int J Pharm* 169:45-54.

Ishikawa K (1996). "Flexible member for use as a medical bag". US Patent 5480394.

Itälä A, Ylänen HO, Yrjans J, Heino T, Hentunen T, Hupa M, Aro HT (2002). "Characterization of microrough bioactive glass surface: surface reactions and osteoblast responses *in vitro*". *J Biomed Mater Res* 62:404-411.

Jeyanthi R, Mehta RC, Thanoo BC. and DeLuca PP (1997). "Effect of processing parameters on the properties of peptide-containing PLGA microspheres".

*J Microencapsul* 14:163-174.

Jendrossek D (2002). "Extracellular polyhydroxyalkanoate depolymerises: the key enzyme of PHA degradation". *Biopolymers: Polyesters II (Vol. 3b) - Properties and chemical synthesis.* (Eds.) Steinbuechel A. and Doi Y. Weinheim, Wiley-VCH: pp 41.

Ji Y, Li X-T, Chen G-Q (2008). "Interactions between a poly(3-hydroxybutyrate-co-3-hydroxyvalerate-co-3-hydroxyhexanoate) terpolyester and human keratinocytes" *Biomaterials* 29:3807-3814.

Jones NL, Cooper JJ, Waters RD and Williams DF (2000). "Resorption profile and biological response of calcium phosphate filled PLLA and PHB7V". *Synthetic bioabsorbable polymers for implants.* (eds) Agarwal CM, Parr JE, Lin ST, America Society for Testing and Materials, West Conshohocken: pp 69.

Juni K, Nakano M and Kukota M (1987). "Controlled release of aclarubicin, an anti-cancer antibiotic, from poly- $\beta$ -hydroxybutyric acid microspheres". *J Control Rel* 4:25-32.

Kai Z, Ying D and Guo-Qiang C (2002). "Effects of surface morphology on the biocompatibility of polyhydroxyalkanoates". *Biochem Eng J.* 16:115-123.

Kang KI, Choi SH, Shin DS, Yoon SC (2001) "Surface modification of polyhydroxyalkanoate films and their interaction with human fibroblasts". *Int. J. Biol. Macromol* 28: 205-212

Kassab AC, Xu K, Denkbaz EB, Dou Y, Zhao S, Piskin E (1997). "Rifampicin carrying polyhydroxybutyrate microspheres as potential chemoembolization agent". *J Biomater Sci Polymer Edn.* 8:947-961.

Khang G, Kim SW, Cho JC, Rhee JM, Yoon SC, Lee HB (2001). "Preparation and characterization of poly(3-hydroxybutyrate-co-3-hydroxyvalerate) microspheres for the sustained release of 5-fl uorouracil". *Biomed Mater Eng* 11:89 -103.

- Kharenko AV, Iordanskii AL (1999). "Diltiazem release from matrices based on polyhydroxybutyrate". *Proc Int Symp Control Rel Bioact Mater* 26:919-920.
- Kim HW, Chung CW, Kim SS and Kim YB, Rhee YH (2002). "Preparation and cell compatibility of acrylamide-grafted poly(3-hydroxyoctanoate)". *Int J Biol Macromol* 30:129-135.
- Kim HW, Chung CW and Rhee YH (2005). "UV-induced graft copolymerization of monoacrylate-poly(ethylene glycol) onto poly(3-hydroxyoctanoate) to reduce protein adsorption and platelet adhesion". *Int J Biol Macromol* 35:47-53.
- Kim, H. W., Knowles, J. C. & Kim, H. E (2004). "Development of hydroxyapatite bone scaffold for controlled drug release via poly(1-caprolactone) and hydroxyapatite hybrid coatings". *J Biomed Mater Res Part B: Appl Biomater.* 70:240-249.
- Kim DY, Kim HW, Chung MG and Rhee YH (2007) "Biosynthesis, modification and biodegradation of bacterial medium chain length polyhydroxyalkanoates". *The J of Microbiol* 45:87-97.
- Kose GT, Korkusuz F, Korkusuz P, Purali N, Ozkul A (2003). "Bone on PHBV matrices: an *in vitro* study". *Biomaterials* 24:4999-5007.
- Köse GT, Korkusuz F, Özkul A, Soysal Y, Özdemir T, Yildiz C and Hasirci V (2005). "Tissue engineered cartilage on collagen and PHBV matrices". *Biomaterials* 26:5187-5197.
- Kostopoulos L and Karring T (1994). "Guided bone regeneration in mandibular defects in rats using bioresorbable polymer". *Clin Oral Impl Res* 5:66-74.
- Korsatko VW, Wabnegg B, Tillian HM, Egger G, Pfranger R, Walser V (1984). "Poly-D-(-)-3-hydroxybutyric acid-a biodegradable carrier for long term medication dosage.

Studies on compatibility of poly-D-(-)-3hydroxybutyric acid implantation tablets in tissue culture and animals”. *Pharm Ind* 46:952-954.

Knowles JC, Mahmud FA and Hastings GW (1991). “Piezoelectric characteristics of Polyhydroxybutyrate based composite”. *Clinical Materials* 8:155-158.

Kubota M, Nakano M and Juni K (1988). “Mechanism of enhancement of the release rate of alcarubicin from poly- $\beta$ -hydroxybutyric acid microspheres by fatty acid esters”. *Chem Pharmaceut Bull* 36:333-337.

Kokubo T, Kushitani H, Sakka S, Kitsugi T and Yamamuro T (1990). “Solutions able to reproduce in vivo surface structure changes in bioactive glass ceramic A-W”. *J Biomed Mater Res* 24:721-734.

Kokubo T, Hata K, Nakamura T and Yamamura T (1991). “Apatite formation on ceramics, metals and polymers induced by CaO-SiO<sub>2</sub>-based glass in simulated body fluid”. *Bioceramics*. (Eds.) Bonfield W, Hastings GW, Tanner KE. Butterworth-Heinemann, Oxford.

Kurcok P, Kowalczyk M, Adamus G, Jedlinski Z, Lenz RW (1995). “Degradability of poly( $\beta$ -hydroxybutyrate)s. Correlation with chemical microstructure”. *J Macromol Sci A* 32:875-880.

Kumagai Y and Doi Y (1992a). “Enzymatic degradation and morphologies of binary blends of microbial poly(3-hydroxybutyrate) with poly( $\epsilon$ -caprolactone), poly(1,4 butylene adipate) and poly(vinyl acetate)”. *Polym Degrad Stabil* 36:241-248.

Kumagai Y, Kanetsawa Y and Doi Y (1992b). “Enzymatic degradation of microbial poly(3-hydroxybutyrate) films”. *Macromol Chem* 193:53-57.

Labuzek S, Radecka I (2001). “Biosynthesis of PHB tercopolymer by *Bacillus cereus*

UW85". *J Appl Microbiol.* 90:353-357.

Langer R and Tirrell DA (2004). "Designing materials for biology and medicine". *Nature* 428:487-492.

- (2006). "Determination of gentamycin in different matrices by a new sensitive high-performance liquid chromatography-mass spectrometric method". *J Antimicrob Chemother* 58:557-63.

Lee SY (1995). "Review bacterial polyhydroxyalkanoates". *Biotechnol Bioeng* 49:1-14.

Lee SC, Oh JT, Jang MH, Chung S Il (1999). "Quantitative analysis of polyvinyl alcohol on the surface of poly(D, L-lactide-co-glycolide) microparticles prepared by solvent evaporation method: effect of particle size and PVA concentration". *J Control Rel* 59:123-132.

Liu Q, Chen G-Q (2008). "In vitro biocompatibility and degradation of terpolyester 3HB-co-4HB-co-3HHx, consisting of 3-hydroxybutyrate, 4-hydroxybutyrate and 3-hydroxyhexanoate". *J Biomater Sci Polymer Edn* 19:1521-1533.

Li H and Chang J (2004). "Fabrication and characterization of bioactive wollastonite/PHBV composite scaffolds". *Biomaterials* 25:5473-5480.

Li H and Chang J (2005). "Preparation, characterization and *in vitro* release of gentamicin from PHBV/wollastonite composite microspheres". *J Control Rel* 107(3):463-473.

, MI, Guterres, SS, Pohlmann, AR (2007). "Microparticles prepared with poly(hydroxybutyrate-co-hydroxyvalerate) and poly(-caprolactone) blends to control the release of a drug model". *J Microencapsul* 24:175-186.

- Liu Q, Chen G-Q (2008). "In vitro biocompatibility and degradation of terpolyester 3HB-co-4HB-co-3HHx, consisting of 3-hydroxybutyrate, 4-hydroxybutyrate and 3-hydroxyhexanoate". *J Biomater. Sci. Polymer Edn* 19:1521-1533.
- Lu B, Wang ZR and Yang H (2001). "Long-acting delivery microspheres of levonorgestrel-poly(3-hydroxybutyrate):their preparation, characterization and contraceptive tests on mice". *J Microencapsul* 18:55-64.
- Lu H, Solomon R. Pollack, Paul D (2001). "45S5 Bioactive glass surface charge variations and the formation of a surface calcium phosphate layer in a solution containing fibronectin". *J Biomed Mater Res* 54:454-461.
- Ljungberg C, Johansson RG, Bostrom KJ, Novikov L and Weiberg M (1999). "Neuronal survival using a resorbable synthetic conduit as an alternative to primary nerve repair". *Microsurgery* 19:250-264.
- Luklinska ZB and Bonfield W (1997). "Morphology and ultrastructure of the interface between hydroxyapatite-polyhydroxybutyrate implant". *Sci Mater Med* 8:379-383.
- Luklinska ZB and Schluckwerder H (2003). "In vivo response to HA polyhydroxybutyrate/polyhydroxyvalerate composite". *J Microsc* 211:121-129.
- Luo L, Wei X, Chen GQ (2009). "Physical Properties and Biocompatibility of Poly(3-hydroxybutyrate-co-4-hydroxybutyrate)". *J Biomat Sci* 20:1537-1553.
- MacNeil S (2007) "Progress and opportunities for tissue-engineered skin". *Nature* 445, 874-880
- Malm T, Bowald S, Bylock A and Busch C (1992). "Prevention of postoperative pericardial adhesions by closure of the pericardium with absorbable polymer patches-An experimental study". *J Thorac Cardiovasc Surg* 104:600-607.

Marschessault RH, Monasterios CJ, Morin FG and Sundararajan PR (1990). "Chiral poly( $\beta$ -hydroxyalkanoates): an adaptable helix influenced by the alkane side-chain" *Int J of Biological Macromol* 12:158-165.

Marois Y, Zhang Z, Vert M, Beaulieu L, Lenz RW (1999). "In vivo biocompatibility and degradation studies of polyhydroxyoctanoate in the sealant for the polyester arterial prosthesis". *Tissue Eng* 5:369-386.

Martin DP and Williams SF (2003). "Medical applications of poly-4-hydroxybutyrate: a strong flexible absorbable biomaterial". *Biochem Eng J* 16:97-105.

Marti A (2000). "Inert Bioceramics ( $Al_2O_3$ ,  $ZrO_2$ ) for medical applications". *Injury* 31 (Suppl 4):33-36.

Martin MA, Miguens FC, Rieumont J, Sanchez R (2000). "Tailoring of the external and internal morphology of poly-3-hydroxy butyrate microparticles". *Colloids Surf. B: Biointerf.* 17:111-116.

Miyamoto S, Akiyama SK, Yamada KM (1995). "Synergistic roles for receptor occupancy and aggregation in intergin transmembrane function". *Science* 267:883-885.

McLeod BJ, Haresign W, Peters AR, Humke R and Lamming GE (1988). "The development of subcutaneous delivery preparations of GnRH for the induction of ovulation in acyclic sheep and cattle". *Animal Reprod. Sci.* 17:33-50.

Merino V, López A, Kalia YN and Guy RH (1999). "Electrorepulsion versus electroosmosis: effect of pH on the iontophoretic flux of 5-fluorouracil". *Pharm Res* 16: 671-758.

Metcalfe AD, Ferguson MWJ (2007). "Tissue engineering of replacement skin : the crossroads of biomaterials, wound healing, embryonic development, stem cells and regeneration". *J R Soc Interface* 4:413-437.

Miao X, Tan DM, Li J, Xiao Y, Crawford R (2008). "Mechanical and biological properties of hydroxyapatite/tricalcium phosphate scaffolds coated with poly(lactic-co-glycolic acid)". *Acta Biomater* 4:638-645.

Milner KR, Siedlecki CA (2007). "Submicron poly(L-Lactic acid) pillars affect fibroblasts adhesion and proliferation". *J Biomed Mater Res A* 82:80-91.

Misra SK, Valappil SP, Roy I, Boccaccini AR (2006). "Polyhydroxyalkanoate (PHA) /inorganic phase composites for tissue engineering applications". *Biomacromol* 7:2249-2258.

Misra SK, Nazhat SN, Valappil SP, Moshrefi-Torbati M, Wood RJK, Roy I, Boccaccini AR (2007). "Fabrication and characterization of biodegradable poly(3-hydroxybutyrate) composite containing Bioglass". *Biomacromol* 8:2112-2119.

Misra SK, Mohn D, Brunner T J, Stark W J, Philip SE, Roy I, Salih V, Knowles JC, Boccaccini AR (2008). "Comparison of nanoscale and microscale bioactive glass on the properties of P(3HB)/Bioglass composites". *Biomaterials* 29:1750-1761.

Misra SK, Philip SE, Chrzanowski, Nazhat SN, Roy I, Knowles JC, Salih V, Boccaccini AR (2009). "Incorporation of vitamin E in Poly (3-hydroxybutyrate)/Bioglass composite films: effect on surface properties and cell attachment". *J R Soc Interface* 6:401-409.

Misra SK, Ansari TI, Valappil SP, Mohn D, Philip S E, Stark W J, Roy I, Knowles JC, Salih V, Boccaccini AR (2010). "Poly(3-hydroxybutyrate) multifunctional composite scaffolds for tissue engineering applications". *Biomaterials* 31:2806-2815.

Mosahebi A, Fuller P, Wiberg M and Terenghi G (2002). "Effect of allogeneic Schwann cell transplantation on peripheral nerve regeneration". *Exp. Neurol* 173:213-223.

Mourino V and Boccaccini AR (2009). "Bone tissue engineering therapeutics: controlled

drug delivery in three-dimensional scaffolds”. *J R Soc Interface* 7:209-227.

Morita T, Sakamura Y, Horikiri Y, Suzuki T, Yoshino H (2000). “Protein encapsulation into biodegradable microspheres by a novel S/O/W emulsion method using poly(ethylene glycol) as a protein micronization adjuvant”. *J Control Rel* 69:435-444.

Murata N, Takashima Y, Toyoshima K, Yamamoto M, Okada H (2008). “Anti-tumor effects of anti-VEGF siRNA encapsulated with PLGA microspheres in mice”. *J Control Rel* 126:246-254.

Nakamura S and Doi Y (1992). “Microbial synthesis and characterization of Poly(3-hydroxybutyrate-co-4-hydroxybutyrate”. *Macromol* 25:4237-4828.

Naraharisetti PK, Lewa MDN, Fub Y-C (2005). “Gentamicin-loaded discs and microspheres and their modifications: characterization and *in vitro* release”. *Biomaterial* 77B:329-337.

Naraharisetti PK, Lee HCG, Fu Y-C, Lee D-J, Wang C-H (2006). “*In Vitro* and *In Vivo* Release of Gentamicin from Biodegradable Discs”. *J Biomed Mater Res Part B:Appl* 77:329-337.

Navarro M, Michiardi A, Castano O and Planell JA (2008). “Biomaterials in orthopaedics”. *J R Soc Interface* 5:1137-1158.

Nellore RV, Bhagat HR (1997). “Structural stability and *in vitro* biological activity of Ribonuclease A during microencapsulation into biodegradable polymers”. *Drug del* 4:49-55.

Nelson T, Kaufman E, Kline J and Sokoloff L (1981). “The extraneural distribution hydroxybutyrate”. *J Neurochem.* 37:1345-1348

- Nebe B, Forster C, Pommerenke H, Fulda G, Behrend D, Bernewski U, Schmitz KP, Rychly J (2002). "Structural alterations of adhesion mediating components in cells cultured on poly-hydroxy butyric acid". *Biomaterials* 22:2425-2434.
- Ni J and Wang M (2002). "In vitro evaluation of hydroxyapatite reinforced polyhydroxybutyrate composite". *Mater Science Eng. C* 20:101-109.
- Nobes GAR, Marchessault RH and Maysinger D (1998). "Polyhydroxyalkanoates: Materials for Delivery Systems". *Drug Del* 5:167-177.
- Norman J (2006). "Methods for fabrication of nanoscale topography for tissue engineering scaffolds". *Annals of biomed eng*, 34:89-101.
- Novikov LN, Novikova LN, Mosahebi A, Wiberg M, Terenghi G, Kellerth JO (2002). "A novel biodegradable implant for neuronal rescue and regeneration after spinal cord injury". *Biomaterials* 23:369-376.
- Ostomel TA, Shi Q, Tsung C-K, Liang H, Stucky GD (2006). "Spherical Bioactive Glass with enhanced rates of hydroxyapatite deposition and haemostatic activity". *Small* 11:1261-1265.
- Palau M-M, Franco L, Puiggali J (2008). "Microspheres of New Alternating Copolyesters derived from Glycolic acid units for controlled drug release". *J Appl Polym Sci* 110:2127-2138.
- Palazzo B, Sidoti MC, Tampieri A, Sandri M, Bertolazzi L, Galbusera F, Dubini G, Vena P. and Contro R. (2005). "Controlled drug delivery from porous hydroxyapatite grafts: an experimental and theoretical approach". *Mater Sci Eng C* 25:207-213.
- Paul DR, Harris FW (1976). "Controlled release polymeric formulations". *ACS Symposium Series*. 33:1976.

Park G T (1994). "Degradation of poly (DL-lactic acid) microspheres: Effect of molecular weight". *J Control Rel* 30:161-173.

Palau M-M, Franco L, Puiggali J (2008). "Microspheres of New Alternating Copolyesters derived from Glycolic acid units for controlled drug release". *J Appl Polym Sci* 110:2127-2138.

Pramanik N, Bhargava P, Alam S, Pramanik P (2006). "Processing and properties of nano-and macro-hydroxyapatite/poly(ethylene-co-acrylic acid) composites". *Poly Comp* 27:633-641.

Prashar A, Locke IC and Evans CS (2002). "Cytotoxicity of lavender oil and its major components to human skin cells". *Cell prolif* 37:221-229.

Patil S, Sandberg A, Heckert E, Self W, Seal S (2007). "Protein adsorption and cellular uptake of cerium oxide nanoparticles as a function of zeta potential". *Biomaterials* 28:4600-4607.

Patrick CW and King TW (1999). "Development and *in vitro* characterization of vascular endothelial growth factor (VEGF)-loaded poly(DL-lactic-co-glycolic acid)/poly(ethylene glycol) microspheres using a solid encapsulation/single emulsion/solvent extraction technique". *J Biomed Mater Res* 51:383-390.

Pezzatini S, Morbidelli L, Solito R, Paccagnini E, Boanini E, Bigi A (2000). "Nanostructured HA crystals up-regulate FGF-2 expression and activity in microvascular endothelium promoting angiogenesis". *Bone* 41:523-534.

Peschel G, Dahse H-M, Konrad A, Weiland GD, Mueller PJ, Martin DP, Roth M (2007). "Growth of Keratinocytes on porous films of poly(3-hydroxybutyrate) and poly(4-hydroxybutyrate) blended with hyaluronic acid and chitosan". *J Biomed Mater Res* 85 A:1072-1081.

- Pouton C, Akhtar S (1996). "Biosynthetic polyhydroxyalkanoates and their potential in drug delivery". *Adv Drug Deliv Rev* 18:133-162.
- Poletto FS, Jager E, M I Re, Guterres SS, Pohlmann AR (2007). "Rate-modulating PHBHV/PCL microparticles containing weak acid model drugs". *Int J Pharm* 345:70-80.
- Preusting H, Nijenhuis A and Witholt B (1990). "Physical characteristics of poly(3-hydroxyalkanoates) and poly(3-hydroxyalkenoates) produced by *Pseudomonas oleovorans* grown on aliphatic hydrocarbons". *Macromolecules* 23:4220-4224.
- Qiu QQ, Ducheyne P, Ayyaswamy P (2000). "New bioactive, degradable composite microspheres as tissue engineering substrates". *J Biomed Mater Res* 52(1):66-76.
- Qua XH, Wua Q, Zhanga KY and Chen GQ (2006). "In vitro studies of poly(3-hydroxybutyrate-co-3-hydroxyhexanoate) based polymers: Biodegradation and tissue reactions". *Biomaterials* 27:3540-3548.
- Rainer A, Giannitelli SM, Abbruzzese F, Traversa E, Licoccia S, Trombetta M (2008). "Fabrication of bioactive glass-ceramic foams mimicking human bone portions for regenerative medicine". *Acta Biomat* 4:362-369.
- Renard E, Tanguy PY, Samain E, Guerin P (2003). "Synthesis of novel graft polyhydroxyalkanoates". *Macromol Symp* 197:11-18.
- Rezwan K, Chen QZ, Blaker JJ and Boccacinni AR (2006). "Biodegradable and bioactive porous polymer/inorganic composite scaffolds for bone tissue engineering". *Biomaterials* 27:3413-3431.
- Rezwan K, Lorenz PM, Rezwan M, Janos V, Textor M and Gauckler LJ (2004). "Bovine serum albumin adsorption on colloidal AlO particles. A new model based on Zeta Potential and UV-Vis measurements". *Langmuir* 20:10055-10061.

- Rivard CH, Chaput CJ, DesRosiers EA, Yahia LH and Selmani A (1995). "Fibroblast seeding and culture in biodegradable porous substrate". *J Appl Biomater* 6:65-68.
- Rosca ID, Watari F, Uo M (2004). "Microparticle formation and its mechanism in single and double emulsion solvent evaporation". *J Control Rel* 99:271-280.
- Robertson BC, Zydney AL (1990). "Protein adsorption in asymmetric ultra filtration membranes with highly constricted pores". *J Colloid Interface Sci* 134:563-575.
- Sadowski B (1988). "PHB and BIOPOL as resorbable osteosynthesis material" (In German), MD Thesis, University of Wurzburg.
- Sampath SS, Garvin K and Robinson D.H (1992). "Preparation and characterization of biodegradable poly(L-lactic acid) gentamicin delivery systems". *Int J Pharm* 78:165-174.
- Sandor M, Ensore D, Weston P and Mathiowitz E (2001). "Effect of protein molecular weight on release from micron-sized PLGA microspheres". *J Control Rel* 76:297-311.
- Sanharawi M El, Kowalczyk L, Touchard E, Omri S, Kozak Yde, Behar-Cohen F (2010). "Protein delivery for retinal diseases: From basic considerations to clinical applications". *Prog in Ret and Eye Res* 29:443-465.
- Sahoo SK, Panyam J, Prabha S, Labhasetwar V (2002). "Residual polyvinyl alcohol associated with poly(D,L-lactide-co- glycolide) nanoparticles affects their physical properties and cellular uptake". *J Control Rel* 82:105-114.
- Saito T, Tomita K, Juni K, Ooba K (1991). "In vivo and in vitro degradation of poly(3-hydroxybutyrate) in rat". *Biomaterials* 12:309-312.
- Saito Y, Nakamura S, Hiramitsu M and Doi Y (1996). "Microbial synthesis and properties of Poly(3-hydroxybutyrate-co-4-hydroxybutyrate)". *Polym Int* 39:169.

Sanchez R, Schripsema J, Da Silva, LF, Taciro MK, Pradella GC and Gomez GC (2003). "Medium-chain-length polyhydroxyalkanoic acids (PHAmcl) produced by *Pseudomonas putida* IPT 046 from renewable sources". *Eur Poly J* 39:1385-1394.

Scandola M, Ceccorulli G, Pizzoli M, Gazzano M (1992). "Study of the crystal phase and crystallization rate of bacterial poly(3-hydroxybutyrate-co-3-hydroxyvalerate)". *Macromol* 25:1405-1410.

Sendil D, Gursel I, Wise D L, Hasirci V (1999). "Antibiotic release from biodegradable PHBV microparticles". *J Control Rel* 59:207-217.

Selhuber-Unkel M, Garcia L, Kessler H and Spatz JP (2008). "Cooperativity in adhesion cluster formation during initial cell adhesion". *Biophys J* 95:5424-5431

Siepmann J, Peppas NA (2001). "Modeling of drug release from delivery systems based on hydroxypropyl methylcellulose". *Advd Drug Deliv Rev* 48:139-157.

Shishatskaya EI and Volova TG (2004). "A comparative investigation of biodegradable polyhydroxyalkanoate films as matrices for *in vitro* cell cultures". *J Mater Sci Mater Med* 15:915-923.

Shishatskaya EI, Goreva AV, Voinova ON, Inzhevatin EV, Khlebopros RG, and TG Volova (2007). "Evaluation of Antitumor Activity of Rubomycin Deposited in Absorbable Polymeric Microparticles". *Bull Exp Biol Med* 145:358-361.

Shih W-J, Chen Y-H, Shih C-J, Hon M-H, Wang M-C (2007). "Structural and morphological studies on poly(3-hydroxybutyrate acid) (PHB)/chitosan drug releasing microspheres prepared by both single and double emulsion processes". *J of Alloys and Comp* 434-435:826-829.

Sodian R, Hoerstrup SP, Sperling JS, Daebritz S, Martin DP (2000a). "Early *In*

*vivo* experience with tissue engineered trileaflet heart valves”. *Circulation* 102:111-122

Sodian R, Hoerstrup SP, Sperling JS, Martin DP, Daebritz S (2000b). “Evaluation of biodegradable, three dimensional matrices for tissue engineering of heart valves”. *ASAIO J* 46:107-110.

Soderling EK. Herbst EW. Larmas and Yli-Urpo A (1996). “Protein adsorption to bioactive glass with special reference to precorrosion”. *J of Biomed Mat Res* 31:525-531.

Solberg BD, Gutow AP, Baumgaertner MR (1999). “Efficacy of gentamicin-impregnated resorbable hydroxyapatite cement in treating osteomyelitis in a rat model”. *J Orthop Traum* 13:102-106.

Sokolsky Papkov-Marina, Agashi K, Olaye A, Shakesheff K and Domb A (2007). “Polymer carriers for drug delivery in tissue engineering”. *Advd Drug Del Rev* 59:187-206.

Sotome S, Uemura T, Kikuchi M, Chen J, Itoh S, Tanaka J, Tateishi T, Shinomiya K (2004). “Synthesis and in vivo evaluation of a novel hydroxyapatite/ collagen–alginate as a bone filler and a drug delivery carrier of bone morphogenetic protein”. *Mater Sci and Eng C* 24:341-347.

Steinbüchel A and Valentin HE (1995). “Diversity of bacterial polyhydroxyalkanoic Acids”. *FEMS Microbiol. Lett.* 128:219-228.

Steinbüchel A and Eversloh TL (2003). “Review: Metabolic engineering and pathway construction for biotechnological production of relevant polyhydroxyalkanoates in microorganisms”. *Biochem Eng J* 16:81-96.

Stephens D, Li L, Robinson D, Chen S, Chang H-C, Liu RM, Tian Y, Ginsburg, EJ, Gao X, Stultz T (2000). “Investigation of the *in vitro* release of gentamicin from a

polyanhydride matrix". *J Control Rel* 63:305-317.

Stock UA, Sakamoto T, Hatsuoka S, Martin DP, Nagashima M *et al.* (2000). "Patch augmentation of the pulmonary artery with bioabsorbable". *J Thorac Cardiovasc Surg* 120:1158-1167.

Stoeffele TG, Grunow M and Hahn U (1996). "A General Ribonuclease Assay Using Methylene Blue". *Anal Biochem* 240:24-28.

Sudesh K, Abe H and Doi Y (2000). "Synthesis, structure and properties of polyhydroxyalkanoates: biological polyesters". *Prog Polym. Sci* 25:1503-1555.

Suzuki T, Deguchi H, Yamane T, Shimizu S, and Gekko K (1998). "Control of molecular weight of poly- $\beta$ -hydroxybutyric acid produced in fed-batch culture of *Protomonas extorquens*". *Appl Microbiol Biotechnol* 27:487-491.

Tanahashi M, Kokubo T, Minoda M, Miyamoto T, Nakamura T, Yamamuro T (1994). "Apatite coating on organic polymers by a biomimetic process". *J Am Ceram Soc* 77:2805.

Tajima K, Igari T, Nishimura D, Nakamura M, Satoh Y, Munekata M (2003). "Isolation and characterization of *Bacillus* sp. INT005 accumulating polyhydroxyalkanoate (PHA) from gas field soil". *J Biosci Bioeng* 95:77-78.

Tesema Y, Raghvan D and Stubbs J (2004). "Bone cell viability on collagen immobilized poly(3-hydroxybutyrate-co-3-hydroxyvalerate) membrane: Effect ON surface chemistry". *J Appl Polym Sci* 93:2445-2453.

Teixeira AI, Nealey PF and Murphy CJ (2004). "Responses of human keratocytes to micro-and nanostructured substrates". *J of Biomed Mat Res Part A*, 71A:369-376.

- Tezcancer A, Burga K and Hasirci V (2003). "Retinal pigment epithelium cell culture on surface modified poly(hydroxybutyrate-co-hydroxyvalerate)". *Biomaterials* 24:4573-4583.
- Unverdorben M, Spielberger A, Schywalsky M, Labahn D, Hartwig S *et al.*, (2002). "A polyhydroxybutyrate biodegradable stent:Preliminary experience in the rabbit". *Cardiovasc Interv Radiol* 25:127-132.
- Vainionpää S (1986). "Biodegradation of polyglycolic acid in bone tissue: an experimental study on rabbits". *Arch Orthop Trauma Surg* 104:333-338.
- Van Der Walle GAM, de Koning GJM, Weusthuis RA and Eggin G (2001). "Properties, Modifications and Applications of Biopolyesters". *Adv in Biochem Eng/ Biotech* 71:263-291.
- Valappil SP, Misra SK, Boccaccini AR, Roy I (2006). "Biomedical applications of polyhydroxyalkanoates, an overview of animal testing and *in vivo* responses". *Expert Rev Med Dev* 3:853-868.
- Valappil SP, Misra SK, Boccaccini AR, Keshavarz T, Bucke C, Roy I (2007). "Large scale production and efficient recovery of PHB with desirable material properties, from the newly characterized *Bacillus cereus* SPV". *J of Biotechnol* 132:251-258.
- Vallet-Regí M, Balas F, Colilla M and Manzano M (2008). "Bone-regenerative bioceramic implants with drug and protein controlled delivery capability". *Prog Solid State Chem* 36:163-191.
- Volova T, Shishatskaya E, Sevastianov V, Efremov S and Mogilnaya O (2003a). "Results of biomedical investigations of PHB and PHB/PHV fibers". *Biochem Eng J.* 16:125-133.

Wang Z, Itoh Y, Hosaka Y, Kobayashi I, Nakano Y, Maeda I, Umeda F, Yamakawa J, Kawase M, Yagi K (2003). "Novel Transdermal Drug delivery system with Polyhydroxyalkanoate and Starburst Polyamidoamine Dendrimer". *J Biosci and Bioeng* 95:541-543.

Wang YW, Wu Q and Chen GQ (2004). "Attachment, proliferation and differentiation of osteoblasts on random biopolyester 3--hydroxyhexanoate) scaffolds". *Biomaterials* 25: 669-675.

Wang YW, Wu Q, Chen J and Chen GQ (2005a). "Evaluation of three-dimensional scaffolds made of blends of hydroxyapatite and poly(3-h3hydroxyhexanoate) for bone reconstruction". *Biomaterials* 26:899.

Wang YM, Yang F, Wu Q, Chen YC, Yu PHF, Chen J and Chen GQ (2005b). "Effect of composition of poly(3-hydroxybutyrate-co-3-hydroxyhexanoate on growth of fibroblast and osteoblast". *Biomaterials* 26:755-761.

Wang Y, Lu L, Zheng Y, Chen X (2006). "Improvement in hydrophilicity of PHBV films by plasma treatment". *J of Biomed Mat Res Part A* 76A 3:589-595.

Wang Y, Wang X, Wei K, Zhao N, Zhang S, Chen J (2007). "Fabrication, characterization and long-term in vitro release of hydrophilic drug using PHBV/HA composite microspheres". *Mat Lett* 61:1071-1076.

Wang C, Ye W, Zheng Y, Liu X, Tong Z (2007). "Fabrication of drug-loaded biodegradable microcapsules for controlled release by combination of solvent evaporation and layer-by-layer self-assembly". *Int J Pharm* 338:165-173.

Wahlgren M, Arnebrant T (1991). "Protein adsorption to solid surfaces". *Trends Biotechnol* 6:201-208.

Ward PG, Roo GD, Connor KEO (2005). "Accumulation of Polyhydroxyalkanoate from Styrene and Phenylacetic Acid by *Pseudomonas putida* CA-3". *Appl and Enviorn Microbiol* 71:4 2046-2052.

Webster T J, Siegel R W and Bizios R (1999). "Osteoblast adhesion on nanophase Ceramics". *Biomaterials* 20:221-227.

Wei G and Ma PX (2004). "Structural and properties of nano-hydroxyapatite/polymer composite scaffolds for bone tissue engineering". *Biomaterials* 25:4749-4757.

Wei X, Hu Y-J, Xie W-P, Lin R-L, Chen G-Q (2008). "Influence of poly(3-hydroxybutyrate-co-4-hydroxybutyrate-co-3-hydroxyhexanoate) on growth and osteogenic differentiation of human boe marrow-derived mesenchymal stem cells". *J Biomed Mater Res* 90A:894-905.

Williams SF and Martin DP, Horowitz DM and Peoples OP (1999). "PHA applications: addressing the price performance issue I. Tissue engineering". *Int J Biol Macromol* 25:111-121.

Wilkinson JF and Williamson DH (1958). "The isolation and estimation of the poly-  $\beta$ -hydroxybutyrate inclusion of *Bacillus* species". *J Gen Microbiol* 19:198-209.

Williams SF and Martin DP (2005). "Applications of PHAs in medicine and pharmacy". Weinheim, Germany, Marchessault RH (Eds)Wiley-VCH.

Wozniak MA, Modzelewska K, Kwong L, Keely PJ (2004). "Focal adhesion regulation of cell behaviour". *Biochem Biophys Acta* 1692:103-119.

Wu TJ, Huang HH, Lan CW, Lin CH, Hsu FY *et al.*, (2004). "Studies on the microspheres comprised of reconstituted collagen and hydroxyapatite". *Biomaterials* 25:651.

Xi J, Zhang L, Zheng ZA, Chen GQ, Gong Y (2008). "Preparation and evaluation of porous poly(3hydroxybutyrate-co-3hydroxyhexanoate)-hydroxyapatite composite scaffolds". *J Biomater Appl* 22:293-307.

Xynos ID, Edgar AJ, Buttery LDK, Hench LL and Polak JM (2001). "Gene expression profiling of human osteoblasts following treatment with the ionic products of Bioglass 45S5 dissolution". *J Biomed Mater Res* 55:151-157.

Yagmurlu MF, Korkusuz F, Gürsel I, Korkusuz P, Örs Ü, Hasirci V (1999). "Sulbactam-cefoperazone polyhydroxybutyrate-co-hydroxyvalerate (PHBV) local antibiotic delivery system: *In vivo* effectiveness and biocompatibility in the treatment of implant-related experimental osteomyelitis". *J Biomed Mater Res* 46:494-503.

Yang Y, Chung TS, Ng NP (2001). "Morphology, drug distribution, and in vitro release profiles of biodegradable polymeric microspheres containing protein fabricated by double-emulsion solvent extraction/evaporation method". *Biomaterials* 22:231-241.

Yang M, Zhu S, Chen Y, (2004). "Studies on bone marrow stromal cells affinity of poly (3-hydroxybutyrate-co-3-hydroxyhexanoate)". *Biomaterials* 25:1365-1373.

Yang H, Fumitaka Horii (2008). "Investigation of the structure of poly(vinyl alcohol)-iodine complex hydrogels prepared from the concentrated polymer solutions". *Polymer* 49:785-791.

Yasin M, Holland SJ, Jolly AM and Tighe BJ (1989). "Polymers for biodegradable medical devices. VI. Hydroxybutyrate-hydroxyvalerate copolymers: accelerated degradation of blends with polysaccharides". *Biomaterials* 10:400-412.

Ying TH, Ishii D, Mahara A, Murakami S, Yamaoka T, Sudesh K, Samian R, Fujita M, Maeda M and T Iwata T (2008). "Scaffolds from electrospun polyhydroxyalkanoate

copolymers: Fabrication, characterization, bioabsorption and tissue response” *Biomaterials* 10:1307-1317.

Yunos DM, Bretcanu O, Boccaccini AR (2008). “Polymer–bioceramic composites for tissue engineering scaffolds”. *J Mater Sci* 43:4433-4442.

Zhao K, Deng Y, Chen CJ, Chen G-Q (2003). “Polyhydroxyalkanoates (PHA) scaffolds with good mechanical properties and biocompatibility”. *Biomaterials* 24:1041-1048.

Zhu J, Snow DD, Cassada DA, Monson SJ, Spalding RF (2001). “Analysis of oxytetracycline, tetracycline and chlortetracycline in water using solid-phase extraction and liquid chromatography-tandem mass spectrometry”. *J of Chromatography A* 177-186.

Zhang Y, Zhang MQ (2002). “Three-dimensional macroporous calcium phosphate Bioceramics with nested chitosan sponges for load-bearing bone implants”. *J Biomed Mater Res* 61:1-8.

Zhao K, Deng Y, Chen CJ, Chen G-Q (2003). “Polyhydroxyalkanoates (PHA) scaffolds with good mechanical properties and biocompatibility”. *Biomaterials* 24:1041-1048.

Zhu Y, & Kaskel S (2009). “Comparison of the *in vitro* bioactivity and drug release property of mesoporous bioactive glasses (MBGs) and bioactive glasses (BGs) scaffolds”. *Microporous Mesoporous Mater* 118:176-182.

Zinn M, and Hany R (2005). “Tailored material properties of polyhydroxyalkanoates through biosynthesis and chemical modification”. *Adv Eng Mater* 7:408-411.

## **List of Publications**

1. Francis L *et al.*, (2010). “Multi-functional P(3HB) microsphere/45S5 Bioglass-based composite scaffolds for bone tissue engineering”. *Acta biomaterials*.
2. Francis L *et al.*, (2010).“The Influence of Tetracycline Loading on the Surface Morphology and Biocompatibility of Films made from P(3HB) Microspheres”. *Advanced Biomaterials*.
3. Francis L *et al.*, (2010). “Using electrophoretic deposition to identify protein charge in biological medium”. *J. Appl. Electrochemistry* (Manuscript submitted).
4. Francis L *et al.*, (2011). Controlled delivery of gentamicin using Poly(3-hydroxybutyrate) microspheres. *Int J of Mat Sci* (Manuscript submitted).